

# UNIVERSITE DE LIMOGES

ECOLE DOCTORALE SCIENCES ET INGÉNIERIE POUR L'INFORMATION

FACULTE DES SCIENCES ET TECHNIQUES

*Laboratoire : XLIM*

*Département : C<sup>2</sup>S<sup>2</sup>*

**Année : 2012**

**Thèse N° 40-2012**

## Thèse

pour obtenir le grade de

DOCTEUR DE L'UNIVERSITÉ DE LIMOGES

Spécialité : Électronique des Hautes Fréquences, Photonique et Systèmes

Présentée et soutenue par

**Sajjad AHMED**

Le 16 Novembre 2012

## **Système de mesures temporelles 4-canaux à échantillonnage entrelacé ultra haute fréquence basé sur des amplificateurs « Track & Hold » pour la caractérisation impulsionnelle d'amplificateurs de puissance non linéaires**

---

Thèse dirigée par **Denis BARATAUD** et **Guillaume NEVEUX**

### JURY :

<b>Jean-Michel NEBUS</b>	Professeur, Université de Limoges	<b>Président</b>
<b>Yves Rollain</b>	Professeur, Vrije Universiteit Brussel	<b>Rapporteur</b>
<b>Juan-Mari Collantes</b>	Professeur, Université du Pays Basque de Bilbao	<b>Rapporteur</b>
<b>Denis BARATAUD</b>	Professeur, Université de Limoges	<b>Examineur</b>
<b>Guillaume NEVEUX</b>	Maître de Conférences, Université de Limoges	<b>Examineur</b>
<b>M.VANDEN BOSSCHE</b>	Ingénieur, NI Belgium NV/SA	<b>Examineur</b>
<b>Tony GASSELING</b>	Ingénieur, AMCAD-ENGINEERING	<b>Examineur</b>
<b>Michel STANISLAWIAK</b>	Ingénieur, Thales Air Systems – TR6	<b>Examineur</b>
<b>Tibault REVEYRAND</b>	Ingénieur d'Etudes CNRS	<b>Invité</b>



# UNIVERSITE DE LIMOGES

ECOLE DOCTORALE SCIENCES ET INGÉNIERIE POUR L'INFORMATION

FACULTE DES SCIENCES ET TECHNIQUES

*Laboratoire : XLIM*

*Département : C<sup>2</sup>S<sup>2</sup>*

**Année : 2012**

**Thèse N°40-2012**

## Thèse

pour obtenir le grade de

DOCTEUR DE L'UNIVERSITÉ DE LIMOGES

Spécialité : Électronique des Hautes Fréquences, Photonique et Systèmes

Présentée et soutenue par

**Sajjad Ahmed**

Le 16 Novembre 2012

## **Système de mesures temporelles 4-canaux à échantillonnage entrelacé ultra haute fréquence basé sur des amplificateurs « Track & Hold » pour la caractérisation impulsionnelle d'amplificateurs de puissance non linéaires**

---

Thèse dirigée par **Denis BARATAUD** et **Guillaume Neveux**

### JURY :

<b>Jean-Michel NEBUS</b>	Professeur, Université de Limoges	<b>Président</b>
<b>Yves Rollain</b>	Professeur, Vrije Universiteit Brussel	<b>Rapporteur</b>
<b>Juan-Mari Collantes</b>	Professeur, Université du Pays Basque de Bilbao	<b>Rapporteur</b>
<b>Denis BARATAUD</b>	Professeur, Université de Limoges	<b>Examineur</b>
<b>Guillaume NEVEUX</b>	Maître de Conférences, Université de Limoges	<b>Examineur</b>
<b>M.VANDEN BOSSCHE</b>	Ingénieur, NI Belgium NV/SA	<b>Examineur</b>
<b>Tony GASSELING</b>	Ingénieur, AMCAD-ENGINEERING	<b>Examineur</b>
<b>Michel STANISLAWIAK</b>	Ingénieur, Thales Air Systems – TR6	<b>Examineur</b>
<b>Tibault REVEYRAND</b>	Ingénieur d'Etudes CNRS	<b>Invité</b>

*“People who have no hold over their process of thinking are likely to be ruined by liberty of thought. If thought is immature, liberty of thought becomes a method of converting men into animals”.*

Mohammad Iqbal  
November 9, 1877 – April 21, 1938

*To my parents*

*To all, I care about*



## **Acknowledgements**

First of all, I thank Allah, the almighty, for giving me the strength to carry on this research and for blessing me with many great people who have been my greatest support. The results achieved during my research work would not have been possible without the guidance and the help of several individuals who in one way or another contributed and extended their valuable assistance in the preparation and completion of this study.

Especially I would like to record my gratitude to **Denis BARATAUD**, professor at University of Limoges and **Guillaume NEVEUX**, maître de Conférences at University of Limoges who were my thesis advisor and co-advisor respectively. Their supervision, advice, and guidance from the very early stage of this research and their encouraging remarks helped me to gain an extraordinary experience throughout the work. They provided a great friendly environment where one can openly discuss the ideas floating in the mind and their overwhelming response helped my growth as a student.

I gratefully thank **Jean-Michel NEBUS**, professor at University of Limoges and **Tibault REVEYRAND**, ingénieur d'Etudes CNRS for their scientific inputs and some great discussions with the later helped me to think in different dimensions. I would also like to thank the department secretary **Marie Claude LEROUGE** for helping me with all the official documental work which would not have been possible for me, to manage alone.

Many thanks go in particular to **Yves Rollain**, Professor at Vrije Universiteit Brussel, for accepting to be my examiner and lending his precious time for extensively reading the thesis and giving his critical comments for improving the script particularly the scientific language. I would also like to thank **Juan-Mari Collantes**, Professor at University of Pays Basque de Bilbao, who in the midst of all his activities accepted to be the other examiner and gave valuable and constructive remarks.

My special gratitude to **M.VANDEN BOSSCHE**, engineer at NI Belgium, NV/SA, **Tony GASSELING**, engineer at AMCAD-ENGINEERING and **Michel STANISLAWIAK**, engineer at Thales Air Systems – TR6 for their availability and interest in my research work. Their support and encouraging remarks nourished my intellectual maturity.

I am indebted to all my colleagues whom I have worked with during the last three years namely: Ala Saleh, Khaled Khoder, George, Ali, Aladin Ramadan, Saad el din, Christophe, Abdullah, Patrick, Pierre, kassem and karthik. We altogether shared some great moments and developed strong bonding and friendship.

A ton of thanks to all my friends, cousins who always supported me during the good and hard times and making my educational process a success.

Finally I would like to thank my parents and sisters for all their love, encouragement and supporting me in all my pursuits. My uncle “M. Iqbal” who gently offered counsel and unconditional support throughout my life. Thank you all for being there whenever I need you.

# Index Table

---

<b>GENERAL INTRODUCTION</b> .....	<b>11</b>
<b>CHAPTER I :</b> .....	<b>15</b>
<b>THE TIME-DOMAIN MEASUREMENT SYSTEM AND ITS IMPORTANCE.</b>	<b>15</b>
<b>INTRODUCTION</b> .....	<b>17</b>
<b>I. RADAR COMMUNICATION</b> .....	<b>18</b>
<b>I.1. OPERATING PRINCIPLES OF A RADAR SYSTEM</b> .....	<b>18</b>
I.1.1. TRANSMITTED AND RECEIVED SIGNALS [1], [2] .....	18
I.1.2. FREQUENCY BASED RADAR APPLICATION [5], [6].....	22
I.1.3. ROLE OF POWER AMPLIFIER IN RADAR COMMUNICATIONS [8] .....	23
<b>II. EMERGENCE OF WIDE BAND GAP SEMICONDUCTORS</b> .....	<b>23</b>
<b>II.1. PROS AND CONS OF SEMICONDUCTORS</b> .....	<b>23</b>
II.1.1. ADVANTAGES AND PROPERTIES OF SEMICONDUCTORS [9], [10].....	23
II.1.2. UNDESIRE EFFECTS OF SEMI-CONDUCTORS [16], [17], [18] .....	25
<b>II.2. RF PULSED SIGNALS AND COMPLEXITIES</b> .....	<b>26</b>
II.2.1. RF PULSED SIGNALS [19].....	26
II.2.1.1. RF measurement complexity.....	32
II.2.1.2. Pulse to pulse stability [22], [23].....	32
II.2.1.2.1. Standard deviation method .....	34
II.2.1.2.2. RMS method.....	34
<b>III. TIME-DOMAIN MEASUREMENT SYSTEMS</b> .....	<b>35</b>
<b>III.1. IMPORTANCE OF TIME-DOMAIN MEASUREMENT</b> .....	<b>35</b>
III.1.1. BASIC TIME-DOMAIN MEASUREMENT SETUP ARCHITECTURE .....	36
III.1.2. DETERMINING THE BOTTLENECK [25], [26].....	37
<b>III.2. RF DOWN-CONVERSION</b> .....	<b>41</b>
III.2.1. MICROWAVE MIXERS [30], [31] .....	41
III.2.1.1. Mixer specifications [31], [32].....	43
III.2.2. SAMPLERS [33].....	45
III.2.2.1. Basic architecture.....	45
III.2.2.2. Charge sampling [38].....	52
III.2.2.3. Sub-sampling Down-conversion.....	54



<b>IV. PRE EXISTING TIME-DOMAIN INSTRUMENTS .....</b>	<b>58</b>
<b>IV.1. SAMPLER BASED INSTRUMENTS .....</b>	<b>58</b>
IV.1.1. VECTOR NETWORK ANALYZER (VNA) .....	58
IV.1.2. LARGE SIGNAL NETWORK ANALYZER (LSNA) .....	60
IV.1.2.1. Modulated signals.....	62
<b>IV.2. MIXER BASED INSTRUMENTS.....</b>	<b>64</b>
IV.2.1. VECTOR SIGNAL ANALYSIS.....	64
IV.2.2. NON-LINEAR VECTOR NETWORK ANALYZER (NVNA) [49], [50] .....	68
<b>IV.3. DIGITAL STORAGE OSCILLOSCOPE (DSO) [50].....</b>	<b>69</b>
<b>CONCLUSION.....</b>	<b>72</b>
<b>BIBLIOGRAPHIE .....</b>	<b>73</b>
<b>CHAPTER II : .....</b>	<b>77</b>
<b>DESCRIPTION OF A TRACK &amp; HOLD AMPLIFIER .....</b>	<b>77</b>
<b>INTRODUCTION.....</b>	<b>79</b>
<b>I. TRACK AND HOLD OPERATION .....</b>	<b>79</b>
<b>I.1. TRACK AND HOLD CIRCUIT (T/H).....</b>	<b>79</b>
<b>I.2. TRACK AND HOLD AMPLIFIER [THA].....</b>	<b>80</b>
I.2.1. OPERATING PRINCIPLE OF THA.....	84
<b>II. CHARACTERIZATION OF THA.....</b>	<b>89</b>
<b>II.1. INPHI THA .....</b>	<b>89</b>
II.1.1. MEASUREMENT SETUP.....	90
II.1.2. DC POWER .....	91
II.1.3. LINEARITY.....	91
II.1.3.1. Measurement of 1dB compression point .....	91
II.1.3.2. Intermodulation distortion (IMD) .....	92
II.1.3.3. Third Order Intercept (TOI) point.....	93
II.1.4. BANDWIDTH OF OPERATION.....	94
<b>II.2. CHARACTERIZATION OF THE THA WITH A DIFFERENTIAL AMPLIFIER .....</b>	<b>96</b>
<b>II.3. COMPARISON OF THA AND SAMPLER CHARACTERISTICS.....</b>	<b>97</b>
<b>CONCLUSION.....</b>	<b>101</b>

<b>BIBLIOGRAPHIE .....</b>	<b>102</b>
<b>CHAPTER III :.....</b>	<b>103</b>
<b>ENVELOPE MEASUREMENT TEST BENCH .....</b>	<b>103</b>
<b>INTRODUCTION.....</b>	<b>105</b>
<b>I. INPHASE AND QUADRATURE (IQ) SAMPLING .....</b>	<b>106</b>
<b>I.1. IQ DATA .....</b>	<b>106</b>
I.1.1. QUADRATURE SAMPLING.....	109
<b>II. CALIBRATION .....</b>	<b>112</b>
II.1.1. INTRODUCTION.....	112
II.1.2. CALIBRATION STANDARDS.....	115
II.1.3. ERROR VECTOR CALCULATION [5].....	118
<b>III. TIME-DOMAIN MEASUREMENT SETUP .....</b>	<b>126</b>
<b>III.1. SINGLE CHANNEL ACQUISITION OF TIME-DOMAIN DATA.....</b>	<b>126</b>
III.1.1. ANALOGY OF THE MEASUREMENTS OF THE PROPOSED SYSTEM AND VECTOR SIGNAL ANALYZER .....	131
<b>III.2. 4-CHANNEL TIME-DOMAIN MEASUREMENT TEST-BENCH.....</b>	<b>134</b>
III.2.1. MEASUREMENT RESULTS.....	136
III.2.1.1. CW Measurement .....	137
III.2.1.2. Pulsed Measurements.....	138
III.2.1.3. Two-tone Measurements.....	142
III.2.1.4. Digital pre-distortion .....	145
<b>CONCLUSION.....</b>	<b>150</b>
<b>BIBLIOGRAPHIE .....</b>	<b>151</b>
<b>CHAPTER IV:.....</b>	<b>153</b>
<b>RF TRANSIENTS MEASUREMENT.....</b>	<b>153</b>
<b>INTRODUCTION.....</b>	<b>155</b>
<b>I. COHERENT TIME-INTERLEAVED SYSTEM.....</b>	<b>157</b>

<b>I.1. AN ADAPTION OF SUB-SAMPLING PRINCIPLE .....</b>	<b>157</b>
I.1.1. REAL SAMPLING FREQUENCY CALCULATION .....	157
I.1.2. DE-SCRAMBLING OF SAMPLES.....	160
I.1.3. EXAMPLE EXPLAINING CTIS .....	160
<b>II. CW MEASUREMENT SYSTEM DESCRIPTION AND RESULTS.....</b>	<b>162</b>
<b>II.1. CW WAVE MEASUREMENT.....</b>	<b>162</b>
II.1.1. CW MEASUREMENT SETUP AND CALIBRATION .....	162
II.1.2. AUTOMATED MEASUREMENT SETUP FOR CW SIGNAL.....	165
II.1.3. CW MEASUREMENT RESULTS .....	167
<b>II.2. MEASUREMENT OF A BROADBAND AMPLIFIER .....</b>	<b>169</b>
II.2.1. CW PERFORMANCE.....	169
II.2.2. QUASI SQUARE SIGNAL MEASUREMENT RESULTS .....	171
<b>III. PULSED SIGNAL MEASUREMENTS AND RESULTS.....</b>	<b>175</b>
<b>III.1. PULSED SIGNAL MEASUREMENT TEST SETUP .....</b>	<b>176</b>
<b>III.2. ISSUES RELATED TO PULSED SIGNAL EXCITATION .....</b>	<b>177</b>
III.2.1. EFFECT OF THE BANDWIDTH IN PULSED SIGNAL.....	177
III.2.2. SPECTRUM CORRECTION.....	181
III.2.3. RF TRANSIENTS IN PULSED SIGNAL .....	182
<b>III.3. PULSED SIGNAL AUTOMATED TEST SETUP .....</b>	<b>187</b>
III.3.1. RESULTS FOR THE PULSED SIGNAL MEASUREMENT .....	189
III.3.1.1. 1us pulse repetition period .....	189
III.3.1.2. 50us pulse repetition period .....	191
III.3.1.3. Power sweep characterization.....	194
III.3.2. PULSED SIGNAL MEASUREMENT UNDER LOAD-PULL CONDITIONS .....	196
<b>CONCLUSION.....</b>	<b>200</b>
<b>BIBLIOGRAPHY.....</b>	<b>201</b>
<b>GENERAL CONCLUSION &amp; PERSPECTIVES .....</b>	<b>203</b>
<b>PUBLICATIONS RELATIVE TO THIS THESIS.....</b>	<b>209</b>
<b>ABSTRACT.....</b>	<b>211</b>

# List of Figures

---

## Chapter I

---

Figure I. 1: Transmitted and back scattered radar signal. ....	19
Figure I. 2: Transmit and receive time instant during a pulse.....	20
Figure I. 3 : Architecture of radar transmitter. ....	21
Figure I. 4 : Pulse profile.....	27
Figure I. 5: Principle Frequency domain representation of pulse .....	28
Figure I. 6: RF pulsed signal. ....	31
Figure I. 7 : Point to point pulse stability measurement.....	33
Figure I. 8 : Block diagram of frequency translation circuit .....	37
Figure I. 9 : Basic block diagram of ADC .....	37
Figure I. 10 : ADC performance w.r.t. sampling frequency and resolution.....	40
Figure I. 11 : Circuit symbol for a mixer .....	41
Figure I. 12 : RF down-conversion principle .....	42
Figure I. 13 : Power conversion of mixer.....	44
Figure I. 14 : Analogy between a sampler and a mixer.....	46
Figure I. 15 : Circuit symbol for sampler.....	47
Figure I. 16 : Harmonic mixing principle of a sampler.....	47
Figure I. 17: Characteristic of SRD.....	48
Figure I. 18 : Block diagram for sampler circuit.....	49
Figure I. 19 : Block diagram of sampler based frequency translation .....	50
Figure I. 20 : Transient response of sampler. ....	51
Figure I. 21 : Basic charge sampling principle.....	52
Figure I. 22: Block diagram of sub-sampling circuitry .....	54
Figure I. 23 : Illustration of down conversion process.....	57
Figure I. 24: Architecture for incident and reflected signal acquisition.....	59
Figure I. 25 : Basic LSNA architecture.....	61
Figure I. 26 : Adapted Local oscillator setup for modulated signal .....	62
Figure I. 27 : Transient response of the SRD for adapted LO configuration.....	63
Figure I. 28: Harmonics mixing response for adapted LO configuration .....	64
Figure I. 29 : Basic block diagram of VSA.....	65
Figure I. 30: IQ representation .....	66
Figure I. 31: Phase and magnitude transition in different modulating signals.....	67
Figure I. 32 : NVNA architecture for incident and reflected wave acquisition .....	69
Figure I. 33: Basic block diagram of DSO.....	71

## Chapter II

---

Figure II. 1: Basic T/H circuit .....	79
Figure II. 2: Transient response of ideal T/H circuit.....	80

Figure II. 3: Block diagram of basic THA circuit.....	81
Figure II. 4: Basic T/H circuit.....	82
Figure II. 5: Block diagram of simulated THA schematic in ADS.....	84
Figure II. 6: Clock Signal.....	85
Figure II. 7: Operating principle of SW1 (track and hold).....	86
Figure II. 8: Operating principle of SW2 (track and hold).....	87
Figure II. 9: Complete operating principle of THA.....	88
Figure II. 10: Output Voltage THA with and without EFA.....	88
Figure II. 11: Inphi THA (1321TH).....	89
Figure II. 12: Measurement setup for THA characterization.....	90
Figure II. 13: 1dB compression point of THA @ different CLK frequencies.....	92
Figure II. 14: Intermodulation distortion [IMD].....	93
Figure II. 15: Input and output third order intercept points.....	94
Figure II. 16: RF bandwidth of THA.....	95
Figure II. 17: Insertion loss w.r.t. Intermediate Frequency.....	95
Figure II. 18 Measurement setup for differential amplifier.....	96
Figure II. 19: Characterization of differential amplifier (II.9.a) Insertion loss w.r.t. Intermediate Frequency (II.9.b). RF Bandwidth of differential amplifier. (II.9.c). Output power and 1dB compression point.....	97
Figure II. 20: Output power and conversion loss ( $L_c$ ) of the Agilent Sampler.....	98
Figure II. 21: Block diagram of down conversion phenomenon using sampler.....	99
Figure II. 22: Comparison of THA and Sampler based down conversion circuitry.....	100
Figure II. 23: Main characteristics of THA and Sampler based systems.....	100

## Chapter III

Figure III. 1: Polar representation of a sine wave.....	106
Figure III. 2: Time-domain convolution of rectangular and comb dirac function.....	108
Figure III. 3: Constellation diagram when phase =0.....	108
Figure III. 4: Single channel down-conversion setup.....	109
Figure III. 5: Samples acquired by ADC.....	111
Figure III. 6: IQ data for Quadrature sampling.....	112
Figure III. 7: Basic time-domain measurement test-bench.....	113
Figure III. 8: Measurement and ref planes.....	114
Figure III. 9: Open circuit of coaxial type.....	116
Figure III. 10: Short circuit of coaxial type.....	117
Figure III. 11: load circuit of coaxial type.....	117
Figure III. 12: SOL standards at input port.....	120
Figure III. 13: SOL standards at output port.....	121
Figure III. 14: A through connection between port 1 and port 2.....	122
Figure III. 15: K factor amplitude calculation.....	123
Figure III. 16: K factor phase calculation.....	125
Figure III. 17: Block diagram of single channel measurement system.....	126
Figure III. 18: Direct RF measured time-domain pulsed input waveform at saturation.....	128
Figure III. 19: Direct RF measured time-domain pulsed output waveform at saturation.....	129
Figure III. 20: Direct RF corrected time-domain pulsed input waveform at saturation.....	129
Figure III. 21: Direct RF corrected time-domain pulsed output waveform at saturation.....	130

Figure III. 22: Demodulated amplitude within each pulse at input (A) and output (B) of DUT .....	130
Figure III. 23: Demodulated phase within each pulse at input (A) and output (B) of DUT ..	131
Figure III. 24: Block diagram of VSA based measurement system.....	132
Figure III. 25: Amplitude and Phase Demodulation of a pulse using VSA based setup .....	132
Figure III. 26: Comparison of Pout & Gain for AUT @ 2.5GHz .....	133
Figure III. 27: AM/PM characteristics @ 2.5GHz .....	133
Figure III. 28: Block diagram of 4-channel measurement system .....	135
Figure III. 29: Nitronex (NPTB00050B) 50W PA.....	136
Figure III. 30: Measured gain and output power of Nitronex 50W PA .....	137
Figure III. 31: Measured drain and power added efficiency .....	137
Figure III. 32: Measured AM-PM conversion .....	138
Figure III. 33: Measured corrected time-domain pulsed input waveform .....	139
Figure III. 34: Measured corrected time-domain pulsed output waveform .....	139
Figure III. 35: Extracted envelop and phase information at input and output within a pulse	140
Figure III. 36: Power characteristics for three different measurement setups .....	141
Figure III. 37: Am/PM characteristics for three different measurement setups.....	141
Figure III. 38: Measured time-domain two-tone voltage waveforms @ gain compression...	142
Figure III. 39: Demodulated envelope amplitude @ gain compression.....	143
Figure III. 40: Demodulated envelope phase @ gain compression .....	143
Figure III. 41: Dynamic AM/AM @ gain compression.....	144
Figure III. 42: Dynamic AM/PM @ gain compression.....	144
Figure III. 43: Output Current and voltage waveform at compression and the load and source reflection coefficients .....	145
Figure III. 44: Calculated two-tone normalized envelop information .....	146
Figure III. 45: Extracted two-tone phase variation .....	147
Figure III. 46: Generated DPD envelop and phase .....	148
Figure III. 47: Generated I signal with DPD .....	148
Figure III. 48: Generated Q signal with DPD .....	149
Figure III. 49: Extracted pulsed envelop and phase information .....	149

## Chapter IV

---

Figure IV. 1: De-scrambling phenomenon in CTIS.....	159
Figure IV. 2: Example explaining CTIS sampling and de-scrambling procedure.....	161
Figure IV. 3: Block diagram of measurement setup for CW measurement.....	163
Figure IV. 4: Phase error correction using a HPR and Lecroy oscilloscope.....	164
Figure IV. 5: Block diagram of measurement setup for CW measurement.....	166
Figure IV. 6: Measured voltage and current waveforms at the input and output port .....	167
Figure IV. 7: Measured DC characteristics of the PA.....	168
Figure IV. 8: Measured Power characteristics. ....	168
Figure IV. 9: Measured AM/PM characteristics and input impedance.....	169
Figure IV. 10: Corrected input, output voltage and current waveforms. ....	170
Figure IV. 11: Measured Power characteristics for non-linear amplifier. ....	171
Figure IV. 12: Block diagram for time-domain test setup for quasi-square signal generation and measurement.....	172
Figure IV. 13: Quasi-square input and corresponding output voltage and current waveforms. ....	173

Figure IV. 14: Measured Power characteristics of quasi-square signal. ....	174
Figure IV. 15: Quasi-square input, output voltage and current waveforms and the frequency spectrum at input and output .....	175
Figure IV. 16: Block diagram of the time-domain setup for pulsed signal measurement. ....	176
Figure IV. 17: Acquired pulsed signal at the input port and its spectrum.....	178
Figure IV. 18: Block diagram for calibration and digital filtering. ....	179
Figure IV. 19: Block diagram of measurement setup for CW measurement. ....	179
Figure IV. 20: Pulsed profile for different correction bandwidths (a-e represent bandwidth from 2.5GHz-200MHz).....	181
Figure IV. 21: Block diagram of the measurement system in through mode. ....	183
Figure IV. 22: corrected Pulse modulated RF signal with a pulse period of 1 $\mu$ s and 10% duty cycle in through connection. ....	184
Figure IV. 23: Reflections at the beginning and end of the pulse. ....	184
Figure IV. 24: Pulse modulated RF signal with a pulse period of 50 $\mu$ s and 5% duty cycle in through connection. ....	185
Figure IV. 25: Reflections at the beginning and end of the pulse. ....	185
Figure IV. 26: Pulse modulated RF signal with a pulse period of 50 $\mu$ s and 10% duty cycle. ....	186
Figure IV. 27: Reflections at the beginning and end of the pulse. ....	186
Figure IV. 28: Block diagram of the measurement setup for Pulsed signal.....	188
Figure IV. 29: Input and output voltage and current waveforms @ 1 $\mu$ s pulse period. ....	190
Figure IV. 30: Pulse profile @ 1 $\mu$ s pulse period.....	190
Figure IV. 31: Input and output voltage and current waveforms @ 50 $\mu$ s pulse period. ....	192
Figure IV. 32: Input and output voltage and current transients @ 5 $\mu$ s pulse width.....	192
Figure IV. 33: Input and output voltage and current waveforms @ 50 $\mu$ s pulse period. ....	193
Figure IV. 34: Input and output voltage and current transients @ 10 $\mu$ s pulse width. ....	193
Figure IV. 35: Power characteristics in pulsed mode.....	194
Figure IV. 36: Input and load impedance @ $f_0$ .....	195
Figure IV. 37: Pulse detection to calculate average power .....	195
Figure IV. 38: Input and output voltage and current waveforms @ 50 $\mu$ s pulse period and 25+j54 $\Omega$ load.....	196
Figure IV. 39: Input and output voltage and current transients @ 10 $\mu$ s pulse width and 25+j54 $\Omega$ load.....	197
Figure IV. 40: Input and output voltage and current waveforms @ 50 $\mu$ s pulse period and 11+j4.78 $\Omega$ load.....	197
Figure IV. 41: Input and output voltage and current transients @ 10 $\mu$ s pulse width and 11+j4.78 $\Omega$ load.....	198
Figure IV. 42: Input and output voltage and current waveforms @ 50 $\mu$ s pulse period and 68+j127 $\Omega$ load.....	198
Figure IV. 43: Input and output voltage and current transients @ 10 $\mu$ s pulse width and 68+j127 $\Omega$ load.....	199

# List of abbreviations

---

RADAR: RAdio Detection And Ranging.

RF: Radio Frequency

SSPA: Solid State Power Amplifier.

WBG: Wide Band Gap

HEMT: High Electron Mobility Transistor.

GaN: Gallium Nitride.

AlGaN: Aluminium Gallium Nitride.

InP: Indium Phosphide.

GaAs: Gallium Arsenide.

Si: Silicon.

SiC: Silicon Carbide.

ADC: Analog to Digital Converter

PRI: Pulse Repetition Interval

PRF: Pulse Repetition Frequency

PW: Pulse Width

CW: Continuous Wave

$f_c$ : Carrier frequency

LSNA: Large Signal Network Analyzer

VSA: Vector Signal Analyzer

NVNA: Non-linear Vector Network Analyzer

DSO: Digital Storage Oscilloscope

PAE: Power Added Efficiency

TOI: Third Order Intercept Point

IM: Inter-modulation Distortion

SNR: Signal to Noise Ratio



SFDR: Spurious Free Dynamic Range

LO: Local oscillator

IF: Intermediate Frequency

SRD: Step Recovery Diode

DUT: Device Under Test

HPR: Harmonic Phase Reference

THA: Track and Hold Amplifier

T/H: Track and Hold

EFA: Emitter Follower Amplifier

SOLT: Short, Open, Load, Through calibration

# General Introduction

---



The rapid growth in telecommunications in terms of power and bandwidth has led to revolutionary advances in device technologies. Wide band-gap semiconductors have proved quite attractive to process high power modulated communication signal in particular one thinks about RADAR applications. Presently a large effort is being made to exploit the maximum properties of these WBG semiconductor devices, primarily GaN HEMTs. For accurate characterization of such a device it is necessary that the behavior of the device is measured under modulated signal excitation. When operated under these modulated signals the devices are affected by dynamic non-linearity that includes low frequency memory effects such as trapping, thermal and electrical effects. In case of pulsed signals, it is very important to have information about the pulse to pulse behavior of the device or system under test. This means that the complete phase and amplitude spectral characteristics of the input and output pulses are known.

Present state of the art RF measurement instruments utilize samplers or mixers to overcome the frequency limitations imposed by the analog-to-digital convertors (ADC). The RF signal to be measured is down converted to a baseband IF before digitization. Next, different data processing techniques are adopted to extract the amplitude and phase information of the associated spectrum. In doing so, as the signal is translated to a baseband signal (larger time period) the information about RF transients could be lost. In this work, an effort was made to extract the time-domain information of RF transients at both ports of RF devices, circuits or sub-systems. To achieve this, it was necessary to define a new frontend instrument which has less analog component density and is closer to the ADC so that the measured information could be processed digitally. The measurement system should also be working at a very high sampling rate, to reconstruct the measured RF signal and observe the complete RF transient information.

In chapter I the basics of radar communications are discussed. The pulse modulated signal and the complexities involved in the measurement of pulsed signals are described. The basic building blocks of the time-domain measurement setup and its limiting factors are discussed. For the frequency down conversion the two basic instruments based on samplers and mixers are thoroughly evaluated and described in terms of architecture and working principle (sub-sampling or harmonic mixing). In the end, the existing time-domain measurement instruments are analyzed and the different frequency down conversion and phase referencing techniques used in these instruments are explained.

Chapter II focuses on the heart of this work where a new instrument based on a Track and Hold Amplifier (THA) is proposed to replace the conventional sampler or mixer used for the down conversion of signals. The complete working principle of THA is explained and a commercially available 13 GHz 2 Gsamples/s THA was fully characterized in terms of power handling and linearity. The advantages and disadvantages offered by THA over other instruments are presented.

Chapter III describes the measurement and data processing technique adopted to extract the envelope and phase information of the RF signal. To evaluate the performance of THA in time-domain measurement, a single channel test set up was built. The input and output envelope waveforms of the DUT were sequentially acquired. The complete processes needed to remove the linear systematic errors as well as absolute calibration are discussed. A fully calibrated 4-channel time-domain envelope measurement setup is built and is used to characterize a nonlinear GaN power amplifier in terms of power and linearity using a continuous wave (sinusoidal) and pulse modulated signals. In this chapter it's also shown that the proposed envelope measurement setup works similar to a commercially available VSA but is capable of 4-channel.

In chapter IV ways to enhance the sampling frequency of the proposed 4-channel time-domain measurement system are discussed and presented using the properties offered by the THA. It also explains the procedure to convert the proposed 4-channel VSA into a 4-channel oscilloscope. The sampling frequency of  $100f_C$  for CW signal and  $10f_C$  for pulsed modulated signal was achieved. Complete characterization of non-linear 50 W PA operated under CW and pulse modulated excitation signals is presented. The measured RF transient response for pulse modulated signal is presented for the first time using the proposed setup. The effect of the instrumentation on the pulse profile is also analyzed along with capabilities of the test bench in a load pull environment. In the end, a conclusion is drawn and future perspectives to improve the test-bench are presented.

## **CHAPTER I:**

# **The Time-Domain Measurement System and its Importance**

---



## Introduction

The need for broadband applications and high power in wireless communications has encouraged new advances in the field of solid-state devices. One of the significant advancements is the use of wide band-gap (WBG) semiconductors. This large band-gap, high electron mobility, and high-breakdown voltage make them good candidates for use in the design of high-power microwave amplifiers, particularly for radar applications. Simultaneously, these high-power devices have induced many undesirable effects that hamper on the performance of high-power amplifiers (PAs) such as trapping, electrical, and thermal effects. These are often termed as memory effects. To extract the inherent properties of WBG devices and minimize the low-frequency memory effects occurring in non-linear high-power devices, it is necessary to characterize them in the time-domain with modulated signals. In the past, time-domain measurements of multi-sines for radio communications and pulsed-modulated signals for radar applications have been performed [8], [53]. Each system has its own advantages and disadvantages and physical limitations.

In this chapter the basic theoretical operating principles of radars and its applications are discussed. The complexities of pulse modulated signal measurements are thoroughly evaluated and discussed. It also describes the basic architectures of time domain measurements systems and the physical limitations involved in the measurement process. The frequency down-conversion principle and the operation of the instruments that realize it are explained. A complete characterization and working principle of sampler based setups is discussed. Types of mixers presently existing and their characteristic are thoroughly evaluated. Theoretical and technological limitations of analog to digital convertors are presented. In the end working the principles of existing time domain measurements systems like Large Signal Network Analyzer (LSNA), the Vector Signal Analyzer (VSA), the Non-linear the Vector Network Analyzer (NVNA) and the Digital Storage Oscilloscope (DSO) are explained.



# I. RADAR COMMUNICATION

## I.1. Operating Principles of a RADAR System

### I.1.1. Transmitted and received signals [1], [2]

Radar is an electronic and electromagnetic system that uses radio waves to detect and locate objects. Radar operates by transmitting a specifically designed radio frequency waveform and then waits for a short period of time to receive the reflected signal also called an echo, before a new transmitted signal is sent out. As the name implies, the **RA**dio **D**etection **A**nd **R**anging (RADAR), it is used to detect the remotely situated target of interest and to determine its location. The radar signal which is generated by a very powerful transmitter hits the target with a microwave signal, which is then reflected and the attenuated signal is received by a highly sensitive receiver. The transmitted signal is scattered after reflection but the signal reflected in exactly the opposite direction (also called back scattering) is captured by the radar. Radio waves propagate in free space therefore possess properties, which include speed, frequency, and power and display many phenomena such as refraction, attenuation, absorption, scattering and reflection. The speed and radiation properties of radio waves are fundamental to the theory of radar operation. TEM Electromagnetic waves are composed of both an electric and a magnetic field, both of which oscillate perpendicular to each other and the direction of propagation [1]. These transverse waves can be identified by certain characteristics, such as wavelength and frequency.

The frequency and wavelength of electromagnetic waves are affected by relative motion known as the Doppler Effect [3], [4]. Only the radial (approaching or receding) component of motion produces this phenomenon. If the source of an electromagnetic wave is approaching the observer, the frequency increases and the wavelength decrease. If the source is receding, the frequency decreases and the wavelength increase. The motion of an object causes a wavelength shift  $\Delta\lambda$  that depends on the speed and the direction of the object movement. The size of the frequency shift is given by:

$$\Delta\lambda = \frac{\lambda_{stationary} v_{radial}}{c} \quad \text{Eq:-1}$$

Where

$\lambda_{stationary}$  = wavelength when the source is at rest

$v_{radial}$  = speed of the source moving along the line of sight (m/s).

$c$  = speed of light (m/s) in vacuum.

Radars use the Doppler Effect to determine a target's velocity. Many radars use the Doppler information only to determine the direction of the target motion, whereas others determine the speed of motion. Radars transmit radio waves that contains a set of wavelengths (or frequencies), which then reflect off the target as shown in Fig. I.1. In this case the target acts as a secondary source. Its speed can be determined from the difference in the wavelength (or frequency) of the transmitted beam and reflected beam.

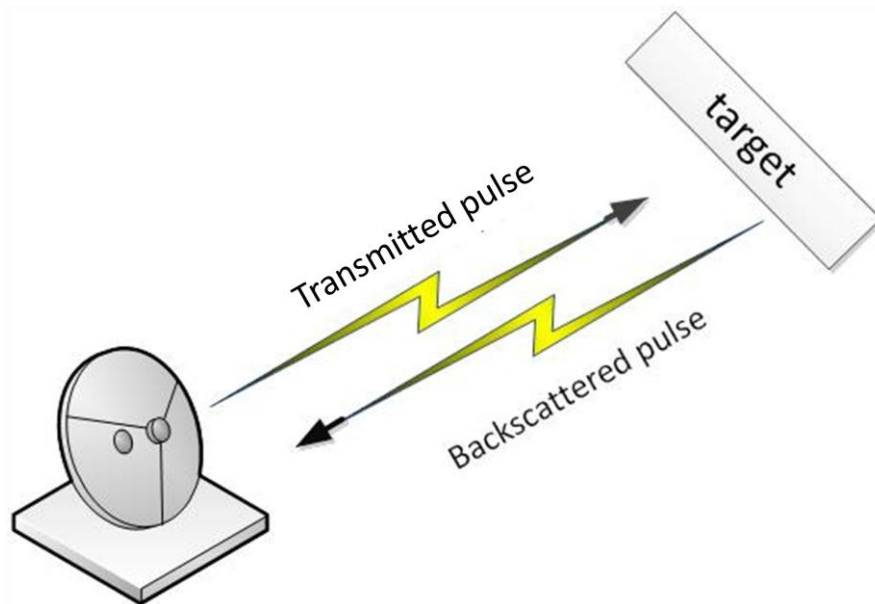


Figure I. 1: Transmitted and back scattered radar signal.

The radar signals are time dependent and synchronization between the transmitted and the received signal is required. The transmitted signal consists of a series of pulsed modulated signals [4], [5]. It transmits during a pulse width  $\tau$  and then it waits for the reflected signal (echo) for a period of time equal to  $T - \tau$  before radiating the next pulse as explained in Fig. I.2.

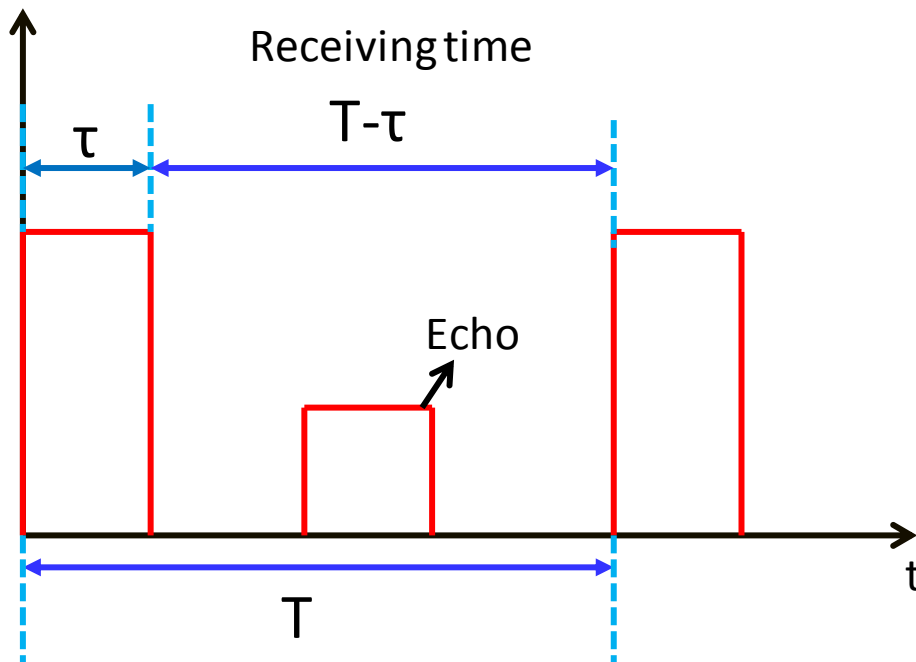


Figure I. 2: Transmit and receive time instant during a pulse.

The time interval between the beginning of the first pulse and the beginning of the second pulse is called pulse repetition interval  $T$  and is reciprocal is the pulse repetition frequency, which is a count of the number of pulses per second as shown in Eq.2. The higher the PRF larger is the average power transmitted by the radar.

$$T = \frac{1}{\text{PRF}} \quad \text{Eq:-2}$$

The pulse width plays an important role in the detection of the target which means that if the pulse width increases, the transmitted signal energy also increases. If the pulse period is kept constant then the time to receive the back scattered signal decreases. For a non modulated pulse signal the power reflected from the target to the antenna could be calculated using the following relation Eq.3 [5], [6]:

$$P_R = \frac{P_T G_T^2 \lambda^2 \sigma}{(4\pi)^3 R^4 L} \quad \text{Eq:-3}$$

Where  $P_T$ =transmitted power [W]

$\lambda$ = Wavelength

$A_T$ = receiver antenna aperture [ $\text{m}^2$ ]

- $\sigma$  = target radar cross-section [ $m^2$ ]
- R =range between radar and target [m]
- L= aggregate of system losses

The sensitivity increases with the increase in pulse width and PRF. The received signal power is much lower than the transmitted signal power so the **dynamic range** of the receiver plays an important role. The dynamic range is depends upon the properties of antenna, the pulse width of the signal and the total losses occurred in the transmitter path as explained in Fig.I.3. The following Eq.4 gives the signal to noise ratio (SNR) for a single pulse:

$$SNR = \frac{P_T G_T^2 \lambda^2 \sigma}{(4\pi)^3 R^4 K T_s B L} \quad \text{Eq:-4}$$

- Where  $P_T$  =transmitted power [W]
- $G_T$  = antenna transmitted gain
- $A_T$  = receiver antenna aperture [ $m^2$ ]
- B = receiver bandwidth
- $\sigma$  = target radar cross-section [ $m^2$ ]
- R =range between radar and target [m]
- K= Boltzmann’s constant
- $T_s$  = system noise temperature
- L= aggregate of system losses

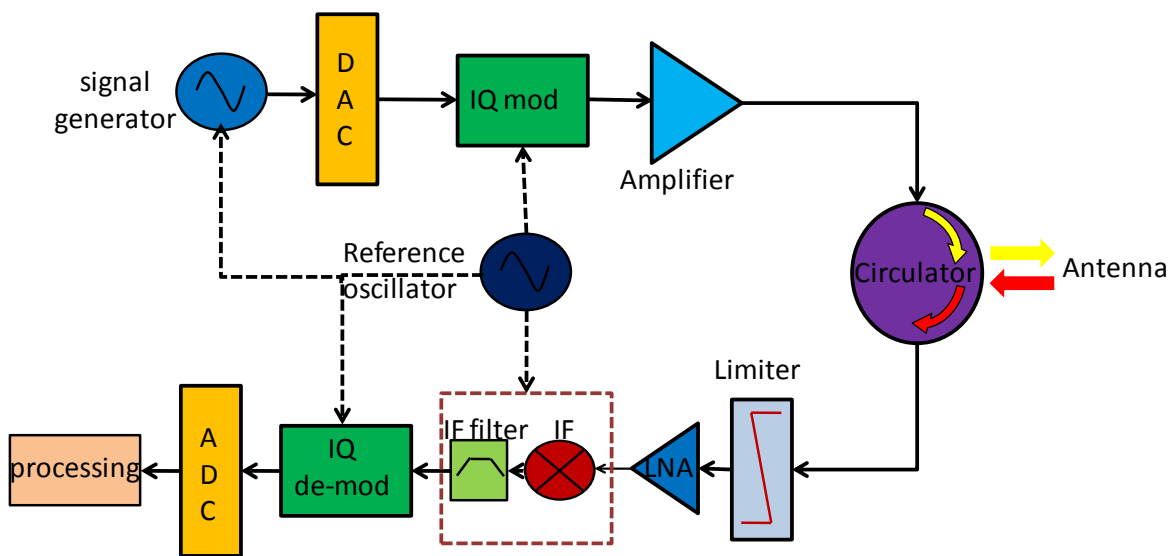


Figure I. 3 : Architecture of radar transmitter.

### I.1.2. Frequency Based Radar application [5], [6]

The operating frequency plays an important role in the performance of the radars as it affects the radar beam propagation. At the low frequency extremes, radar beams will refract in the atmosphere and can be caught in "atmospheric ducts" resulting in long ranges while at the higher frequencies, the radar beam will behave much like visible light and travel in very straight lines. Very high frequency radar beams suffer high losses and are not suitable for long range systems.

The frequency also affects the beam-width. For the same antenna size, low frequency radar will have a larger beam-width than high frequency ones. In order to keep the beam-width constant, low frequency radar will need a large antenna. The table I.1 describes the frequency dependent applications [7].

Band	Freq (GHz)	Application
mm	40 - 100	short range targetting radars
Ka	26.5 - 40	airport surface detection equipment
K	18 - 26.5	airport surface detection equipment
Ku	12.5 – 18	maritime, civil & military navigation
X	8 - 12.5	maritime, civil & military navigation
C	4.0 - 8.0	military surveillance
S	2.0 - 4.0	special airport surveillance radars
L	1.0 - 2.0	air route surveillance radars
UHF	0.3 - 1.0	communication, broadcasting & air defence system

Table I.1: Frequency dependent application of Radar systems

In radar communications the radar transmitter and receiver play an important role. The radar transmitter subsystem generates the radiofrequency (RF) energy required for the illumination of a remotely situated target of interest. The transmitter stage consists of a power amplifier, an analog or digital modulator and a very high power, power supply that provides the high voltages and currents that are typically required in modern radar transmitters. The peak powers generated by the radar transmitter can range from milliwatts to gigawatts depending on the application. The average radiated power of a radar system and the effective antenna aperture, establish the maximum operating range of radars. The maximum radar

range can be increased by increasing either the antenna size or the average output power of the radar transmitter.

### I.1.3. Role of power amplifier in radar communications [8]

The performance of the radar system is directly related to performance of the power amplifiers which in turn is determined by its technological features and the applied operating mode. The RF power amplifier section of the transmission chain of the radar system consists of several stages. To achieve the desired transmission power, multiple power amplifiers are placed in parallel and their output power is combined. Historically travelling wave tube devices were utilized to generate high output microwave power, which are inherently less efficient, quite large in size and have reliability issues. Recently, solid state amplifiers (SSPA Solid State Power Amplifier) have taken over the power amplification process. They show distinct advantages in terms of transition frequency and size. Solid state power amplifiers also offer wide range of other advantages over travelling wave tubes which include higher bandwidth, greater efficiency, instantaneous start-up (as no warm up period is required) more reliable operation and less expensive power supplies and improved mean time between (MTBF) failure. They also offer the opportunity to work with longer pulse widths while maintaining the desired power levels.

## **II. Emergence of Wide Band Gap Semiconductors**

### **II.1. Pros and cons of semiconductors**

#### II.1.1. Advantages and properties of semiconductors [9], [10]

Since the onset of radio there has been a constant research on innovative uses of RF technology. RF signals are just the electromagnetic waves capable of carrying energy across empty spaces. To investigate methods of transmitting and receiving signals and to avoid interference, improving detection and capacity these RF signals were used in modulated way i.e. under varying conditions for the amplitude, the phase and the time. The widespread successes of cellular systems, wireless data networks and military communications have made modulation schemes utterly complex.

A major contributor in the performance of a wireless communication system is the power amplifier. It contributes a major share in the cost of a wireless system. The performance of a power amplifier is characterized by its efficiency, output power, bandwidth, linearity and its thermal characteristics. One of the primary components for a power amplifier to meet the ever increasing demands of the world of telecommunications is the power transistor. An improved device technology allows meeting the challenges faced by the designers to achieve better results.

Among power transistor design semiconductors play a vital role. The emergence of Wide Band Gap semiconductor devices have made them a strong contender in the application of the microwave frequency systems due to their high electric breakdown field strength, which enables high power density, high electron saturation velocity and high operating temperature[10], [11]. These attractive features offer tremendous advantages in the design of high power amplifiers. The high output power density reduces the device size which leads to low impedance devices making input and output matching easier and lower loss. The high break down voltage assists to operate at higher voltages which reduce the need for voltage conversion and achieving high efficiencies. High band gap devices inherently have high linearity so less power back off is required from the transistor power rating to achieve adequate linearity. This allows the transistors to operate at higher set points on efficiency versus power curve. Table I.2 now compares some of the intrinsic properties of some materials used in the RF semiconductor industry [12], [13], [14], and [15]:

Materials	Bandgap [eV]	Electron mobility [Cm <sup>2</sup> /Vs]	Saturated peak electron velocity [1*10 <sup>7</sup> cm/s]	Critical breakdown field [1*10 <sup>6</sup> V/cm]	Thermal conductivity [W/cm-K]	Relative dielectric constant [ε <sub>r</sub> ]
Si	1.1	1500	1.0	0.3	1.5	11.8
GaAs	1.42	8500	1.0	0.4	0.5	12.8
SiC	3.26	700	2	2	4.5	10
GaN	3.49	900	1.5	3.3	1.7	9
AlGaN/GaN	3.49	>2000	2.7	3.3	1.7	9
Diamond	5.6	2200	2.7	5	20-30	5.5

Table I.2: Intrinsic properties of semi-conductors

A large energy gap results in low intrinsic concentration of charges and a high resistance to ionization from radiation. The wide band-gap semiconductors also have a relatively low dielectric constant, which allows obtaining reduced capacitance loading. High

thermal conductivity is extremely important since many of the electronic devices of interest are intended for high power applications and the performance of these devices depends upon the ability to extract the heat due to the dissipated power. The thermal conductivity of GaN is essentially equal to that of Si while the thermal conductivity of SiC is factor of three higher. This is one of the reasons that SiC is an attractive substrate for GaN devices, as well as for SiC epitaxial growth. The wide band-gap of SiC and GaN results in a high critical electric field for breakdown, which is on the order of 1-5 MV/cm. This is almost an order of magnitude larger than for Si and GaAs. The high breakdown voltage permits high drain bias voltages to be applied to the devices, which is necessary to obtain high RF output power in a normal load.

### II.1.2. Undesired effects of semi-conductors [16], [17], [18]

These high power devices have also induced some undesired effects on power amplifiers called memory effects. Memory effects are defined as a distortion of the phase and amplitude response of the device over the modulation bandwidth. These memory effects can arise from multiple sources, which include bias circuit effects, self heating and trapping effects. Memory effects can be divided into two major categories based on their causes: the electrical and the thermal memory effects.

The frequency dependence of the bias and matching networks result in the load and source impedance change over the modulation bandwidth. These electrical effects cause the dominant portion of the memory effects. Thermal memory effects on the other hand are caused by electro-thermal couplings. The high power that is dissipated in the active components increases temperature of the bulk material and this affects the mobility of carriers in the channel and reduces the diffusion coefficient thus decreasing the flow of current. Thermal memory effects can also occur due to self heating (high biasing of the transistor) and external power injection into the device.

Memory effects in the power transistors are one of the most critical points for designers of power amplifiers. In the particular case of RADAR or other wideband modulation schemes, the excitation of system consists of repetitive pulse trains [52]. A pulse train contains a number of successive pulses with a uniform or a variable pulse width. The pulse period within the pulse train normally remains constant. When the first pulse of a pulse train arrives, the power amplifier is operating at a steady-state temperature and after each pulse it cools down until the next pulse arrives. Note that the temperature of the device for the



second pulse would not be the same as it was for the first pulse. The device heats up during the first pulse and cools down only partially. As a result, the temperature for the second pulse is higher. This phenomenon builds up from pulse to pulse and the slow memory effects associated with the thermal behavior shift the characteristics of the transistor from one pulse to another.

## II.2. RF Pulsed Signals and complexities

### II.2.1. RF pulsed signals [19]

Most of the communication signals are continuous which means that the amplitude (AM), phase (PM) or frequency (FM) of the RF signal might change with time but the RF signal is always present up to some extent. For high power non-linear devices the self heating and memory effects discussed previously severely affect the performance figure when excited in the continuous wave mode. During on wafer measurements of power amplifiers devices, heat sinks are difficult or even impossible to implement and this limits the range of measurement power levels. Using pulsed stimulus signals, the device can be characterized at the higher peak power levels up to saturation to which the devices will be subjected in their intended use. If the devices are excited in pulsed mode, they can be operated at higher peak power level at a reduced risk of device breakdown and a better control of operating temperature. A pulsed RF signal consists of a burst (pulses) of RF signal where no RF signal present in between the bursts. The most general case of a pulsed RF signal consists of train of pulses with a fixed pulse width (PW) (Fig.I.4) which are spaced by a fixed time interval, or a repetition period, (T). Commonly the amplitude of the RF pulses in a pulse train is kept constant. Pulses that are spaced at a fixed time interval arrive at a repetition rate that is referred to as the pulse repetition interval (PRI).

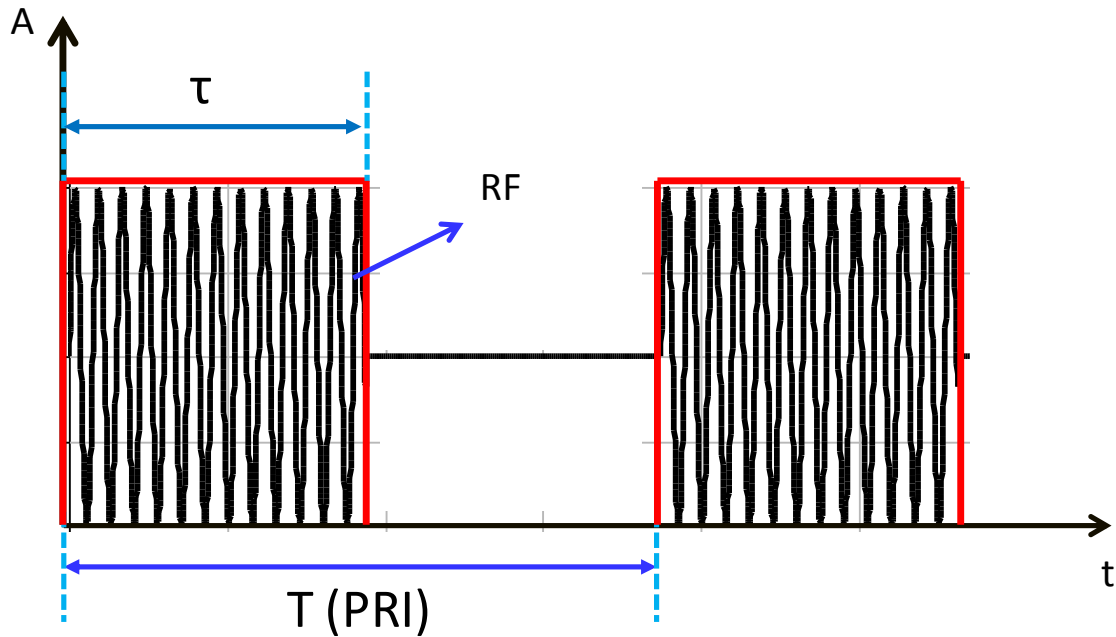


Figure I. 4 : Pulse profile

Pulse width  $\tau$  is the time duration for which the device is active. It is an important quantity because it relates to peak and the average power in the determination of total energy output. This affects the power of the reflected signal, the required power supply capacity and the cooling requirements of the transmitter. Power measurements are classified as either peak pulse power ( $P_P$ ) or average power ( $P_{AVG}$ ) [4], [19]. The actual power transfer in a pulsed RF signal occurs during the pulses, but most power measurement methods measure the effects of the RF energy over entire period to obtain an average value of the power. Frequently it is necessary to convert from peak power ( $P_P$ ) to average power ( $P_{AVG}$ ) using the following relation Eq.5 and Eq.6.

$$Duty\ cycle\ (\%) = \frac{\tau}{T} * 100 \quad \text{Eq:-5}$$

$$P_{AVG}(W) = P_P(W) * \left(\frac{\tau}{T}\right) \quad \text{Eq:-6}$$

Where  $\tau = pulse\ width$

$T = pulse\ repetition\ interval\ (PRI)$

The ratio of the average power to the peak pulse power is the duty cycle and represents the percentage of time the power is present. In pulsed applications the power measurement and peak power calculations are performed by assuming the rise time ( $\tau_R$ ) and the fall time ( $\tau_F$ ) of the pulses are equal to zero and that the effect of transients is negligible. The pulse is then called a block pulse.

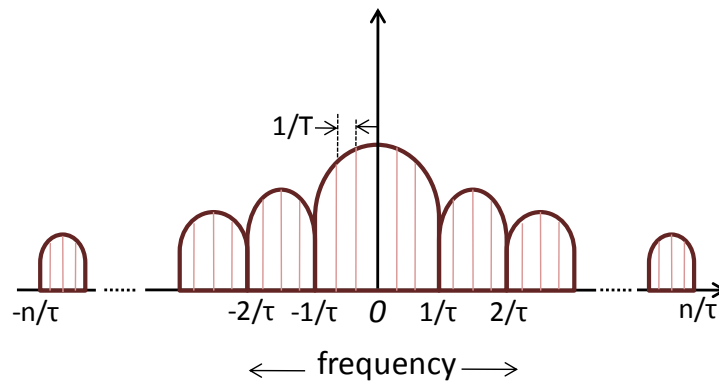


Figure I. 5: Principle Frequency domain representation of pulse

It is very important that the spectrum of the block pulse ( $\tau_R = \tau_F = 0$ ) is investigated as it produces multiple harmonics and interferes with the frequencies outside the allocated band as the bandwidth of RF pulsed spectrum is infinite. The Fig.I.5 describes the frequency domain representation of the pulse which is a sinc function and could mathematically be defined as:

$$\text{Sinc } x = \begin{cases} \frac{\sin \pi x}{\pi x} & \text{for } x \neq 0 \\ 1 & \text{for } x = 0 \end{cases} \quad \text{Eq:-7}$$

Note that the spectrum of the pulsed signal is spread over infinite number of lobes and that the bandwidth of the lobes in the spread spectrum depends on the pulse width ( $BW=1/\tau$ ). The spacing between the lines of the spectrum depends upon the pulse repetition interval (T) and is  $1/T$ . If  $\tau$  remains constant while T increases, the number of side-lobes remains the same, but the density of the spectral lines increases and vice versa. If the repetition rate T remains constant, while  $\tau$  increases, then the lobe width decreases and vice versa. If the  $\tau$  approaches T, the spectrum will approach the "one lobe", case i.e., a single spectral line. The periodicity of the lobes remains constant with constant  $\tau$ .

Until now, we have discussed pulsed signals without their relation to the carrier frequency. This relation could be expressed as simple multiplication in the time domain and convolution in the frequency-domain of the rectangular periodic pulse envelope signal of width  $\tau$ , pulse repetition interval  $T$  and a carrier frequency  $f_0$ . The mathematical computation of the RF pulsed signal spectrum is shown below:

Let the carrier be:

$$s(t) = \cos(2\pi f_c t) \quad \text{Eq:-8}$$

And the envelope be:

$$p(t) = \sum_{n=-\infty}^{\infty} \text{rect}\left(\frac{t - nT}{\tau}\right) \quad \text{Eq:-9}$$

Where  $\tau$  = width of rectangle

$T$  = repetition period

$$\text{rect}(x) = \begin{cases} 1 & |x| \leq 1 \\ 0 & |x| > 1 \end{cases}$$

Using Euler's identity

$$s(t) = \frac{e^{j2\pi f_c t} + e^{-j2\pi f_c t}}{2} \quad \text{Eq:-10}$$

In time domain we multiply the two signals to get

$$u(t) = s(t) \times p(t) \quad \text{Eq:-11}$$

$$u(t) = \cos(2\pi f_c t) \times \sum_{n=-\infty}^{\infty} \text{rect}\left(\frac{t - nT}{\tau}\right) \quad \text{Eq:-12}$$

While in frequency domain we convolve the spectra

$$u(f) = s(f) * p(f) \quad \text{Eq:-13}$$

Where

$$s(f) = \frac{1}{2}\delta(f - f_c) + \frac{1}{2}\delta(f + f_c) \quad \text{Eq:-14}$$

$$p(f) = \sum_{k=-\infty}^{\infty} \text{sinc}(f\tau) e^{-j2\pi f n T} \quad \text{Eq:-15}$$

Where  $e^{-j2\pi f n T}$  = time delay of pulsed train

$$u(f) = \left[ \frac{1}{2}\delta(f - f_c) + \frac{1}{2}\delta(f + f_c) \right] * \left[ \sum_{k=-\infty}^{\infty} \text{sinc}(f\tau) e^{-j2\pi f n T} \right] \quad \text{Eq:-16}$$

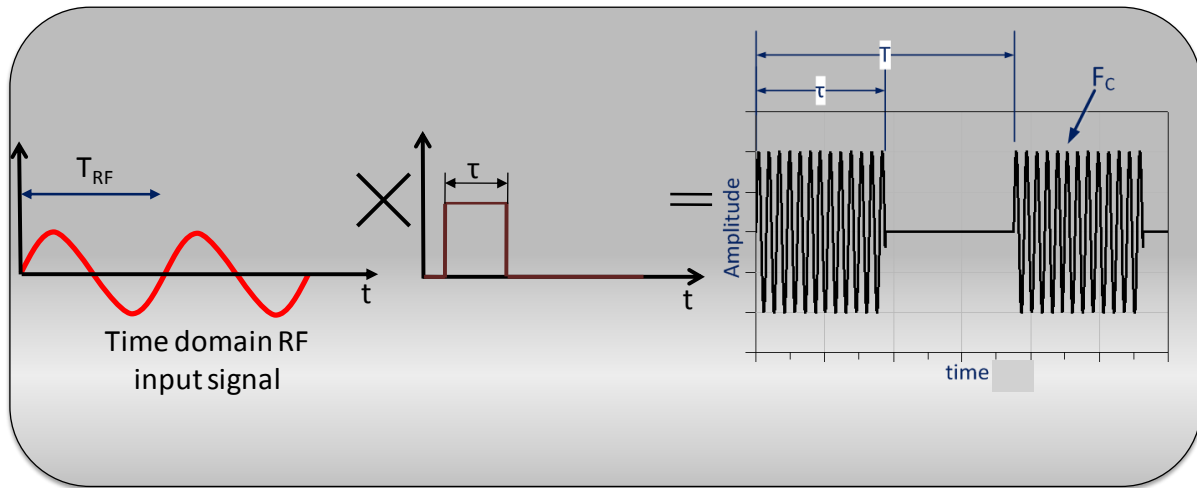
$$u(f) = \frac{1}{2} \sum_{k=-\infty}^{\infty} \left[ \delta(f - f_c) * \text{sinc}(f\tau) e^{-j2\pi f n T} + \delta(f + f_c) * \text{sinc}(f\tau) e^{-j2\pi f n T} \right] \quad \text{Eq:-17}$$

$$u(f) = \left[ \begin{array}{c} \frac{1}{2} \text{sinc}((f - f_c)\tau) \sum e^{-j2\pi(f-f_c)nT} + \\ \frac{1}{2} \text{sinc}((f + f_c)\tau) \sum e^{-j2\pi(f+f_c)nT} \end{array} \right] \quad \text{Eq:-18}$$

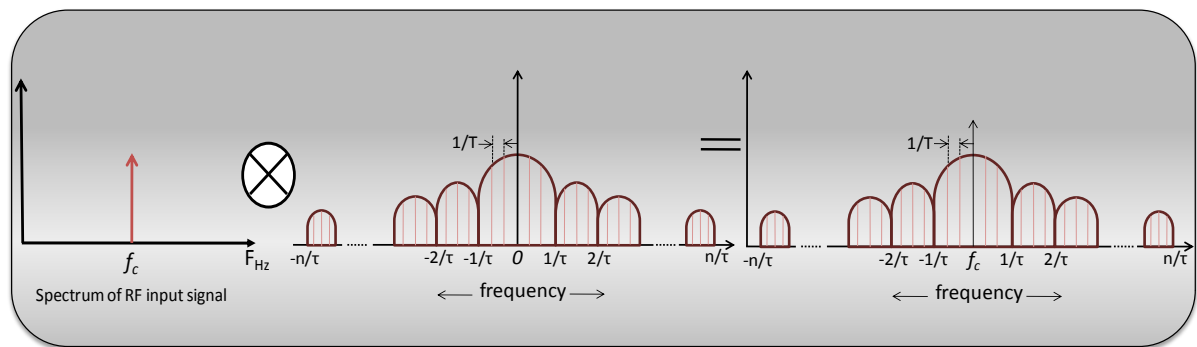
Using Poissons formula:

$$\sum_{-\infty}^{\infty} e^{-j2\pi f n T} = \frac{1}{T} \sum_{-\infty}^{\infty} \delta\left(f - \frac{n}{T}\right) \quad \text{Eq:-19}$$

$$u(f) = \left[ \begin{array}{c} \frac{1}{2} \text{sinc}((f - f_c)\tau) \frac{1}{T} \sum_{n=-\infty}^{\infty} \delta\left(f - f_c - \frac{n}{T}\right) + \\ \frac{1}{2} \text{sinc}((f + f_c)\tau) \frac{1}{T} \sum_{n=-\infty}^{\infty} \delta\left(f + f_c - \frac{n}{T}\right) \end{array} \right] \quad \text{Eq:-20}$$



(a) Multiplication in Time-domain



(b) Convolution in frequency domain

Figure I. 6: RF pulsed signal.

As in the case of Continuous Wave (CW) signals the sidebands are produced above and below the carrier frequency which is true for pulsed signal as well. Remember that periodic RF pulsed signal consists of multiple harmonics. Fig.I.6 represents the spectral plot of the pulsed RF signal where each spectral line represents the modulation product of the carrier frequency  $f_c$  and the modulating pulse repetition frequency with its harmonics. The each frequency spectral line can be represented as follows:

$$F_{SL} = f_c + \frac{n}{PRI} \quad \text{Eq:-21}$$

Where  $n= 1, 2, \dots, N$

$F_{SL}$  = frequency spectral line

$f_c$  = carrier frequency

PRI= pulse repetition interval = T

The main lobe of the system contains the carrier frequency located at the centre of the lobe. The amplitudes of the spectral lines of the lobe vary as a function of frequency using the following relation:  $\sin(f\tau/2)/f\tau/2$ . The frequency of the spectral lines within the lobes is affected by the pulsed repetition interval of the pulse signal. The width of lobes in the spectral display of pulsed waveforms remains constant as long as there is no change in the pulse width. The bandwidth of the main lobe is  $2/\tau$  Hz. The bandwidth of the side lobe is also related to the modulating pulse width by relation  $1/\tau$  Hz. The theoretical spectrum of the pulsed signal has an infinite bandwidth which means that it contains an infinite number of side lobes.

### *II.2.1.1. RF measurement complexity*

As described earlier the pulsed signal produces multiple harmonics and the occupied bandwidth of a pulsed signal is infinite. Fortunately when frequency increases the associated reduction in amplitude of the side lobes is sufficient to keep the power of the signal finite. This phenomenon is known as reciprocal spreading in Fourier analysis [20], [21]. As a consequence the receivers with fixed band-width detection measure a reduced signal level when the pulse width is decreased. This phenomenon is known as pulse desensitization and the dynamic range losses associated with this phenomenon is represented by the following relation:

$$\text{Dynamic range loss} = 20 \log \left( \frac{\tau}{T} \right) \quad \text{Eq:-22}$$

$$\text{Where } \left( \frac{\tau}{T} * 100 \right) = \text{duty cycle [\%]}$$

This relation leads us to the fact that the SNR of the measurement system decreases with the decreasing pulse width and is called desensitization due to CW receiver.

### *II.2.1.2. Pulse to pulse stability [22], [23].*

A practical pulsed characterization is often difficult due to the presence of an inconsistent pulse width and pulse repetition frequency. Therefore, practical applicability requires that the pulse to pulse stability is calculated. Pulse to pulse stability is obtained as the amplitude and phase variation of the spectrum between successive pulses presenting a burst microwave signal. The radars ability to sum the signals of each receiver and integrate the

power of multiple target returns is highly sensitive to these phase and amplitude fluctuations. Pulse to pulse stability can be related to intrinsic or extrinsic causes in the transmitter module.

Extrinsic causes

- The instabilities caused during signal generation (local oscillator noise, mixer noise, multiplier or filter phase noise)
- Electronic perturbations (parasitic coupling between transmitter modules)

Intrinsic cause

- Thermal variation within the device is the premier cause for phase and amplitude instability within the burst of wide pulses and larger duty cycles.
- Irregularities in biasing circuitry when the system is excited by a pulsed signal.

Pulse to pulse stability is calculated using the demodulated base-band signals around the carrier frequency only to avoid taking into account the distortion of the envelope due to harmonic distortion. When a burst of RF pulse signal is generated n number of points within the first pulse are selected. To calculate pulse to pulse stability same number of points (n) at same time instants of each successive pulse within the same burst are also selected.

For example if a burst contains three pulses then n number of points (as shown in Fig.I.7) are selected at same time instants on the three pulses and the phase ( $\theta$ ) and amplitude (A) of these points is extracted (envelope or instantaneous). In these calculations n (no. of points within a pulse) remains constant while i changes for each pulse which means that stability is calculated for same time instant in pulses within the burst.

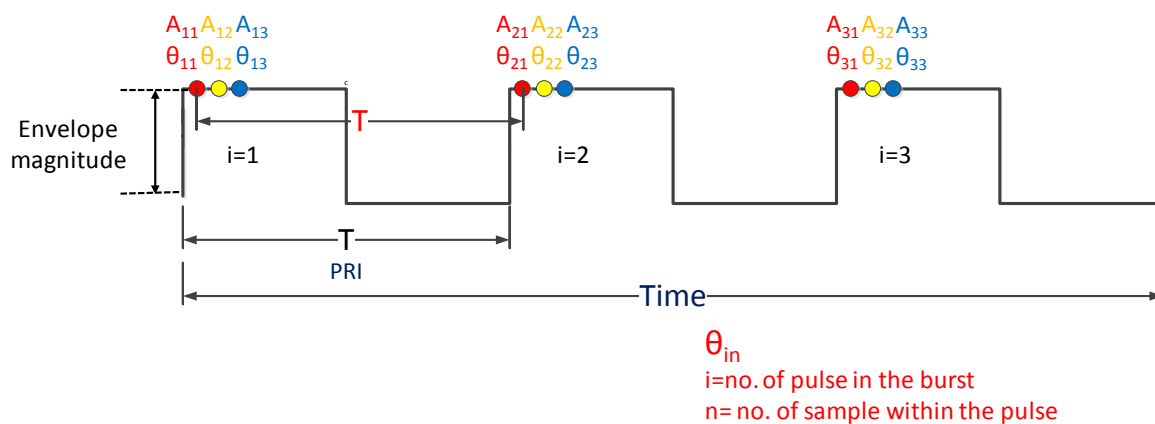


Figure I. 7 : Point to point pulse stability measurement.



Two temporal methods are normally used to calculate pulse to pulse stability described as followed [22], [23]:

- 1) Standard deviation method
- 2) RMS method

These methods are sketched below:

#### II.2.1.2.1. Standard deviation method

Phase stability in dB for burst of N pulses is calculated using the following relations where

n= number of sample inside the pulse

i= number of pulse in the burst

$$S_n(\phi) = -10 * \log \frac{1}{N} \sum_{i=1}^N (\phi_{in} - \phi_{avg(n)})^2 \quad \text{Eq:-23}$$

$$\phi_{avg(n)} = \frac{1}{N} \sum_{i=1}^N (\phi_{in}) \quad \text{Eq:-24}$$

Amplitude stability in dB for burst of N pulses is calculated by :

$$S_n(A) = -10 * \log \frac{\frac{1}{N} \sum_{i=1}^N (A_{in} - A_{avg(n)})^2}{(A_{avg(n)})^2} \quad \text{Eq:-25}$$

$$A_{avg(n)} = \frac{1}{N} \sum_{i=1}^N (A_{in}) \quad \text{Eq:-26}$$

Total stability is calculated by

$$S_n(\text{dB}) = -10 * \log(10^{-S_n(A)/10} + 10^{-S_n(\phi)/10}) \quad \text{Eq:-27}$$

#### II.2.1.2.2. RMS method

Phase stability in dB for N burst of pulses

$$S_n(\phi) = -10 * \log \frac{1}{N-1} \sum_{i=1}^{N-1} (\phi_{in+1} - \phi_{in})^2 \quad \text{Eq:-28}$$

Amplitude stability in dB for N burst of pulses

$$S_n(A) = -10 * \log \frac{\frac{1}{N-1} \sum_{i=1}^{N-1} (A_{in+1} - A_{in})^2}{(A_{\text{avg}(n)})^2} \quad \text{Eq:-29}$$

$$A_{\text{avg}(n)} = \frac{1}{N} \sum_{n=1}^N (A_{in}) \quad \text{Eq:-30}$$

To accurately represent the pulse to pulse stability results it is necessary to clearly indicate the measurement method adopted and the pulse profile of the signal which includes the number of pulses, pulse width and duty cycle (fixed or varied) information. Historically, pulse to pulse stability was measured with a system called PN9002 from Aeroflex. This system was based on the demodulation of the pulsed RF signal with an AM/PM detector and a logic analyzer HP16500 C. This system is no longer commercially available and there is a need for a time domain measurement system to analyze both envelope and carrier distortion. Many time domain measurement systems have been developed in the past 15 years based on different techniques. Some of these are discussed in the coming sections.

### III. Time-Domain Measurement Systems

#### III.1. Importance of time-domain measurement

Historically most measurements intended for non-linear device characterization have been performed in the frequency domain. This gives accurate spectral information regarding the carrier, the harmonics, the modulation and the potential presence of spurious signals. Spectrum analyzers are the most commonly used instruments for frequency domain analysis. These instruments possess a good dynamic range but don't give any information regarding the phase of the RF spectrum [24]. To compare the obtained measurement results with the much improved simulations tools used for designing of high-power microwave amplifiers force us to accurately characterize the (high power) non-linear device at saturation and under wide

range of excited signals and operating conditions. While a spectrum analysis only unveils the power spectrum and does not fully characterizes the non-linear behavior.

An accurate characterization means that an intuitive relationship between input and output signals is established and the phase and amplitude of the complex spectrum are perfectly known. Accurate and complete measurements should capture the real behavior one encounters in the actual system. Many of today's RF signals are modulated and therefore they change the behaviour from one instant to another. They may hop frequencies or have a complex modulation that can dynamically change. All these modulation activities induce disturbance like random transients, interference, inter-modulation etc but one thing common among this entire phenomenon is time dependency. If the measurement is made in a time-domain all the information could be retrieved.

This necessity generates the need to have a time-domain test bench that is capable of handling high power levels up to several 10s of Watts and possess a high bandwidth. Many commercial time domain measurement setups exist, exhibiting tremendous capabilities [34], [41], [42]. However there is still room left for the instruments that increase the bandwidth and the dynamic range.

### III.1.1. Basic time-domain measurement setup architecture

Fig.I.8 describes the basic time-domain measurement setup (each step is explained in detail in later sections).The primary step for a time-domain analysis is the conversion of the RF frequency signal to a lower frequency due to the technological constraints of individual blocks used in the architecture. Traditionally samplers and mixers have been used for this purpose. They down-convert the RF frequency signal depending on the RF clock signal. A continuous wave signal clock is used for mixers while a comb generator serves as clock signal for sampler. This down-conversion stage is followed by Intermediate Frequency (IF) circuitry which consists of amplifiers and band-pass filters. Finally the analog IF signal is digitized by an analog to digital convertor.

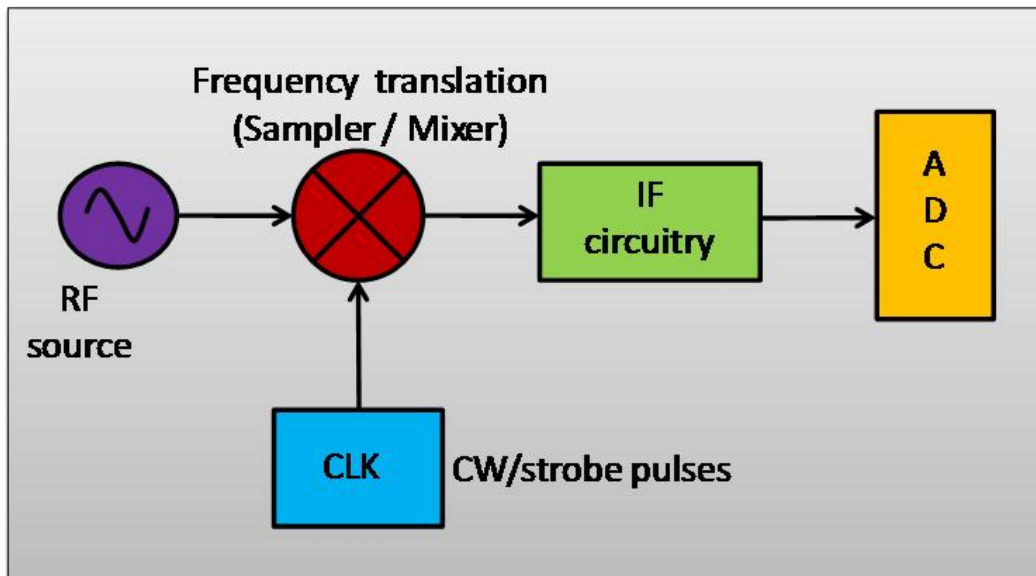


Figure I. 8 : Block diagram of frequency translation circuit

### III.1.2. Determining the Bottleneck [25], [26]

The analog to digital convertor (ADC) is one of the basic building blocks of time domain based measurement setup. It is an essential part of the signal processing and becomes the bottleneck of the signal processing system. Analog to digital converters (ADCs) translate analog signals which are characteristic of most phenomena in the “real world” to a digital data stream for a variety of applications. They are often used in advanced telecommunications. Fig.I.9 describes the block diagram of the basic ADC [25]. The analog signal  $x(t)$  is sampled at time instances  $t = k/fs$ , where  $k = 0, 1, 2, \dots$  and  $fs$  denotes the sampling frequency. The samples  $x[k]$  are then quantized, which yields the digital representation of  $x(t)$ , i.e., the quantized samples  $y[k]$ .

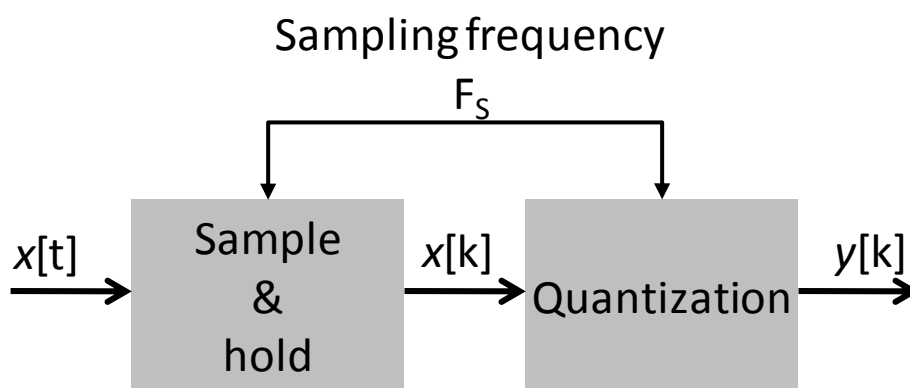


Figure I. 9 : Basic block diagram of ADC

The performance of the digital signal processing and communication systems is generally limited by the speed and the precision of the digital representation of the analog input signal. The conversion or sampling rate roughly corresponds to the bandwidth of the signal. The bandwidth of the analog input signal fed to the analog-to-digital converter (ADC) needs to be limited to one half of the conversion rate. In addition, note that the centre frequency of the signal may, reside at any frequency, as long as the width of the frequency band is  $f_s/2$ . The maximum sampling rate and the resolution of the ADC are inversely proportional to each other and a physical bound (energy-time uncertainty) to the digital representation of analog signals exists which is explained by W. Hisenburg's uncertainty principle [25]. This bound involves a theoretical limit to the sampling rate which corresponds to the bandwidth ( $BW=f_s/2$ ) that can be used for maximum data rate.

Resolution of an ADC can be determined using quasi-static or dynamic methods. Quasi-static is more theoretical while dynamic method involves signal to Noise Ratio (SNR), spurious Free Dynamic Range (SFDR) and noise power ratio (NPR) which are very important for high-speed applications and provide a more accurate measure of ADC performance than the stated-number-of-bits. These quantities are determined from the spectral analysis of the converted signals. Usually fast Fourier transform (FFT) of a sequence of ADC output samples is analyzed.

The SNR of an ADC is defined as the ratio of the root-mean-square (rms) signal amplitude to the square-root of the integral of the noise power spectrum over the frequency band of interest which ranges from (0-  $f_s/2$ ) Hz for a Nyquist convertor. The noise spectrum contains contributions from all the error mechanisms present [27], [28]. These include quantization noise, circuit noise, aperture uncertainty, and comparator ambiguity. The SNR could be represented by the following equation [26], [34]:

$$\text{SNR (dB)} = 6.02N + 1.76 \quad \text{Eq:-31}$$

In practical ADC's, additional error mechanisms are present which may also be characterized as white noise with the same expression for SNR, except that N represents  $N_{\text{eff}}$ , an effective number of bits. The notation for effective number of bits (ENOB) is given by:

$$\text{ENOB} = (\text{SNR (dB)} - 1.76) / 6.02 \quad \text{Eq:-32}$$

Effective Number of Bit indicates the quality of an ADC, used for digital conversion.

SFDR is the ratio of the single-tone signal amplitude to the largest spur whether harmonically related or not within the spectrum of interest. The effective number of bits associated with SFDR is

$$\text{SFDR (bits)} = \text{SFDR(dBc)} / 6.02 \quad \text{Eq:-33}$$

Two figures of merit namely P and F are commonly used to evaluate the performance of ADC emphasizing efficiency with respect to dissipated power, SNR, and SFDR.

P is the product of the effective number of quantization levels, times the sample rate [26]:

$$P = 2^{\text{ENOB}} \times f_s \quad \text{Eq:-34}$$

F, involves dissipated power ( $P_{\text{dis}}$ ) and is given by the following equation:

$$F = (2^{\text{ENOB}} \times f_s) / P_{\text{dis}} \quad \text{Eq:-35}$$

Fig I.10 describes the performance [29] of different ADC's and the area in the upper left-hand corner of the graph is generally accomplished by ADCs integrated with digital ICs such as microcontrollers or low-cost, high-volume application specific ICs which may combine analog, mixed-signal, and extensive digital circuitry. The area in the lower right-hand corner represents an area that is either impossible for all practical purposes or is only possible for low volume applications where cost is a low priority.

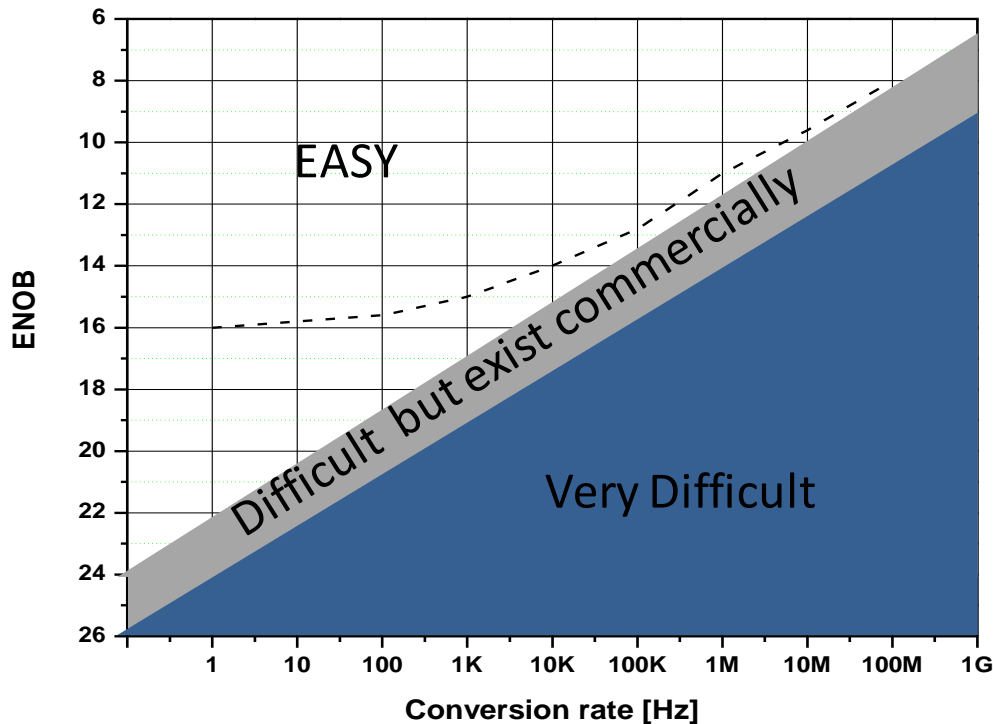


Figure I. 10 : ADC performance w.r.t. sampling frequency and resolution

Considering the performance of an ADC, we know that the bandwidth and the resolution are inversely proportional to each other and the resolution is decreased by one bit when  $f_s$  is doubled. The bandwidth of an ADC can be defined in several ways. One is simply to specify the -3dB bandwidth of the ADC input stage or track and hold circuit. Another is to consider the frequency at which the spectral power of the ADCs digital output signal is reduced by 3dB. Perhaps the most stringent definition would be the analog frequency for which the ADCs signal to noise ratio performance is reduced by 3dB.

To achieve a good compromise between bandwidth and dynamic range for time domain measurement systems the commercially available ADC's that can be used have a sampling frequency  $f_s$  of around 400MHz and a resolution of 12 bits. There are ADC's available in the market with sampling frequency of as high as 1GHz but with a much lower resolution. This means that to overcome the practical limitations of the ADC the RF should be down-converted.

### III.2. RF Down-conversion

Due to the technological limits of ADC, the down conversion of an RF signal is a key component in a time-domain analysis system. Many different instruments and techniques can be used for this purpose. Most commonly used among them are the mixers and the samplers.

#### III.2.1. Microwave mixers [30], [31]

Ideal microwave mixers translate the frequency of RF signals and are critical components in modern radio frequency (RF) transceiver systems. It converts the RF spectral power at one frequency into power at another frequency to make signal processing easier and compatible with the ADC. A mixer is a three port device (Fig.I.11) where two ports are termed as input ports while a third port is the output port. The two input ports are the RF port where the RF frequency to be translated is fed and the local oscillator port (LO) which acts as the “gate” of the mixer in the sense that the mixer can be considered “ON” when the LO voltage is a large and “OFF” when the LO voltage is a small. The LO port is typically driven with either a sinusoidal continuous wave (CW) signal or a square wave signal. The choice to apply a CW or square wave signal depends on the application and the type of mixer. The output port is termed as the Intermediate Frequency (IF) port and is either the sum or difference of the frequency of the inputs (Fig.I.12).

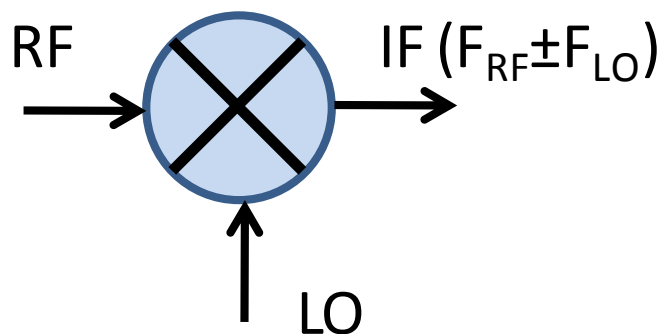


Figure I. 11 : Circuit symbol for a mixer



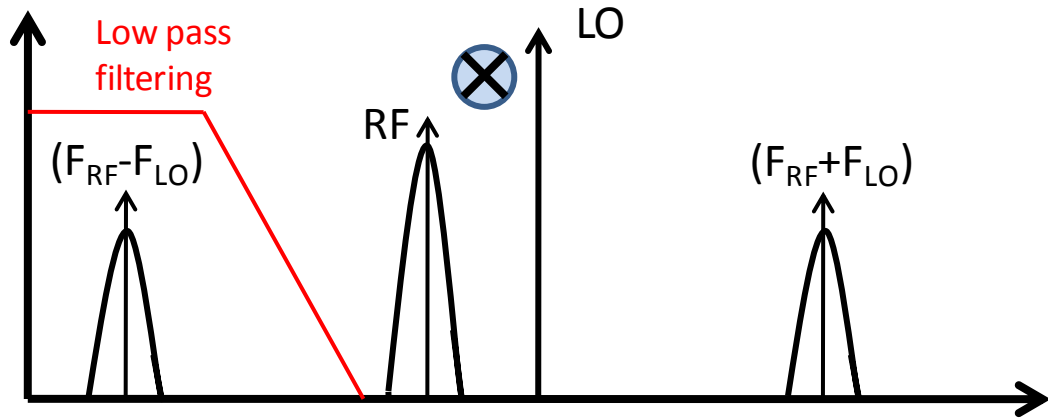


Figure I. 12 : RF down-conversion principle

In the first approximation, a mixer can be seen as a circuit realizing a multiplication of the RF signal and the LO signal. Generally speaking the LO frequency is higher than the RF. The frequency components located at frequencies that are higher than the RF signal are removed by low pass filtering. The multiplication process of the two input signals can be represented mathematically as follows:

$$S_{LO}(t) = A \sin(\omega_{LO}t + \theta_{LO}) \quad \text{Eq:-36}$$

$$\delta_{RF}(t) = B \sin(\omega_{RF}t + \theta_{RF}) \quad \text{Eq:-37}$$

$$S_{LO}(t)\delta_{RF}(t) = A \sin(\omega_{LO}t + \theta_{LO})B \sin(\omega_{RF}t + \theta_{RF}) \quad \text{Eq:-38}$$

$$\sin \alpha \sin \beta = \frac{1}{2} [\cos(\alpha + \beta) - \cos(\alpha - \beta)] \quad \text{Eq:-39}$$

Using the trigonometric identity in Eq.39 one obtains

$$S_{IF}(t) = \frac{AB}{2} [\cos(\omega_{LO}(t) + \theta_{LO}) + (\omega_{RF}(t) + \theta_{RF})] - [\cos(\omega_{LO}(t) + \theta_{LO}) - (\omega_{RF}(t) + \theta_{RF})] \quad \text{Eq:-40}$$

$$S_{IF}(t) = \frac{AB}{2} [\cos(\omega_{LO}(t) + \omega_{RF}(t)) + (\theta_{LO} + \theta_{RF})] - [\cos(\omega_{LO}(t) + \omega_{RF}(t)) - (\theta_{LO} + \theta_{RF})] \quad \text{Eq:-41}$$

A mixer could either be a passive device (made of passive elements, such as diodes) or an active device (made of active elements, such as transistors). Active or passive implementations are used depending on the application, and each has both advantages and disadvantages. A passive implementation that uses diodes as nonlinear elements or FETs as

passive switches exhibits a conversion loss rather than a conversion gain. This may impact the overall signal to noise ratio of the system, so in this case an LNA is usually added prior to the mixer.

Passive mixers are widely used due to their simplicity, their wide bandwidth, and their potentially good intermodulation distortion (IMD) performance. Active mixers are mostly used for an RFIC implementation. They are configured to provide conversion gain, a good isolation between the signal ports, and require less power to drive the LO port. They can be monolithically integrated with other signal processing circuitry and are less sensitive to load-matching. There are three basic classifications for both active and passive mixers:

*Unbalanced* mixers have an IF output consisting of  $f_s$ ,  $f_{LO}$ ,  $f_s - f_{LO}$ ,  $f_s + f_{LO}$ , and other spurious outputs. They will also exhibit little isolation between each of the mixer's three ports, resulting in undesired signal interactions and feed through of the signal to another port.

*Single-balanced* mixers will at least strongly attenuate the feed through of either the original input signal *or* the LO (but not both). They send less of the above mixing products on to the output than the unbalanced type.

*Double-balanced* mixer, or *DBM* for short, supplies superior IF-RF-LO inter-port isolation, while outputting only the sum and difference frequencies of the input signal and the local oscillator, while attenuating both the LO at the RF port and RF at the LO port.

### *III.2.1.1. Mixer specifications [31], [32]*

When choosing a mixer, there exist certain performance parameters which are taken into account depending on the specifications of the receiver. These parameters are explained in Fig. I.13 as follows:

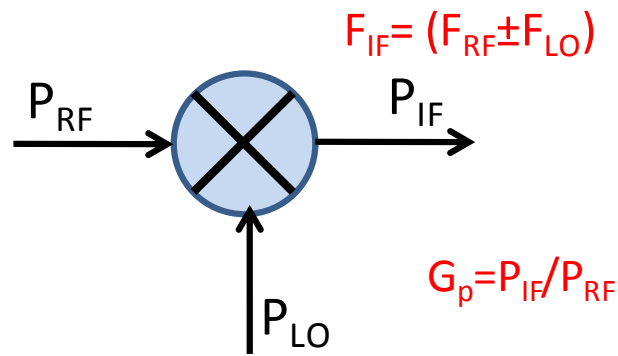


Figure I. 13 : Power conversion of mixer

**Conversion loss/gain  $G_p$**  is the ratio of the output power (IF) to the input power (RF) expressed in dB. The conversion gain measures the signal gain in an active mixer, while the conversion loss measures the loss in a passive mixer. Losses that occur can stem from transmission line losses, balun mismatch, diode series resistance, and mixer imbalance. In addition, the wider the frequency ranges for the three ports, the worse the conversion loss.

**Isolation** represents the amount of "leakage" or "feed-through" between the mixer's LO, RF, and IF ports. This ratio between leakage and signal value is represented in dB. The most important of these isolation specifications is the LO attenuation at the IF and RF ports. LO feed through is a major problem in receiver and transmitter system design, while the RF to LO isolation is normally of little concern due to the low RF input power levels.

**Noise figure (NF)** The noise added by the mixer itself, and equals the difference between the signal to noise ratio at the input of the mixer and the signal to noise ratio at the output of the mixer, in dB. When the mixer is driven with the proper LO drive level, the NF will equal the conversion loss.

**Dynamic Range** is the amplitude range over which a mixer can operate without degradation of performance. It is bounded by the conversion compression point for high input signals, and by the noise figure of the mixer for low level input signals. The 1 dB compression point is generally taken to be the top of the dynamic range of a mixer because the input RF power that is not converted into desired IF output power is instead converted into heat and higher order

intermodulation products. The intermodulation products that begin to appear when RF power is increased beyond the 1 dB compression point can begin to obscure the desired IF output.

**Intercept Point**, measured in dBm, is a figure of merit for intermodulation product suppression. There exist two types of intercept points commonly specified as input (IIP) and output intercept point (OIP). Input intercept point is the level of input RF power at which the output power levels of the undesired intermodulation products and IF products would be equal. Normally as input RF power increases, the mixer compresses the power level of the intermodulation products to avoid interception with the IF output power. So, input and output intercept points are theoretical and are calculated by extrapolating the output power of the intermodulation and IF products past the 1 dB compression point until they equal each other. A high intercept point is desirable because it means the mixer can handle more input RF power before causing undesired products to rival the desired IF output product and essentially means the mixer has a greater dynamic range. Dynamic range, 1 dB compression point, and intercept point are all interrelated, but it has been shown that, in general, no dB-for -dB rule of thumb exists to easily correlate 1 dB compression point with intercept point.

### III.2.2. Samplers [33]

#### *III.2.2.1. Basic architecture*

As we have discussed in the previous sections that the most important performance aspect of an RF receiver is the down-conversion phenomenon due to the limitations posed by the ADC. This makes the sampling process a critical step to implement before digitization of the RF signal. A sampler is another device that's used for down-conversion of an RF signal into an IF signal. For a sampler the strobe signal is no longer a CW signal but a sequence of narrow periodically repetitive pulses. This signal could be viewed as a sum of numerous mixers working at harmonic frequencies of the local oscillator signal as shown in Fig.I.14.

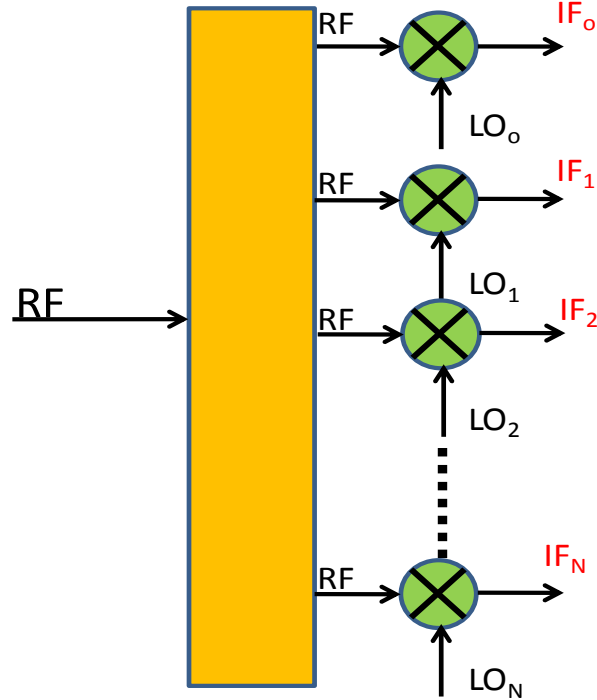


Figure I. 14 : Analogy between a sampler and a mixer

Sampling process is commonly referred to as sub-sampling because the frequency driving the pulse strobe signal is lower than the fundamental RF signal to be down-converted. The spectral contents of the resulting sub-sampled signal waveform are highly dependent on the relationship between the sampling rate employed and the minimum and maximum number of frequency components present in analog input signal. To produce the desired IF as shown in Fig. I.15 the LO conversion frequency can be chosen from the set of sampling frequencies present in the pulse train and is given by the Eq.42:

$$F_{IF} = F_{RF} - nF_{LO} \quad \text{Eq:-42}$$

Where

$F_{IF}$  = Intermediate frequency

$F_{RF}$  = Radio frequency

$F_{LO}$  = Frequency of local oscillator

$n$  = an integer called sampling ratio

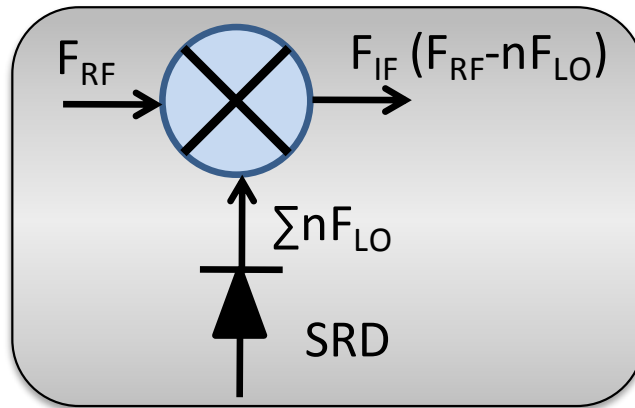


Figure I. 15 : Circuit symbol for sampler

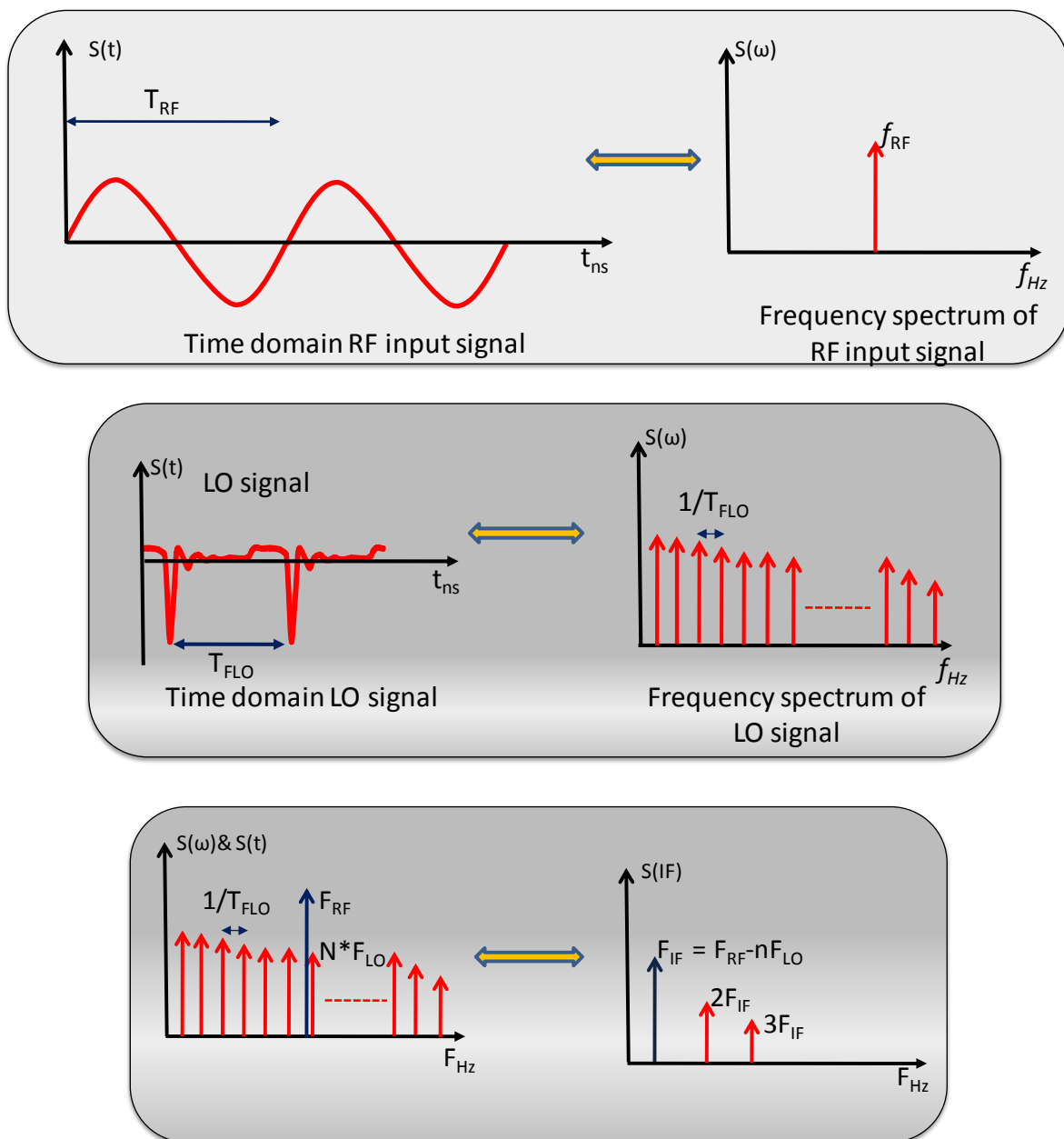


Figure I. 16 : Harmonic mixing principle of a sampler.

Fig.I.16 describes the time and frequency domain representation of the input (RF and LO) and output signal (IF) [33], [34]. The local oscillator signal is a sequence of stroboscopic pulses. In a real setup, they can be generated by a Step Recovery Diode (SRD) [35] which is a strongly nonlinear semiconductor device. It generates one short electrical pulse in each period when driven by a sine wave. The repetition period of the pulses is set by the period of the sine wave.

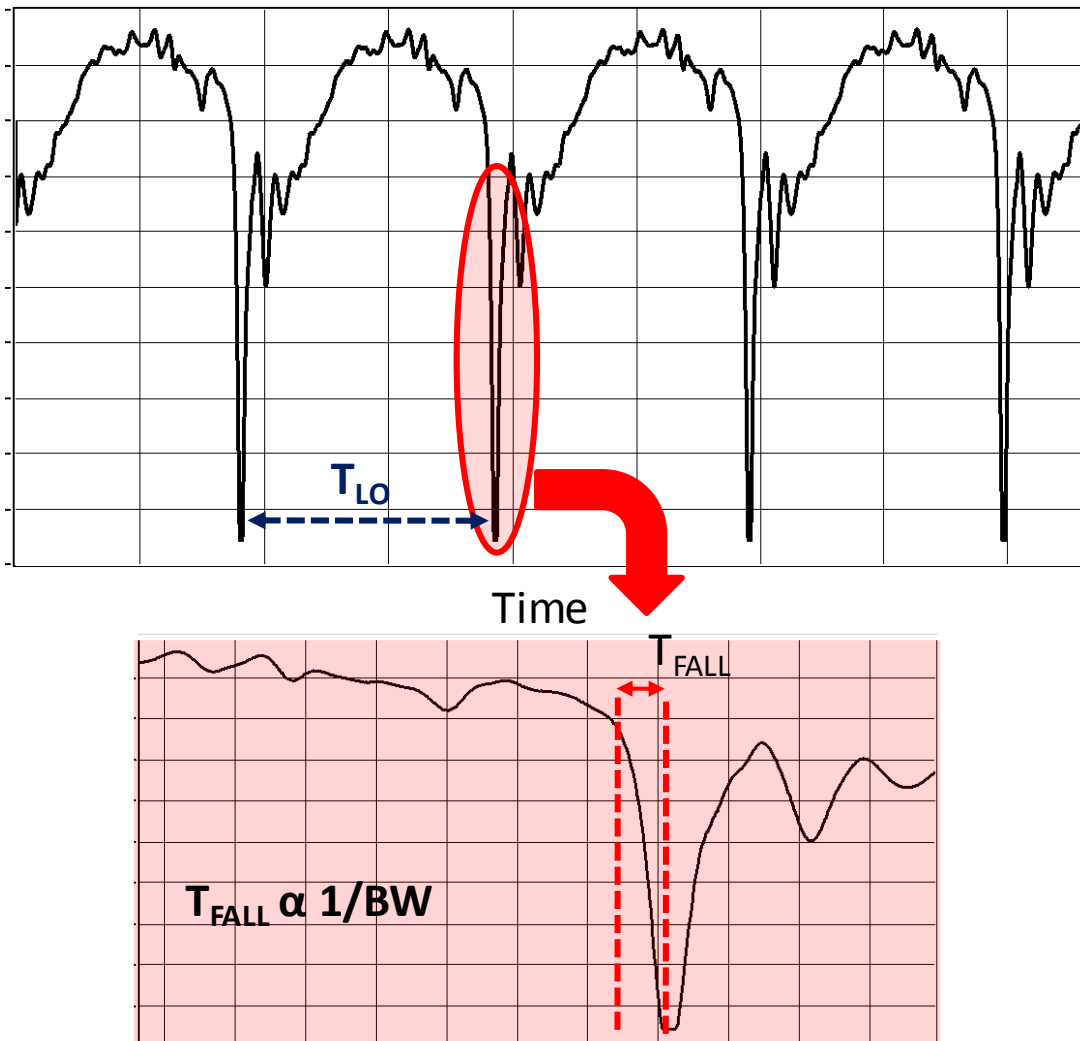


Figure I. 17: Characteristic of SRD

The fall time Fig. I.17 of the short electrical pulses produced by SRD determines the RF bandwidth of the diode i.e. the number of harmonics produced. This fall time also known as storage time is the time taken by the minority carriers to return to their original position once the diode is reversed biased. When all the charge is transferred the reverse current stops immediately and this immediate change in state produces a steep edge, resulting in harmonics

and is called the transition time. A lower fall time corresponds to higher bandwidth while a higher fall time decreases the bandwidth. This pulse generating circuit works independently of the sampling head. Different pulse repetition frequencies can be generated depending upon the application and the requirements. The IF contains a number of spectral components due to harmonics mixing thus require IF pass-band filter. The cutoff frequency of these filters is dependent upon the maximum sampling rate of the ADC ( $f_{ADC(min)} \geq 2 * f_c$ ).

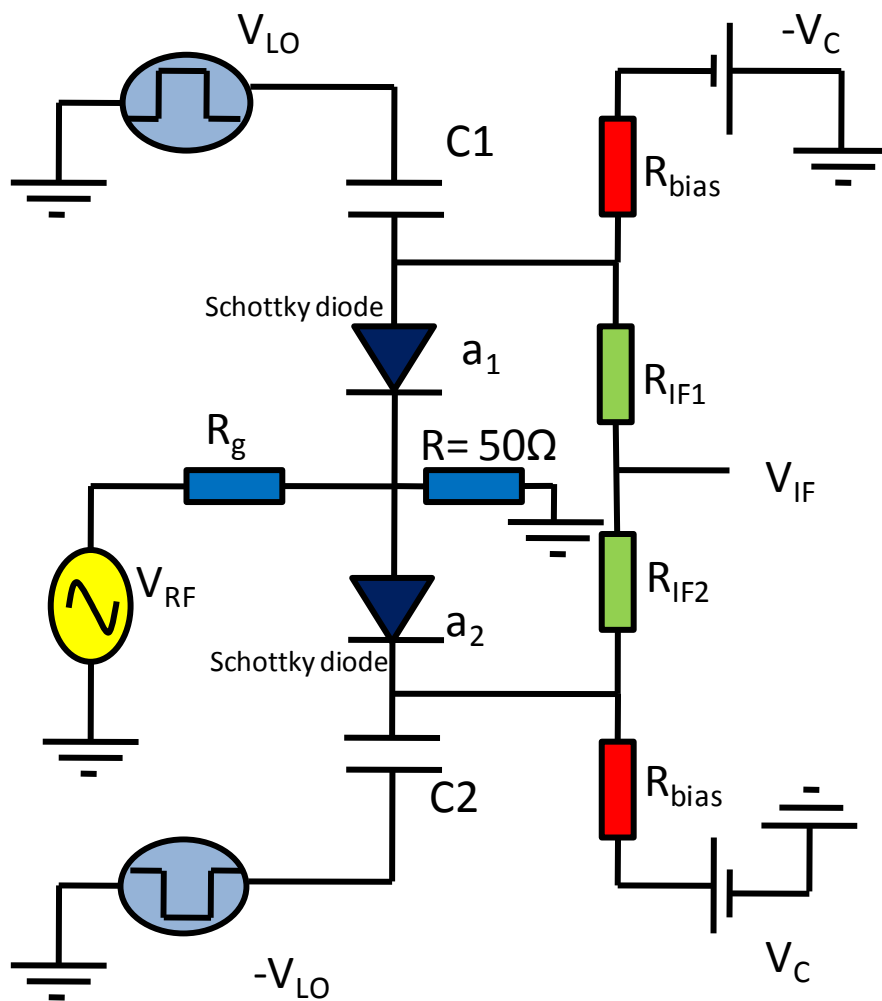


Figure I. 18 : Block diagram for sampler circuit.

The operating principle of the sampling heads where the sub-sampling is performed is based on Schottky diodes. The sub-sampling is performed due to the fact that the repetition rate of the pulses in LO signal is much lower than the RF signal. As exhibited in the Fig.I.18 the sampling head [33], [34] [36], [37] is shown that's based on a symmetrical architecture with a differential LO signal applied at the two diodes. Initially, when there is no signal



present at the LO the Schottky diodes are reverse biased due to the dc voltages  $V_C$  and  $-V_C$ . In this case the RF signal is absorbed by the  $50\Omega$  load and as the diodes act as an open circuit the charge capacitors  $C1$  and  $C2$  discharge through the resistors  $R_{IF1}$  and  $R_{IF2}$  to IF path. Now when the two LO signal are active the diode  $a_1$  and  $a_2$  are forward biased (short circuit) and  $C1$  and  $C2$  are charged for the time period equal to the fall time of the LO signal. During the off state of the pulse of LO signal the capacitors  $C1$  and  $C2$  discharge through IF path. Ideally the amplitude of the voltage  $V_{IF}$  at the IF port should be equal to the  $V_{RF}$  but in reality the internal resistances at the two path are not equal and the far less level of  $V_{IF}$  is achieved. This level could also be increased by increasing the fall time of the pulse of the LO signal (charging the capacitors  $C1$  and  $C2$  for longer time) but that would be at the expense of the RF bandwidth of the strobe signal. Thus the sampling efficiency of the sampler is very low and high gain linear amplifiers are required at the IF path before the IF filter.

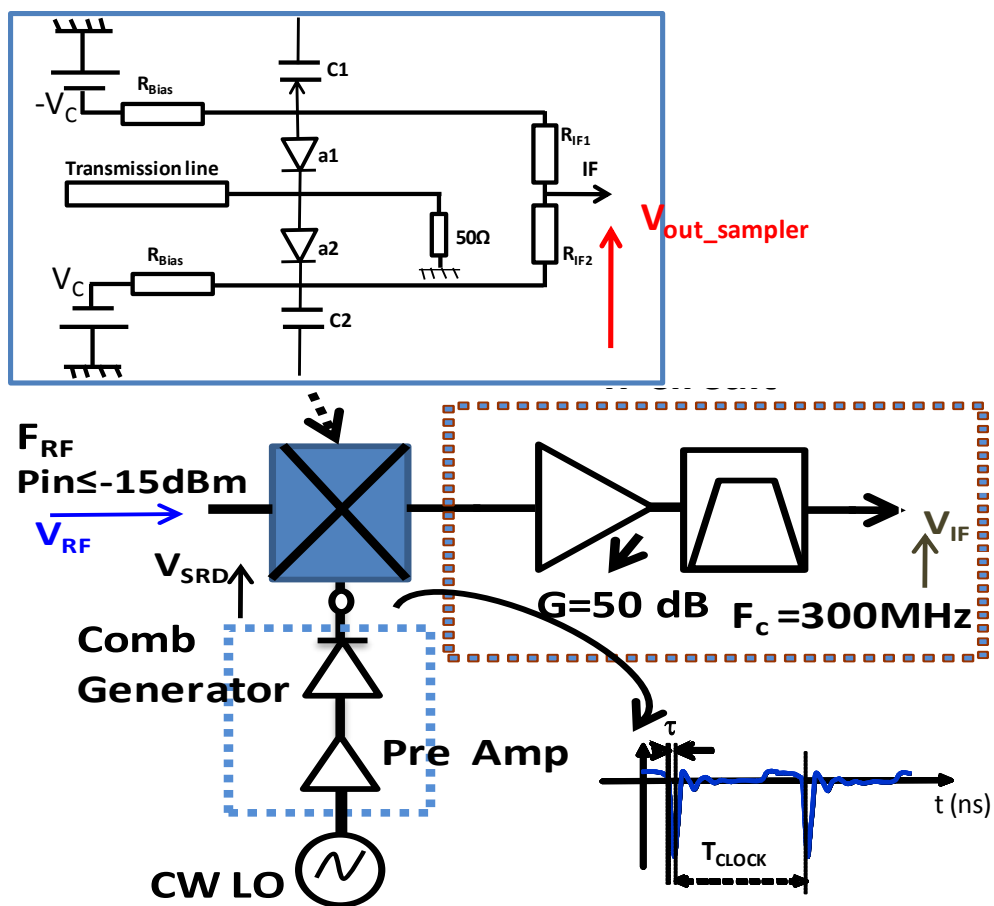


Figure I. 19 : Block diagram of sampler based frequency translation

Fig.I.19 describes the block diagram of the circuit used to simulate the sampling principle using sampler based down conversion phenomenon which implies charge sampling technique [38]. The simulation results are shown in Fig.I.20. The sampling efficiency of the sampler is very low, which means that the conversion loss of the sampler is very high (typically 40 dB). The maximum input power to the sampler is also limited, making it necessary to include an IF circuitry comprising a linear amplifier (around 55 dB gain) and a low pass filter before sending this data to ADC. The linearity of IF circuitry is very important to avoid distortion of the actual measured data. The IF circuitry also integrates the IF signal at the output of the sampler.

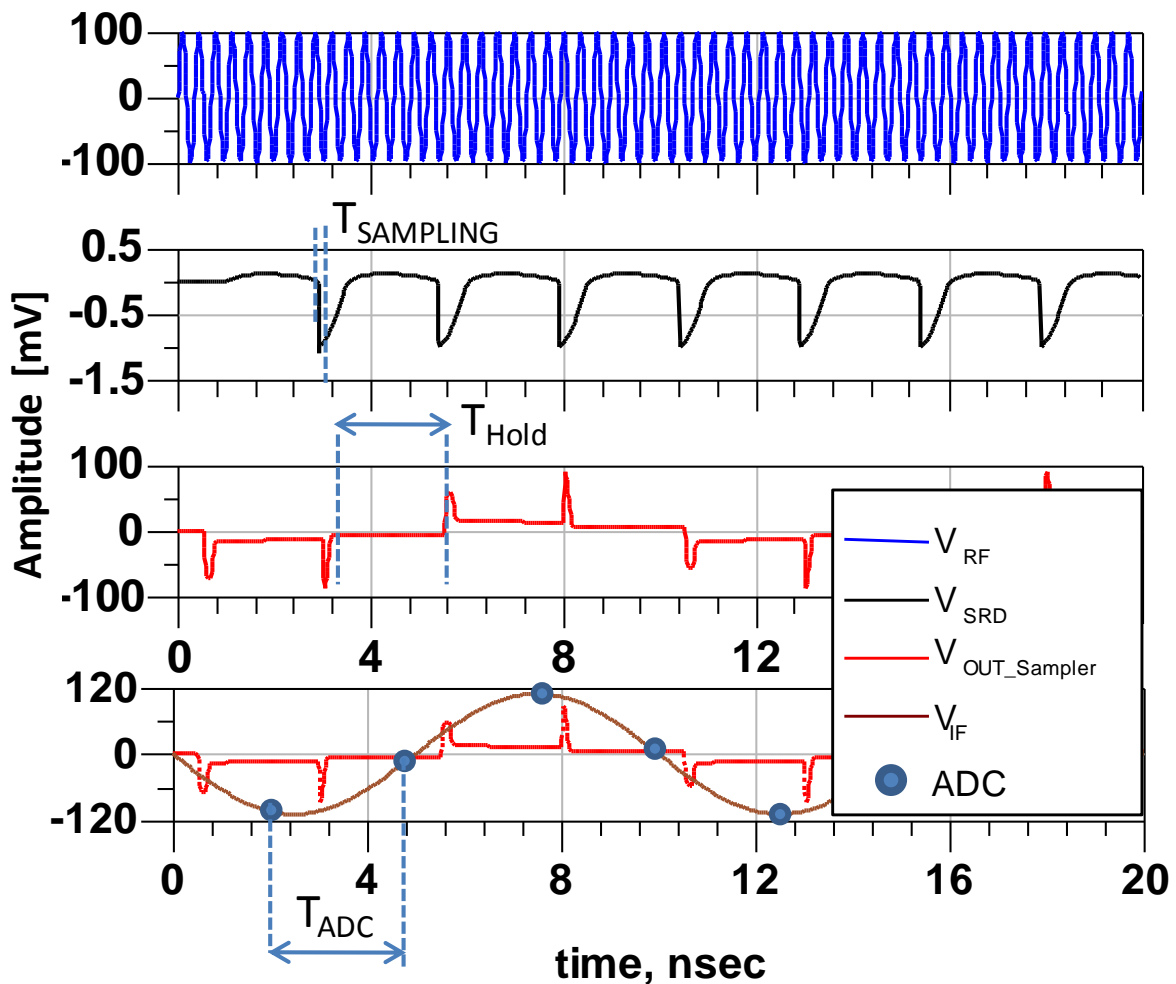


Figure I. 20 : Transient response of sampler.

III.2.2.2. Charge sampling [38]

This sampling phenomenon as discussed is known as charge sampling technique. Charge sampling integrates the input current instead of tracking input voltage to realize a high speed and low voltage sampling. It utilizes the linear charging behaviour of the capacitor ( $C_1$  &  $C_2$ ) as shown in Fig. I.18 to store and measure the amount of charge. A simplified principle of operation of the charge sampling consists of charging phase, a discharging phase and a holding phase. It can be described by two switches and a capacitor in parallel as described in Fig.I.18. The switches S1 and S2 are controlled by clock signals in differential mode.

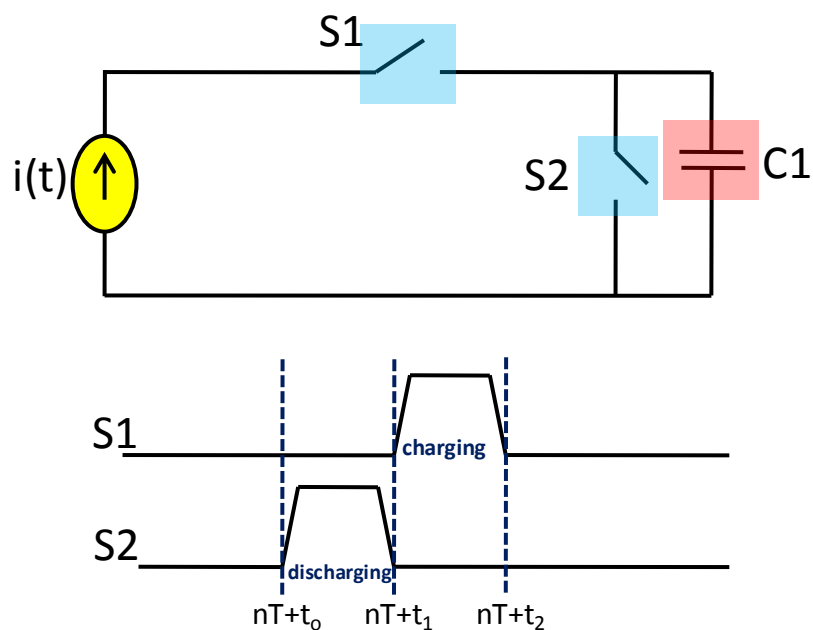


Figure I. 21 : Basic charge sampling principle.

The current source  $i(t)$  is assumed to be the input signal to be sampled while  $C$  is the hold capacitance. The two switches operate on the differential clocks  $S_1$  and  $S_2$  and let the capacitors charge and discharge when the corresponding clock turns on the switch. Fig.I.21 shows that when switch  $S_2$  is turned on between  $nT+t_0$  to  $nT+t_1$  the capacitor is discharged while  $S_1$  between  $nT+t_1$  to  $nT+t_2$  charges the capacitor [39].

$$v(nT + t_2) = \frac{1}{C_1} \int_{nT+t_1}^{nT+t_2} i(t) u(t) dt \quad \text{Eq:-43}$$

Where  $u(t)$  is the unit step function and  $T$  is the sampling period.  $n$  represents the  $n$ th charging period

$$= \frac{1}{C} \int_{-\infty}^{\infty} i(t)[u(t - (nT + t_1)) - u(t - (nT + t_2))]dt \quad \text{Eq:-44}$$

Let

$$fo(t) = u(-t + \Delta t) - u(-t) \quad \text{Eq:-45}$$

Where  $\Delta t = t_2 - t_1$  and using Eq.43 and 44

$$v(nT + t_2) = \frac{1}{C} \int_{-\infty}^{\infty} i(t) fo(nT + t_2 - t_1)dt \quad \text{Eq:-46}$$

This gives us that the stored charge is the convolution of sampling frequency  $f_o(t)$  and the current  $i(t)$ .

As the sampling signal which is a pulsed signal, we know that the frequency domain representation of it would be a sinc function and Eq.46 is represented as multiplication of Fourier transforms of  $f_o(t)$  and  $i(t)$ .

$$V_s(f) = I(f) \times F_o(f) \quad \text{Eq:-47}$$

Where

$$F_o(f) = \frac{\Delta t}{T} \text{sinc}(\pi f \Delta t) \quad \text{Eq:-48}$$

So the final spectrum of the charge spectrum is

$$V_s(f) = \Delta t / TC \sum_{i=-\infty}^{\infty} I(f - ifs) . Fo(f - ifs) \quad \text{Eq:-49}$$

$$V_s(f) = \Delta t / TC \sum_{i=-\infty}^{\infty} I(f - ifs) . \text{sinc}(\pi \Delta t (f - ifs)) \quad \text{Eq:-50}$$

The charge sampling bandwidth is directly determined from the signal integrating window (Charging time) while the phase shift is linearly proportional to the frequency. The output voltage is dependent on the value of the capacitance and the current which is not



$$S_{LO}(t) = \sum_{n=-\infty}^{\infty} P(t - nT_o) \quad \text{Eq:-52}$$

The signal at the output of sampler is

$$S_{IF}(t) = S_{RF}(t) \times S_{LO}(t) \quad \text{Eq:-53}$$

Now replacing Eq.51 and 52 in Eq. 53 yields Eq.54 the signal shape at IF port

$$S_{IF}(t) = S_{RF}(t) \times \left[ \sum_{n=-\infty}^{\infty} (P(t - nT_o)) \right] = \sum_{i=-N}^N S_{IF_i}(t) \quad \text{Eq:-54}$$

$$\text{Where } S_{IF_i}(t) = A_i e^{j\omega_o t} \sum_{n=-\infty}^{\infty} P(t - nT_o)$$

Eq.54 represents the time domain output of the harmonic mixer within the sampler. It corresponds roughly to the multiplication of RF signal with the pulse train which consists an of infinite number of delayed versions of p(t). The mixing process could also be described in frequency domain, hence taking the Fourier transform of  $S_{IF_i}(t)$  gives

$$Y_i(f) = \int_{-\infty}^{\infty} S_{IF_i}(t) e^{-j\omega t} dt \quad \text{Eq:-55}$$

$$Y_i(f) = \int_{-\infty}^{\infty} A_i e^{j\omega_o t} \left[ \sum_{n=-\infty}^{\infty} P(t - nT_o) \right] e^{-j\omega t} dt \quad \text{Eq:-56}$$

Simplifying Eq 56 using the following relation

$$\text{Now } e^{-j\omega t} * e^{j\omega_o t} = e^{j2\pi(if_{RF} - f)t}$$

$$Y_i(f) = A_i \sum_{n=-\infty}^{\infty} \int_{-\infty}^{\infty} P(t - nT_o) e^{j2\pi(if_{RF} - f)t} dt \quad \text{Eq:-57}$$

Substituting  $t' = t - nT_o$  in Eq.57 and further simplifying

$$Y_i(f) = A_i \sum_{-\infty}^{\infty} \int_{-\infty}^{\infty} P(t') e^{j2\pi(if_{RF} - f)(t' + nT_o)} dt' \quad \text{Eq:-58}$$

$$Y_i(f) = A_i \left( \sum_{-\infty}^{\infty} e^{j2\pi n \left( \frac{if_{RF} - f}{f_{LO}} \right)} \right) \left( \int_{-\infty}^{\infty} p(t') e^{j2\pi(if_{RF} - f)t'} dt' \right) \quad \text{Eq:-59}$$

Using the poissons formula:

$$\sum_{n=-\infty}^{\infty} e^{2\pi f k T} = \sum_{k=-\infty}^{\infty} \delta\left(f - \frac{k}{T}\right) \quad \text{Eq:-60}$$

helps to simplify the Eq.59 where p(f) represents the Fourier transform of the pulse signal.

$$Y_i(f) = A_i f_{LO} \left( \sum_{k=-\infty}^{\infty} \delta(f - if_{RF} + kf_{LO}) \right) p(f - if_{RF}) \quad \text{Eq:-61}$$

$$Y_i(f) = A_i f_{LO} \left( \sum_{k=-\infty}^{\infty} \delta(f - if_{RF} + kf_{LO}) \right) p^*(kf_{LO}) \quad \text{Eq:-62}$$

Eq.62 represents a complex function with magnitude  $A_i$  and is a series of periodic repetitions and harmonic products at the output of sampler. All the intermodulation products indexed by  $k$  appear at output with an equidistant frequency grid with distance  $F_{LO}$ . It could be seen in Fig.I.23 that RF signal of 1 GHz with 20 harmonics is fed into the sampler and the LO frequency is chosen to be 9.998 MHz. At the IF port a series of intermodulation products corresponding to the RF harmonics are appeared. The IF signal needs to be filtered to eliminate all aliasing products.

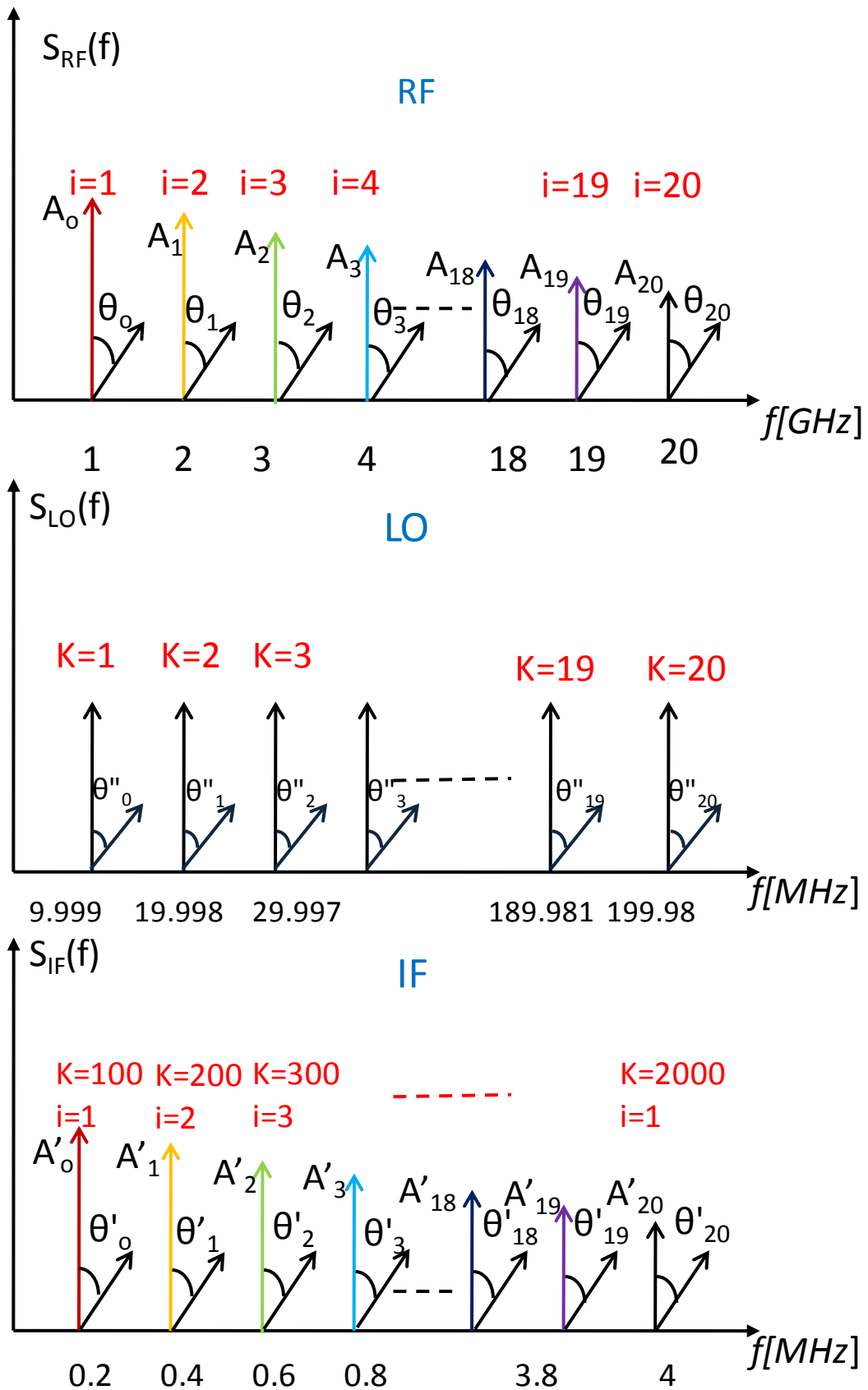


Figure I. 23 : Illustration of down conversion process



## **IV. Pre Existing Time-domain Instruments**

The ever growing need for an increase of the data rate in telecommunication systems has lead RF engineers to innovative ideas in terms of design, realization and measurement of RF devices and instruments. The power amplifier is still one of the most important constituents in a transmitter system has seen vigorous modernization in terms of device technology and driven RF signals (modulation schemes). The use of high power, wide bandwidth and vector modulated data signals have enforced innovative approaches, when it comes to characterization and modeling of power amplifiers in particular.

For high power applications, such as radars, it is very difficult to characterize devices in CW operation as it increases the risk of device or component destruction. To avoid this problem radar signals utilize pulsed modulation techniques. Pulsed modulation enables the use of components at larger signals amplitudes while reducing the risk of destruction by thermal overload. The control of the width and pulse repetition frequency of the pulse train is used to set the thermal state of the transistor. This allows one to limit or control the influence of the self-heating. An amplifier driven with a high power level during the pulses undergoes numerous parasitic effects due to self heating and trapping effects, thus changing the magnitude and its phase significantly.

Different measurement techniques have been developed in the past for pulsed and CW characterization of systems and devices and some of them are described as below.

### **IV.1. Sampler Based Instruments**

#### **IV.1.1. Vector network analyzer (VNA)**

Different instrumentation techniques have been utilized in the past to characterize the linear and non-linear behavior of circuits and devices. A Vector Network Analyzer (VNA) [43] is the most notable among them for linear characterization. A VNA measures the devices in terms of scattering parameters (s-parameters) which are the ratio of an incident and a scattered wave at the input and output ports of the Device Under Test (DUT). The term scattering refers to the obstruction and discontinuity faced by the electromagnetic waves when passing along dissimilar wave guiding structure. When a device is excited by a signal, one

part of the wave passes through the device while the rest is reflected back due to unmatched impedances present at the ports. The incident and the reflected waves can be separated and measured by two directional couplers. One of these is connected at each port of the DUT and in case of PA they are connected at the input and output ports of the DUT as shown in Fig 1.24.

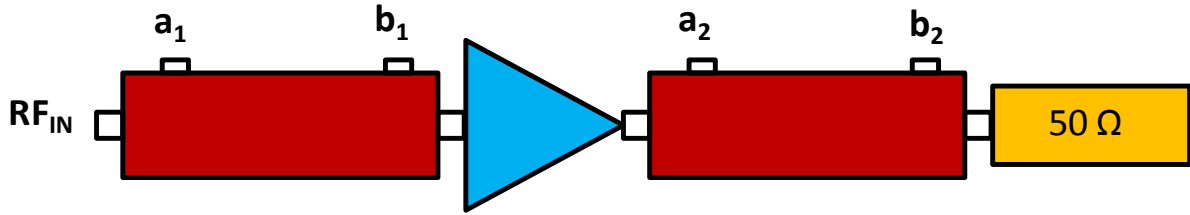


Figure I. 24: Architecture for incident and reflected signal acquisition

The S-parameters [40] of a two port network are defined as the relation between incident and reflected waves at the ports of DUT, where each port is terminated with characteristic impedance  $Z_0$ .

$$S_{11}(f) \text{ (input port voltage wave reflection coefficient)} = \frac{b_1(f)}{a_1(f)_{a_2=50\Omega}} \quad \text{Eq:-63}$$

$$S_{12}(f) \text{ (reverse voltage wave gain)} = \frac{b_1(f)}{a_2(f)_{a_1=50\Omega}} \quad \text{Eq:-64}$$

$$S_{21}(f) \text{ (forward voltage wave gain)} = \frac{b_2(f)}{a_1(f)_{a_2=50\Omega}} \quad \text{Eq:-65}$$

$$S_{22}(f) \text{ (output port voltage wave reflection coefficient)} = \frac{b_2(f)}{a_2(f)_{a_1=50\Omega}} \quad \text{Eq:-66}$$

The S-parameters of a 2 port network which give the relation between the incident and reflected waveforms are represented in a matrix form as under:

$$\begin{bmatrix} b_1 \\ b_2 \end{bmatrix} = \begin{bmatrix} S_{11} & S_{12} \\ S_{21} & S_{22} \end{bmatrix} \begin{bmatrix} a_1 \\ a_2 \end{bmatrix} \quad \text{Eq:-67}$$

#### IV.1.2. Large signal network analyzer (LSNA)

As seen from the equations that the s-parameters are ratio of the incident and reflected waves and are based on the superposition principle which means they are only valid for linear time-invariant systems. If the scattering parameters are measured at two different incident power levels, the two measurements are to be identical. Note that to enforce small signal operation in devices, the power incident to the DUT in a VNA is chosen to be very small. The representation of S-parameters which is a ratio is neither sufficient nor adequate to describe the nonlinear behavior of the devices. It is important to note that, under the linearity assumption required for the operation of the VNA itself, the stimulus frequency will be the only frequency that is present and there will be no spectral contributions at other frequencies (e.g., harmonics or intermodulation distortion products) present. All this leads us to the fact that these measurements are true for passive devices and for linear operation of devices which could be represented by linear equation.

To represent the behavior of nonlinear devices waves can still be used and instead of measuring the ratios of the incident and reflected waves at one frequency, the true waveforms were captured in one take even if the device is driven to saturation [44], [45]. The time-domain traveling voltage waves ( $a_{IN}, b_{IN}, a_{OUT}, b_{OUT}$ ) can be transformed into a current and a voltage (VI) waveform using the following algebraic equations.

$$a_{IN}(t) = \frac{1}{2}(v_1(t) + i_1(t)Z_o) \quad \text{Eq:-68}$$

$$b_{IN}(t) = \frac{1}{2}(v_1(t) - i_1(t)Z_o) \quad \text{Eq:-69}$$

$$a_{OUT}(t) = \frac{1}{2}(v_2(t) + i_2(t)Z_o) \quad \text{Eq:-70}$$

$$b_{OUT}(t) = \frac{1}{2}(v_2(t) - i_2(t)Z_o) \quad \text{Eq:-71}$$

Where  $Z_o = 50\Omega$  and

$$V_{IN}(t) = a_{IN}(t) + b_{IN}(t) \quad \text{Eq:-72}$$

$$I_{IN} = \frac{1}{Z_o} (a_{IN}(t) - b_{IN}(t)) \quad \text{Eq:-73}$$

$$V_{OUT} = a_{OUT}(t) + b_{OUT}(t) \quad \text{Eq:-74}$$

$$I_{OUT} = \frac{1}{Z_o} (a_{OUT}(t) - b_{OUT}(t)) \quad \text{Eq:-75}$$

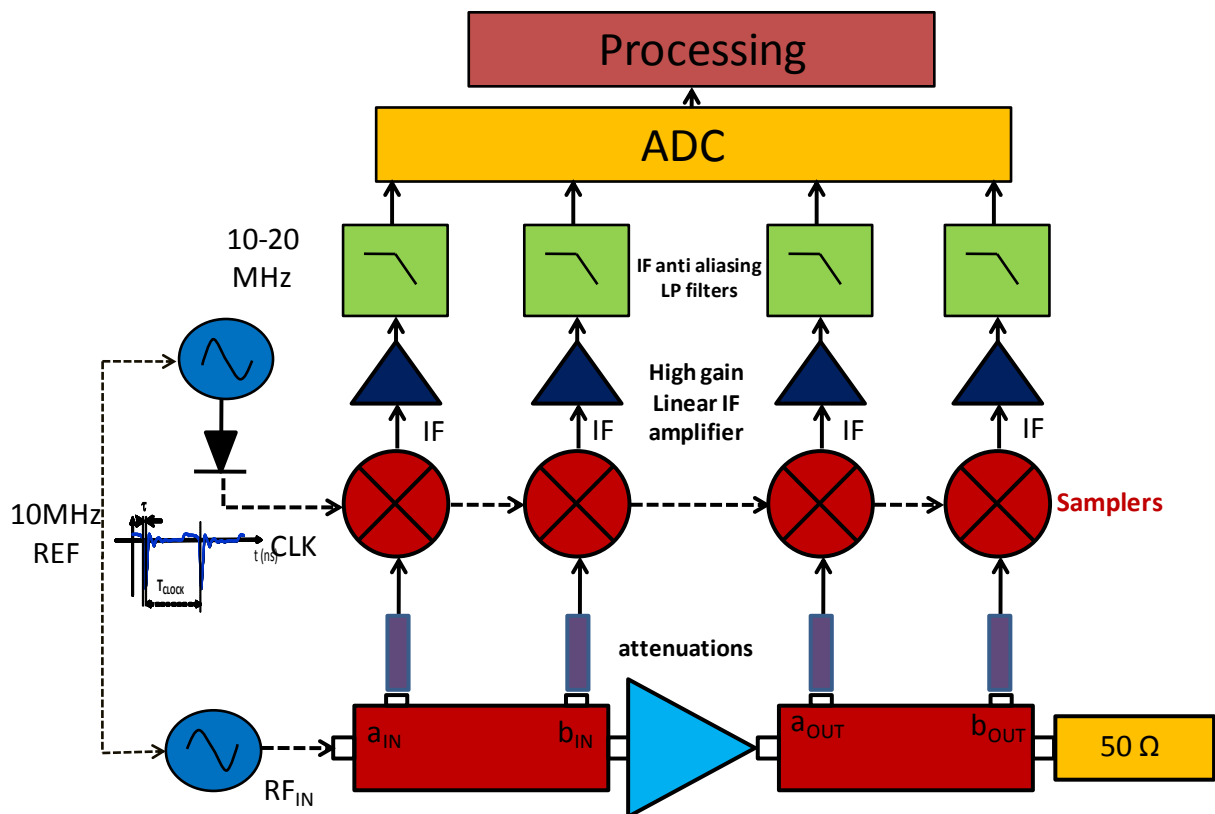


Figure I. 25 : Basic LSNA architecture

The Large Signal Network Analyzer (LSNA) is a sampler based instrument which means that RF to IF conversion is based on the harmonic sampling principle. It converts all the spectral components coherently to similar components located at a lower frequency. The acquired signals are attenuated to an acceptable level before being sent to the input channels of a four-channel broadband RF–IF converter to avoid compression. The sampler which operates as a charge sampler utilizes a pulsed clock which is provided by a Step Recovery Diode (SRD) operating at frequency ranging from (10-20) MHz. When the synthesizer frequency is properly chosen, an undistorted low-frequency copy of time-domain waves is found. The sampling efficiency of the sampler is very low therefore high gain linear

amplifiers are used at the IF port to amplify the IF signal. These amplifiers are followed by low pass filters (often called anti-aliasing filters) to ensure anti-alias filtering. A high resolution ADC's (8-12bits) digitizes the acquired time-domain waveforms simultaneously. The harmonic sub-sampling converts the RF signal to a baseband signal, hence low bandwidth ADC's can be utilized.

#### IV.1.2.1. Modulated signals

The spectrum of CW signals can easily be down converted using the sub-harmonic sampling principle. Distortion free low frequency replicas of the signals are obtained by a smart selection of  $F_{LO}$ . When the device is excited with a modulated signal a complex spectrum is obtained and if the bandwidth of its spectrum is larger than half the sampling frequency ( $f_s$ ) then the down-converted spectral components are scrambled and in worst cases could fall on the top of each other [46]. Thus for broadband modulated signal descrambling of the spectral components is necessary to accurately obtain the time-domain waveform and this could be a difficult process. To combat this problem a complex clock circuitry was proposed [46] which practically slows down the train of pulses coming from the SRD as explained in FigI.26.

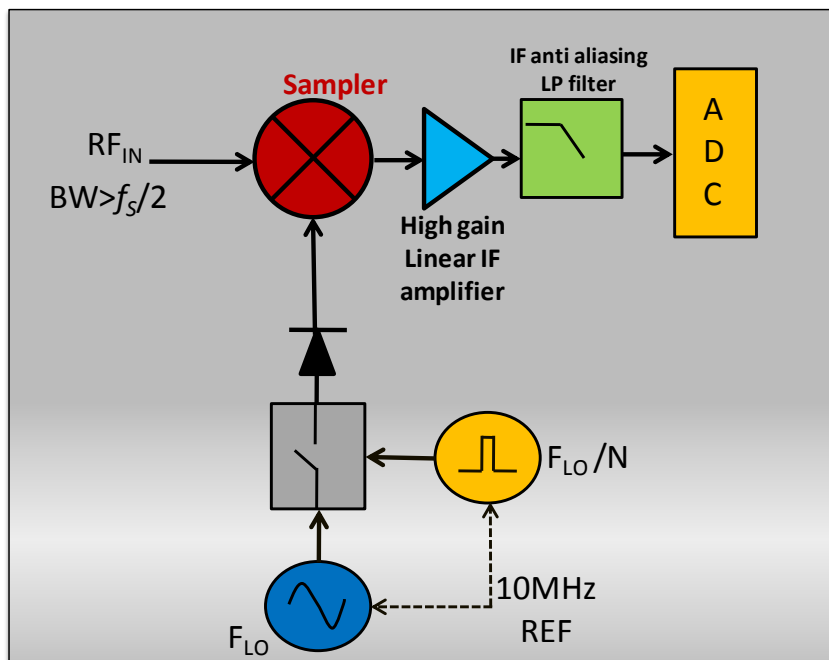


Figure I. 26 : Adapted Local oscillator setup for modulated signal

Fig.I.26 explains the single channel of an LSNA where a switch is connected between the  $F_{LO}$  synthesizer and the SRD. The switch is steered by a pulsed signal with a duty cycle whose frequency is an integer multiple (N) of the  $F_{LO}$ . The value of integer multiple (N) and the duty cycle is chosen such that only one out of the N successive periods of  $F_{LO}$  is allowed to pass as shown in Fig. 1.27

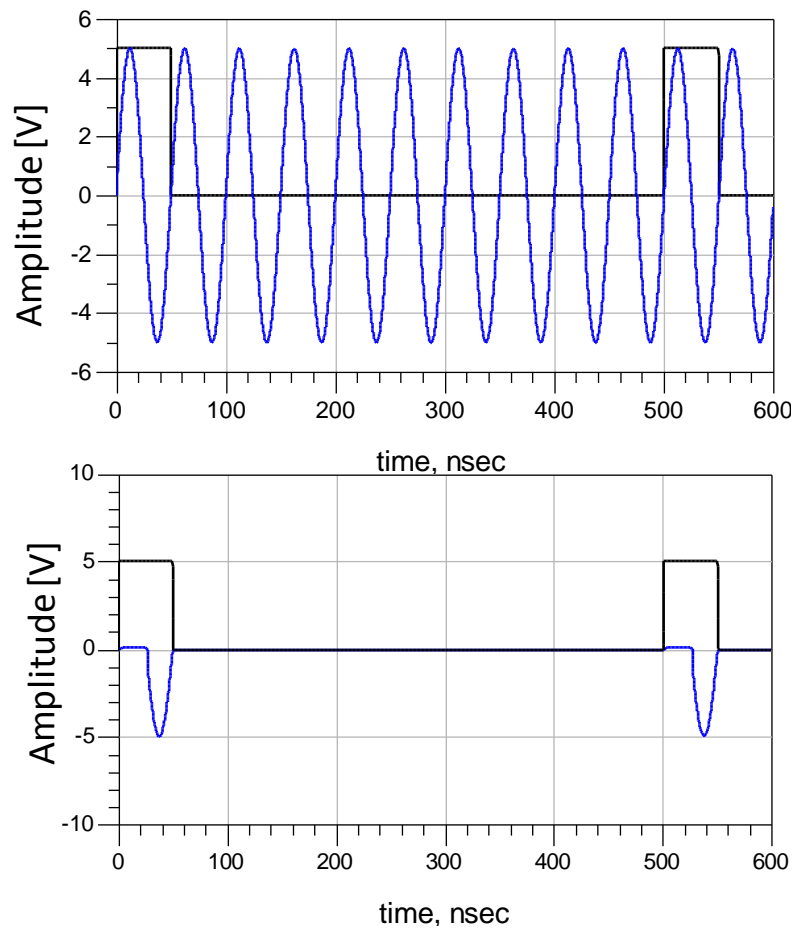


Figure I. 27 : Transient response of the SRD for adapted LO configuration

The Fig.I.27 displays the transient response of the clock circuitry when the  $F_{LO}$  is chosen to be 19.98 MHz and the value of N is chosen to be 10. The 10% duty cycle was selected which means that only one period of  $F_{LO}$  was allowed to pass through the SRD. By doing this, the measured samples are consecutive samples of the RF time-domain waveform, which are automatically in the correct order. Hence, a “slowed-down” version of the RF signal is obtained without reshuffling the measured samples. The spectral bandwidth of the SRD remains the same but much more narrow spectral resolution between the components is obtained Fig.I.28. This process has limited effects on the characteristics of the sampler. The

signal-to-noise ratio will, however, be reduced by an amount proportional to the duty cycle change (lower sampling frequency).

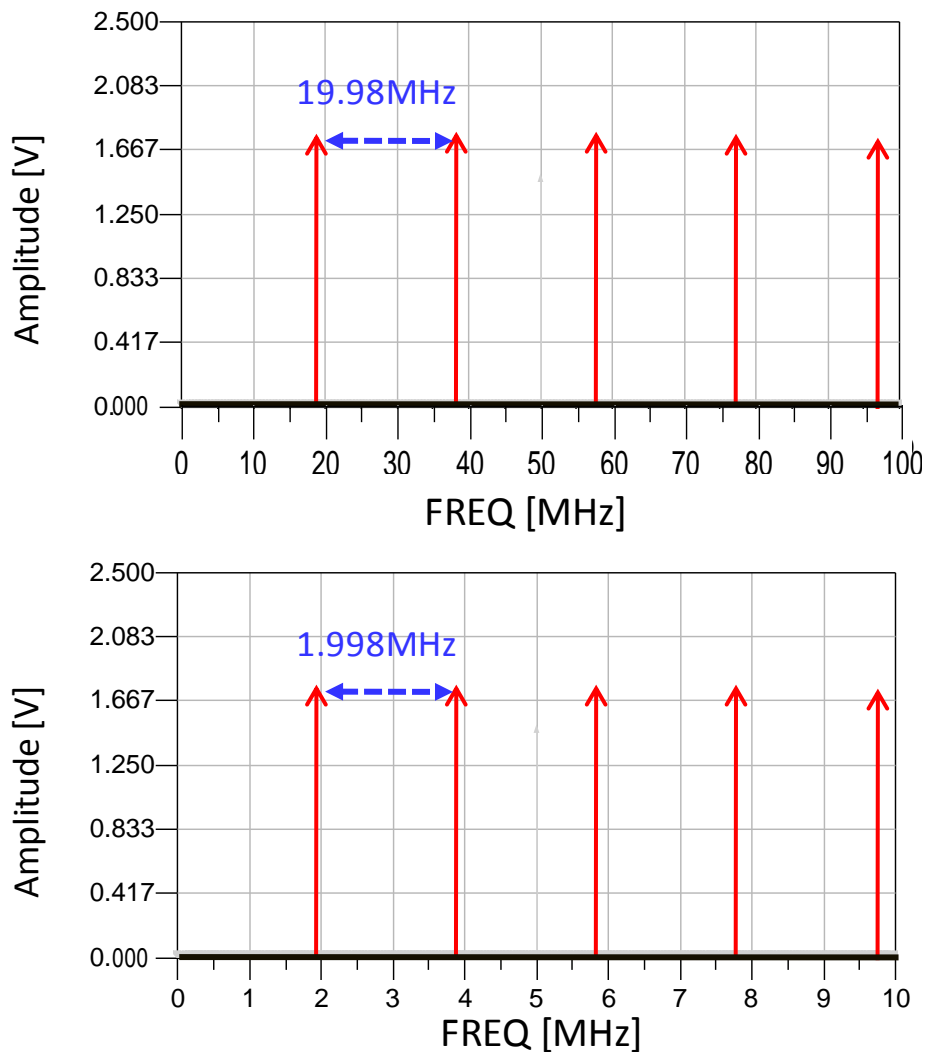


Figure I. 28: Harmonics mixing response for adapted LO configuration

## IV.2. Mixer Based Instruments

### IV.2.1. Vector signal analysis

Another possible solution is to use a mixer based instrument, commonly known as Vector signal analysis (VSA) [41], [42] has the capability to vector detect an input RF signal which means that the phase between RF signals and amplitude of the RF signal are accurately obtained. The architecture of the VSA is explained in Fig.I.29. It is composed of two parts,

the analog and the digital part. The analog part focuses on the frequency translation while the digital part processes the data in digital domain. A significant characteristic of the VSA is that it is designed to measure and manipulate complex data in RF and microwave ranges, and contains an additional modulation-domain analysis capability. The VSA could fundamentally be termed as a digital system that uses DSP to perform spectrum analysis based on FFTs, and uses the demodulator algorithms to perform vector-modulation analysis. The analog signal acquired by the time-sampling technique must be digitized in the time-domain, and then the FFT algorithm computes the spectra.

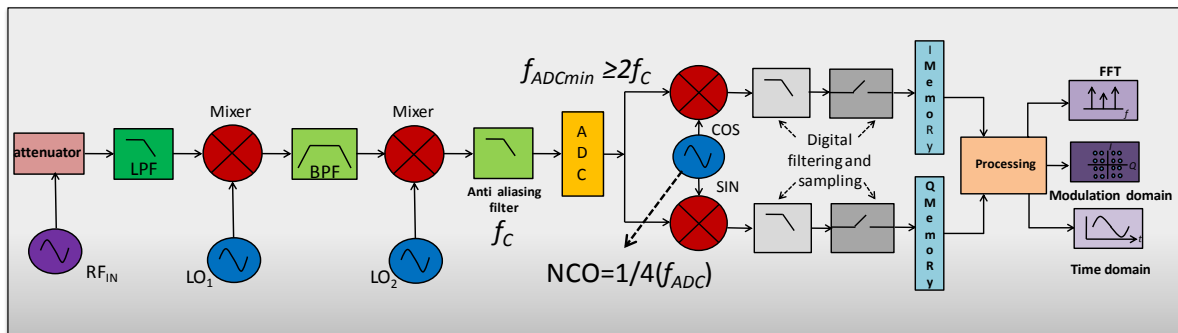


Figure I. 29 : Basic block diagram of VSA.

The frequency down conversion stage may consist of multiple stages and mixers are used for this purpose. Depending upon the RF frequency the LO frequency is adjusted automatically to down convert a part of the RF signal to desired IF. An anti aliasing filter precedes the ADC in order to nullify the frequency components which are not part of the desired IF signal. The resulting signals are translated as follows:

$$f_{IF} = f_{RF} - f_{LO} \tag{Eq:-76}$$

If the input RF signal is composed of a modulated signal around a carrier and its harmonics, the VSA requires the successive measurements of the modulation around the successive carrier  $f_c$  upto  $nf_c$ . The phase information between harmonics is lost in the process due to the sweep of local oscillator for the down conversion process. Therefore a specific sampling technique is adapted to extract the complex envelop around the carrier frequency. An ADC digitizes the IF signal by obeying the Nyquist criterion which states that the sampling frequency should be at least twice the maximum frequency component to accurately reconstruct the sampled signal.



Next an IQ demodulator is used to generate vector modulation [41], [42], [43]. The IQ demodulator generates signal in terms of I and Q components which is hardware implementation from rectangular to polar coordinates. The I-Q modulator receives the I and Q baseband signals as inputs and mixes them with the same local oscillator (LO) but with a 90 degree phase shift. The I information modulates the carrier producing the in-phase component. The Q information modulates a 90-degree phase shifted version of the carrier producing the quadrature component. These two orthogonal modulated carrier signals are summed together producing the composite I-Q modulated carrier signal. The quadrature relationship between I and Q signals means that these two signals are truly independent.

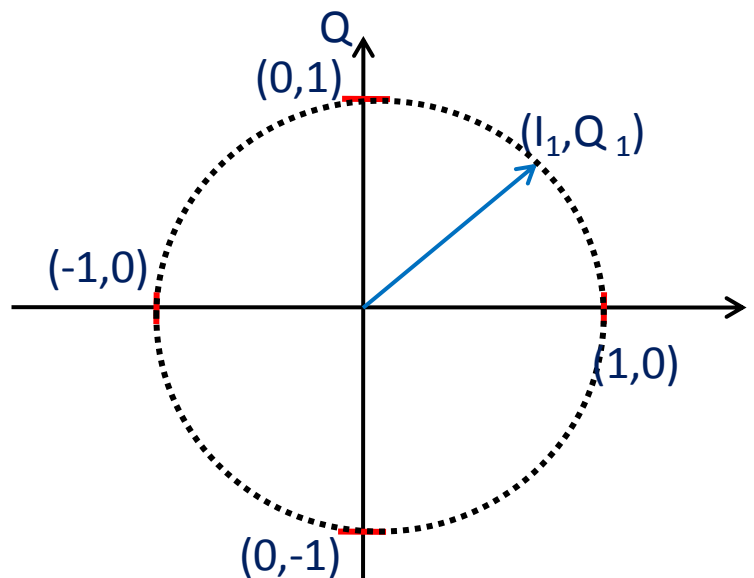


Figure I. 30: IQ representation

In most digital communication systems, the frequency of the carrier is fixed so only phase and magnitude need to be considered. The phase and magnitude can be represented in polar or vector coordinates as a discrete point in the I-Q plane as exhibited in Fig.I.30. The DSP algorithms work on these complex time signals to demodulate almost any modulation format. The demodulator also produces ideal I-Q reference waveforms that are synthesized from the actually recovered bits. The I-Q measured and I-Q reference waveforms are subtracted to produce I-Q error waveforms. The I-Q error waveforms are analyzed to specify the modulation quality, which can be viewed in various data formats and display outputs.

The most widely used modulation quality metric in digital communications systems is error vector magnitude (EVM). The error vector is the vector difference at a given time between the ideal reference signal and the measured signal.

The vector diagram, more commonly called the IQ diagram in the digital modulation, shows the recovered complex, I-Q baseband signal at all moments in time as is shown in Fig 1.30. It shows the states and the transitions between them as the signal moves from symbol to symbol on time. A vector drawn from the origin to a point on the vector diagram corresponds to the instantaneous complex voltage at that instant in time.

IQ data provides useful information to view analog modulation signal characteristics around the carrier frequency, such as AM and PM. An un-modulated continuous wave (CW) signal would simply show us as a single stationary point with a constant magnitude and phase. An AM signal has its trajectory along a fixed line through the origin and only the magnitude of the signal changes. In PM the relative change in phase is the controlling parameter as shown in Fig 1.31. In vector modulation, in which both the amplitude and phase can change simultaneously, the vector trajectory changes in both magnitude and phase.

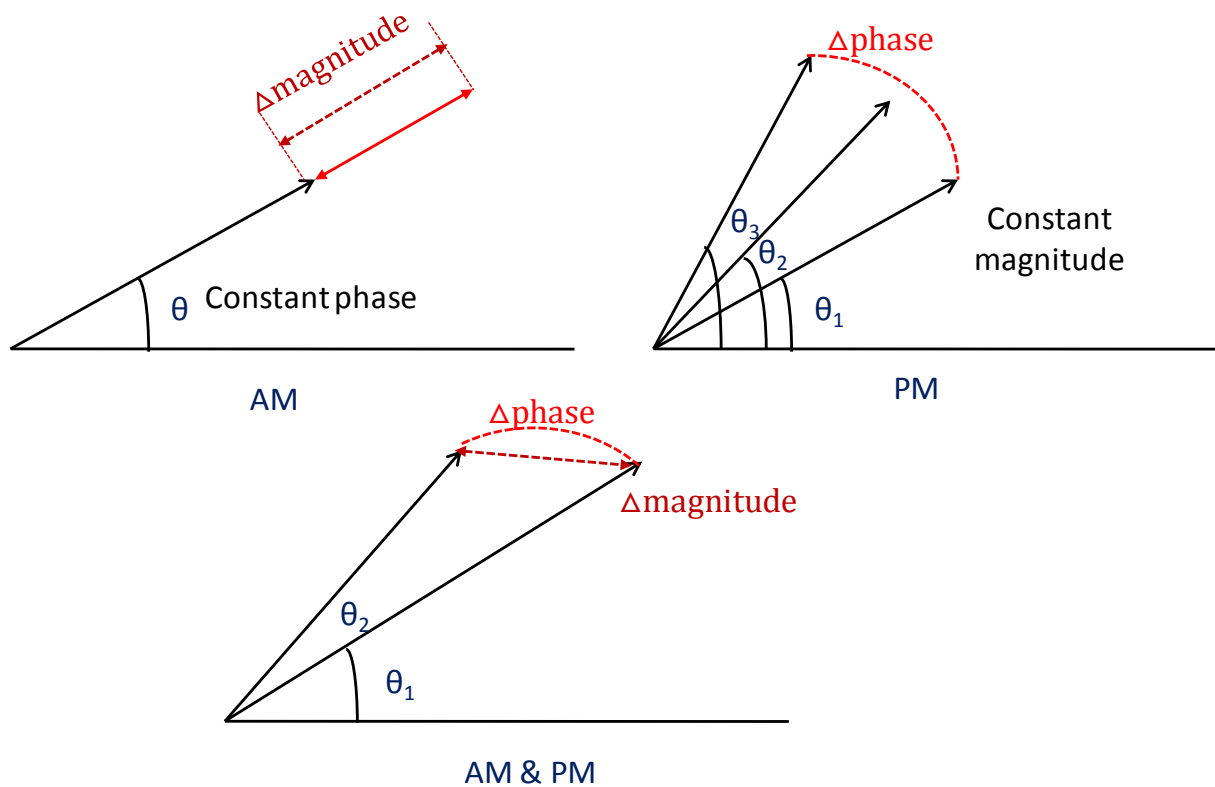


Figure I. 31: Phase and magnitude transition in different modulating signals

Applying trigonometric identities to the I(t) and Q(t) components allows us to extract the instantaneous amplitude, A(t), and phase,  $\varphi(t)$ . This is the AM and PM modulation. The amplitude modulation, AM, is the variation of the carrier magnitude, A(t), versus time and is extracted from I(t) and Q(t) by taking the square root of the sum of the squares of I(t) and Q(t).

$$A(t) = \sqrt{I(t)^2 + Q(t)^2} \quad \text{Eq:-77}$$

Phase modulation, PM, is the phase variation,  $\varphi(t)$ , versus time and is equal to:

$$\varphi(t) = \arctan(Q(t)/I(t)) \quad \text{Eq:-78}$$

#### IV.2.2. Non-linear Vector Network Analyzer (NVNA) [49], [50]

The non-linear vector network analyzer uses mixers to down-convert the RF spectrum into an IF spectrum. For the LSNA the harmonic sampling principle is used for down-conversion. This means that the whole spectrum is down converted in a single acquisition due to the use of the multi harmonic clock (SRD). In a mixer based instrument such as the NVNA only one frequency component is down converted at a time. This means that each spectral line that is to be measured by the NVNA needs then to be down converted separately. Hence the measurement requires a signal sweep at the local oscillator. The phase of the spectral lines is therefore not aligned and changes by an unknown value. To counter this phase indeterminacy a harmonic phase reference (HPR) signal is used as a time reference measured by a fifth channel as depicted in Fig.I.32. To correctly stitch together all spectral lines, the phase is compensated with respect to phase of the reference. This HPR is excited by a CW signal which remains fixed during the complete measurement sweep and the harmonics generated by this reference signal have a static and a priori known phase relationship. The reference frequency is chosen to be the highest common divisor of the frequencies of all spectral lines in the signals that are present at the measurement ports, or a sub-harmonic of that frequency. One harmonic of the reference signal will then be present at each measurement frequency of interest.



$$Acquisition\ time(s) = \frac{No.\ of\ samples(storage\ length\ N_s)}{Sampling\ frequency(f_s)} \quad Eq:-79$$

Most commercially available DSO's allow the user to increase the acquisition time only by reducing the sampling frequency as the memory depth is fixed. This is not always desirable as it can lead to aliasing of the signal and the loss of small details like signal glitches that can seriously restrict the usefulness of a DSO.

Sampling as discussed before is the process of converting the analog signal into a number of discrete values for the purpose of storage, processing and display. Ideally the magnitude of each sampled point should be equal to the amplitude of the input signal at the time instant at which it is sampled. Although there exists different operating principles for DSOs, but roughly speaking they can be divided into two main categories depending upon the type of sampling technique [52]:

- 1) Real time oscilloscopes
- 2) Equivalent time oscilloscopes

### **1) Real time oscilloscopes**

A real time oscilloscope repetitively samples a periodic or aperiodic signal at full rate in a single shot. This means that the ADC operates at the maximum sampling rate obeying Nyquist theorem. This phenomenon offers a great challenge for DSOs to accurately characterize high frequency transient events as these events should be acquired at one take. In order to capture a waveform, the ADC sampling rate needs to be significantly faster (atleast  $\geq 2f_s$ ) than the frequency of the incoming waveform. Real-time oscilloscopes use an interleaved ADC technology to achieve sampling rates as high as 50 Gsamples/s and bandwidths as high as 20 GHz. DSO's are also capable of acquiring tens or hundreds of millions of samples. They post process these waveforms to obtain information on various properties of the signal, including jitter or microwave modulation properties.

### **2) Equivalent time oscilloscopes**

Using the equivalent time sampling technique the oscilloscope can acquire a signal that has bandwidth larger than its sampling rate. This principle works for periodic signals where samples can be acquired from multiple repetitions with one or more samples taken

during each repetition. Several triggering techniques are used for capturing the samples and the acquired samples need time realignment to obtain leakage free spectral waveforms. Using this technique a maximum virtual sampling rate of 100 Gsamples/s has been achieved.

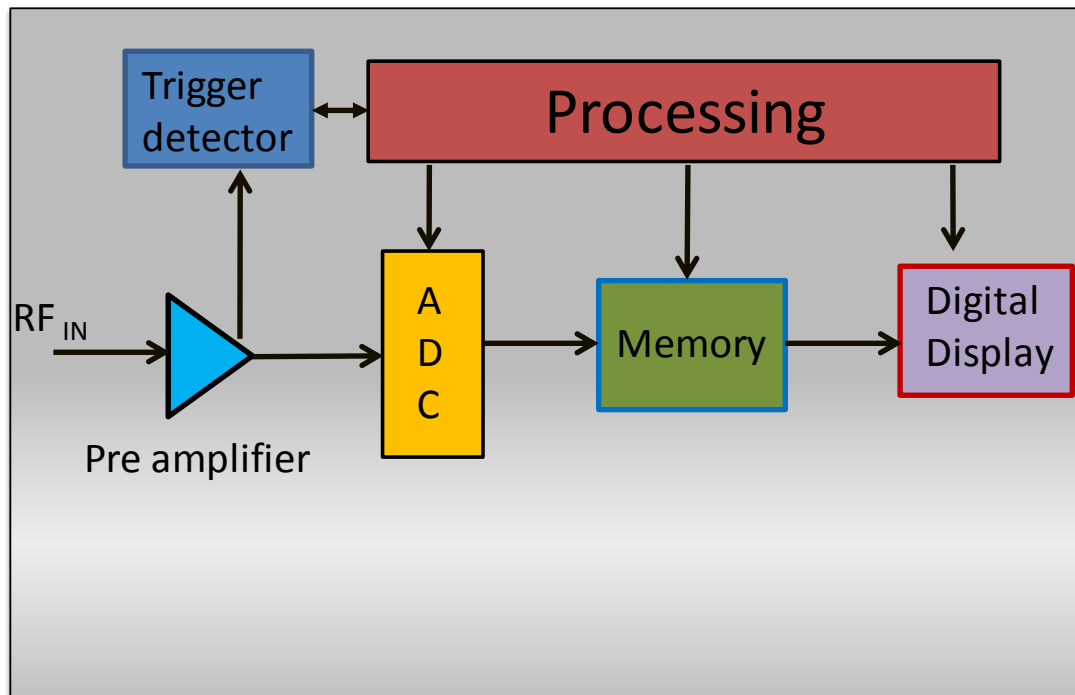


Figure I. 33: Basic block diagram of DSO

Fig.I.33 shows the basic block diagram of a Digital storage oscilloscope [50], [51]. The analogue signal to be measured is fed into a pre-amplifier, which conditions its amplitude so that it falls well within the input range of the Analogue to Digital Converter (ADC) and the trigger detector. When the amplified voltage crosses a threshold set by the user the trigger unit signals the device to start recording one or more samples. The ADC samples the output of the pre-amplifier at a regular low sampling frequency with a preset delay and the digital output from the ADC is then stored in consecutive locations in the memory.

## **Conclusion**

This chapter addresses the importance of time-domain measurement system for the pulsed characterization of high power devices particularly in radar applications. RF pulsed modulated signals and pulse to pulse stability profiling is thoroughly discussed. Issues related to pulse spectrum bandwidth are also highlighted. The architecture of basic time-domain measurement system and the theoretical and technological limitations associated are presented. The operating principle of frequency down-conversion instruments like mixers and samplers are discussed. In the end the existing time domain measurement systems and their associated operation techniques are presented. This part also discusses the complete signal acquisition using sub-sampling in sampler based systems and mixing phenomenon in mixer based system along with different data processing techniques involved.

## BIBLIOGRAPHIE :

---

- [1] Lav Varshney, "Radar principles", Syracuse research cooperation, *October 29, 2002*.
- [2] Tracy V. Wallace, Randy J. Jost, and Paul E. Schmid "Radar transmitters", *chapter 10, Vol. 1*.
- [3] E. J. Barlow, "Doppler Radar", I.R.E. Proceedings, *Vol. 37, April 1949*, pp. 340-355.
- [4] US Naval research, "Electronic warfare and Radar systems engineering handbook" Naval air systems command, avionics department, Washington DC, *1 April 1997*.
- [5] Merrill I. Skolnik, "Introduction to radar systems" *3<sup>rd</sup> edition McGraw hill 2001*.
- [6] Greg Goebel, "Basic Principles of Radar" v2.1.4, *Chapter 1 of 6, 2011*.
- [7] Waves and frequency ranges <http://www.radartutorial.eu/07.waves/wa04.en.html>
- [8] Francesco Fornetti, "Optimisation of GaN HEMTs and amplifiers for radar applications", Doctoral Dissertation, university of Bristol, *December 2010*.
- [9] Ahmed Sajjad, "Design and realization of Power amplifiers for hig power applications based on wide bandgap technologies", master thesis, university of Gavle, *January 2009*.
- [10] Chris Harris, "Wide Bandgap Revolution", Cree Sweden AB, [www.emcomp.se](http://www.emcomp.se).
- [11] Ric Borges, "GaN Electronic Devices for High Power Wireless Application", *Sep 2001*, [www.rfdesign.com](http://www.rfdesign.com).
- [12] R. T. Kemerley, H. B. Wallace and M. N. Youder, "Impact of wide bandgap microwave Devices on DOD systems," Proc. IEEE, pp. 1059, vol. 90, no. 6, *2002*.
- [13] Mishra, U.K. & Parikh, 2002 "AlGaN/GaN HEMTs-an overview of device operation and applications" Proceedings of the IEEE, vol. 90, issue 6, pp.1022-1031.
- [14] Trew R.J, "Wide bandgap semiconductor transistors for microwave power Amplifiers" *Microwave Magazine IEEE*, vol. 1, issue 1, pp 46-54, *Mar. 2000*.
- [15] Burk Jr., A.A., et al, 1999 "SiC and GaN wide bandgap semiconductor materials and devices", *Solid-State Electronics*, vol. 43, no. 8, pp. 1459-1464.
- [16] Prejs, A. et al., "Thermal Analysis and its application to High Power GaN HEMT Amplifiers". *IEEE MTTs International Microwave Symposium IMS*, p.917-920 *June 2009*.
- [17] Jingchang Nan, Jiuchao Li, "Analysis and simulation of memory effects on microwave power amplifiers". International workshop on information security and application, Qingdao, China, *November 21-22, 2009*, pp 205-208.
- [18] P. Draxler, I. Langmore, T.P. Hung and P.M. Asbeck, "Time-domain characterization of power amplifiers with memory effects" *IEEE MTT digest*, vol. 2, pp 803-806, *2003*.
- [19] Application note HP, "Spectrum analysis....Pulsed RF". Hewlett-Packard, *November, 1971*.
- [20] Fabien De Groote, Olivier Jardel, Tibault Reveyrand, Jean Pierre Teyssier, Raymond Quere, "Very small duty cycle for pulsed time-domain transistor characterization", *European Microwave Association journal*, vol. 4, p112- 117, *June 2008*.



- [21] Morris Engeleson, Len Garret “The pulse desensitization factor”, *Microwave Journal*, vol.41 June 1998.
- [22] C.Salmer, PH. Eudeline, PA. Rolland “Pulse to pulse stability of solid state transmitter module for radars application”, 28<sup>th</sup> *European Microwave conference*. pp. 79-84, Amsterdam, 1998.
- [23] M. Cicolani, A. Gentile, S. Maccaroni, L. Marecialli, “Pulse to pulse stability characteristics of robust design centered high performance low cost T/R module”3<sup>rd</sup> *European RADAR conference*. pp. 258-261, Manchester, UK, SEP 2006.
- [24] Tektronix. “Fundamentals of real time spectrum analysis” application notes
- [25] Stefan Krone, Gerhard Fettweis, “Fundamental limits to communications with analog to digital conversion at the receiver” 2009 IEEE 10th Workshop on Signal Processing Advances in Wireless Communications, Perugia, Italy 21-24 June 2009.
- [26] Robert H Walden, “Analog-to-digital converter survey and analysis” *IEEE journal on selected areas in communications*, vol. 17, pp. 539-550, April 1999.
- [27] Ed Crean, Paul Hiller, “A wide dynamic range radar digitizer” *Summit technical media*, September 2008, [www.highfrequencyelectronics.com](http://www.highfrequencyelectronics.com).
- [28] Saiyu Ren, “Broad bandwidth high resolution analog to digital converters: theory, architecture and implementation” doctoral dissertation. *Wright state university*, 2008.
- [29] Jerry Horn, “Practical limits of analog to digital conversion” chip centre, Mar 2000, <http://www.hit.bme.hu>
- [30] Ferenc Marki, Christopher Marki. “A tutorial for RF and Microwave Mixers” Marki Microwave, Inc. [www.markimicrowave.com](http://www.markimicrowave.com)
- [31] Michael Ellis, “Introduction to mixers” <http://michaelgellis.tripod.com/tutorial.html>.
- [32] Cotter W. Sayre, “Complete wireless design, chapter 7, Mixer design” Mc Graw Hill telecom, June 2008.
- [33] Alaa Saleh. “ Étude de la faisabilité d’une tête d’échantillonnage micro-ondes ” Rapport de stage, University de Limoges.
- [34] M. Abouchahine, “Développement d’un Banc de Caractérisation Fonctionnelle Large Bande (Porteuses et Enveloppes) dans le Domaine Temporel de Dispositifs non linéaires microondes”, doctoral dissertation, 18 Dec 2009, University de Limoges.
- [35] Jian Zhang, Antti V. Raisanen, “Characterization and modeling of step recovery diode”. *Microwave and Optical technology letters*, vol. 17, No. 3, pp. 200-205, Feb 20, 1998.
- [36] Wiltron General Maintenance, “General system description, block and stripline Schematic diagrams”. 361XA/362XA TS MM.
- [37] A. Agoston, “100 GHz through-Line Sampler System with Sampling Rates in Excess of 10 Gsamples/second”, *IEEE MTT-S*, vol. 3, pp. 1519-1521, 2003.

- [38] Gang XU, Jiren Yuan, “Comparison of charge sampling and voltage sampling”, *43<sup>rd</sup> IEEE Midwest Symposium on Circuits and System, Lansing MI, pp. 440-443, 8<sup>th</sup> Nov 2000.*
- [39] Gang XU, Jiren Yuan, “Performance analysis of general charge sampling”, *IEEE transaction on Circuits and System, Volume 5, No.2, pp. 107-111, Feb 2005.*
- [40] J. Verspecht, “Calibration of a measurement system for high frequency non-linear devices”, *Doctoral Dissertation - Vrije universiteit Brussel, November 1995.*
- [41] Agilent “Vector signal analysis basics”, *application note 150-15*
- [42] Rhodes & Schwarz, “Firmware option vector signal analysis”, *operating manual*
- [43] Johan Kirkhorn, “Introduction to IQ-demodulation of RF data”, *report IFTB, NTNU, September 1999, <http://folk.ntnu.no>.*
- [44] Agilent “Understanding the fundamental principles of Vector network analysis”, *application note.*
- [45] J. Verspecht, P. Debie, A. Barel, and L. Martens, “Accurate on wafer measurements of phase and amplitude of the spectral components of incident and scattered voltage waves at the signal ports of a nonlinear microwave device,” in *1995 IEEE MTT-S Int. Microwave Symp. Dig. Vol. 3*, pp. 1029-032, May 1995.
- [46] J. Verspecht, “Large signal network analysis”, *IEEE-Microwave magazine, Vol. 6, Issue 4, pp.82-92, December 1995.*
- [47] Wendy Van Moer, Yves Rolain “An Improved Broadband Conversion Scheme for the Large-Signal Network Analyzer”, *IEEE Trans. Instrumentation and Measurement, Vol. 58, No. 2, pp. 483-487, February 2009.*
- [48] P. S. Blockley, D. Gunyan, and J. B. Scott, “Mixer-based, vector corrected, vector signal/network analyzer offering 300 kHz–20- GHz bandwidth and traceable phase response,” in *IEEE MTT-S Int. Microwave Symp. Dig*, pp. 1497-1500, June 2005.
- [49] Wendy Van Moer and Liesbeth Gommé, “NVNA versus LSNA,” in *IEEE Microwave magazine*, pp. 97-103, Feb 2010.
- [50] Tektronix “XYZ’s of oscilloscopes”.
- [51] Thomas Grocutt, “Digital storage oscilloscope”, April 2000.
- [52] Tektronix “Sampling oscilloscope techniques” technique premier 47W-7209.
- [53] Jad faraj, “Développement et validation d’un banc de caractérisation de transistors de puissance en mode temporel impulsionnel ”, doctoral dissertation, 16 Dec 2010, University of Limoges.



## **CHAPTER II:**

# **Description of a Track & Hold Amplifier**

---



## Introduction

The technological restrictions of an ADC in terms of bandwidth and resolution make down conversion of the RF signal the key component in time-domain analysis. Until recently, the major components used for the down-conversion of microwave spectra into IF spectra have been the sampler or the mixer [1]. Both these components offer diverse specifications but the ever-growing need for bandwidth, dynamic range and reduction of the analog component density in the receiver stimulates research efforts for novel ideas. In this context, a new technique based on a Track and Hold Amplifier (THA) is presented which enables the reduction of the analog IF circuit complexity and offers a wide range of flexibility in terms of bandwidth and signal processing techniques.

## I. Track and Hold Operation

### I.1. Track and Hold circuit (T/H)

The function of the T/H is to Track and then sample an analog input signal and hold finally this value over a certain time span for subsequent processing. The T/H enables a fast acquisition (sample) of the analog signal and then holds the signal at a constant value until the next tracking phase is started. This T&H device converts an analog continuous-time signal into a digital (discrete time) signal [2].

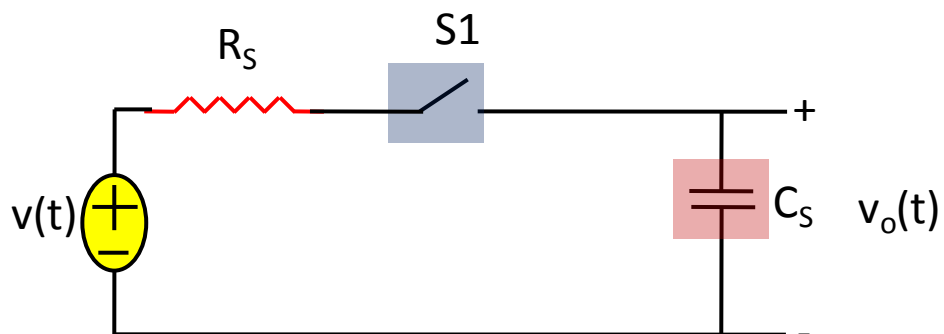


Figure II. 1: Basic T/H circuit

Fig.II.1 illustrates the simplest form of a T/H circuit [2]. The opening and closing instants of the switch are controlled by a sampling

command line called the clock. A transient response of a simple track and hold circuit is depicted in Fig.II.2.

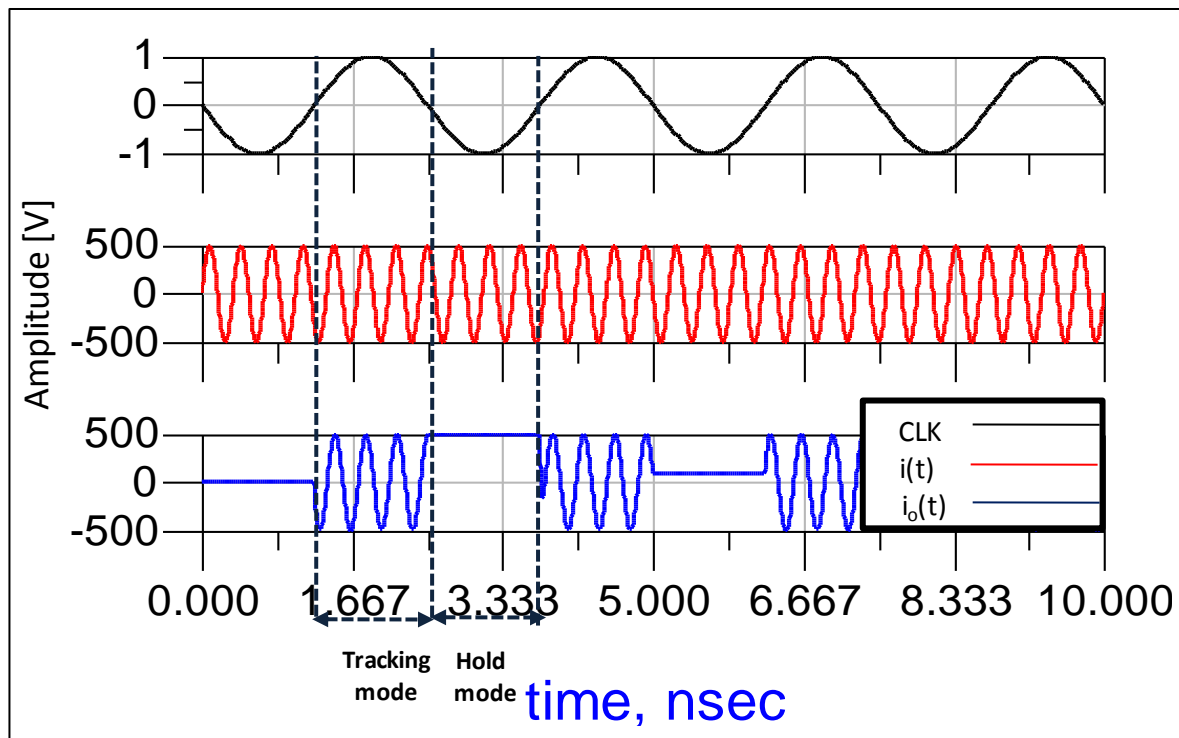


Figure II. 2: Transient response of ideal T/H circuit

It shows that during the one half of the CW clock signal the T&H circuit tracks the RF signal while for the second half when the switch is open it holds on to a constant value.

## I.2. Track and Hold Amplifier [THA]

The architecture of a THA as shown in Fig.2.3 allows a very wideband operation with an extremely fast response to an input signal. Therefore, the current state of the art structure uses the differential open-loop approach and the switching as well as the buffering transistors are bipolar. Regardless of the circuit details all THA's consist of four major components (Fig. II.3) the input amplifier, the energy storage device (capacitor), the output buffer, and the switching circuits. The differential signalling is employed to enhance the operational speed and the noise rejection [3]. The highly linear input amplifier buffers the input signal by presenting high impedance to the signal source and providing a large current gain to charge the hold capacitor. Fast switched emitter-followers are generally used for high-speed THAs

fabricated in bipolar technologies because it offers high-speed of operation [4], [5]. Analog switch connects the input buffer to the hold capacitors in the track mode, and separates them in the hold mode. In the *track* mode the voltage on the hold capacitor tracks the input signal while in the *hold* mode the capacitor retains the voltage present before it is disconnected from the input buffer. The hold capacitors which are the heart of the THAs are the energy storage devices and along with input buffers their size determines the bandwidth of operation.

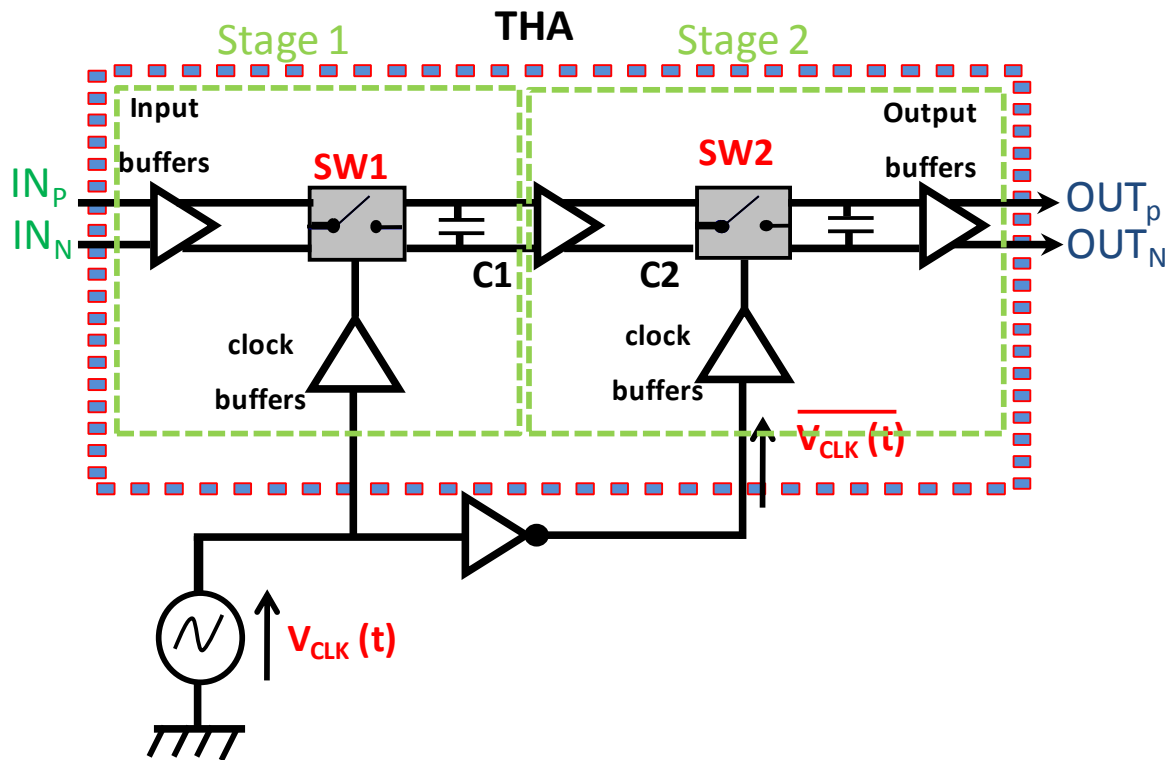


Figure II. 3: Block diagram of basic THA circuit.

The track and hold amplifier as shown in Fig.II.3 is composed of two stages driven by a common sinusoidal differential clock to ensure successive track and hold mode operations. For conventional voltage sampling circuits, as the case of THA, the frequency response is set by the product of resistance and capacitance in the loop [6] as shown in Fig.II.4. The transfer function during the tracking mode is obtained as follows:



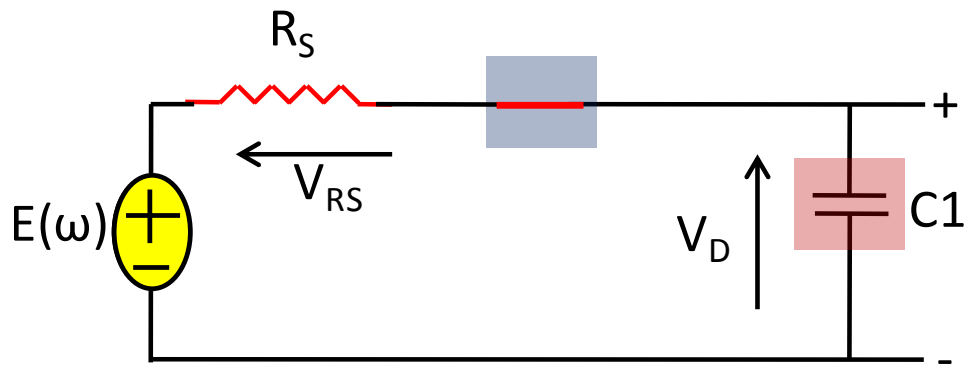


Figure II. 4: Basic T/H circuit

$$H(\omega) = \frac{V_D}{E} \quad \text{Eq:-80}$$

$$-E + V_{RS} + V_D = 0 \quad \text{Eq:-81}$$

$$V_D = \frac{I}{j\omega C} \quad \text{Eq:-82}$$

$$V_{RS} = IR_S \quad \text{Eq:-83}$$

$$E = j\omega CR_S V_D + V_D \quad \text{Eq:-84}$$

$$E = V_D(j\omega CR_S + 1) \quad \text{Eq:-85}$$

$$\frac{V_D}{E} = \frac{1}{j\omega CR_S + 1} \quad \text{Eq:-86}$$

$$\tau = R_S C \quad \text{Eq:-87}$$

$$\frac{V_D}{E} = \frac{1}{j\omega\tau + 1} \quad \text{Eq:-88}$$

Where  $\tau = R_S C_S$

$R_S$ = serial resistance

$C_S$ =hold capacitance

In order to make the phase shift as linear as possible, the value  $\tau\omega$  must be small and the **-3 dB and** bandwidth of the transfer function is also directly related to  $\tau$ . Therefore, the

high frequency performance of voltage sampling is directly limited by the time constant  $\tau$ . The value of the tracking capacitance and serial resistance must be small enough to satisfy the constant group delay and small magnitude attenuation.

The output buffer amplifier biased at relatively large currents to achieve high linearity, offers high impedance to the hold capacitor  $C_1$ , to keep the held voltage from discharging prematurely. The performance of the overall track-and-hold circuit depends upon the quality of the clock signal thus a clock buffer converts the input sine wave into Track/Hold control signals with low clock jitter.

Common errors which contribute in limiting the THA performance could generally be split into two groups:

- Timing-related errors
- Amplitude-related errors

The timing-related errors appear mainly due to the oscillator imperfections which refer to the fact that the output frequency of the oscillator is not exact but varies over the time in a random way. This is expressed by the phase noise and is often expressed in terms of a timing jitter of the oscillator. The amplitude error is a critical measure for a design of THA and is related to the phase error, which is critical measure in an oscillator design and could be expressed in Signal to Noise Ratio (SNR)

$$SNR = -20 \log(\omega * \Delta t_{rms}) \quad \text{Eq:-89}$$

Where  $\omega$  is the angular frequency of the input signal.

$\Delta t_{rms}$  is the RMS quantity of the time error.

The main amplitude-related error that occurs in the design of any THA in a bipolar technology is the so-called feed-through. Feed through [4], [5], [6] results in the appearance of the input signal on the hold capacitor during the hold phase due to the leakage of the signal through the base emitter junction capacitance of the switching transistor. Since high-speed THAs use small hold capacitors to prevent bandwidth reduction, the input signal feed-through is a critical figure for high-speed THAs. Often a feed-through attenuation block is used to attenuate this. Lowering the size of the switching transistor size can reduce the feed-through

effect, but it has also certain limits. Therefore the hold capacitor is to be selected with a minimal capacitance value and the existing feed-through is minimized by a proper compensation.

### I.2.1. Operating principle of THA

The operating principle of THA is described, by performing a transient ADS simulation using ideal components (switches and emitter follower amplifiers). The block diagram of the circuit is presented in Fig. II.5 [8], [9]. Note that THA is composed of two cascaded switches each switch being preceded by an emitter follower amplifier (EFA) (buffer). Each switch is driven by a CW but complementary signal. The emitter follower amplifier acts as buffer stage during the hold period and presents a high input impedance to avoid loading the source or draw current from it. It presents a low output impedance to act as voltage source to the load (buffers are also known as impedance transformers).

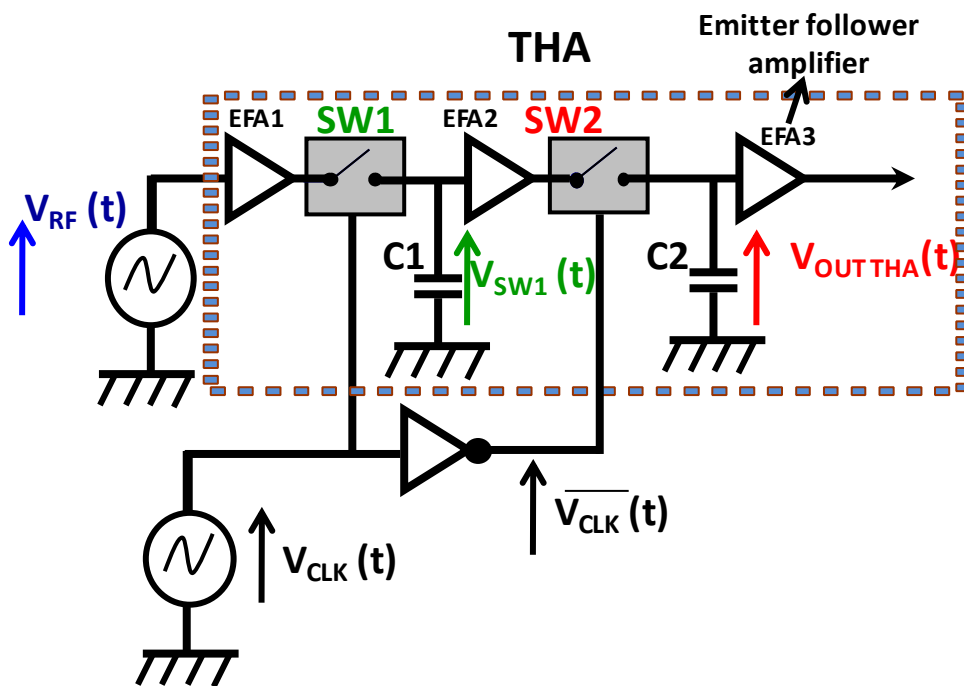


Figure II. 5: Block diagram of simulated THA schematic in ADS

A CW RF signal at 2.5 GHz is applied at the THA input and a transient analysis is performed. Two ideal switches (SW 1 & SW 2) are driven by a sine wave differential signal at 400 MHz (i.e.  $T_{clock}=2.5$  ns) as shown in Fig. II.6.

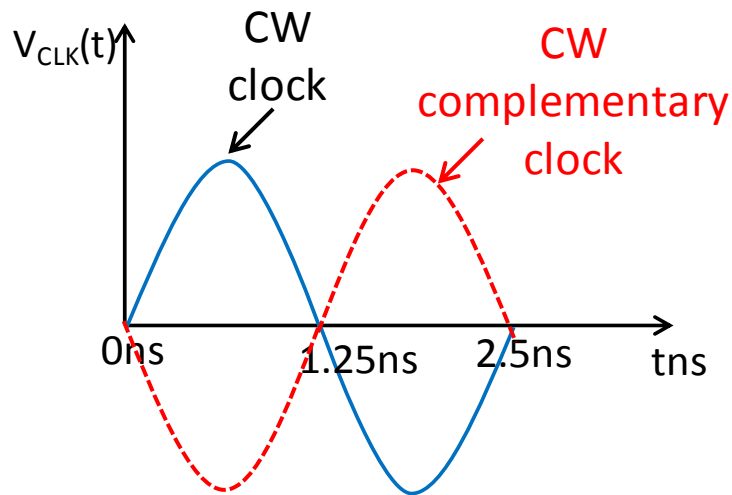


Figure II. 6: Clock Signal

The operation of the THA could be best explained in two stages:

- 1) SW1 tracks and holds the  $RF_{IN}$  signal

$$SW1 \begin{cases} V_{CLK} < 0 (ON) & 0 \leq t \leq \frac{T}{2} \text{ (0ns to 1.25ns) [track mode]} \\ V_{CLK} > 0 (OFF) & \frac{T}{2} \leq t \leq T \text{ (1.25ns to 2.5ns) [hold mode]} \end{cases}$$

- 2) SW2 tracks and holds the output voltage level of SW1

$$SW2 \begin{cases} \overline{V_{CLK}} < 0 (ON) & 0 \leq t \leq \frac{T}{2} \text{ (0ns to 1.25ns) [track mode]} \\ \overline{V_{CLK}} > 0 (OFF) & \frac{T}{2} \leq t \leq T \text{ (1.25ns to 2.5ns) [hold mode]} \end{cases}$$

In stage 1, the SW1 performs two functions on the instruction of the clock signal as explained in Fig. II.7. During the negative half of the clock cycle SW1 tracks the RF signal while during the positive half it holds on to the level at which the hold capacitor is charged. Similarly the SW2 performs same functions and is controlled by an inverted clock. As it precedes SW1 so it tracks and holds the output signal level of SW1 as depicted in Fig II.8

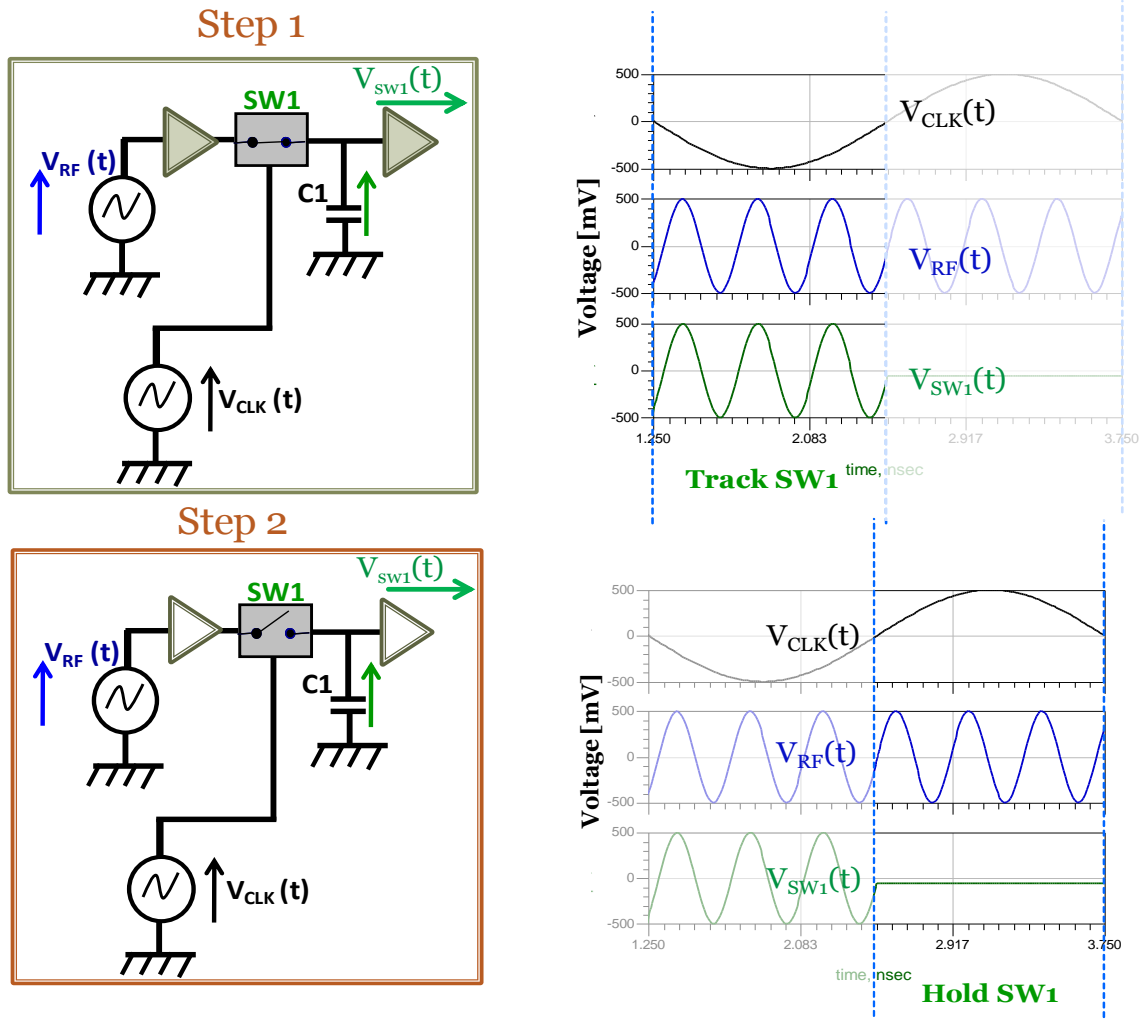


Figure II. 7: Operating principle of SW1 (track and hold)

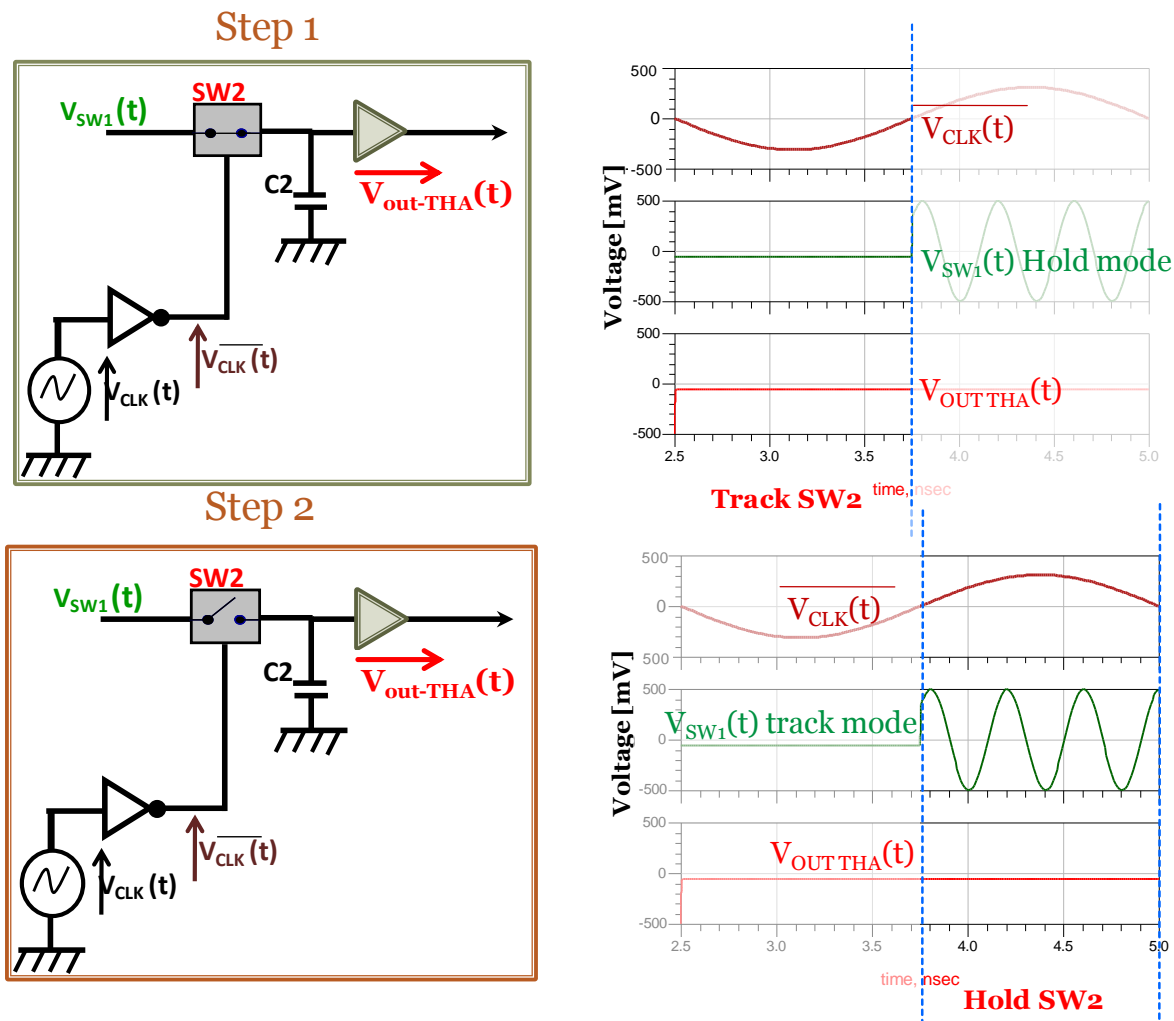


Figure II. 8: Operating principle of SW2 (track and hold)

At the output of the THA constant levels of RF signal (Fig.II.9) are obtained. These are the direct voltage levels of the input RF signal and the sub-sampling principle obeyed by the THA is described by the following equation:

$$T_{clock} = NT_{RF} + \frac{T_{RF}}{4} \tag{Eq:-90}$$

With  $N=6$ ,  $T_{RF}=0.4$  ns and,  $T_{CLK}=2.5$  ns.

It could be seen in this example that the equation is exactly the same as the one used in LSNA principle. The main difference between the two is that the output of THA is directly equals to the value of RF voltage signal due to the use of EFA. Using this sub-sampling principle, the THA output signal can be directly digitized by an ADC without using any IF circuitry. The clock rate of ADC should be higher or equal to the clock rate of THA.

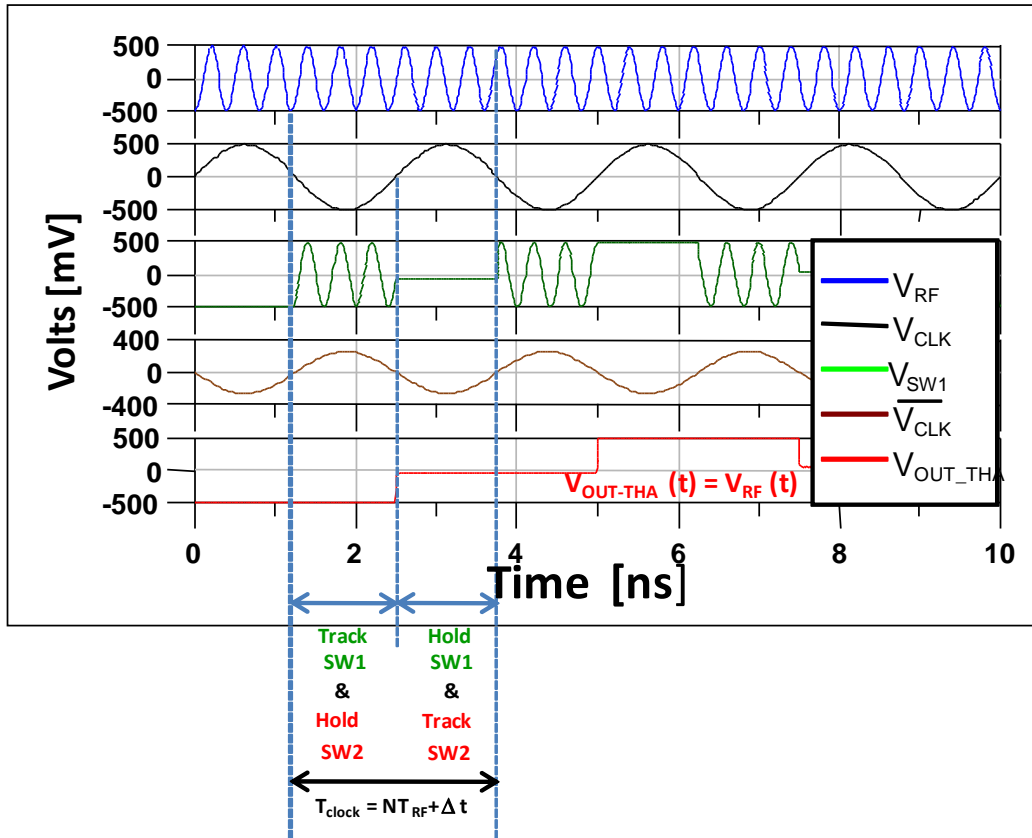


Figure II. 9: Complete operating principle of THA

The THA has an ideal conversion gain equal to unity due to the use of an Emitter Follower Amplifiers (EFA) at the output of each switch. The input EFA is highly linear and is used to decouple the source and the hold capacitance. The simulation result that is obtained here with and without EFA for a single stage is described in Fig. II.10. It can be seen that without using the EFA at the output of switch the capacitor is discharged during the hold state similarly as samplers.

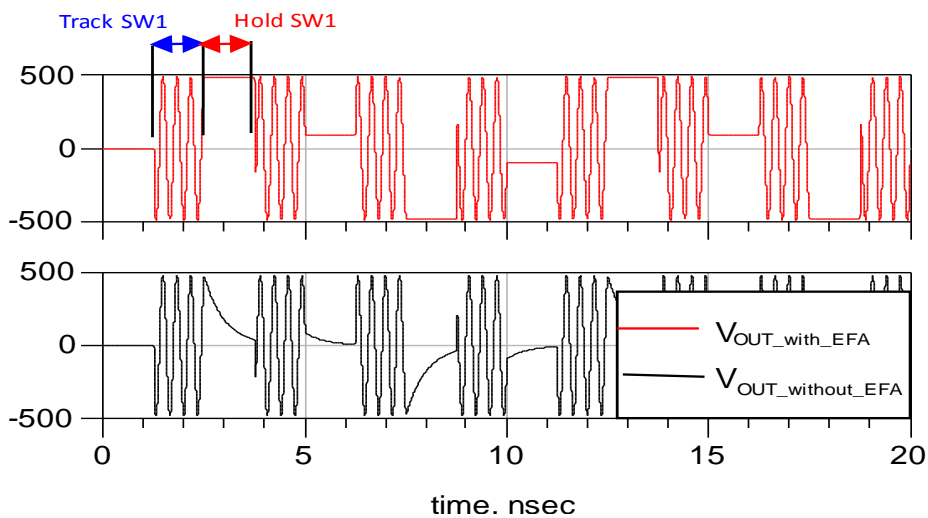


Figure II. 10: Output Voltage THA with and without EFA

## II. Characterization of THA

### II.1. InPHI THA

In order to improve the flexibility of a communication receiver and reduce the number of analog components a commercially available THA based on Indium Phosphide (InP) technology (InPHI 1321TH) is utilized Fig.II.11 [10]. InP technology is the fastest semiconductor technology in production today. Because of its inherent advantages, circuits made in InP typically outperform those made in traditional Gallium Arsenide (GaAs) and Silicon Germanium (SiGe) for high-speed applications. InP technology is also a cost effective solution for circuits. The selected THAs proposed have an analog input bandwidth of 13 GHz at small signal, 10 GHz at 0.5 V<sub>pp</sub> and 8GHz 1V<sub>pp</sub> input. A sampling rate that is as high as 2 GS/s is also achievable. THA's with a bandwidth of 18GHz are also available [11].

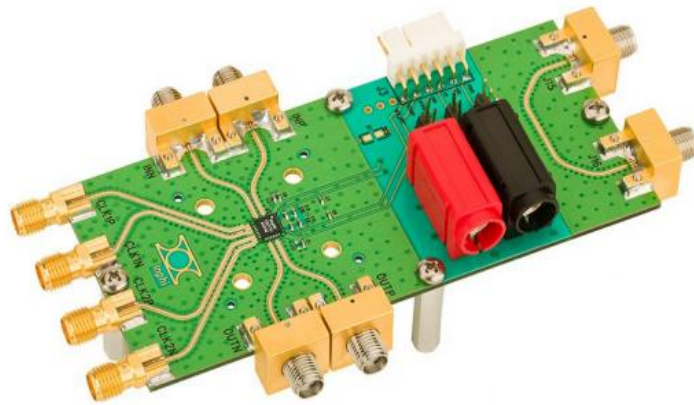


Figure II. 11: Inphi THA (1321TH).

The main characteristics of this Inphi THA are as under:

- Supports 2 GS/s sampling rate
- 13 GHz input bandwidth (small-signal)
- 10 GHz input bandwidth (0.5 V<sub>pp</sub>)
- 8 GHz input bandwidth (1 V<sub>pp</sub>)
- THD < -60 dB (1 GHz 1 V<sub>pp</sub> input)
- THD < -35 dB (10 GHz 0.5 V<sub>pp</sub> input)
- Ultralow aperture jitter: < 50 fs
- 0 dB Gain with up to 1 V<sub>pp</sub> out



- Differential master-slave architecture
- Multiple clock modes
- Fast rise time: < 25 ps (10-90%)
- Adjustable input termination voltage
- Single -5.2 V power supply
- Low power consumption: 1400 mW
- Available in 4mm square QFN package

To verify that the properties specified by the selected THA are indeed obtained under real operation, the THA was characterized in terms of power, linearity and bandwidth.

### II.1.1. Measurement setup

To characterize the THA, the measurement setup as shown in Fig II.12 is used.

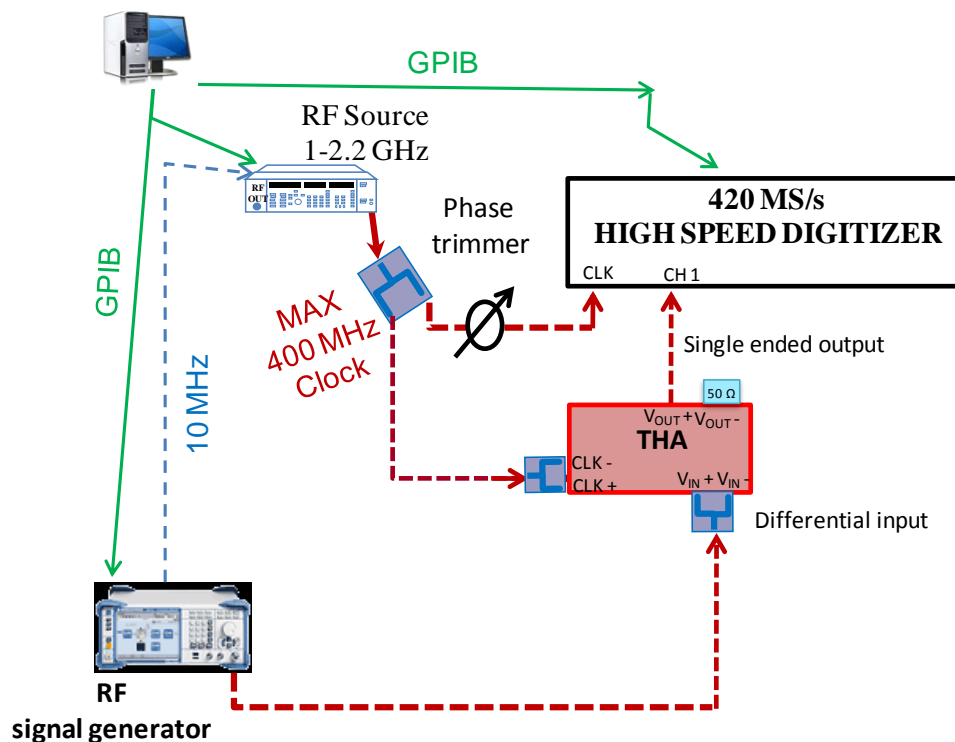


Figure II. 12: Measurement setup for THA characterization.

Both the THA and the ADC are driven by a common sinusoidal clock operating at maximum frequency of 400 MHz. A phase trimmer was provided on the ADC clock path to assure that the ADC sample interval falls within the hold interval of the THA. The THA was fed with a differential input signal but the single ended signal at the output was measured by

the ADC which means that a 3dB loss in power occurs. An RF sine source with a frequency that can be set from 1MHz to 30GHz is used to feed the THA. The two RF generators (Clock and RF input) are synchronized with a 10 MHz reference. All instruments are GPIB controlled and a specific program was developed to automatically perform the measurements. An ADC manufactured by Agilent was utilized that operates at a maximum sampling frequency of 420 Msamples/s and has a dynamic range of 12 bits. To characterize the linearity and the bandwidth the discrete time performance of the THA was evaluated [12].

### II.1.2. DC power

The Inphi (1321 TH) THA operates on a single -5.2V power supply. The measured DC power consumption of the device is

$$V_{ee} = -5.2V$$

$$I_{ee} = 0.26mA$$

$$P_{dissipated} = 1.352 W$$

The THA did not pose any thermal problems since a good thermal interface was provided between the bottom of the package and the ground. It does not require a heat sink when the case temperature does not exceeds maximum temperature of 85 degrees.

### II.1.3. Linearity

For a truly linear amplifier, the output power is a linear function of the input power. A linear amplifier produces an amplified and delayed replica of the input signal at its output, with a negligible or no harmonic distortion. As the THA contains both emitter follower amplifiers with unity gain and an emitter follower switch so both 1 dB gain compression and third-order intercept measurements are performed to determine the linearity of the THA [11], [12].

#### *II.1.3.1. Measurement of 1dB compression point*

When the device is driven to saturation, a nonlinear response appears at the output of the amplifier and the gain of the transistor is reduced. The point where the gain is reduced by

1 dB when compared to the small signal gain is called 1 dB compression point. At this point, the amplifier is no longer in the linear region rather compressing the signal.

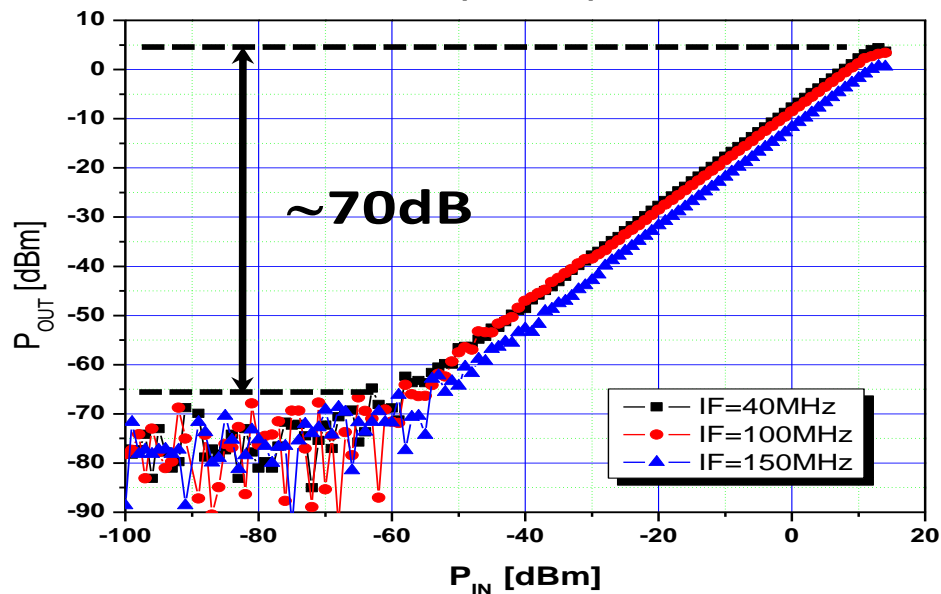


Figure II. 13: 1dB compression point of THA @ different CLK frequencies

In case of the THA the measured value for the 1 dB compression point was  $P_{1dB} = 7$  dBm as can be seen in Fig. II.13. Measurements of the output power versus the input power under three different operating conditions were made. In each experiment the power of  $RF_{IN}$  and the clock frequency is kept constant. It was ensured that the saturation of ADC does not affect the saturation of THA. By sweeping the input power level starting from very low power (close to the noise floor) to the saturation point one can also note that a dynamic range of almost 70 dB is achieved. It could be improved further if a differential amplifier were connected to the output of the THA.

### II.1.3.2. Intermodulation distortion (IMD)

The IMD is a measure for the presence of spectral lines at non harmonic frequencies which occurs for modulated signal having more than one tone. It's best described by inserting a two-tone signal at the input of the DUT. The spectrum at the output of the device consists of the original signals and additional intermodulation signals. These additional signals can cause interference within the original system or in other connected systems. When the intermodulation signals are of sufficiently large amplitude, they can overpower the signal of interest, resulting in interference and in extreme cases, loss of transmitted information. In the

two-tone experiment the device is excited by two equally spaced signals and it generates inter modulation products. These spectral products have frequencies that are obtained as the sum and difference of multiples of the fundamental tones. The most critical among all the possible intermodulation products is usually the third order one (at frequencies  $2f_1-f_2$  and  $2f_2-f_1$ ) as it usually conveys most power [11].

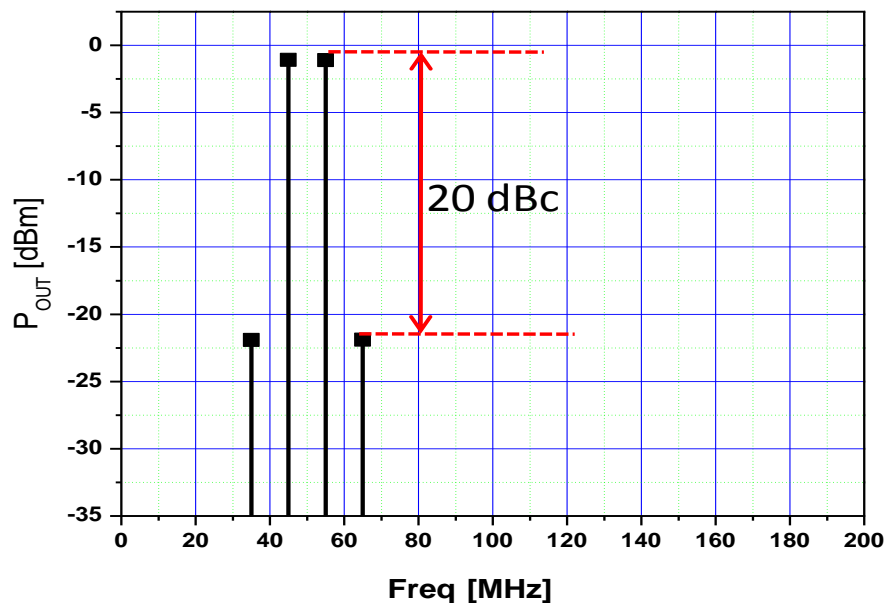


Figure II. 14: Intermodulation distortion [IMD]

As an example a two-tone experiment was performed, to measure the intermodulation distortion in THA. The DUT was excited by a two tone signal at 2.45 GHz with a spacing of 10 MHz (2.445 GHz & 2.455 GHz) and a  $F_{CLK}$  of 100 MHz. The  $RF_{IN}$  power level was set at 1dB compression point of the DUT. Third order harmonics ( $\pm 2f_2-f_1$ ) were noted at 35 MHz and 65 MHz respectively as shown in Fig.II.14. Third order IMD of maximum 20 dBc was noticed.

### II.1.3.3. Third Order Intercept (TOI) point

Intercept points are the points where the slopes of the fundamental linear behavior meet the linear extrapolation of the intermodulation product in a logarithmic chart of the output power versus input power. The third order intercept point is called  $IP_3$ . The input IP is represented as IIP and the output IP as OIP.

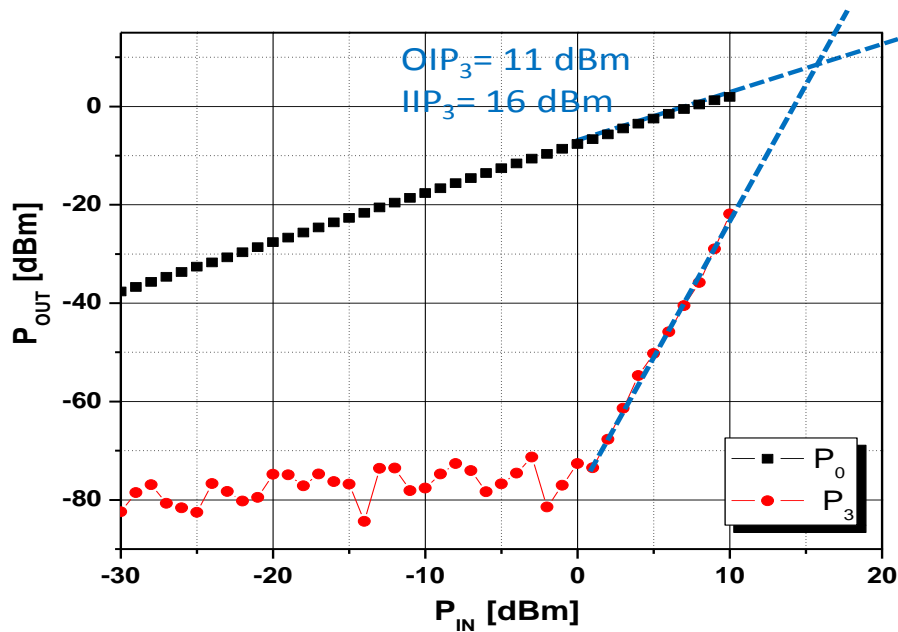


Figure II. 15: Input and output third order intercept points.

Here the THA is excited by two tone signal at fundamental frequency of 2.45GHz and a frequency spacing of 10 MHz. By sweeping the input power, we can plot both the fundamental (P<sub>0</sub>) and third order intermodulation power (P<sub>3</sub>) for both tones in dBm as shown in Fig. II.15. Dashed lines for both the fundamental (P<sub>0</sub>) and third-order (P<sub>3</sub>) powers are linear estimates to the data at input powers [11], [12]. By extrapolating the linear estimates to their intersection, we can calculate the TOI. By convention, TOI is defined as:

$$OIP_n = \frac{P_0 + (P_0 - P_n)}{n - 1} \tag{Eq:-91}$$

Where n = order of the harmonic.

For the measurement shown in Fig.2.13 OIP<sub>3</sub> and IIP<sub>3</sub> of 11dBm and 10dBm respectively were measured. The values obtained for IMD and TOI point are worse than the values obtained for mixer based instruments while similar values are obtained commercially available sampler based instruments.

#### II.1.4. Bandwidth of operation

The bandwidth is measured by sweeping the RF signal into the THA over a broad bandwidth. The insertion loss is measured over the whole band ranging from 1GHz to 27GHz and depicted in Fig. II.16. Note that upto 8 GHz a flat response is obtained which is the RF

bandwidth of the THA as specified in the data sheet. After this point the THA is driven to saturation and the output power level goes into compression.

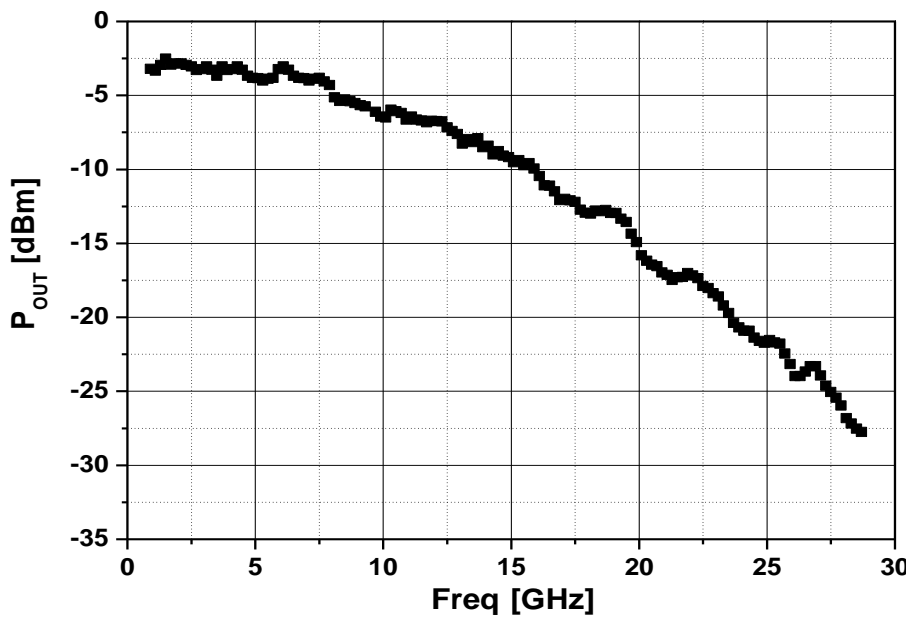


Figure II. 16: RF bandwidth of THA.

Another measurement was made to see the response of the THA over different intermediate frequencies. In this case the clock of the THA and the ADC was kept constant and the RF frequency was swept with a difference of 10 MHz and a fixed power level of 0 dBm.

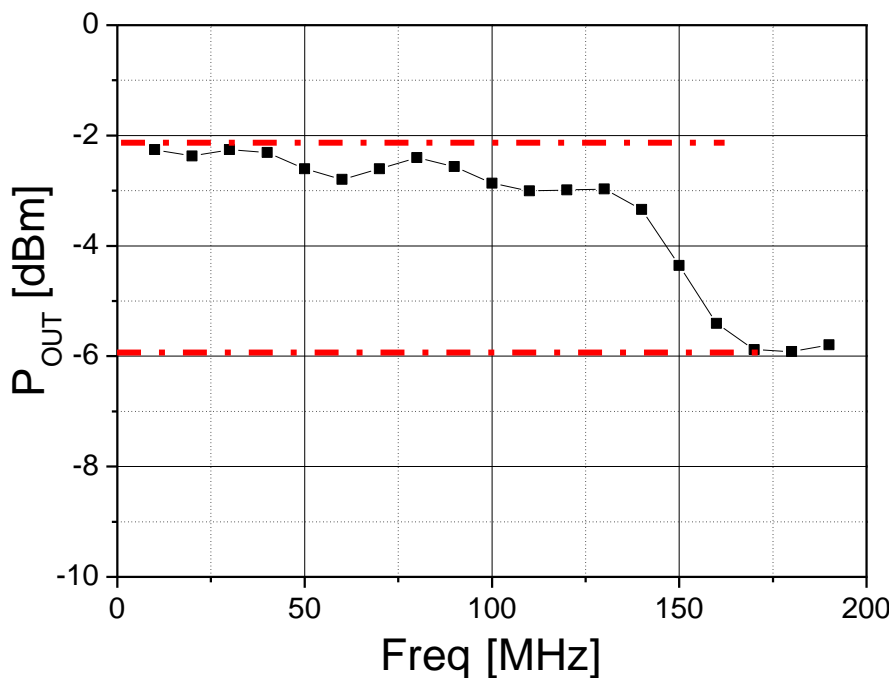


Figure II. 17: Insertion loss w.r.t. Intermediate Frequency

It is observed that the insertion loss varies in the full IF bandwidth from -2 to -6dB this is lower when compared to the sampler as will be discussed in section II.6. To further enhance the performance of THA in terms of noise and output power losses we use a differential amplifier at the output.

## II.2. Characterization of the THA with a Differential Amplifier

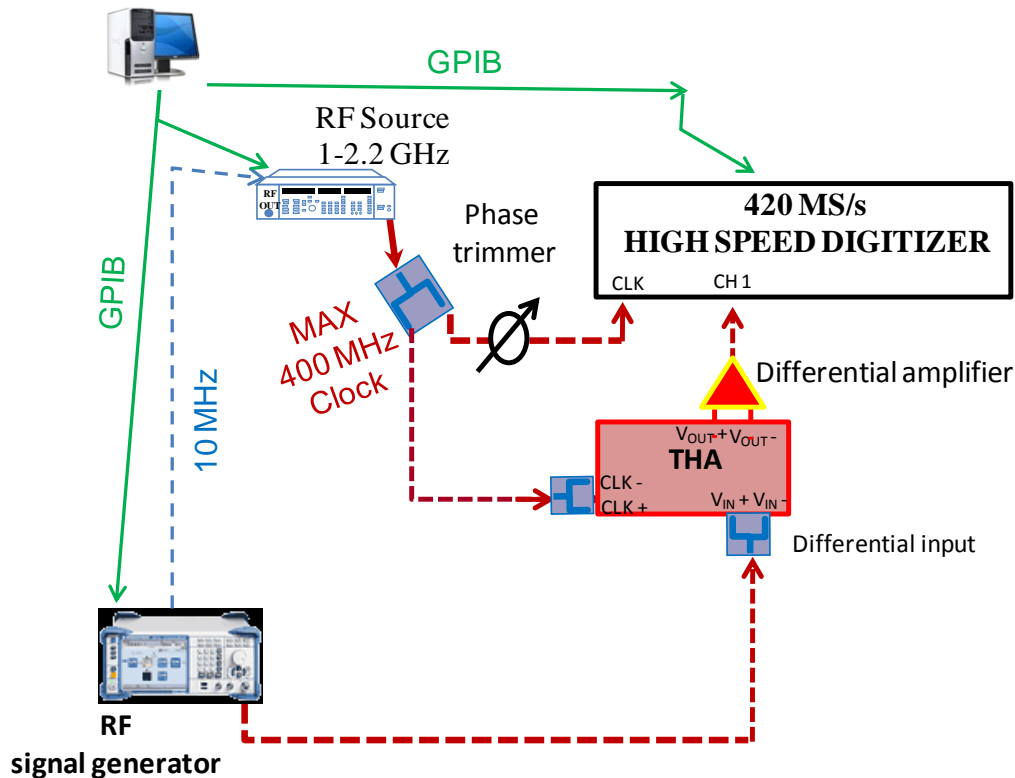
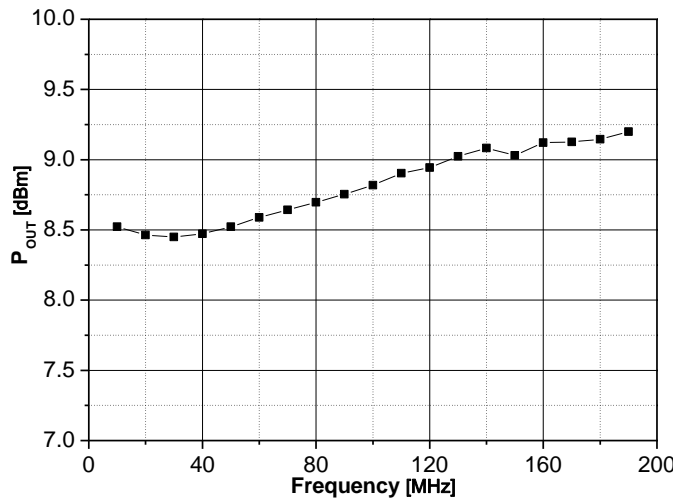
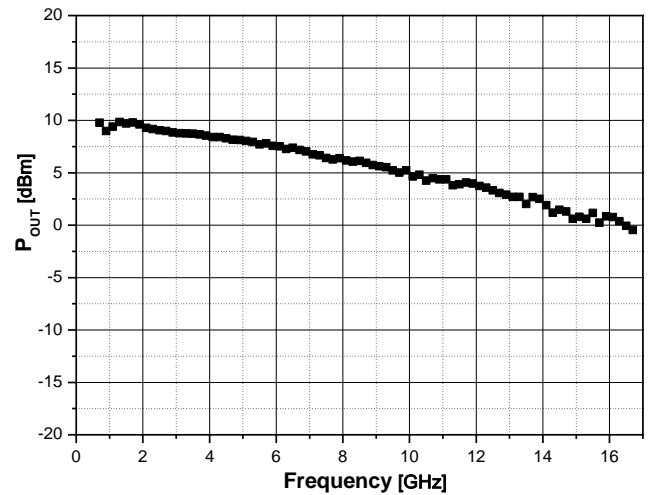


Figure II. 18 Measurement setup for differential amplifier

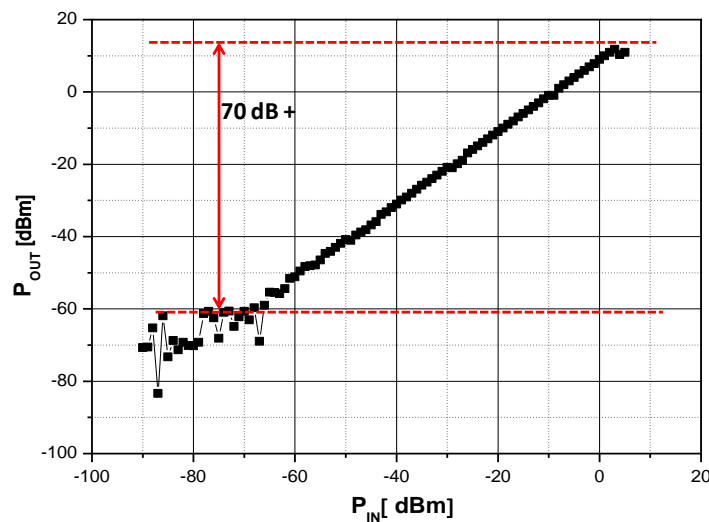
A differential amplifier to single ended by Euvis (L1370) is characterized to be added at the output of the THA. The test setup to characterize differential amplifier with THA based setup is represented in Fig.II.18. The differential signal present at the output of THA is fed into the amplifier which ultimately feeds the single ended signal to the ADC. The results obtained with respect to Gain, output power and bandwidth is depicted in Fig. II.19. A high gain of almost 10 dB is obtained until for an RF of 2 GHz while it depreciates until 4 dB at 13 GHz which is the RF bandwidth of THA. The dynamic range is increased by a few dB by adding the differential amplifier while there is no effect on RF bandwidth as a minimum gain of 5 dB gain is obtained until 13 GHz.



(II.16.a)



(II.16.b)



(II.9.c)

Figure II. 19: Characterization of differential amplifier (II.9.a) Insertion loss w.r.t. Intermediate Frequency (II.9.b). RF Bandwidth of differential amplifier. (II.9.c). Output power and 1dB compression point

### II.3. Comparison of THA and Sampler Characteristics

For comparison, a “conventional” Agilent sampler as used in the 8510 vector network analyzer was characterized in terms of power. The maximum input power here is limited to -15 dBm. A measurement covering a bandwidth of 200 MHz was made, and a conversion loss of around 40 dB was measured (Fig. II.20). As discussed earlier the sampler operates on the principle of charge sampling and charge sampling integrates the charge within a time corresponding to the fall time of the strobe pulse. This time corresponds to the sampling gate window of the sampler. Next, the Schottky diodes are reversed biased and the capacitors are



discharged through IF resistances which correspond to the “hold” mode of the sampler. The IF circuitry is then required to integrate this signal at the output of the sampler. This signal can then be digitized by an ADC having a clock frequency that is at least twice the cut-off frequency of the IF filter.

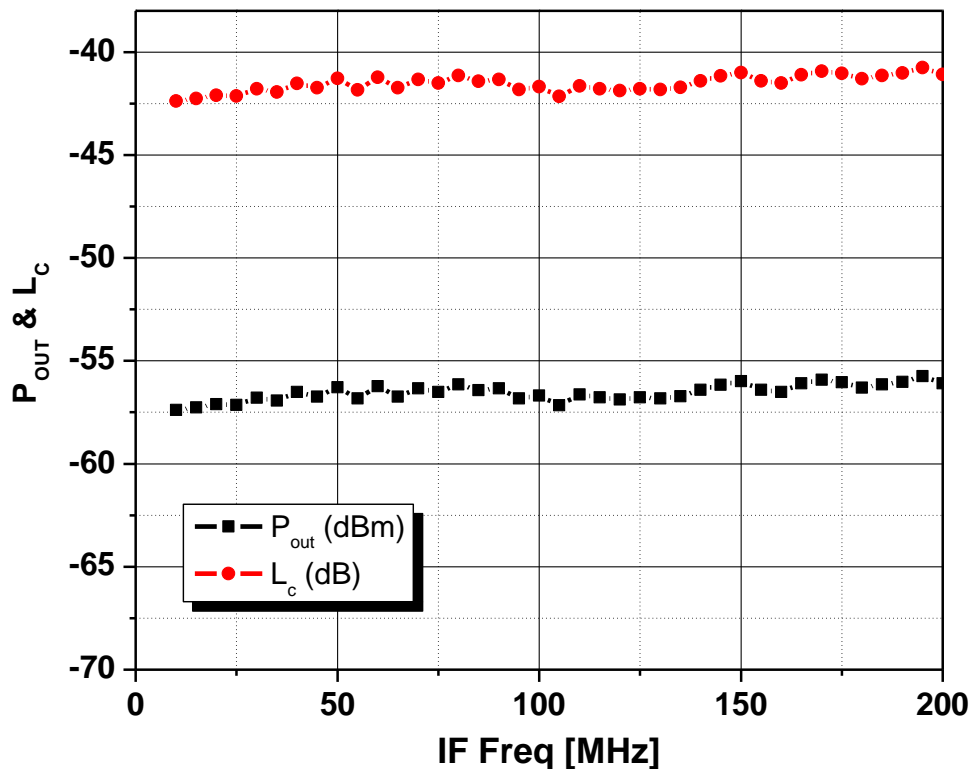


Figure II. 20: Output power and conversion loss ( $L_c$ ) of the Agilent Sampler.

The charge sampling bandwidth is directly dependent upon the width of the signal integrating window so. If the charging time of the capacitor is increased, the maximum useable bandwidth of the strobe signal decreases. The sampling efficiency of the sampler is very low. The conversion loss of the sampler is high (40 dBc). The maximum input power to the sampler is also limited, making it necessary to include IF circuitry comprising a linear power amplifier (around 55 dB gain) and a low pass filter before sending this data to the ADC. The linearity of the IF circuitry is critically important to avoid distortion of the measured data. Therefore a two stage amplification is used and followed by an anti aliasing filter. The component density in the IF path of sampler is therefore very high as shown in Fig. II.20.

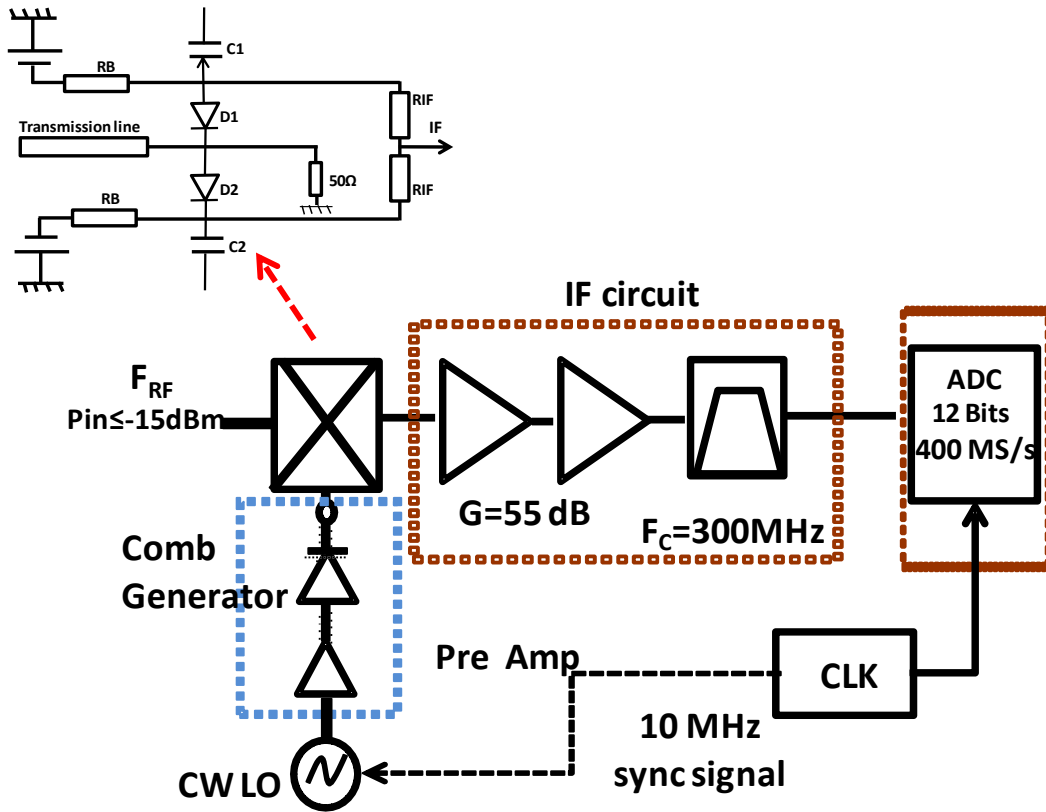


Figure II. 21: Block diagram of down conversion phenomenon using sampler

	IF BW [MHz]	Loss conversion [dBc]	P <sub>MAX</sub> Input [dBm]	RF BW [GHz]	Dynamic Range [dB]
THA	200	≤ 6	10	13	70
Sampler	200	≤ 40	-15	50	55

Table II. 1: Measurement results of INPHI 1321TH and available Agilent 8510 Sampler

A THA offers distinct advantages over sampler in terms of component density as the loss conversion of THA is very low which means that no IF circuitry is required (Fig. II.21). Using the sub-sampling principle, the THA output signal can be directly digitized by an ADC without any IF circuitry. This THA undergoes voltage sampling while sampler implements charge sampling as shown in Fig II.22. In the proposed setup the THA and the ADC share the same CW clock while in sampler based system two separate clocks: namely a pulse strobe signal for sampling and a CW clock ( $F_{ADC\_clock} = 2 * F_{cut\_of\_antialiasing}$ ) for ADC are required.

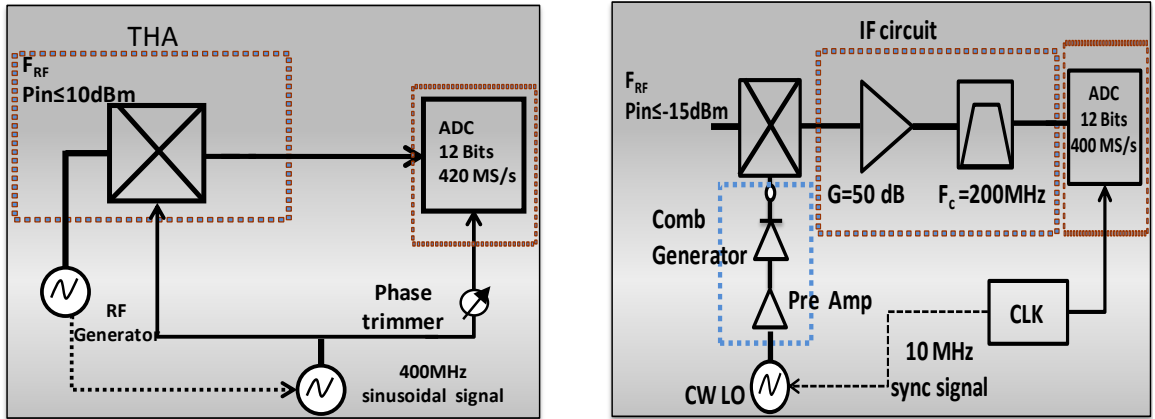


Figure II. 22: Comparison of THA and Sampler based down conversion circuitry

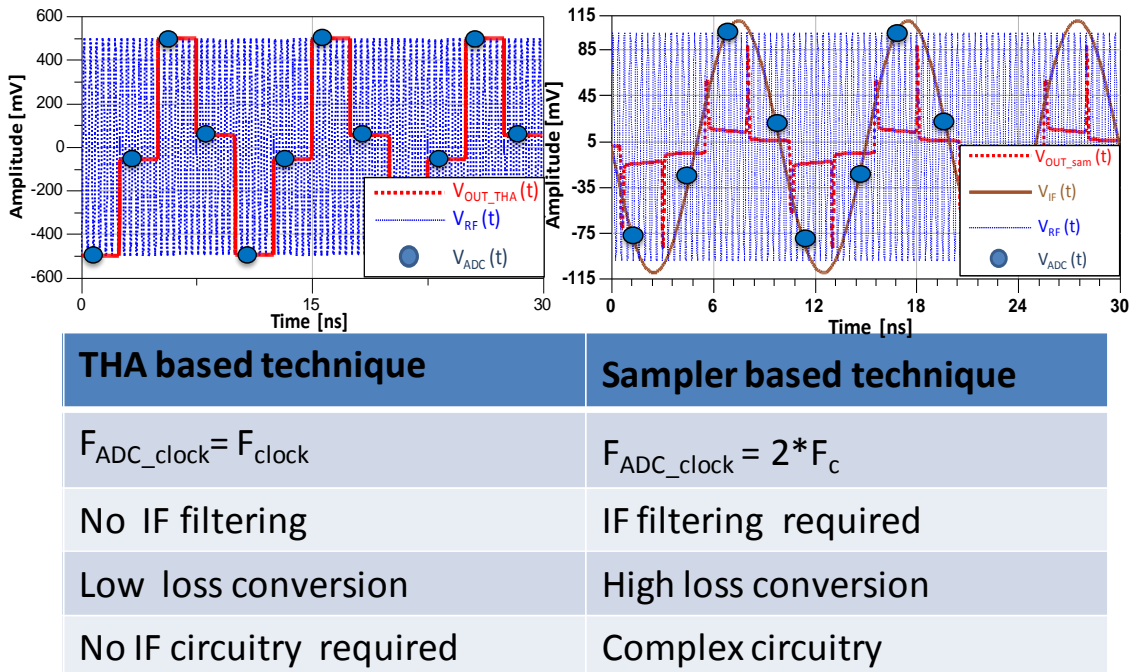


Figure II. 23: Main characteristics of THA and Sampler based systems

The bandwidth of THA in the end is limited by the emitter follower amplifiers (buffers) while the bandwidth of the sampler depends upon the fall time of the narrow pulses generated by the SRD. At the output of the THA constant voltage samples are obtained which are digitized by ADC thus no aliasing is produced. A phase trimmer is required on the ADC clock path to make sure that the ADC sample falls well within the hold interval of the THA. The reduction of the component density in the analog domain and the direct digitization of entire RF spectrum brings more flexibility in the receiver's performance

## Conclusion

Sub-sampling is an important aspect of a time-domain measurement system. It was typically implemented using samplers which operate on the charge sampling principle and have high conversion losses. This complicates the IF path as multiple stages of high gain linear amplifiers are required, and the amplifying stage is followed by a band-pass filter for anti aliasing purposes. In this work a novel technique is presented which is based on the use of THA. The complete working principle of THA has been demonstrated and a commercially available THA has been fully characterized in terms of power, bandwidth and linearity. The advantages of the wideband THA over the sampler are also highlighted for a conventional sub-sampling implementation. The reduction of the component density in the analog domain and the direct digitization of entire RF spectrum bring more flexibility in the receiver's performance. A much improved bandwidth of 200 MHz with enhanced 12-bit dynamic range has been achieved.

---

**BIBLIOGRAPHIE :**

---

- [1] Mark Kahrs, "50 years of RF and microwave sampling" *IEEE Transaction on microwave theory and techniques*, Vol. 51, NO. 6, pp. 1787-1805, June 2003.
- [2] Fang Lin Luo, Hong Ye, M. Rashid, "Digital power electronics and applications" Elsevier Academic press, USA, 2005.
- [3] Douglas Brooks, "Differential signals, rules to live by" circuit design a CMP media publication, ultra CAD design, October 2001.
- [4] Shogo Yamanaka, Kimikazu Sano and Koichi Murata, "A 20-Gs/s Track and Hold amplifier in InP HBT Technology" *IEEE Transactions on Microwave Theory and Techniques*, vol. 58, No. 9, pp. 2334-2339, February 2010.
- [5] J.Lee, A.Leven, J.S. Weiner, Y.Baeyens, Y. Yang, W.J.Sung, J.Frackoviak, R.F.Kopf, Y.Chen, "A6-b 12-GSamples/s track and hold amplifier in InP DHBT technology", *IEEE Journal of solid state Circuits Vol. 38, No. 9, , pp.1533-1539, September 2003*.
- [6] Gang XU, Jiren Yuan, "Comparison of charge sampling and voltage sampling", *43<sup>rd</sup> IEEE Midwest Symposium on Circuits and System, Lansing MI, pp. 440-443, 8<sup>th</sup> Nov 2000*.
- [7] David Smola, Hendrik v.d. Ploeg, Maarten Vertregt, Lucien Breems, Johan Huijsing and Kofi Makinwa, "Ultra high speed sampling track and hold amplifier in SiGe Bi-CMOS technology", *32<sup>nd</sup> European solid states circuit conference, Montreux, Switzerland, 19<sup>th</sup>-21<sup>st</sup> September 2006*.
- [8] Ahmed.S, M. Saad-el-dine, G. Neveux, T. Reveyrand, D. Barataud, J. Nebus, "Time-Domain Measurement System Using Track & Hold Amplifier Applied to Pulsed RF Characterization of High Power GaN Devices", *International Microwave Symposium, June 2011*.
- [9] Ahmed.S, M. Saad-el-dine, G. Neveux, T. Reveyrand, D. Barataud, J. Nebus, "4-Channel, High Dynamic Range Time-Domain Measurement System Using Track & Hold Amplifier Utilized for the Characterization and Linearization of High Power GaN Amplifiers", *International Journal of Microwave and Wireless Technologies*, vol.4, issue 01, pp. 71-79, 2011.
- [10] INPHI datasheet. "INPHI 1321TH 13 GHz 2Gsamples/s", [www.inphi.com](http://www.inphi.com).
- [11] Ahmed Sajjad, "Design and realization of Power amplifiers for hig power applications based on wide bandgap technologies", Master thesis, University of Gavle, January 2009.
- [12] Dale F.Dubbert, Terry L. Hardin, Gilbert G. Delaplain, "Characterization of a track and hold amplifier for application to a high performance SAR", Sandia report, Sandia national laboratories, July 2002, [www.ntis.gov](http://www.ntis.gov).

## **CHAPTER III:**

# **Envelope Measurement Test Bench**

---



## Introduction

Data processing is an important part of any modern measurement system. There are numerous digital or analog data processing techniques associated with measurement instruments. In modern wide band communication systems, that are vector modulated, the measurement of the signals benefit hugely from the capabilities of FFT analysis and other DSP techniques.

The sampling frequency and the resolution of the ADC play an important role when the type of processing is selected. As discussed in the previous chapter, the ADC used in this work is limited to 420Msamples/s taken at a resolution of 12bits. There is no IF circuitry present between THA and the ADC, which means that the ADC directly digitizes the down-converted RF signals. In order to fully utilize these properties an efficient processing technique is utilized so that time-domain waveform with complete non-linear information could be retrieved.

In this chapter we discuss the quadrature modulation/demodulation technique, which has the capability of vector detection (phase and amplitude) of the down-converted RF signal. A complete description of the quadrature sampling system is described. After the processing, this chapter discusses the calibration techniques used for the proposed measurement system. Absolute calibration techniques and their implementation are described. In the beginning, a single channel THA based time-domain measurement setup is built and measurements are made sequentially at the input and output of DUT. The result obtained is verified with the measurements of a commercially available single channel VSA. This device theoretically operates using the same principle. In the end, a four channel measurement test setup is built and a high power amplifier is fully characterized in terms of power and linearity using a continuous wave sinusoidal excitation and modulated signal excitations. The capability of the test bench is highlighted by extracting the two-tone transfer characteristics of PA. Measurements are processed and used for a digital pre-distortion linearization to enhance the linearity performance of the amplifier. The time-domain envelope and the carrier waveforms (voltage and current) along with third-order inter-modulation distortion (IMD) products with and without digital pre-distortion are also presented



## I. Inphase and Quadrature (IQ) Sampling

### I.1. IQ Data

The mathematical representation of a sine wave is

$$s(t) = A_C \cos(\omega_c t + \varphi_C) \quad \text{Eq:-92}$$

There are only three parameters of a sine wave that can be changed over time: the amplitude, the phase, or the frequency. Amplitude modulation (AM) changes only the magnitude of the signal. Phase modulation (PM) modifies only the phase of the signal. Frequency modulation (FM) looks similar to phase modulation, but the frequency is the controlled parameter, rather than relative phase. Phase and frequency are just different ways to view or measure the same signal change. Frequency is simply the rate of change of the phase of a sine wave, so these two parameters of the sine wave equation can be collectively referred to as the phase angle. Therefore, we can represent the instantaneous state of a sine wave with a vector in the complex plane having amplitude (magnitude) and a phase coordinate in a polar coordinate system. The phase is determined relative to a reference signal, which is chosen to be the carrier in most communication systems. The magnitude is either an absolute or a relative value. Polar diagrams are the basis of many displays that are used in digital communications, although it is also common to describe the signal vector in its rectangular coordinates: the  $I$  (In-phase) and the  $Q$  (Quadrature) components.

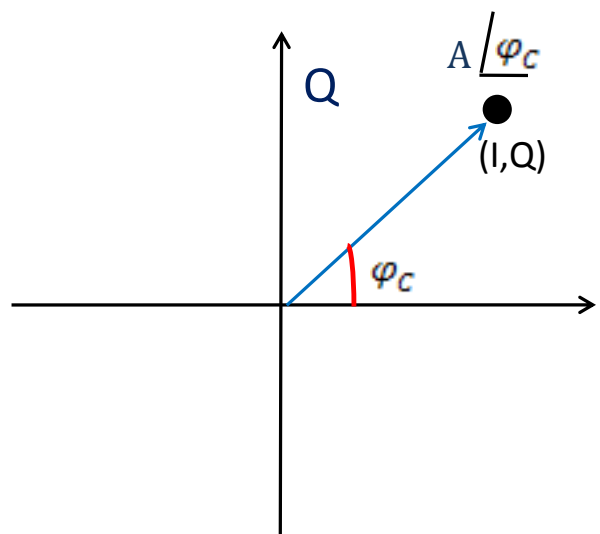


Figure III. 1: Polar representation of a sine wave

The I and Q data can be used to represent the changes in the phase and amplitude of the modulated signal. Given the message IQ data, its information can be encoded onto this sine wave signal as a modulated signal. During the IQ modulation process, the carrier signal modulates (mixes) with this information signal causing phase and amplitude changes. We can easily extract the original information signal by reading the IQ data changes of the resulting modulated carrier signal. The general form of a modulated signal can be expressed as:

$$S_m(t) = A(t)\cos(\omega_c t + \varphi(t)) \quad \text{Eq:-93}$$

Where  $A(t)$  is the time-varying amplitude,  $\omega_c$  is the radian frequency of the carrier ( $2\pi f_c$ ) and  $\varphi_c(t)$  is the time-varying angle. The in-phase and quadrature form can be expressed as:

Using a trigonometric identity

$$S_m(t) = A(t)\cos(\omega_c t)\cos(\varphi(t)) - A(t)\sin(\omega_c t)\sin(\varphi(t)) \quad \text{Eq:-94}$$

$$S_m(t) = I(t)\cos(\omega_c t) - Q(t)\sin(\omega_c t) \quad \text{Eq:-95}$$

$$I(t) = A(t)\cos(\varphi(t)) \quad \text{Eq:-96}$$

$$Q(t) = A(t)\sin(\varphi(t)) \quad \text{Eq:-97}$$

The phase and amplitude information can be obtained from the in-phase/quadrature components by the following equations:

$$\varphi(t) = \tan^{-1} \frac{Q(t)}{I(t)} \quad \text{Eq:-98}$$

$$A(t) = \sqrt{I(t)^2 + Q(t)^2} \quad \text{Eq:-99}$$

The distance between the origin and a point (represented by a black dot in Fig. III.1) will remain constant as long as the amplitude remains the same. This will generate a circle that rotates in the counter-clockwise direction around the origin as the phase of the RF carrier wave increases. For complex modulated signals both the amplitude and the phase vary and the modulation can be represented by a vectorial diagram where baseband signals can be

observed. A simple example explains this phenomenon for a pulse modulated signal. A simple pulse modulated signal is represented by the convolution of a rectangular signal and Dirac comb function as represented Fig. III.2.

$$A(t) = \text{rect}_\tau(t) * \sum_{k=0}^N \delta(t - kt)$$

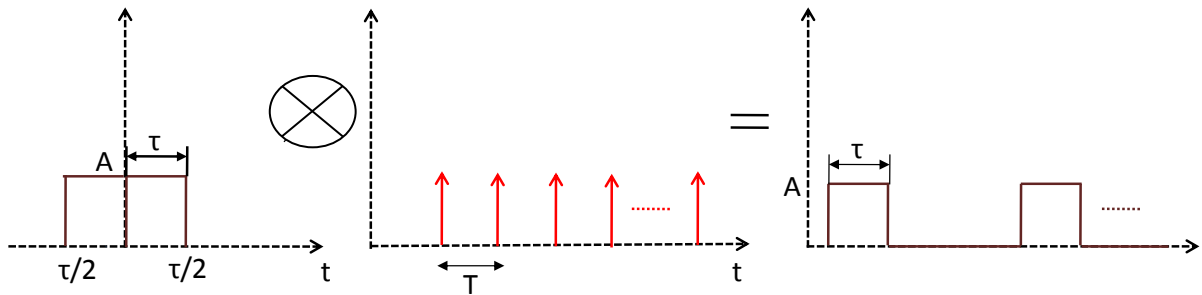


Figure III. 2: Time-domain convolution of rectangular and comb dirac function

If we supposed that  $\varphi(t) = 0$ , then using Eq.96 and 97 the values of  $I(t)$  and  $Q(t)$  are obtained as follows:

$$I(t) = A(t)(\cos(0)) = A(t)$$

$$Q(t) = A(t)(\sin(0)) = 0$$

Thus using Eq. 98 and 99 phase and amplitude values are obtained. The associated constellation diagram is shown in Fig. III.3.

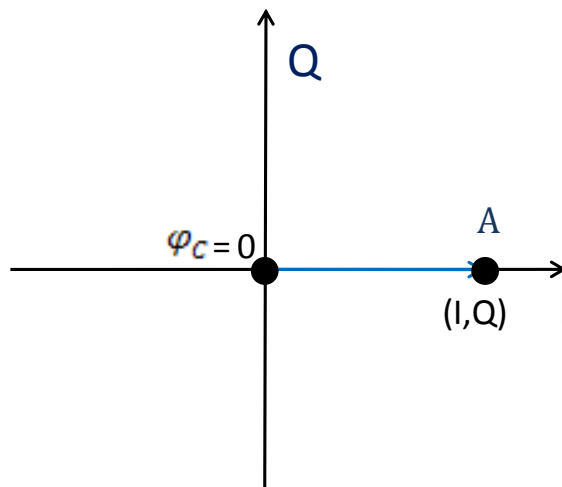


Figure III. 3: Constellation diagram when phase =0

$$\varphi(t) = \tan^{-1} \frac{0}{A(t)} = 0$$

$$A = \sqrt{(A(t))^2 + (0)^2} = A(t)$$

### I.1.1. Quadrature sampling

Magnitude and Phase demodulation of an encoded high frequency carrier signal was always a problem. By reducing the complexity of the IF circuitry in the analog domain and using direct digitization of the entire RF spectrum, more flexibility is brought in the receiver's performance. The boundary between analog to digital conversion and digital computation has been moved as THA and ADC share the same sinusoidal clock without IF analog circuitry.

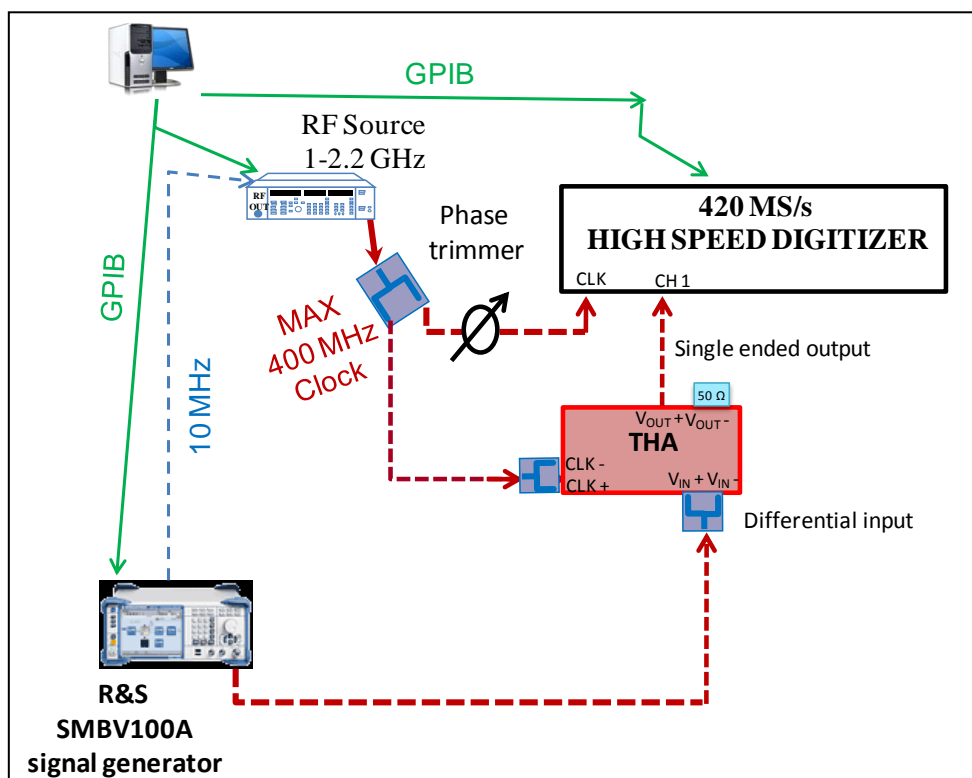


Figure III. 4: Single channel down-conversion setup

The down-conversion channel used in the proposed measurement set up is shown in Fig. III.4 and the sub-sampling quadrature sampling phenomenon is described by the following equation:

$$T_{\text{Sampling}} = NT_C + \frac{T_C}{4} \tag{Eq:-101}$$

Where  $T_C$  = time period of the RF signal  $s(t)$

$N$  = closest harmonic of the sampling frequency

$T_{\text{sampling}}$  = sampling time period of the common clock

Using quadrature sampling the resulting  $T_{IF}$  signal is  $T_{IF} = \frac{T_C}{4}$

If the ratio between  $\frac{F_{\text{sampling}}}{F_{IF}}$  is set to four which means that the ADC samples at exactly four times the IF signal then inphase and quadrature components could easily be extracted by digital mixing.

$$s(t) = A \cos(\omega_{\Delta T} t + \varphi_t) \quad \text{Eq:-102}$$

Where:

$$\omega_{\Delta T} = 2\pi f_{IF} = 2\pi \frac{1}{T_{IF}}$$

If  $\frac{F_{\text{sampling}}}{F_{IF}} = 4$  then,

$$4T_{\text{sampling}} = T_{IF}$$

Eq:-103

$$\omega_{\Delta T} = 2\pi \frac{1}{4T_{\text{sampling}}}$$

Using Eq.102 and 103 we get:

$$s(t) = A \cos\left(2\pi \frac{1}{4T_{\text{sampling}}} t + \varphi_t\right) \quad \text{Eq:-104}$$

Now using Eq.99:

$$s(t_k) = A \cos\left(\frac{\pi t_k}{2T_{\text{sampling}}}\right) \cos(\varphi_{t_k}) - A \sin\left(\frac{\pi t_k}{2T_{\text{sampling}}}\right) \sin(\varphi_{t_k}) \quad \text{Eq:-105}$$

From Eq. 96 and 97

$$I(t_k) = A \cos(\varphi_{t_k})$$

$$Q(t_k) = A \sin(\varphi_{tk})$$

So rewriting Eq. 105 we get

$$s(t_k) = I(t_k) \cos\left(\frac{\pi t_k}{2T_{\text{sampling}}}\right) - Q(t_k) \sin\left(\frac{\pi t_k}{2T_{\text{sampling}}}\right) \quad \text{Eq:-106}$$

$$s(t_k) = I(t_k) \cos\left(\frac{\pi}{2}k\right) - Q(t_k) \sin\left(\frac{\pi}{2}k\right) \quad \text{Eq:-107}$$

Where  $k(\text{sample no.}) = \frac{t_k}{T_{\text{sampling}}}$

$$s(t_k) = \begin{cases} \pm I(t_k), & k = \text{even} \\ \pm Q(t_k), & k = \text{odd} \end{cases} \quad \text{Eq:-108}$$

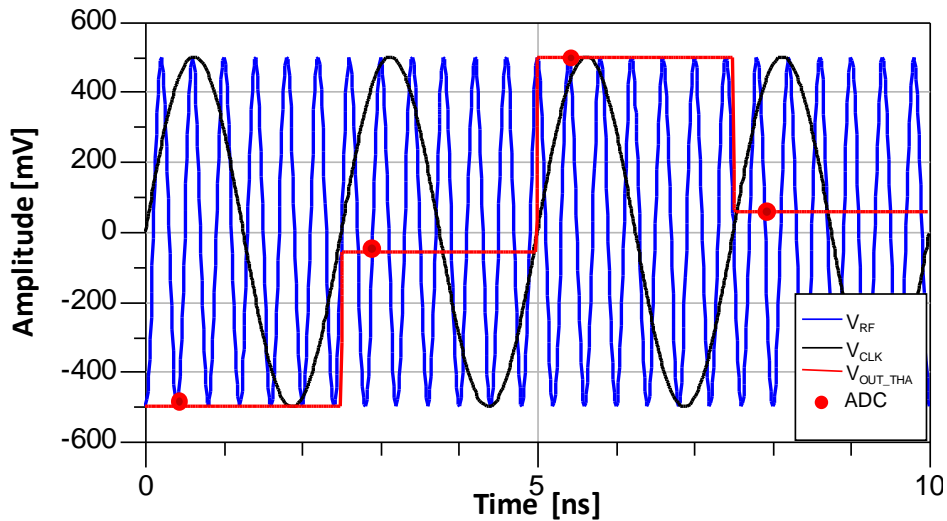


Figure III. 5: Samples acquired by ADC

Fig.III.5 describes the samples acquired by the ADC at the discrete sample values of THA which follows the sub-sampling. The samples could easily be distinguished between I and Q values due to direct RF sub-sampling and digital mixing. The quadrature IQ samples in the IQ diagram have a phase difference of  $\frac{\pi}{2}$  as explained in Fig.III.6.

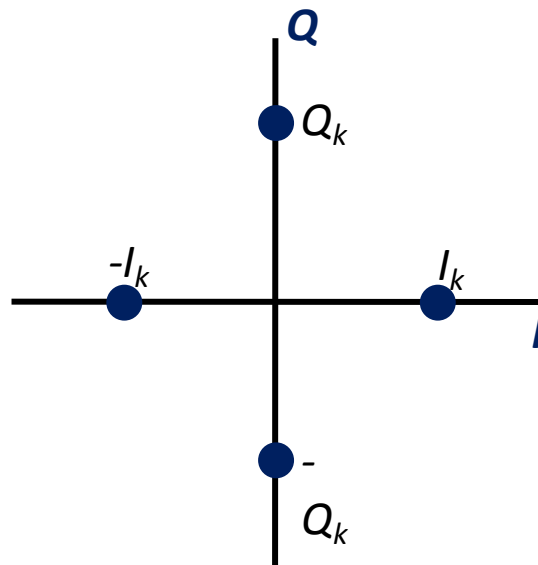


Figure III. 6: IQ data for Quadrature sampling

When the acquired samples are sorted between I and Q data, then the number of samples for the I and the Q become half. To accurately interpret the acquired signal based on the sampling frequency the number of samples should be equal to the acquired samples for both I and Q data. To solve this problem spline interpolation technique was used.

## II. Calibration

### II.1.1. Introduction

The word calibration in RF and microwave engineering signifies removing systematic measurement errors. Broadly speaking, calibration is the process of determining the relationships between the readings obtained by a measuring instrument or system and the applicable units of some defined system of measurement. Systematic errors are repeatable and could be mathematically modeled by using specific correction techniques. Other error like the random errors are non repeatable measurement variations and are unpredictable (jitters). An RF and microwave instrument consists of both active and passive devices as shown in Fig. III.7. Passive devices include the RF cables, couplers, connectors, attenuators and adapters. RF cables when used at microwave frequencies have an electrical length which cannot be neglected compared to the electromagnetic wavelength of the signals. It behaves as a lossy transmission line with a certain delay and characteristic impedance. The skin effect losses also

take place in these cables. The couplers should be accounted for the transmission loss (ideally zero) between the input and output ports and the directivity in the incident and reflected ports. The electrical lengths and delays of the connectors and adapters should also be taken care of.

Active components within the measurement setup include frequency translation circuit (THA in our case) and the ADC. As described in chapter two, these components have been characterized in terms of linearity and made sure that they are not pushed towards saturation. Hence the nonlinear errors can be neglected as long as they are operating in the linear region. The signals at the input and output of these components are sine waves or sum of sine waves representing the high-frequency electromagnetic voltage waves. These signals can be represented by an amplitude and a phase in the frequency domain. Thus a complex numbers are often used and these complex numbers can be thought of being vector quantities. The calibration procedure has to take care of both quantities.

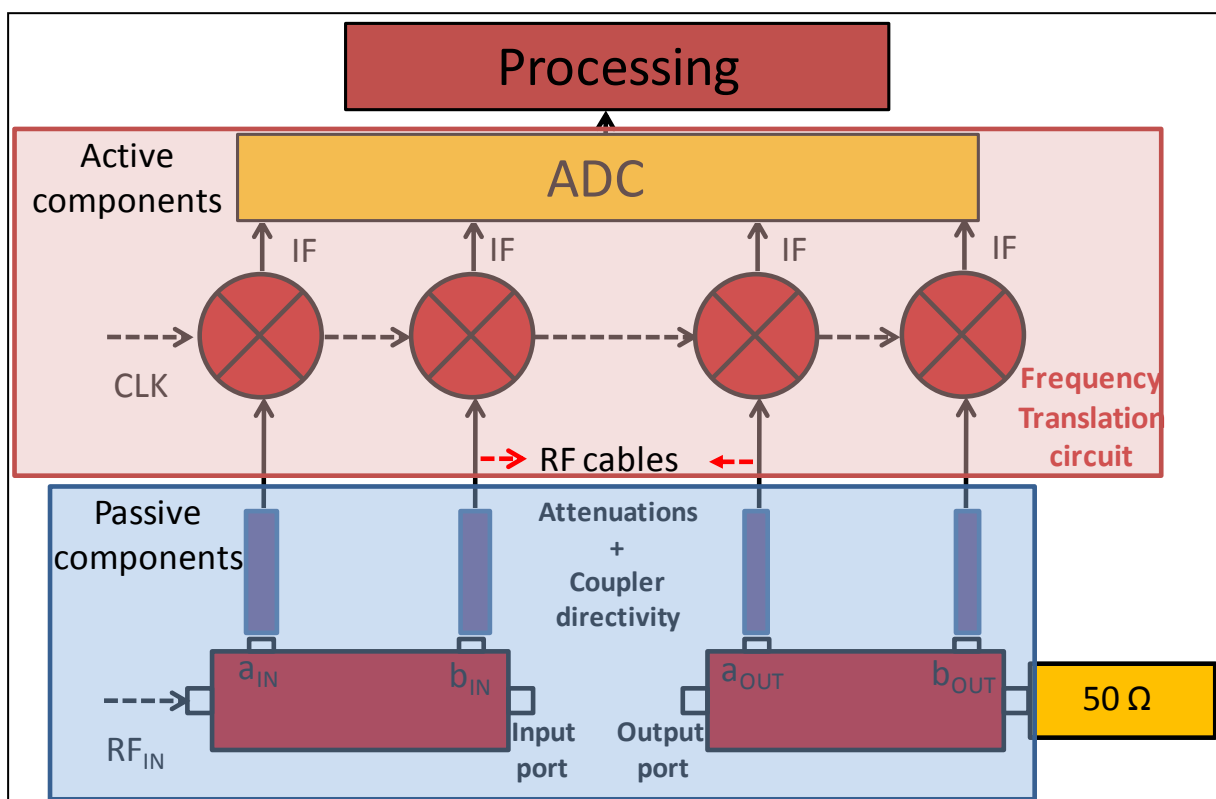


Figure III. 7: Basic time-domain measurement test-bench

At RF the calibration procedure allows to determine the relationship between the waves at two planes: the measurement plane and the reference plane as described in Fig III.8.



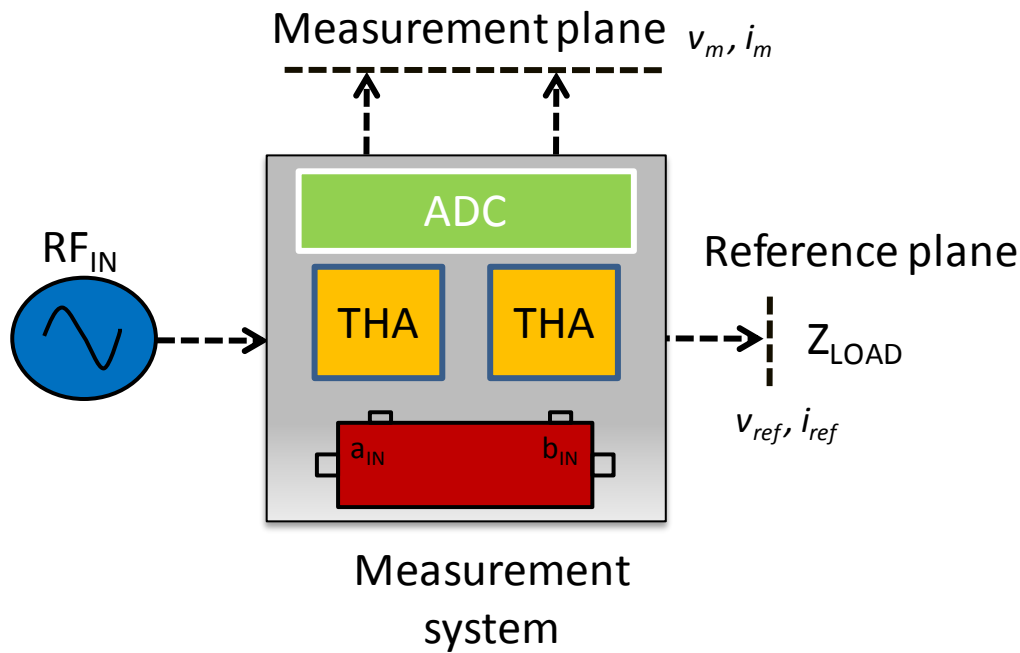


Figure III. 8: Measurement and ref planes

Considering operation at these planes, either the voltage and the current or the incident and the reflected power waves are used during the calibration. The relationship between the two planes could be expressed as simple convolution in time-domain, as for instance:

$$\begin{bmatrix} v_m(t) \\ v_{ref}(t) \end{bmatrix} = \begin{bmatrix} Z_{11}(t) & Z_{12}(t) \\ Z_{21}(t) & Z_{22}(t) \end{bmatrix} * \begin{bmatrix} i_m(t) \\ i_{ref}(t) \end{bmatrix} \quad \text{Eq:-109}$$

Responses      error matrix      excitation

$Z_{ij}(t)$  are the impulse response of the measurement system. To simplify this equation one can work in the frequency domain by simply converting the above relation using Fourier transforms to the frequency domain. The Eq. 109 becomes

$$\begin{bmatrix} V_m(f) \\ V_{ref}(f) \end{bmatrix} = \begin{bmatrix} Z_{11}(f) & Z_{12}(f) \\ Z_{21}(f) & Z_{22}(f) \end{bmatrix} \times \begin{bmatrix} i_m(f) \\ i_{ref}(f) \end{bmatrix} \quad \text{Eq:-110}$$

The convolution process is then replaced by a multiplication and sine wave generators with a variable frequency are used to excite the instrument. Combined with a specific set of well known standards that are connected instead of the DUT in the reference plane allow to extract the coefficients of the error matrix far easier than using time-domain approach. This is the reason why the calibration of RF instruments is commonly performed in the frequency

domain rather than in the time-domain even if the main objective of the measurement is to provide undistorted time-domain waveforms to the user. In this work, a frequency domain calibration approach is adopted for the proposed measurement test set up, even if the samples are acquired in the time-domain. The calibration process then needs preprocessing by the Fourier transforms and post-processing by the inverse Fourier transforms to obtain the waves. The calibration bandwidth is especially important in pulse modulated signals, where the spectrum is spread over a theoretically infinite band. To obtain a correct conversion from the frequency to time-domain the specified bandwidth depends on the pulse repetition period and is to be completely calibrated to reduce errors. This phenomenon is explained in the following chapter.

The calibration can be done in two steps:

- 1) A relative calibration (classical SOLT for S-parameters)
- 2) An absolute calibration (to obtain undistorted multi-harmonic waveforms)

The relative calibration is the procedure followed in the frequency domain by a vector Network Analyzer (VNA). It measures and calibrates the scattering parameters (S-parameters). S-parameters are dimensionless quantities thus relative calibration is done using only the predefined standards. Absolute calibration on the other hand is done with a pre calibrated power meter by measuring voltages waves acquired at the input and output port by the proposed measurement test bench and a power meter at the same time. The power of a voltage waves can be converted into amplitude by making use of the voltage wave characteristic impedance. The measurement result of the test-bench is then compared with the measurement result of the power meter, which is used as the reference standard.

### II.1.2. Calibration standards

Calibration is generally a process of comparison of measurements with the standards in the frequency domain. It involves measuring the actual voltage waves at the incident and reflected ports acquired by the test bench at the input and output of the DUT. The DUT consists of the known calibration standards that are connected at the input and output test ports (measurement planes). The values of the standards are known priori with an accuracy that's higher than the accuracy of the instrument to be calibrated. Different calibration techniques exist based on different error models and set of standards. The definition of

calibration standards and types are adopted for each calibration technique. Typical standards used to perform a calibration are Short, Open and Load. Each standard has precisely known impedance, both in magnitude and phase as a function of frequency. The standard is determined by the use of mathematical models of the electrical characteristics (delay, attenuation and impedance) of each calibration standard. These electrical characteristics can be mathematically derived from the physical dimensions and material properties of each calibration standard or from its actual measured response with a system that has a higher accuracy [7], [8].

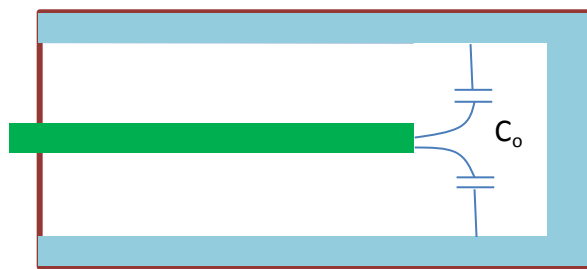


Figure III. 9: Open circuit of coaxial type

The reflection coefficient of an ideal open of zero length has amplitude of 1 and phase of 0 for all frequencies Fig III.9. At microwave frequencies however, the value of the magnitude and phase of an open are affected by radiation loss and capacitive fringing fields, respectively. Radiation losses are considerably reduced using shields. The fringing capacitance could not be removed and causes an additional phase shift. This frequency dependent phase shift can be modeled by a Taylor series approximation. For frequencies until 4 GHz it is sufficient to consider a third order expansion.

$$C_e(f) = C_0 + C_1f^2 + C_2f^3 + C_3f^3 \quad \text{Eq:-111}$$

The impedance and the reflection coefficient resulting from this open standard are defined as

$$Z_{open} = \frac{1}{j\omega C_e(f)} \quad \text{Eq:-112}$$

$$\gamma_{open} = \frac{Z_{open} - Z_o}{Z_{open} + Z_o} \quad \text{Eq:-113}$$

Where  $Z_o$ = characteristic impedance

The values of  $C_0$ ,  $C_1$ ,  $C_2$  and  $C_3$  are provided by the standards manufacturer.

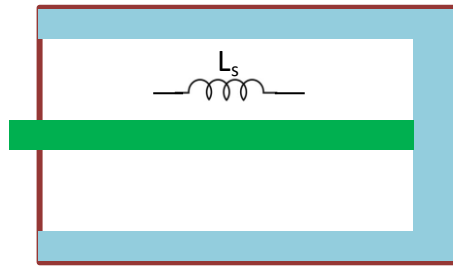


Figure III. 10: Short circuit of coaxial type

The reflection coefficient of an ideal short Fig. III.10 of zero length has a magnitude of 1 and a phase of  $180^\circ$  at all frequencies. At microwave frequencies, however, the residual inductance can produce additional phase shift. Since the inductance is known and repeatable, this phase shift can be accounted for during the calibration. Again a Taylor series approximation of order 3 is used to model the residual inductance.

$$L_s(f) = L_0 + L_1f^2 + L_2f^3 + L_3f^3 \tag{Eq:-114}$$

$$Z_{short} = j\omega L_s(f) \tag{Eq:-115}$$

$$\gamma_{short} = \frac{Z_{short} - Z_0}{Z_{short} + Z_0} \tag{Eq:-116}$$

The values of  $L_0$ ,  $L_1$ ,  $L_2$  and  $L_3$  are provided by the standards manufacturer.

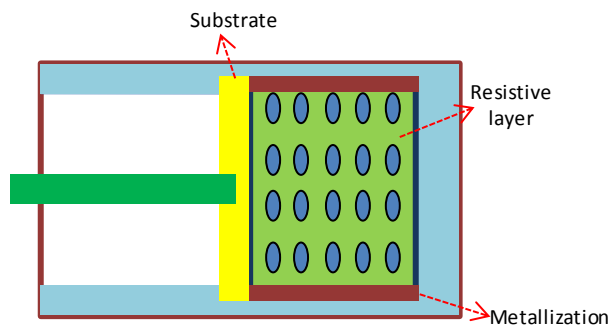



Figure III. 11: load circuit of coaxial type

An ideal load standard Fig.III.11 has reflection coefficient of magnitude 0 and this standard is approximated by a resistive termination the value of which matches the characteristic impedance which is normally 50Ω. For microwave frequencies resistors are best realized as plane circuits.


### II.1.3. Error vector calculation [5]

As discussed earlier a calibration compares measured and a priori known values of set of standards in the frequency domain. This means that the measured values are compared with the known values (SOLT standards in this work) and then based on this comparison a mathematical model of the instrument is formulated. A calibration technique requires an error model and this model is assumed to be linear. The raw measured data and the actual measured data are related by a linear transformation. The model used for this linear relationship is the same as used for relative calibration technique in a VNA. This error model is 16-element matrix and an important assumption made in this error model is that there exists no cross talk between ports. It means that the waves don't have any physical relationship among each other.


$$\begin{bmatrix} a_{c1}^N \\ b_{c1}^N \\ a_{c2}^N \\ b_{c2}^N \end{bmatrix} = \begin{bmatrix} 1 & \beta_1^N & 0 & 0 \\ \gamma_1^N & \delta_1^N & 0 & 0 \\ 0 & 0 & \alpha_1^N & \beta_1^N \\ 0 & 0 & \gamma_1^N & \delta_1^N \end{bmatrix} \begin{bmatrix} a_{m1}^N \\ b_{m1}^N \\ a_{m2}^N \\ b_{m2}^N \end{bmatrix} \tag{Eq:-117}$$



Corrected  
travelling  
waves



Relative  
calibration  
coefficients



Measured raw  
travelling  
waves

Where:

$a_{c1}^N, b_{c1}^N, a_{c2}^N$  and  $b_{c2}^N$  represent the corrected incident and reflected waves at the input (port 1) and output port (port 2) of the DUT. The subscript  $c$  denotes a corrected measurement and subscript 1 denotes the port number.

$a_{m1}^N, b_{m1}^N, a_{m2}^N$  and  $b_{m2}^N$  represent the measured raw incident and reflected waves at the input (port 1) and output port (port 2) of the DUT. The subscript  $m$  denotes raw measurement and subscript 1 denotes port number.

The superscript N stands for the frequency of the calibration. The procedure is to be followed for each frequency of interest. In the case of a pulsed signal the value of N is theoretically infinite but we define a finite value of N to have minimum errors within the bandwidth.

This error model depicts the assumed linear relationship between the measured and the corrected travelling waves that are acquired by the measurement test-bench on a frequency by frequency basis. This error model is not sufficient for multi-harmonics waves. One more complex factor (power and phase constant) is to be added to this model to turn the calibration process to an absolute calibration. The complex constant is multiplied to the error matrix:

$$\begin{bmatrix} a_{c1}^N \\ b_{c1}^N \\ a_{c2}^N \\ b_{c2}^N \end{bmatrix} = K_N e^{j\theta_N} \begin{bmatrix} 1 & \beta_1^N & 0 & 0 \\ \gamma_1^N & \delta_1^N & 0 & 0 \\ 0 & 0 & \alpha_2^N & \beta_2^N \\ 0 & 0 & \gamma_2^N & \delta_2^N \end{bmatrix} \begin{bmatrix} a_{m1}^N \\ b_{m1}^N \\ a_{m2}^N \\ b_{m2}^N \end{bmatrix} \quad \text{Eq:-118}$$

The K factor ( $K_N e^{j\theta_N}$ ) is a complex number which gives information about the absolute power and phase at the input and output ports of the DUT. The phase shift in the vector  $K_N$  is linear and will have no effect other than time delaying both input and output signals.

The first step is a classical S-parameter calibration that determines the 7-error coefficients which is performed by a classical relative calibration. In this work a classical calibrating SOLT standards are used. Short, Open and Load standards are connected at port 1 and port 2 and then a through connection between port 1 and port 2 is established. This leads that to measure these coefficients seven different measurements that are to be performed at each single frequency. The exact priori known reflection coefficients of the standards are pre-calculated using the models defined by the manufacturer.

$$\Gamma_{short} = \frac{b_{c1s}^N}{a_{c1s}^N} \quad \text{Eq:-119}$$

$$\Gamma_{open} = \frac{b_{c1o}^N}{a_{c1o}^N} \quad \text{Eq:-120}$$

$$\Gamma_{load} = \frac{b_{c1L}^N}{a_{c1L}^N}$$

Eq:-121

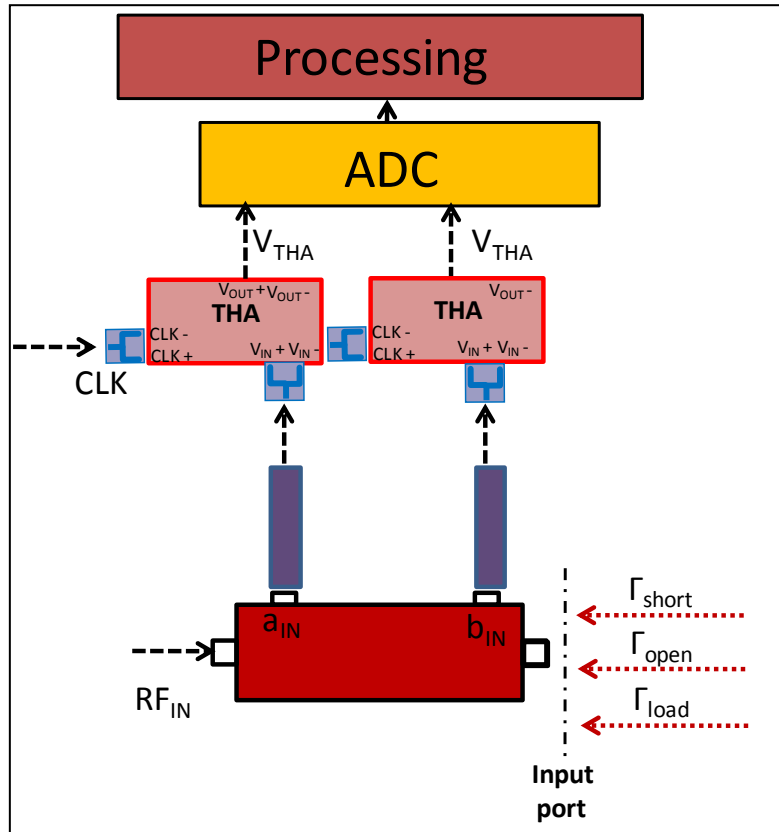


Figure III. 12: SOL standards at input port

Three measurements are made at each port after the connection of a short, an open and a load standard. Using Eq.118 the unknown quantities could be replaced in Eq.119, 120 and 121.

$$\Gamma_{short} (a_{m1s}^N + \beta_1^N b_{m1s}^N) = a_{m1s}^N \gamma_1^N + \delta_1^N b_{m1s}^N \quad \text{Eq:-122}$$

$$\Gamma_{open} (a_{m1o}^N + \beta_1^N b_{m1o}^N) = a_{m1o}^N \gamma_1^N + \delta_1^N b_{m1o}^N \quad \text{Eq:-123}$$

$$\Gamma_{load} (a_{m1L}^N + \beta_1^N b_{m1L}^N) = a_{m1L}^N \gamma_1^N + \delta_1^N b_{m1L}^N \quad \text{Eq:-124}$$

Eq. 122,123 and 124. can be rewritten as follows

$$\Gamma_{short} \beta_1^N b_{m1s}^N - a_{m1s}^N \gamma_1^N - \delta_1^N b_{m1s}^N = -\Gamma_{short} a_{m1s}^N \quad \text{Eq:-125}$$

$$\Gamma_{open} \beta_1^N b_{m1o}^N - a_{m1o}^N \gamma_1^N - \delta_1^N b_{m1}^N = -\Gamma_{open} a_{m1o}^N \quad \text{Eq:-126}$$

$$\Gamma_{load} \beta_1^N b_{m1L}^N - a_{m1L}^N \gamma_1^N - \delta_1^N b_{m1}^N = -\Gamma_{load} a_{m1L}^N \quad \text{Eq:-127}$$

Eq. 125, 126 and 127 represent set of linear equation. It can be represented in matrix form, grouping all the known quantities on the right hand side of the equation. The unknowns  $\beta_1^N, \gamma_1^N, \delta_1^N$  can then be calculated using the matrix relation:

$$\begin{bmatrix} \beta_1^N \\ \gamma_1^N \\ \delta_1^N \end{bmatrix} = \begin{bmatrix} -\Gamma_{short} b_{m1s}^N & -a_{m1s}^N & -b_{m1s}^N \\ -\Gamma_{open} b_{m1o}^N & -a_{m1o}^N & -b_{m1s}^N \\ -\Gamma_{load} b_{m1L}^N & -a_{m1L}^N & -b_{m1s}^N \end{bmatrix}^{-1} \begin{bmatrix} -\Gamma_{short} a_{m1s}^N \\ -\Gamma_{open} a_{m1o}^N \\ -\Gamma_{load} a_{m1L}^N \end{bmatrix} \quad \text{Eq:-128}$$

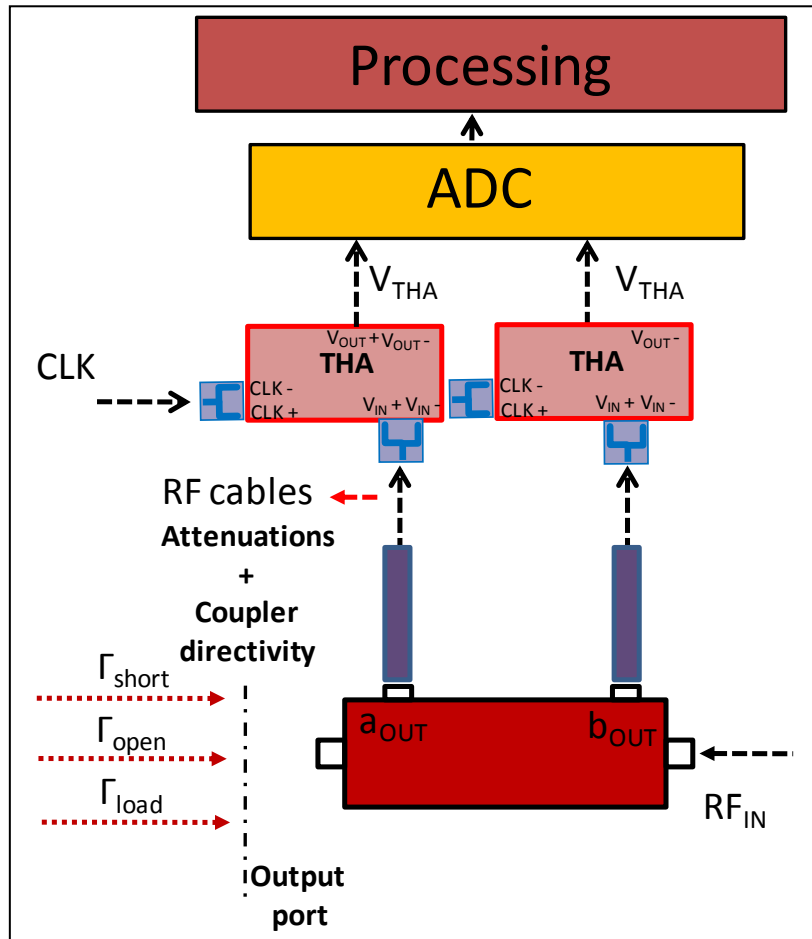


Figure III. 13: SOL standards at output port

Similar measurements are made at port two and this leads to the calculations of  $\beta_2^N, \gamma_2^N, \delta_2^N$  coefficients are calculated.



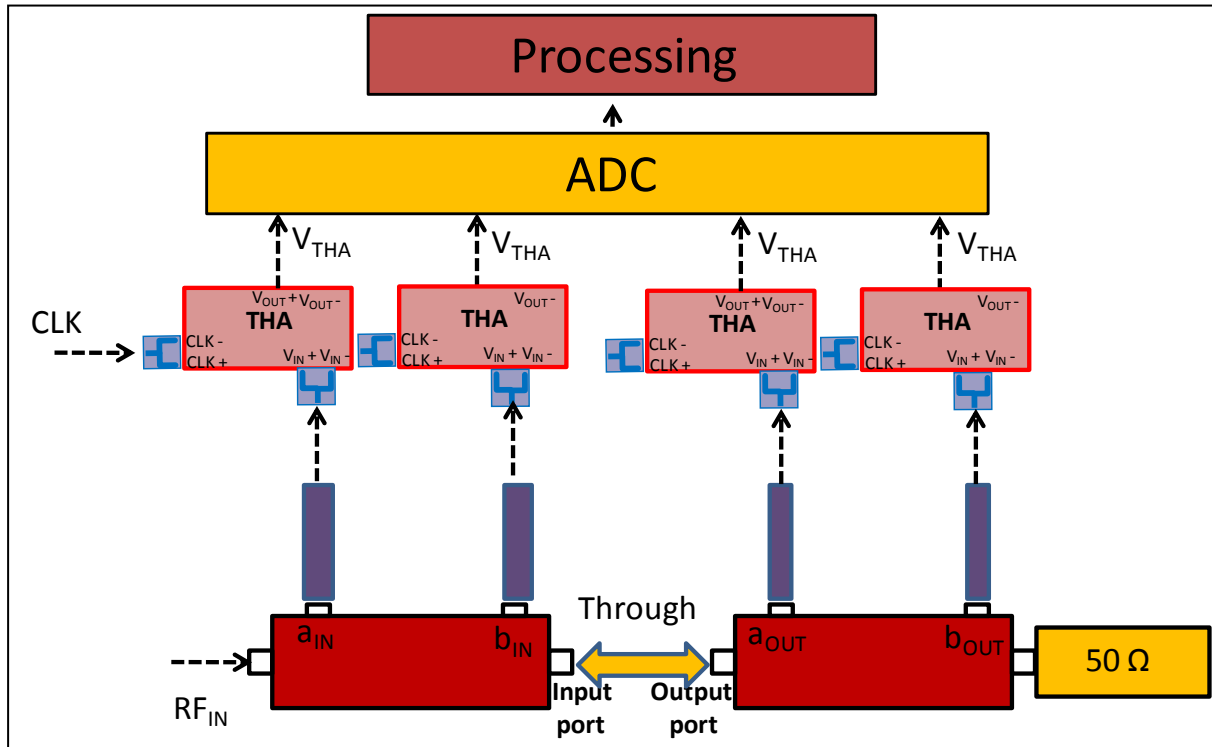


Figure III. 14: A through connection between port 1 and port 2

$$\begin{bmatrix} \beta_{2o}^N \\ \gamma_{2o}^N \\ \delta_{2o}^N \end{bmatrix} = \begin{bmatrix} -\Gamma_{short} b_{m2s}^N & -a_{m2s}^N & -b_{m2s}^N \\ -\Gamma_{open} b_{m2o}^N & -a_{m2o}^N & -b_{m2o}^N \\ -\Gamma_{load} b_{m2L}^N & -a_{m2L}^N & -b_{m2L}^N \end{bmatrix}^{-1} \begin{bmatrix} -\Gamma_{short} a_{m2s}^N \\ -\Gamma_{open} a_{m2o}^N \\ -\Gamma_{load} a_{m2L}^N \end{bmatrix} \quad \text{Eq:-129}$$

Finally one more measurement is made with a through connection is established between port 1 and port 2 see Fig.III.14. The incident signal at port 1 is equal to the incident signal at port 2.

$$\begin{bmatrix} \beta_2^N \\ \gamma_2^N \\ \delta_2^N \end{bmatrix} = \alpha_2^N \begin{bmatrix} \beta_{2o}^N \\ \gamma_{2o}^N \\ \delta_{2o}^N \end{bmatrix} \quad \text{Eq:-130}$$

Theoretically, this relation could be represented as

$$a_{c1}^N = b_{c2}^N \quad \text{Eq:-131}$$

Using Eq. 117

Eq:-132

$$a_{m1s}^N + \beta_1^N b_{m1s}^N = \alpha_2^N (a_{m2}^N \gamma_2^N + \delta_2^N b_{m2}^N)$$

$$\alpha_2^N = \frac{a_{m1s}^N + \beta_1^N b_{m1s}^N}{a_{m2}^N \gamma_2^N + \delta_2^N b_{m2}^N} \quad \text{Eq:-133}$$

The seven unknown correction coefficients in the relative error matrix are calculated using the classical SOLT calibration procedure as explained above. Next, an eighth measurement is performed to determine the amplitude of complex function K at the frequency of calibration. This measurement is performed with a power meter that is connected at port 1. Power is applied to the port 1 RF input as shown in Fig.III.15. The amplitude of the complex number is the maximum amplitude of the sinusoid in time-domain signal.

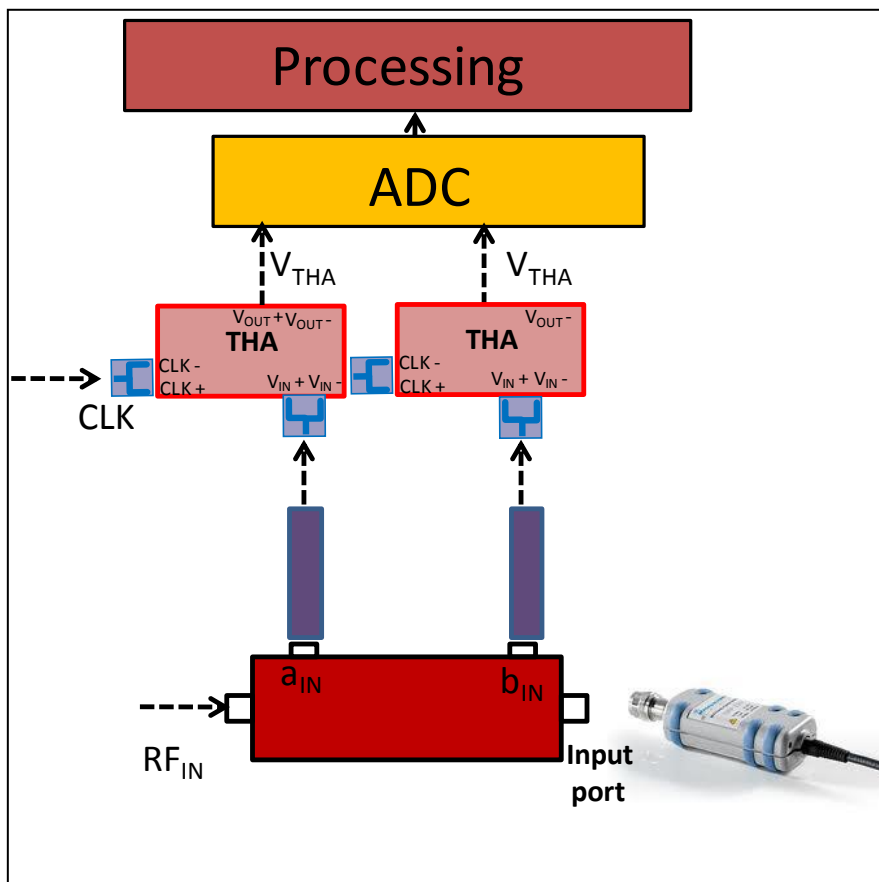


Figure III. 15: K factor amplitude calculation

Using Eq. 118 the power measured by the power meter is equal to the power incident at port 1 by a factor of  $|K|$ . The power which is measured in dBm for each frequency of interest is converted into voltage amplitude.

$$|A_{PM}| = |K_A(a_{m1}^N + \beta_1^N b_{m1}^N)| \quad \text{Eq:-134}$$

$$|K_A| = \left| \frac{A_{PM}}{T_s(a_{m1}^N + \beta_1^N b_{m1}^N)} \right| \quad \text{Eq:-135}$$

Where  $A_{PM} = \sqrt{10^{\frac{P_{dBm}-10}{10}}}$

$T_s =$  transmisson factor of the calibrated power meter

$P_{dBm}$  is the power measured with the calibrated power sensor,  $a_m$  and  $b_m$  are the raw data acquired on the ADC at the desired frequency and  $\beta_1^N$  is the error term defined before.

Accurate time-domain waveform measurements of multi-harmonic signals require a phase calibration on top of well-known relative and power calibration. Finally a ninth measurement is made to determine the phase of complex K factor at each frequency. A harmonic phase reference and a pre-calibrated Lecroy oscilloscope is used for this measurement. The harmonic phase reference generator is characterized by a calibrated broadband sampling oscilloscope. The HPR is composed of a step recovery diode and an amplifier manufactured by Wiltron was excited by a sinusoidal which produces multiple harmonics spaced at the frequency of excitation. A discrete Fourier transformation of the output signal of the HPR returns the phase relationship between all of the relevant harmonics. The oscilloscope is connected to port 1 of the setup and a HPR excites the RF input port as shown in Fig.III.16. In this case only one measurement is needed. The excitation frequency of the HPR is chosen so that it contains all the frequencies of interest within its RF spectrum bandwidth.

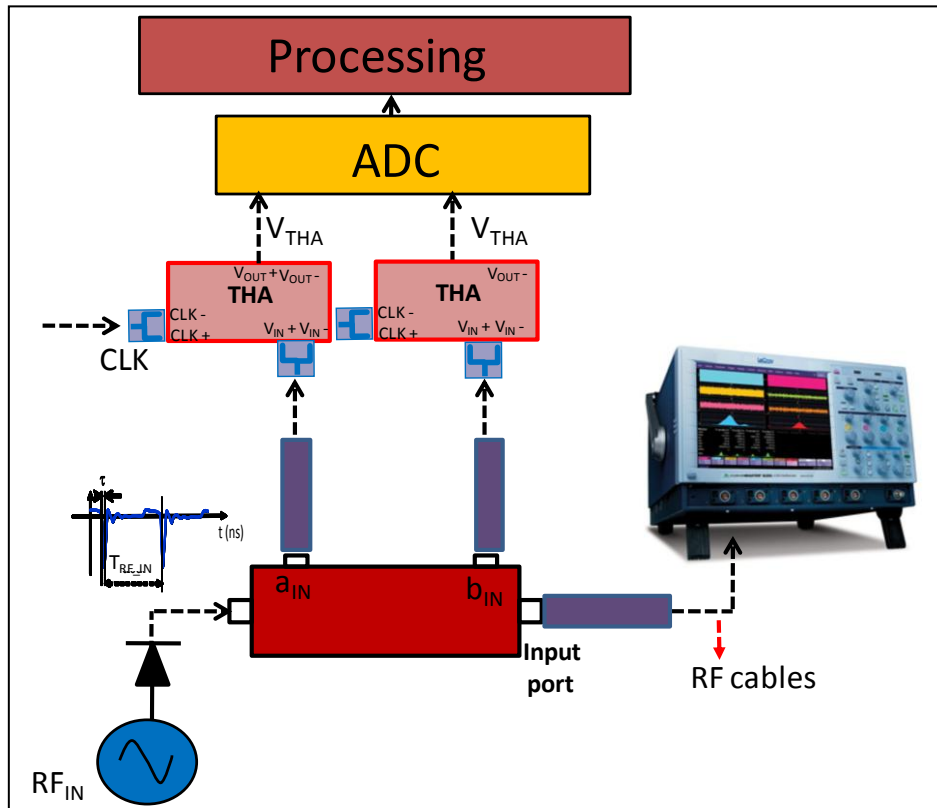


Figure III. 16: K factor phase calculation

The phase response of the attenuators, the connectors and the cable feeding the oscilloscope is compensated by de-embedding of their s-parameters. The relationship between the phase measured by the proposed test-bench and the oscilloscope is represented by:

$$\theta_{LO}^N = \angle K_{\theta} (a_{m1}^N + \beta_1^N b_{m1}^N) \quad \text{Eq:-136}$$

Where N represents all the desired frequencies of calibration.

$$\angle K_{\theta} = \angle \frac{\theta_{LO}^N}{a_{m1}^N + \beta_1^N b_{m1}^N} \quad \text{Eq:-137}$$

### III. Time-Domain measurement setup

#### III.1. Single Channel Acquisition of Time-domain Data

In order to verify the operation of the proposed test bench a single channel time-domain measurement test setup was developed to test and verify the performance of THA based measurement setup. The comparison is made with a commercially available Vector signal analyzer [14]. The complete architecture of the setup is described Fig. III.17. This measurement setup includes only one THA and it was developed to perform input-output time-domain envelope measurements of matched power amplifiers. The input and the output signals are sequentially measured by using two directional couplers, a switch and the 13GHz Bandwidth 2 GS/s THA connected to a dual Channel 420MS/s, high dynamic range (12 bit) analog-to-digital converter (ADC). The pulsed RF signal generated by the R&S SMBV100A generator was linearly amplified to feed the input of the power amplifier under test (AUT). A common clock of 400 MHz (sinusoidal waveform) feeds the THA and the ADC. The pulsed RF signals are then directly sampled by the THA and the ADC is synchronized to a 10 MHz reference signal. The ADC is externally triggered by the RF source.

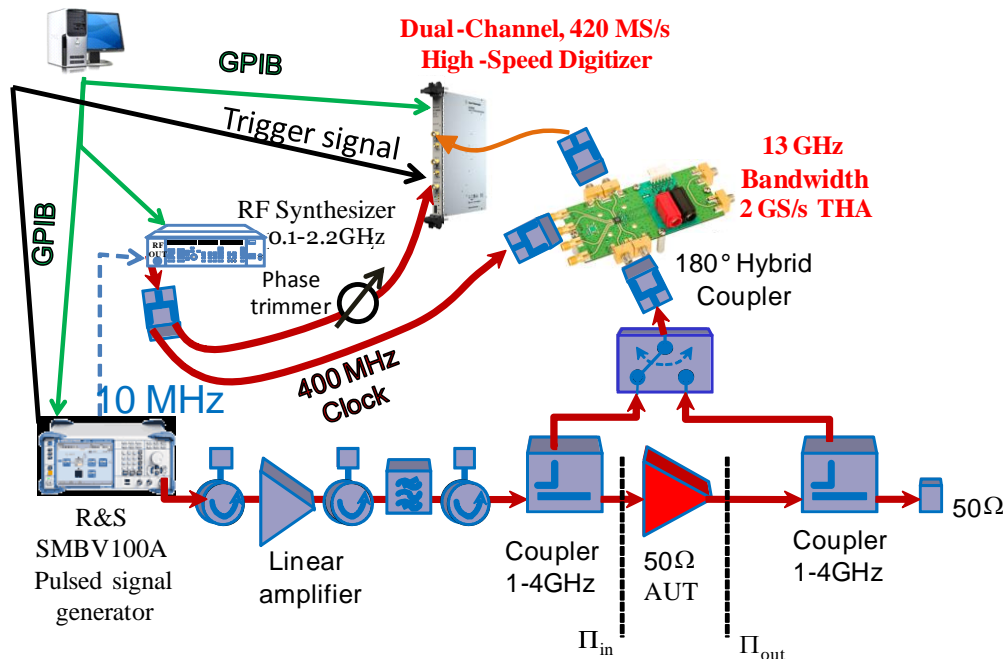


Figure III. 17: Block diagram of single channel measurement system

A simple power and S21 calibration is performed to calculate the error in the measurement system. To determine the amplitude error correction a power calibration was performed using a pulsed power-meter as a power reference. For the phase calibration, a different procedure was followed as the receiver used in our system had single measuring channel, which means that simultaneous measurements of the signals at the input and output of a device under test were impossible. To measure the transfer characteristics (AM/AM and AM / PM) or the linearity of a PA operated under a modulated excitation signal; synchronization between the input and the output signals was required. There are several synchronization procedures which could be applied to the measurement of envelope modulated signals [12], [13]. In this work the time-domain based cross correlation method [11] was adopted, because the time resolution obtained by this method is equal to the sampling time therefore cross correlation calculation can be performed in the frequency domain to allow a better time accuracy. The phase of the cross-spectrum gives us access to the delay between the modulated envelope and the phase rotation between the two local oscillator for sequential acquisition of the input and output signal. This correction step is applied between the input and output of the power amplifier under test to characterize its behaviour.

To assess the test-bench performance, a 50W GaN Nitronex [15] power amplifier is tested. It is driven by a pulsed signal and biased at optimal quiescent current of 330 mA and drain voltage of 28 V. Several burst of pulses were applied to the AUT operating at a carrier frequency of 2.5 GHz. The pulse period is equal to 9 us with 10 % duty cycle. The THA based receiver was fed with a common sinusoidal clock (THA + ADC) of 400 MHz. The presence of narrowband couplers at the input and output port of the AUT ensures suppression of the carrier harmonics and acted as low pass filters, so that the equivalent low pass signal is measured to extract envelope information. The time-domain waveform was sequentially captured at both ports of AUT. Using the sub-sampling the THA down-converts the 2.5 GHz RF signal to 100 MHz.

$$T_{ADC} = NT_{RF} + \frac{T_{RF}}{4} \quad \text{Eq:-138}$$

where N=6

$F_{RF} = 2.5\text{GHz}$

$T_{RF} = 0.4\text{ns}$

$T_{ADC} = 2.5\text{ns} \cong T_{\text{sampling}}$

The measurement of the magnitude and the phase of a high frequency complex modulated carrier signal was always a challenge but the reduced complexity of the IF circuitry eased this somewhat as the boundary between analog circuitry and digital computation was increased. It paved ways for direct pulsed RF sampling that eliminates the need for IQ mixing if the digitizer samples at a rate that is at-least 4 times the IF signal bandwidth as is explained in section I.1.1. The in-phase and quadrature components can be then easily extracted and yield the phase and the amplitude of the RF signal. Fig.III.18 and III.19 represent the directly sampled RF voltage signal at the input and out of DUT and it can be noticed that each period within the burst contains exactly 4 samples at the equally spaced time instants.

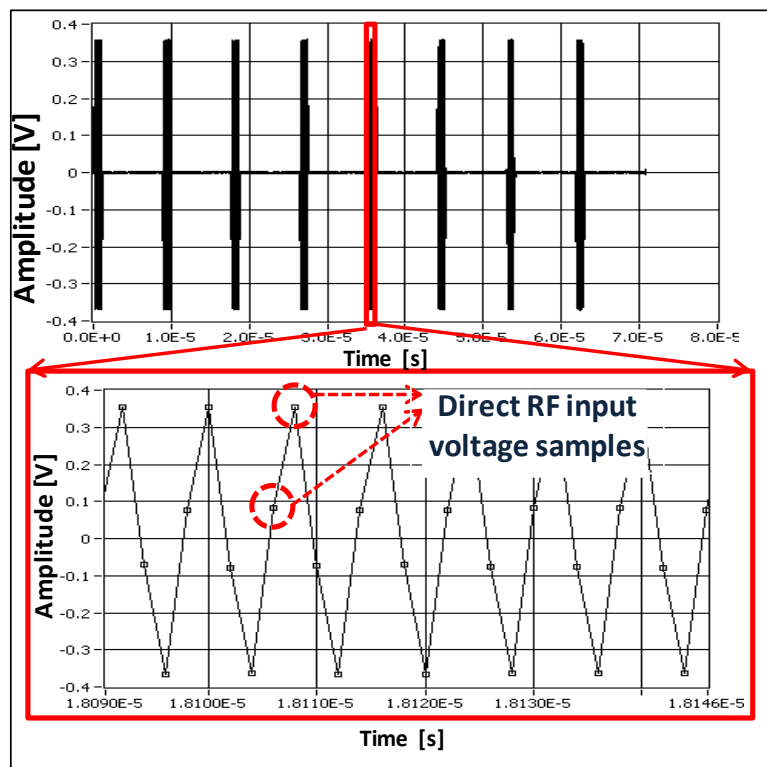


Figure III. 18: Direct RF measured time-domain pulsed input waveform at saturation

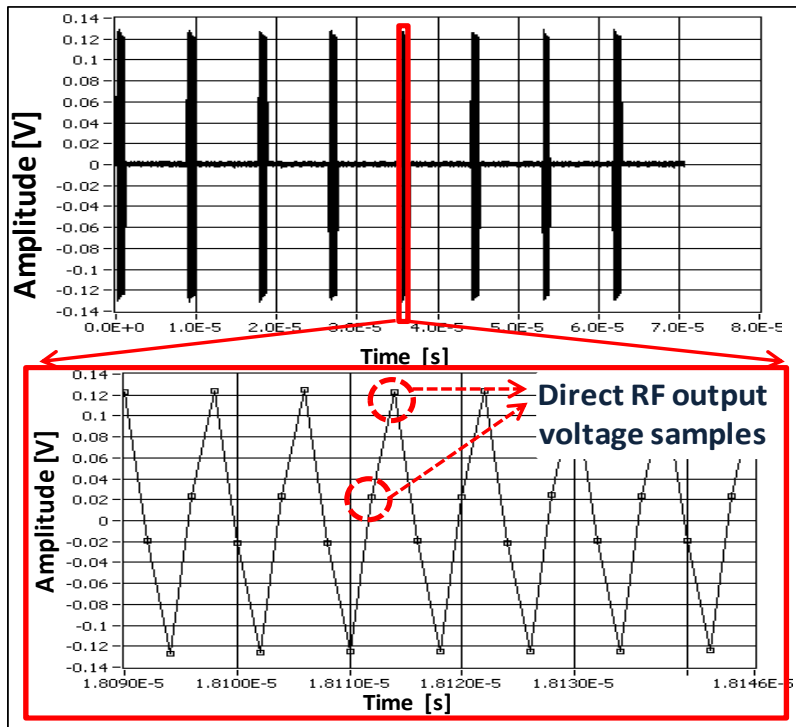


Figure III. 19: Direct RF measured time-domain pulsed output waveform at saturation

The directly sampled RF voltage signals are then calibrated both in phase and amplitude using the error correction matrix as described earlier. The corrected waveforms are depicted in Fig.III.20 and III.21

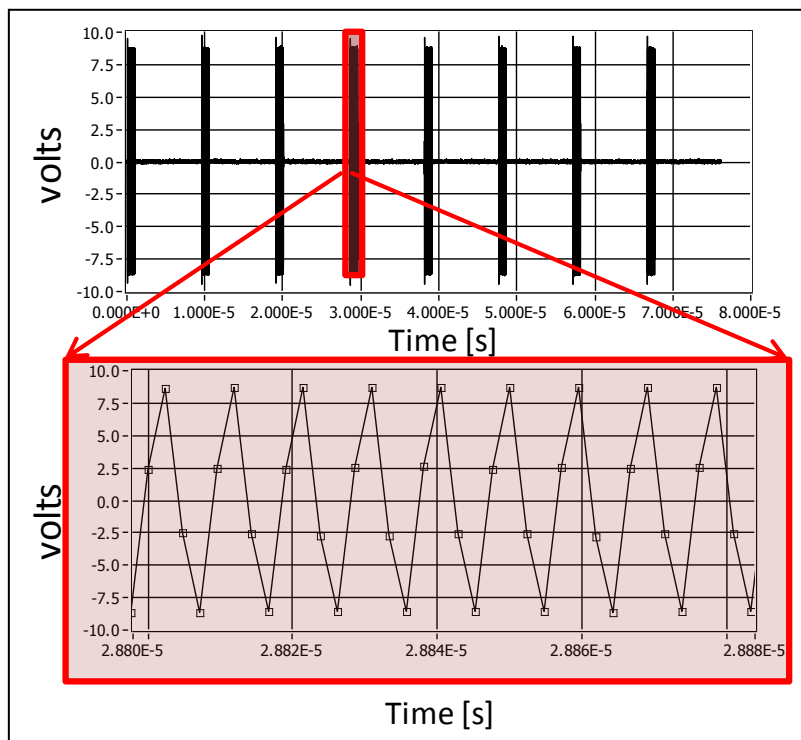


Figure III. 20: Direct RF corrected time-domain pulsed input waveform at saturation



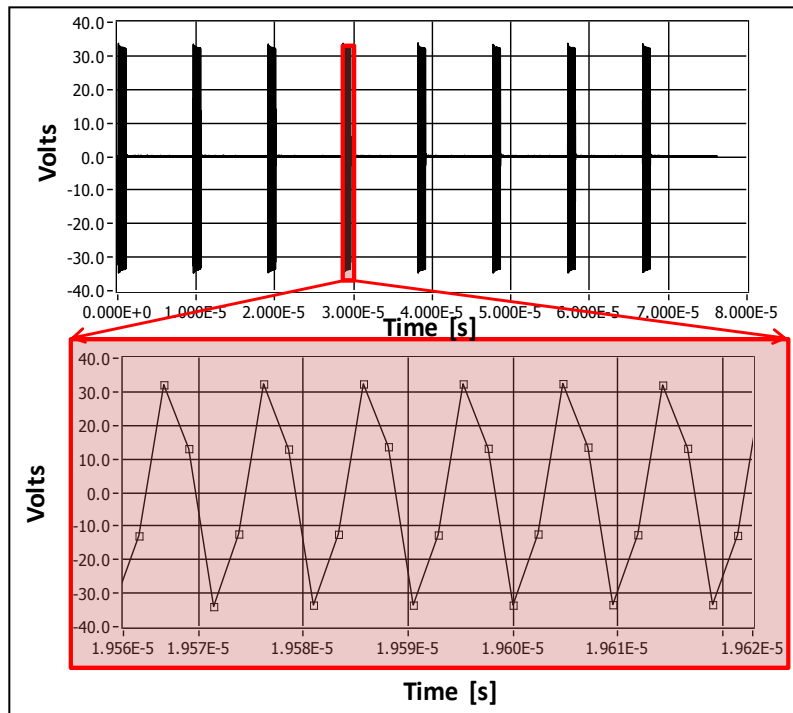


Figure III. 21: Direct RF corrected time-domain pulsed output waveform at saturation

Based on this data the in-phase and quadrature components were computed and the phase and amplitude information was demodulated from the signal as shown below.

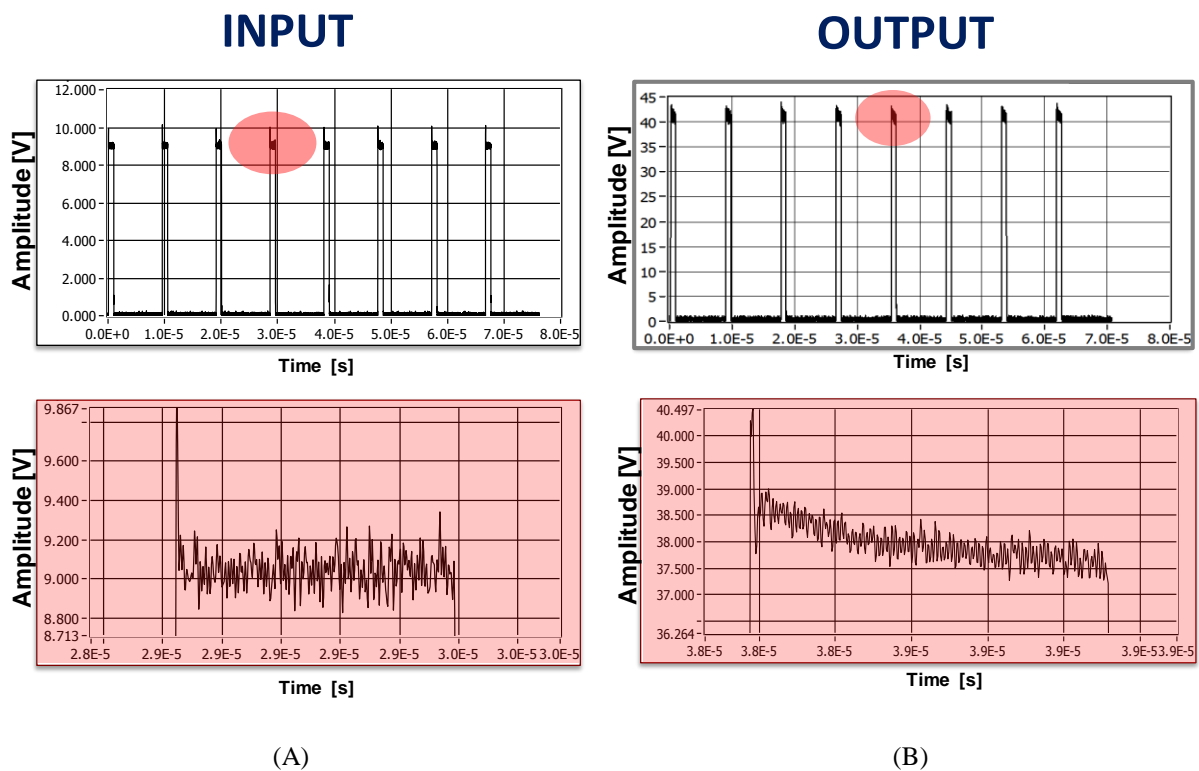


Figure III. 22: Demodulated amplitude within each pulse at input (A) and output (B) of DUT

A small decreasing trend in the amplitude of the de-modulated signal amplitude is present as seen in Fig. III.22. This shows experimentally that memory effects are indeed present during the pulse width at the output. Note that the input amplitude remains constant. The decrease in the amplitude at the output amplitude is most probably due to thermal and trapping effects.

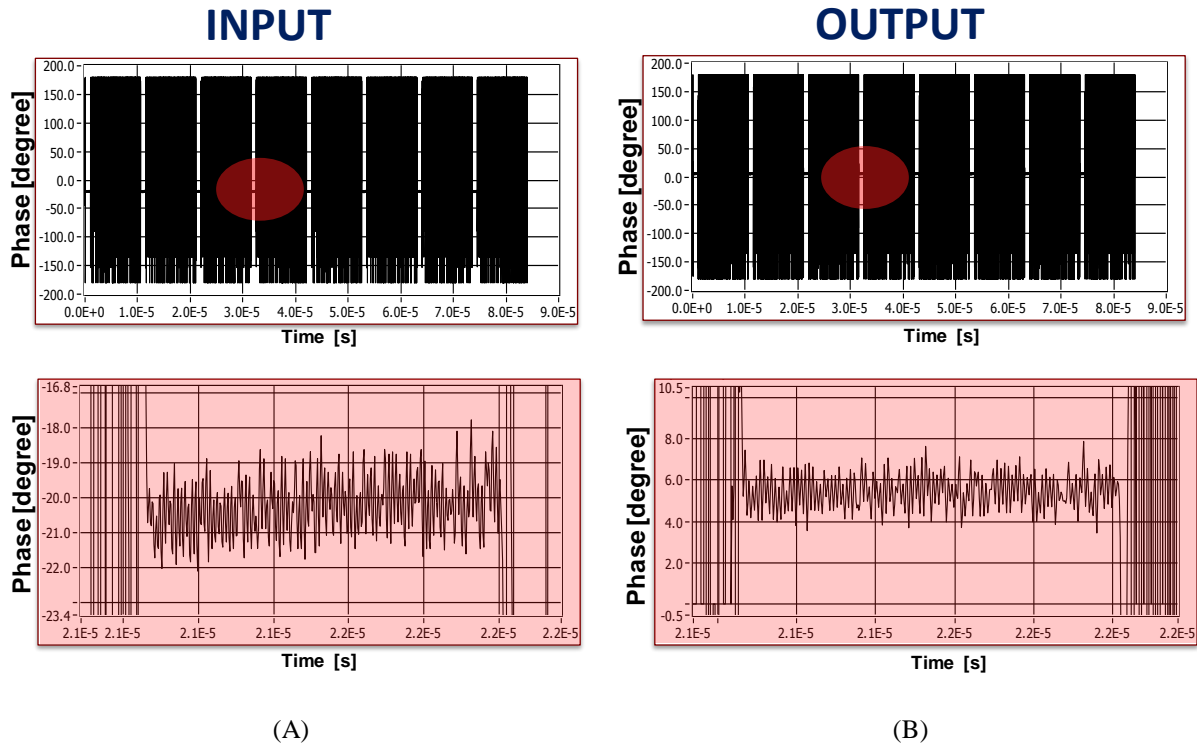


Figure III. 23: Demodulated phase within each pulse at input (A) and output (B) of DUT

As within pulse width the signal is almost constant therefore a constant phase Fig. III.23 could be seen where during the off state of the pulse only noise is measured. Power characteristics of the pulsed signal are depicted in the next section where the measurement is compared with a commercially available VSA.

### III.1.1. Analogy of the measurements of the proposed system and Vector Signal Analyzer

The measured results were validated by comparing the measured data obtained by the proposed measurement setup and the conventional Vector signal Analyzer based on the mixing principle. Similar test bench was used as described in Fig.III.24 where only the THA

based receiver was replaced by R&S FSQ26. The sampling frequency was set to its maximum value of 326.4MHz.

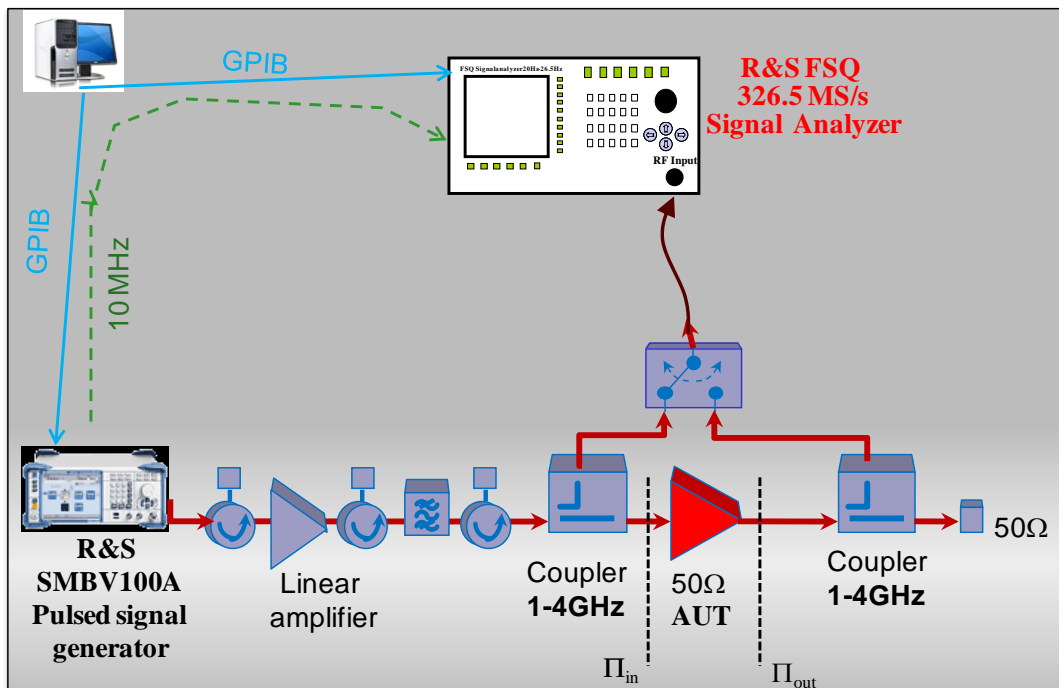


Figure III. 24: Block diagram of VSA based measurement system

The phase and the amplitude information are obtained from the same AUT at the same saturation level. The measurements obtained with the VSA are presented in Fig. III.25. It's observed that identical characteristics are obtained using the two different instruments validating the measured result of THA. The decreasing magnitude envelop measured with the two systems confirms the presence of low memory effects.

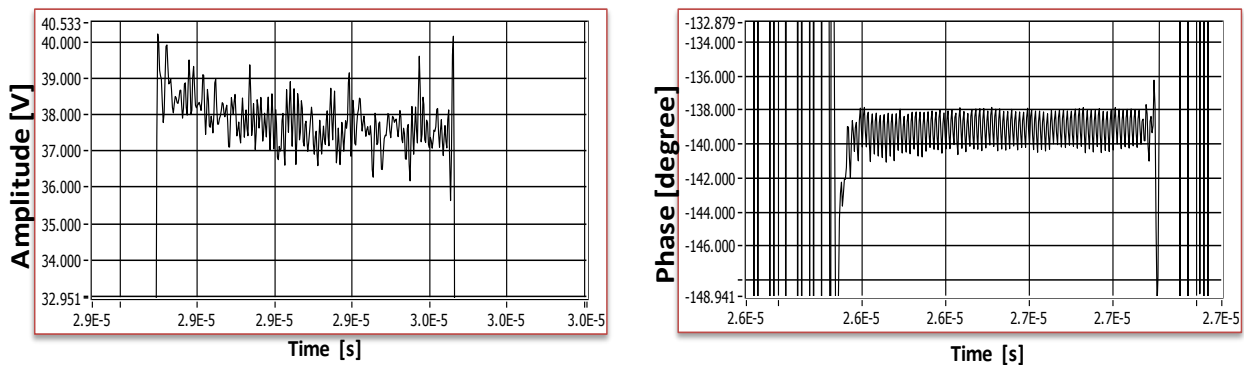


Figure III. 25: Amplitude and Phase Demodulation of a pulse using VSA based setup

An excitation signal that has identical power (section 1.2.2) is used and identical phase calibration and synchronization (section 1.3) procedures are applied to both systems. Fig III.26 demonstrates the measured output power and the gain of the same AUT operated under same biasing conditions (as mentioned earlier). Note that similar power characteristics are obtained for both setups. Similar dynamics are observed on the two test benches even if the two ADC's for the two systems do not have same ENOB. This is due to the fact that the mixer based front end of Rhodes and Schwarz VSA has dynamic range comparable to that of THA.

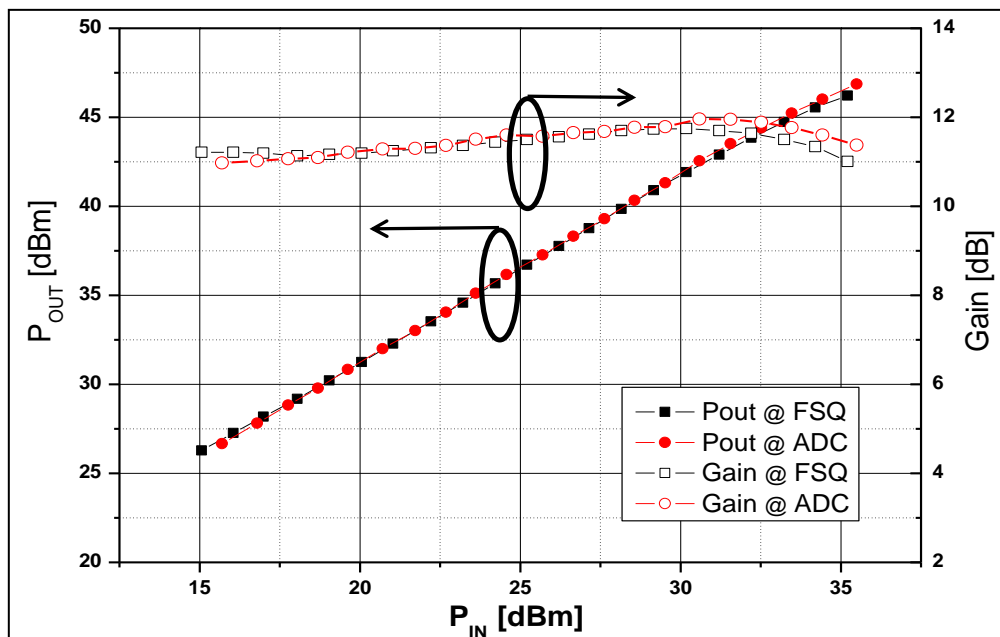


Figure III. 26: Comparison of Pout & Gain for AUT @ 2.5GHz

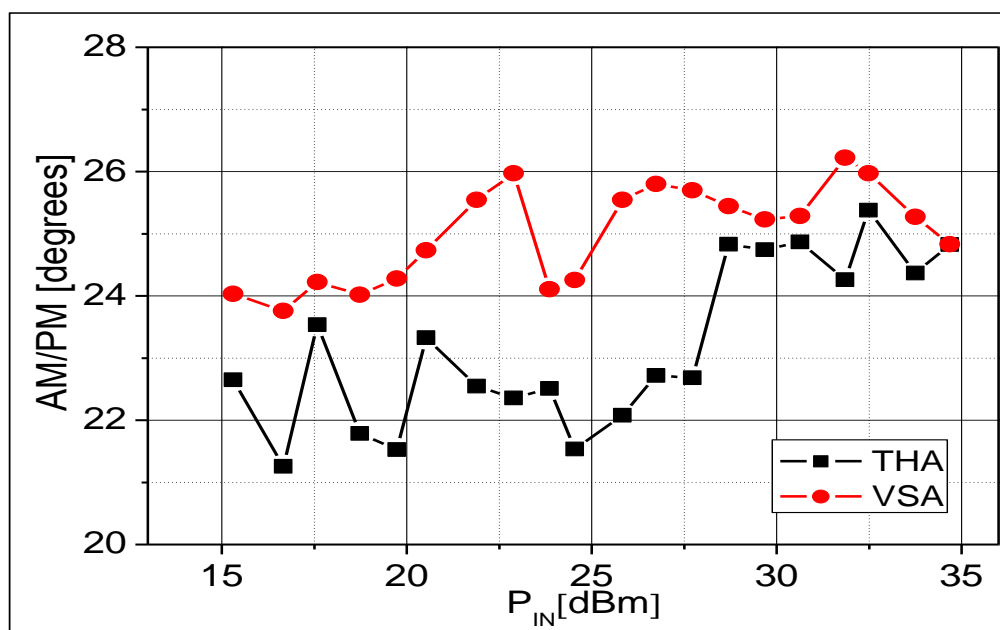


Figure III. 27: AM/PM characteristics @ 2.5GHz

The AM/PM characteristics (Fig. III.27) for the two PA are not the same as different phase error coefficients are applied to the two systems, though the procedure used to calculate them was same. The AM/PM curve for the two measurement systems is not accurate as in both cases the calibration was applied to only fundamental frequency and a constant group delay was supposed. But for pulsed signals the spectrum is spread and requires a calibration to be performed for a large bandwidth with a narrow frequency resolution.

This work presents and validates a time-domain envelope test bench for pulsed characterization of high Power devices. The test bench based on the use of THA is realizable and presents an improved bandwidth of 200 MHz with an enhanced resolution of 12-bits. The reduction of component density in the analog domain and the direct digitization of entire RF spectrum bring more flexibility in the receiver's performance. The use of sub-harmonic sampling enables us to extract both in-phase and quadrature components without the use of digital mixers. The main drawback of this test setup is that to obtain the AM/PM characteristics, a synchronization procedure is required to compensate the two non-synchronous acquisitions (input and output). To overcome this problem the next step was to build a 4-channel setup to extract the pulsed time-domain data for non-linear high power devices as it does not require any extra processing or clock circuitry to extract the synchronized modulated signals.

### **III.2. 4-Channel Time-domain Measurement Test-bench**

Once satisfactory results are obtained from a single channel THA based large signal time-domain measurement, a complete 4-channel test-bench has been built to measure the incident, the transmitted and the reflected envelope signals simultaneously. Even if only two channel setup is required to measure matched power amplifiers but 4 channels set up as seen in Fig. III.28 was built to measure transistors and un-matched PA's under load-pull conditions. The basic architecture includes two broadband couplers (2GHz-18GHz) at the input and the output of the DUT to capture the incident and the reflected signals. As the THA has differential input and output ports, 180° hybrid couplers are added to feed a differential signal to the THA. Note that the output of the THA only consists of a single ended signal that was used to feed the ADC.

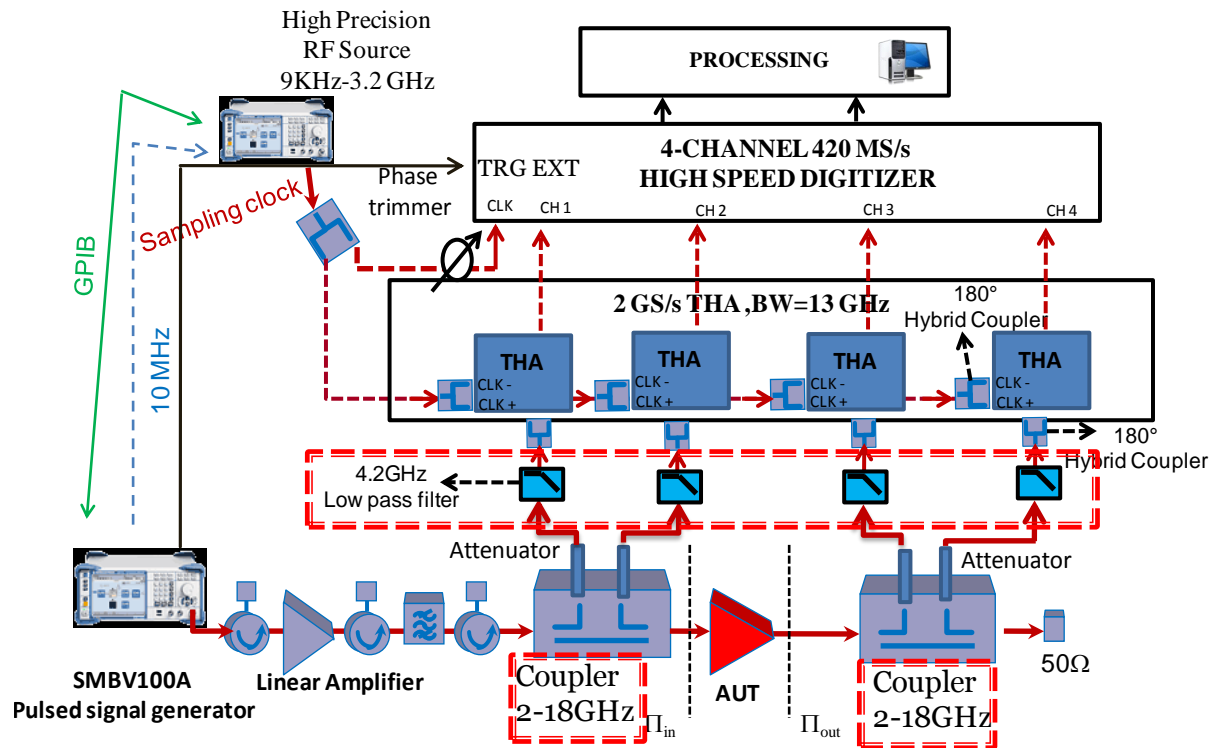


Figure III. 28: Block diagram of 4-channel measurement system

As the proposed test-bench is designed to measure the nonlinearity of a high power device, which means that the device should be driven into saturation. Therefore large attenuators are added to ensure the linearity of both the THA and the ADC. The attenuators were followed by low pass filters with a cut-off frequency of 4.2 GHz to ensure that harmonic the components of the fundamental tone are eliminated at the input and output of AUT. Four commercially available THAs (Inphi 13 GHz bandwidth 2 GS/s) were connected to a four Channel 420 MS/s, high dynamic range (12 bit) analog-to-digital converter (ADC). A common clock of 400 MHz (sinusoidal) feeds the clock of the THAs and the ADC. A R&S signal modulation unit (SMBV100A) was used to generate the modulated RF signals which was linearly amplified and fed the input of the power amplifier under test (AUT). As the same sinusoidal clock is used to feed both the THA and ADC, a phase trimmer was added to ensure that a little delay is added between the sampling instants of THA and ADC. This ensures that the sampling instant of the ADC falls in the hold interval of the THA.

An absolute system calibration was performed to mathematically remove the systematic errors. Two assumptions for the calibration procedure are adopted: The relationship between the measured and the physical quantities is assumed to be linear and the cross talk between ports [5] is assumed to be zero. The goal of the calibration procedure is to

determine the eight unknown complex error coefficients as before. The first seven error coefficients  $\beta_1^N, \gamma_1^N, \delta_1^N, \alpha_2^N, \beta_2^N, \gamma_2^N, \delta_2^N$  are determined by classical relative calibration technique. Subsequently, a power calibration is performed at a relatively high power (20 dBm) by connecting a high power sensor at port 1. At the end of this step, the magnitude of  $K^i$  coefficient was determined. A phase equalization of the input and output voltage waves was then performed assuming a constant group delay over the IF bandwidth. . It should be noted that the measurement system now contains 4 synchronized channels. Therefore, the time alignment as described in section I.3 [12], [11], [13] is no longer required for the instantaneous envelope characterization of the PA with memory. The magnitude and the phase demodulation of encoded high frequency carrier signal are extracted using the direct RF sampling property of the THA. This direct RF sampling eliminates the need for IQ mixing if the digitizer is confined to sample following the relation that is explained in section I.1.1.

### III.2.1. Measurement results

The proposed 4-channel test bench has been used for the characterization of a 50W GaN PA from Nitronex that is shown in Fig. III.29 (NPTB00050B) at 2.5 GHz [14]. The PA is operating at a drain quiescent current of 330 mA and a drain voltage of 28 V.

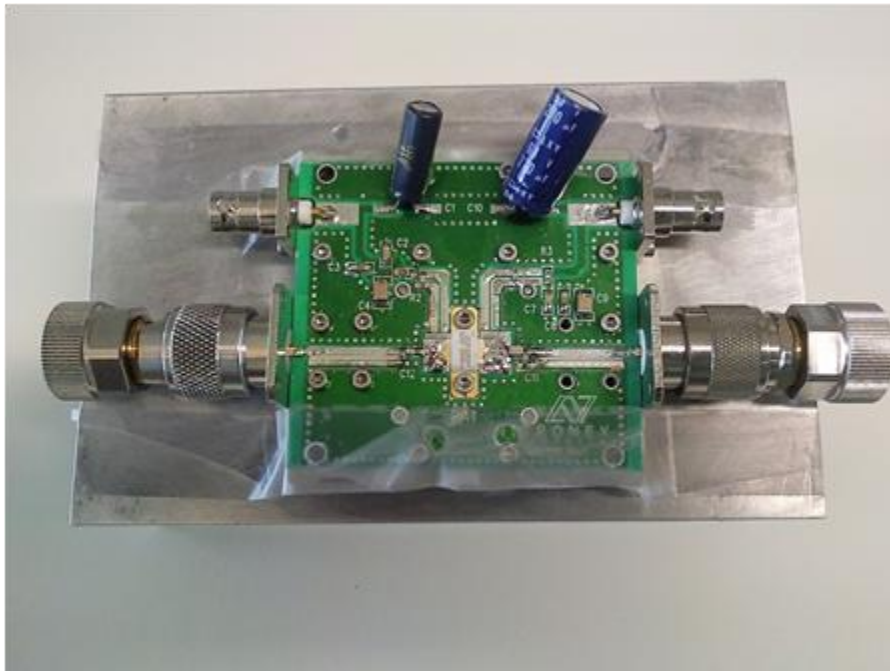


Figure III. 29: Nitronex (NPTB00050B) 50W PA

III.2.1.1. CW Measurement

Measurement results of the 50 W GaN Nitronex power amplifier driven by a continuous RF signal at 2.5GHz are described in this section. Measurement was made using the proposed THA test bench described in Fig.III.28 and compared to an LSNA based test bench [18] to compare the power performance of the PA. The 1 dB compression point output of 45.6 dBm and a power gain of almost 12 dB was measured with both the systems as explained in Fig. III.30.

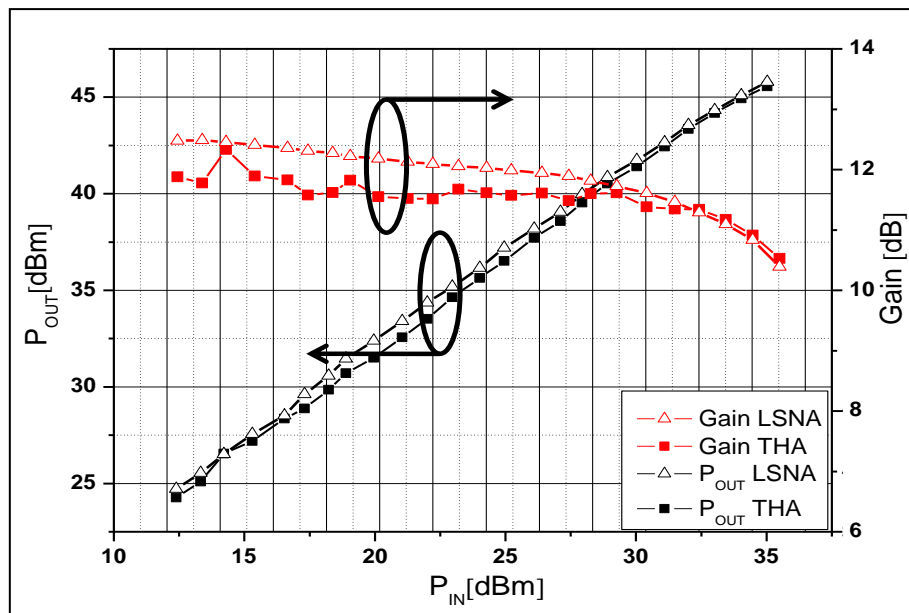


Figure III. 30: Measured gain and output power of Nitronex 50W PA

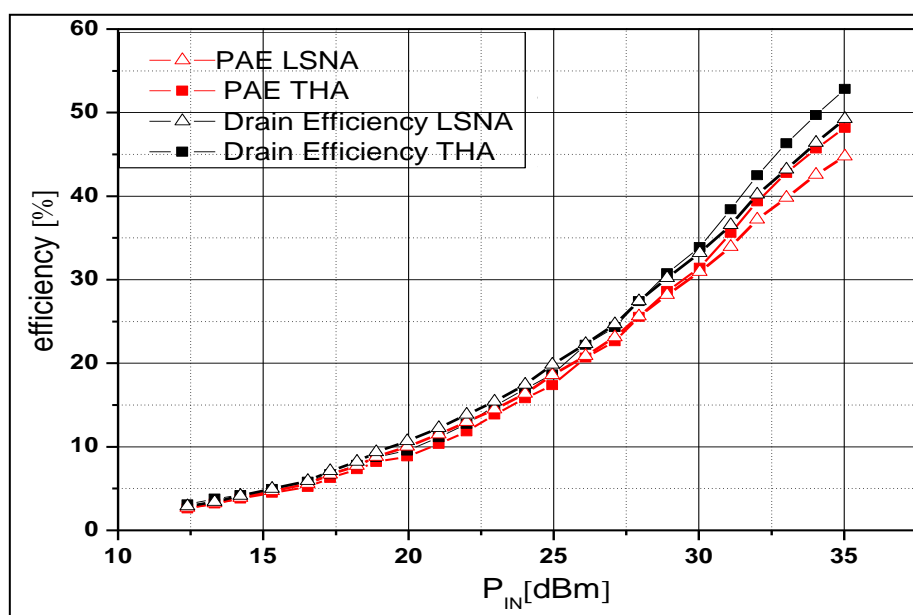


Figure III. 31: Measured drain and power added efficiency



Furthermore, we see in Fig. III.31 that maximum drain efficiency ( $\eta$ ) of 52 % and PAE of 48 % were measured with the THA based system and drain efficiency ( $\eta$ ) of 48 % and PAE of 45 % was recorded with a LSNA.

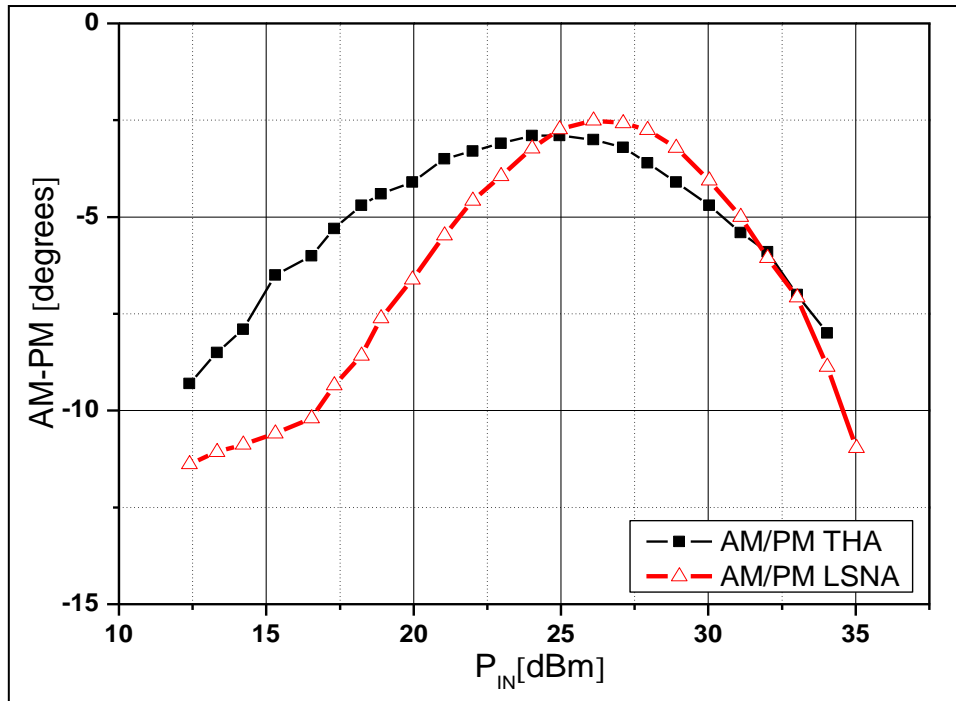


Figure III. 32: Measured AM-PM conversion

A maximum phase variation (Fig. III.32) of almost 9 degrees between both measurement systems (THA and LSNA) was noted with respect to input power variations. An important point to note here is that the AM/PM characteristics measured for the sine wave are very accurate because the spectrum of a sine wave signal is located at one discrete frequency compared to spread spectrum of pulsed signal and also instantaneous measurement was made at input and output of DUT.

### III.2.1.2. Pulsed Measurements

Here a burst of repetitive pulses was applied to the AUT operating at a frequency of 2.5 GHz. The pulse period was chosen equal to 10 us with a 10% duty cycle. The time-domain waveform was simultaneously captured at both ports of AUT. In Fig.III.33 and Fig. III.34, it can be seen that a burst of 8 pulses was captured at the input and the output of the AUT. Within each pulse exactly 4 samples were obtained per RF period.

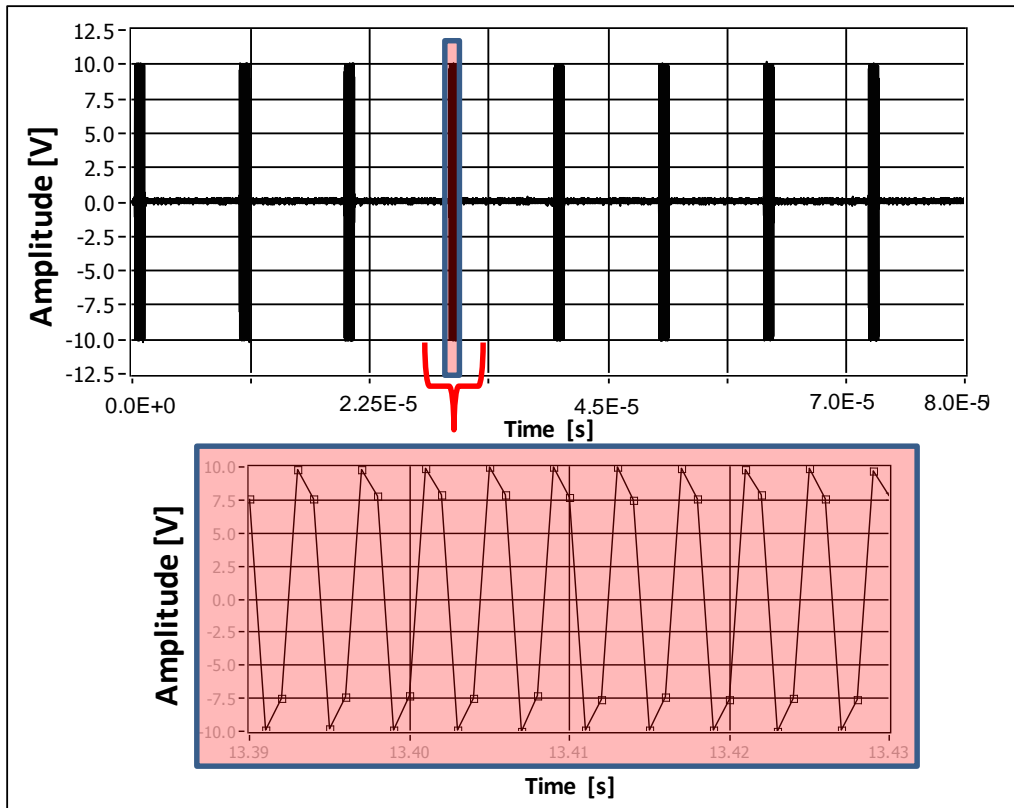


Figure III. 33: Measured corrected time-domain pulsed input waveform

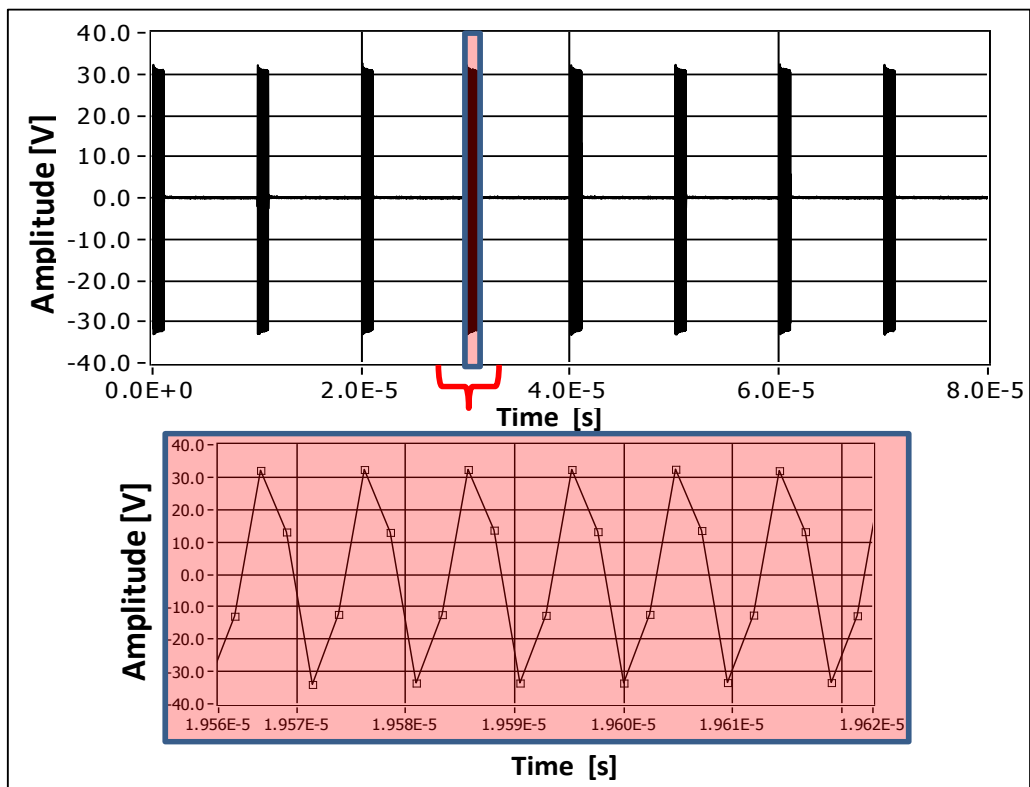


Figure III. 34: Measured corrected time-domain pulsed output waveform

The acquired pulsed waveform is demodulated and the in-phase and quadrature components are computed. The phase and amplitude information is represented in Fig.III.35. Note that similar information as for a single channel measurement is obtained. The signal within the pulse width has a constant envelope, and a constant phase is observed. During the off state of the pulse only noise is measured as shown in Fig. III.36. The pulse amplitude decreases for the output measurement due to the thermal and the trapping effects.

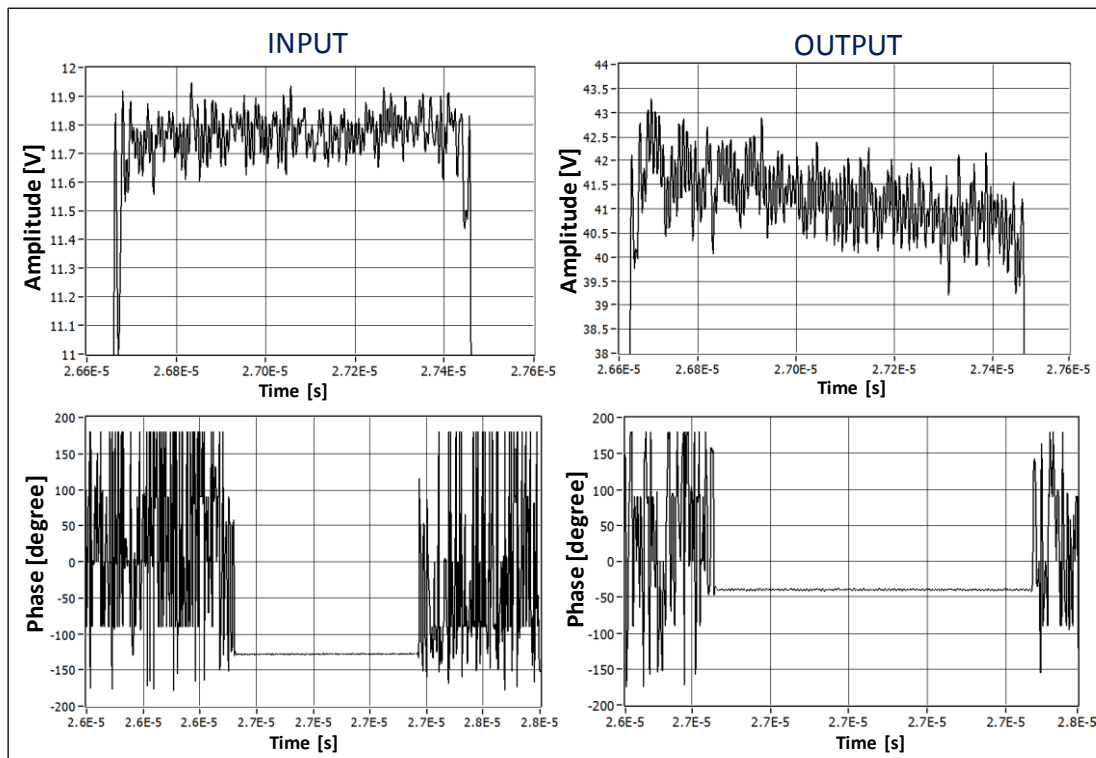


Figure III. 35: Extracted envelop and phase information at input and output within a pulse

The measured power characteristics for the pulsed measurement are shown in Fig.III.36. A good agreement for power and gain characteristic for the three different measurement system could be observed

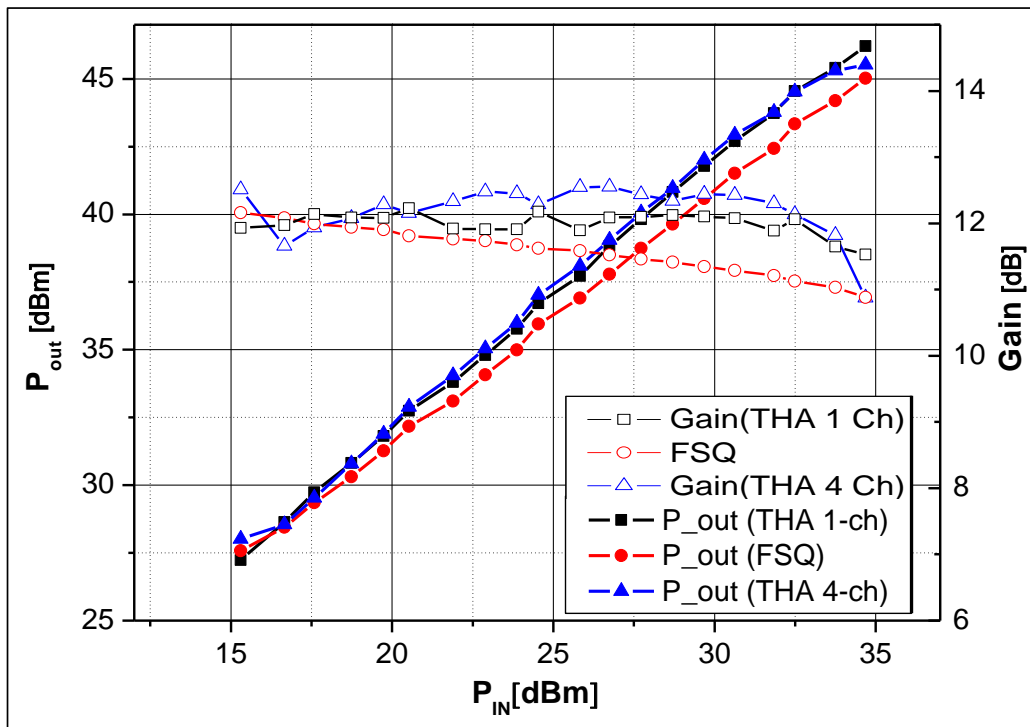


Figure III. 36: Power characteristics for three different measurement setups

The AM/PM data obtained for single channel (VSA and THA base receiver) and 4-channel THA based system is represented in Fig.III.37.

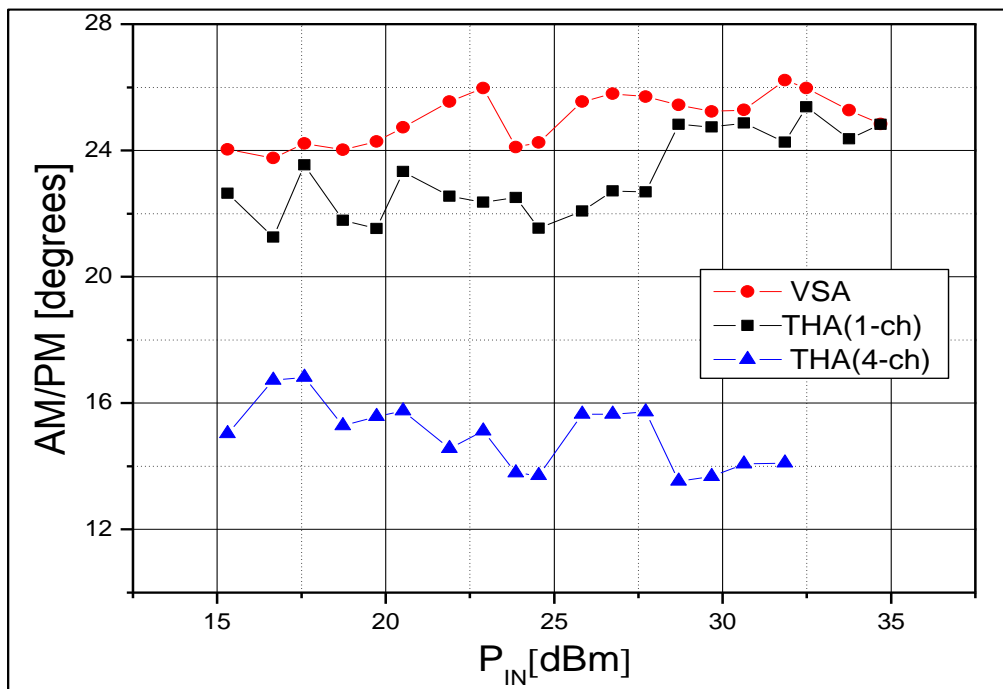


Figure III. 37: Am/PM characteristics for three different measurement setups

The only difference one can notice in this measurement resides in AM/PM data. As the input and output signal were captured instantaneously therefore there was no issue of time alignment but still the AM/PM measurement was not similar to continuous signal measurement due to calibration issues of pulsed signal and the fact that wide band couplers were used for 4-channel acquisition.

### III.2.1.3. Two-tone Measurements

In order to demonstrate the capability of the test setup to directly measure the RF carrier and to extract the envelope characteristics, the power amplifier is characterized in terms of linearity driven by a two-tone signal. The AUT is operated at a frequency of 2.5 GHz with a tone spacing of 1 MHz, and time-domain waveforms are simultaneously captured at both ports of AUT. Fig.III.38 depicts the two-tone time-domain voltage waveforms at the input and output of AUT for an output power of 45 dBm. Exactly 4 samples per IF period were captured and the in-phase and quadrature components were computed to demodulate the amplitude (Fig. III.39) and phase (Fig. III.40) information.

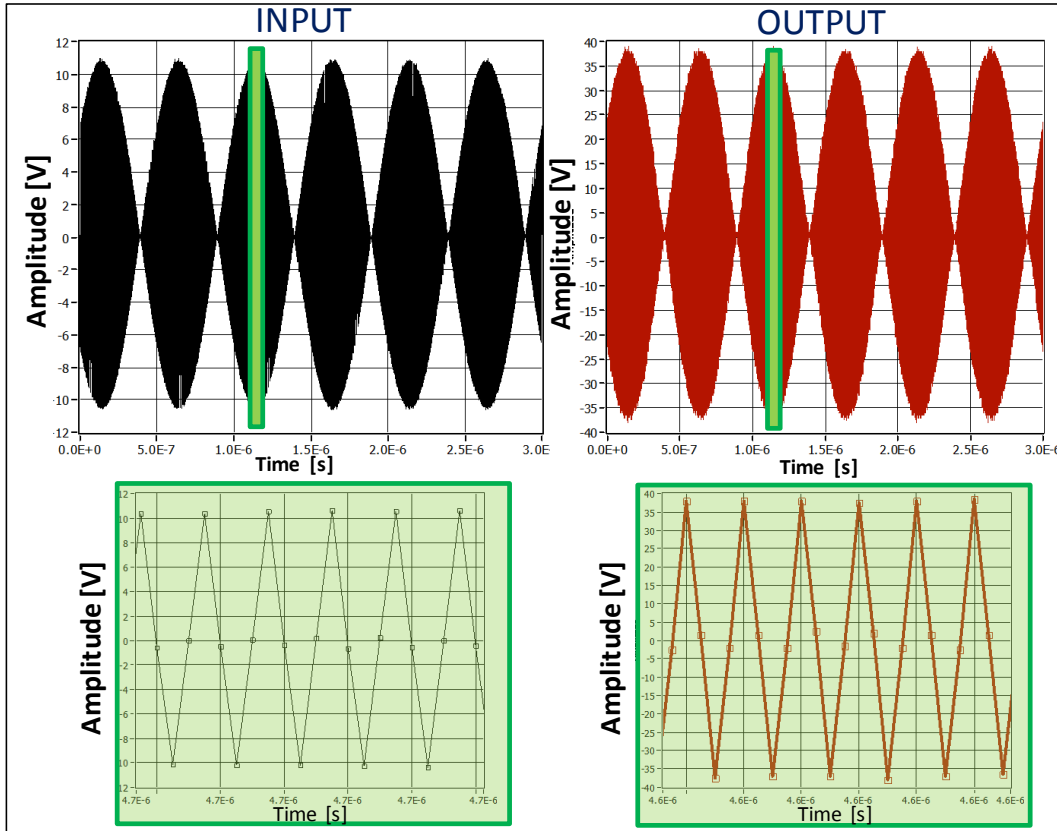


Figure III. 38: Measured time-domain two-tone voltage waveforms @ gain compression

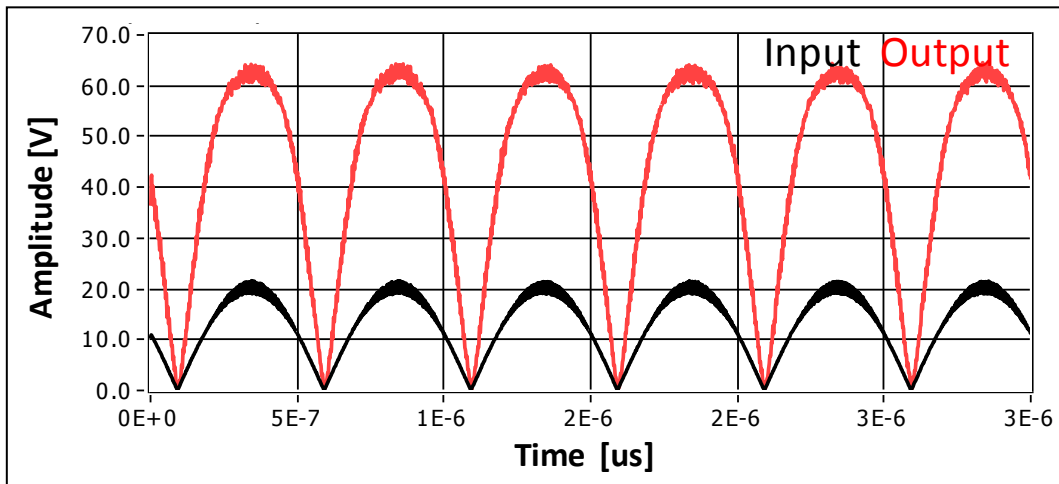


Figure III. 39: Demodulated envelope amplitude @ gain compression

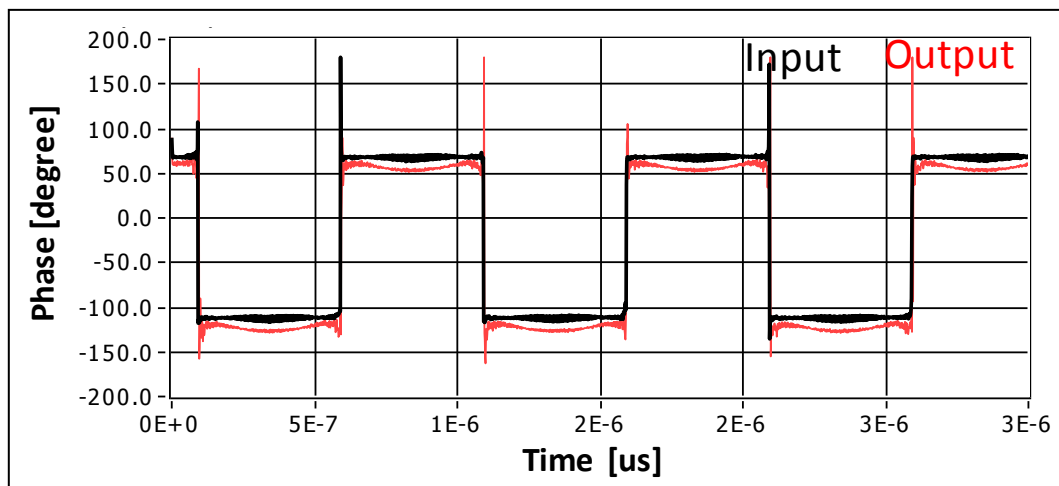


Figure III. 40: Demodulated envelope phase @ gain compression

Two-tone envelope transfer characteristics based on instantaneous AM-AM and AM-PM conversion were also measured. Fig. III.41 shows the dynamic AM-AM curve due to variations in the amplitude of the input and output envelope signals.

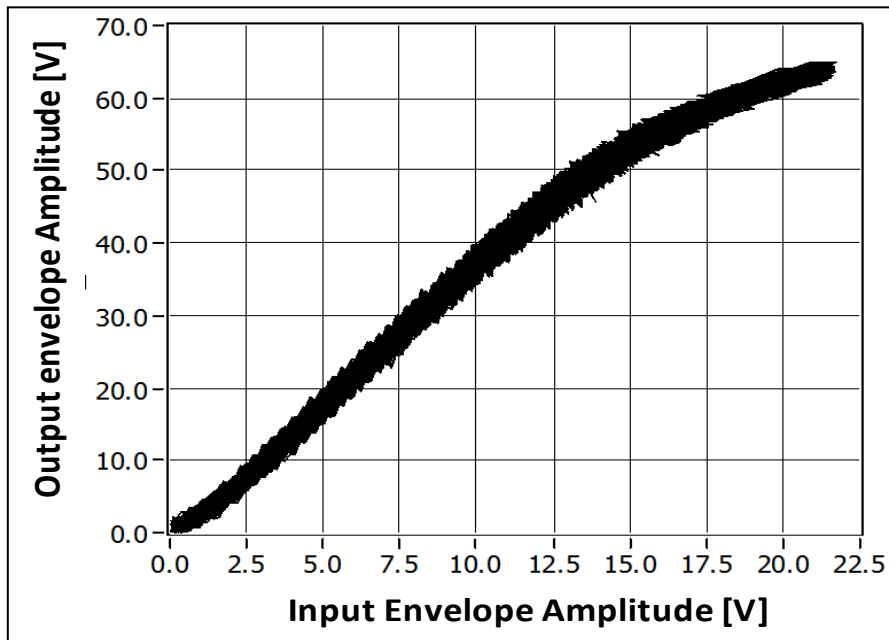


Figure III. 41: Dynamic AM/AM @ gain compression

Fig. III.42 displays the dynamic phase shift occurring at the input and output of power amplifier commonly known as AM-PM conversion. AM-PM conversion gives us information about undesired phase shifts within the amplifier which can cause signal degradation. A maximum of a 12 degree phase shift was noted with the input envelop variation.

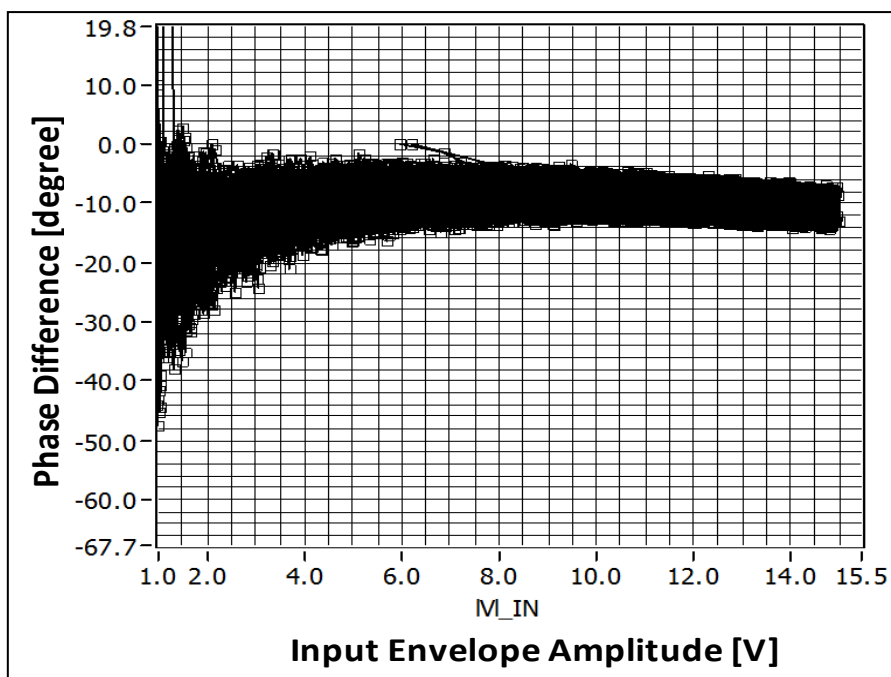


Figure III. 42: Dynamic AM/PM @ gain compression

Fig. III.43 represents the magnitude of the acquired time-domain current  $i_k(t_k)$  and voltage  $v_k(t_k)$  waveforms captured at the output of the amplifier and the input and load reflection coefficients calculated by the captured waveforms at all four ports

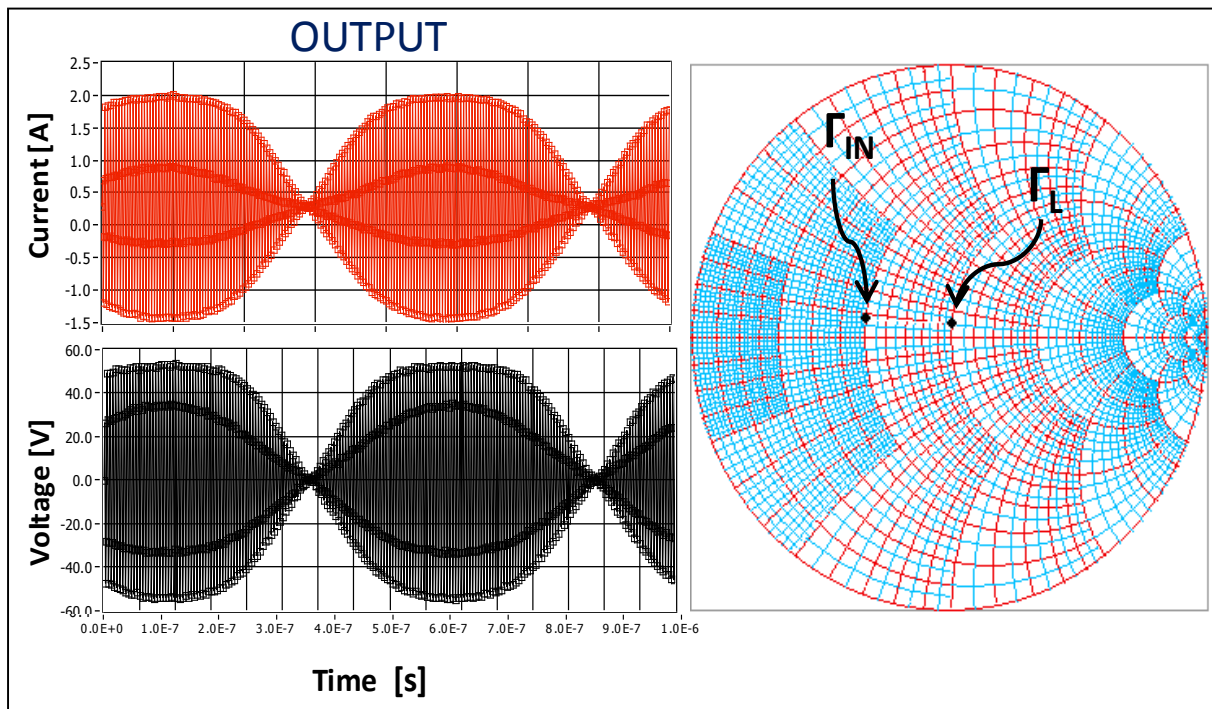


Figure III. 43: Output Current and voltage waveform at compression and the load and source reflection coefficients

#### III.2.1.4. Digital pre-distortion

The generation of unwanted frequency components within an amplifier operating at saturation is a result of the non-linearity of the device. It causes amplitude and phase distortion which leads to interference with other bands and results in the signal spectrum to spread. To compensate the nonlinearities and to improve the linearity many linearization techniques have been used in the past [20], [21]. Digital pre-distortion is quite actively being used for linearizing the non-linear response of a PA and is implemented with digital signal processing techniques. It is known to be able to produce accurate results. DSP techniques are used to pre-distort the baseband signal before modulation, up-conversion, and amplification by the PA. In this work a simple first order baseband pre-distortion technique for memory-less systems was implemented to generate an inverse transfer function of an amplifier prior to the AUT. This results in making the output of the amplifier to become a linear function of the input signal [21], [22]. The aim of this first order linearization approach at the core of this



work is simply to demonstrate the capabilities of our measurement test set-up. Fig.III.41 and III.42 represent the dynamic AM-AM and AM-PM conversion obtained by the measurement of AUT at the input and output ports by the proposed 4-channel time domain measurement system at saturation. The DUT used is the same as describe in the previous section and is excited by a two tone signal with a frequency spacing of 1 MHz. The instantaneous measurement at the input and the output of the amplifier is performed and using the quadrature modulation technique as discussed in the previous section. This helps us to demodulate the I and Q data.

The acquired data is then smoothed and normalized and the resulting data was used to calculate an inverse transfer function by inverting spline functions fitting the average of measured dynamics of the AUT to compensate the compression characteristics of PA. Inverse transfer functions were obtained for each power level, for an accurate representation of each signal. Fig. III.44 represents the normalized average variation of the output envelope amplitude versus the input amplitude calculated from the characteristics of Fig. III.41 and its calculated inverse transfer function.

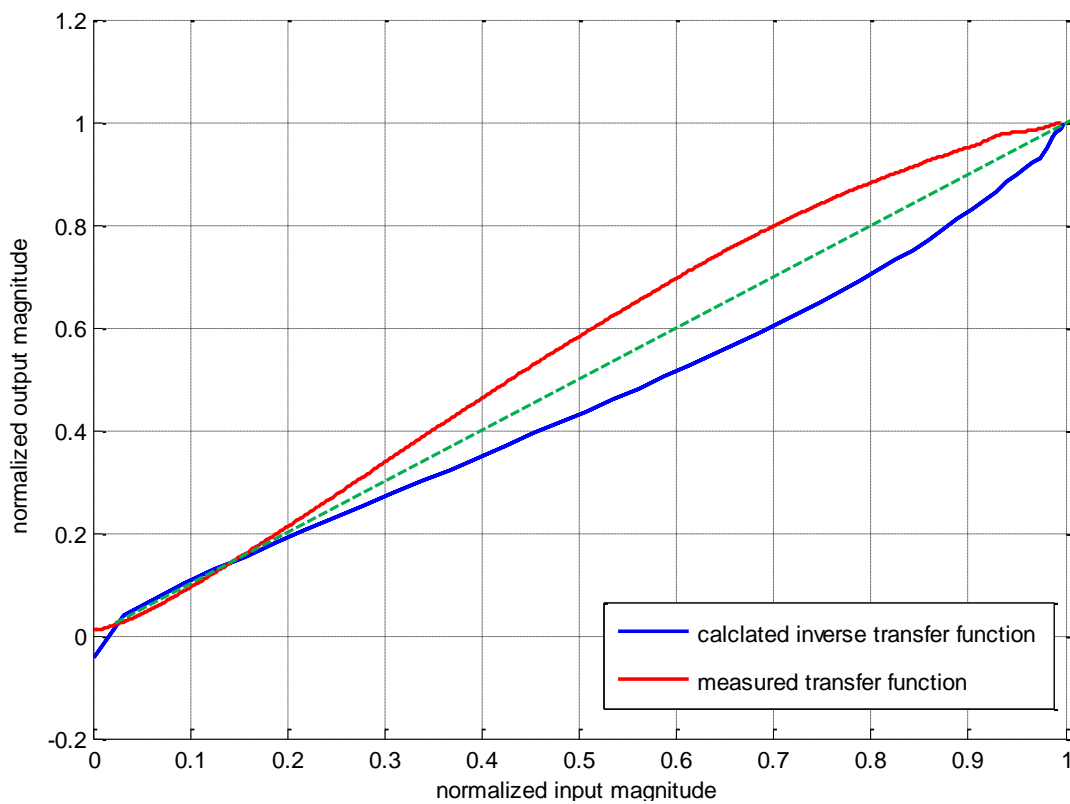


Figure III. 44: Calculated two-tone normalized envelop information

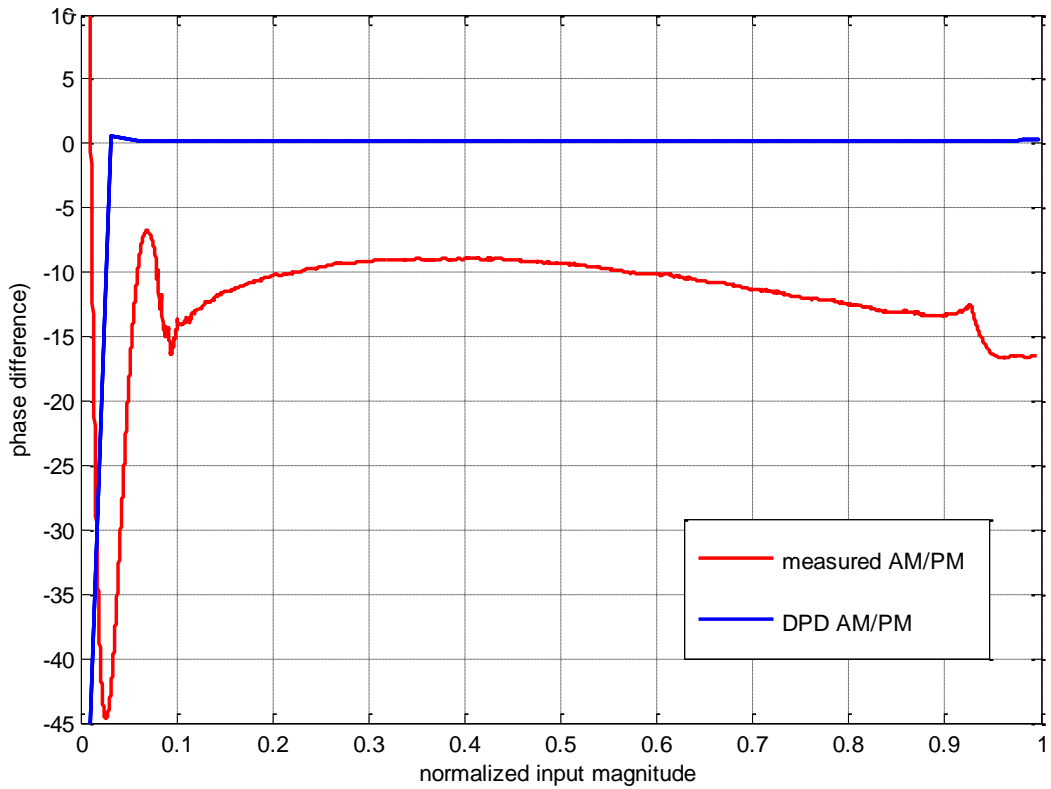


Figure III. 45: Extracted two-tone phase variation

Similarly Fig.III.45 represents the average variation of the phase of the input and output envelope versus the normalized input envelope magnitude and its calculated inverse function. Using these inverse functions a new set of distorted baseband IQ data is obtained which is then sent to the vector signal generator to generate a pre-distorted signal. The distorted envelope and phase obtained from the inverse transfer function is depicted in Fig. III.46.

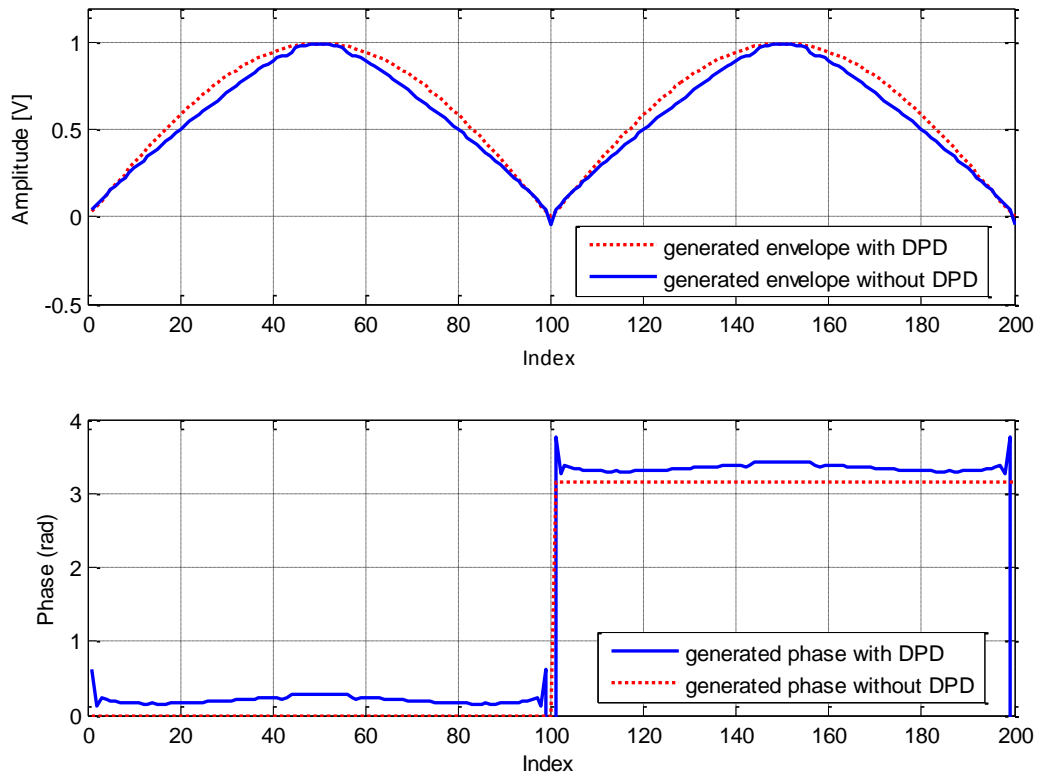


Figure III. 46: Generated DPD envelop and phase

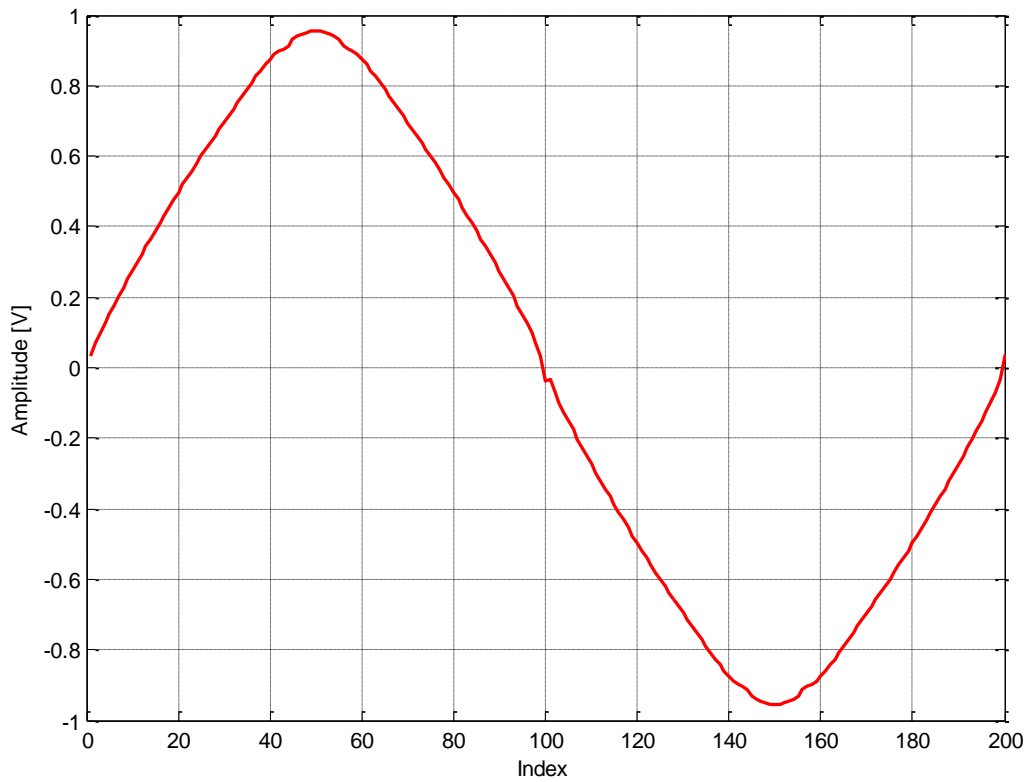


Figure III. 47: Generated I signal with DPD

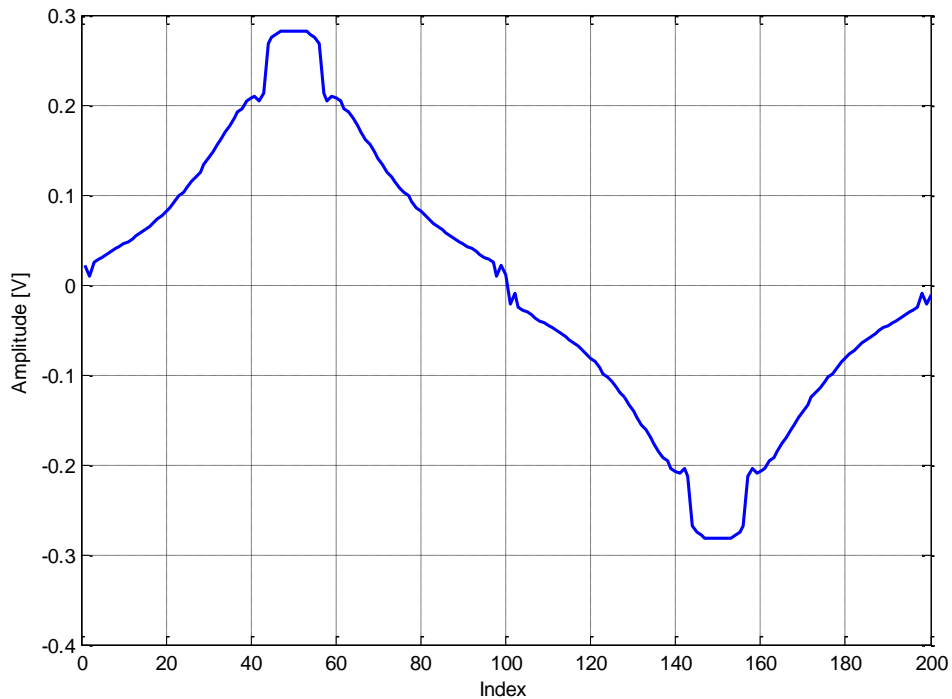


Figure III. 48: Generated Q signal with DPD

Fig. III.47 and III.48 represents the generated distorted baseband IQ signal which is then applied to the AUT for linearization. Encouraging results have been obtained in terms of IMD for the two tone test. Fig. III.49 represents the measured IMD levels and it can be seen that an improvement of 8 dBc has been achieved at saturation, whereas it improves to 16 dBc at 3 dB back off.

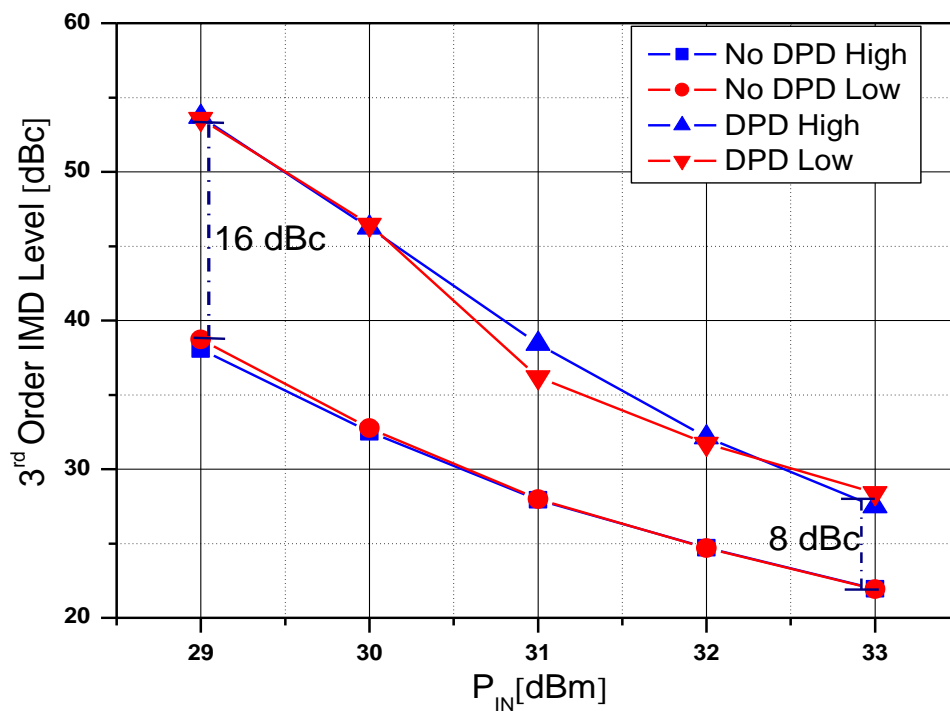


Figure III. 49: Extracted pulsed envelop and phase information

## Conclusion

This chapter presents a quadrature sampling process which is a method to vector detect an RF signal. The reduction of component density in the analog domain and the direct digitization of entire RF spectrum bring more flexibility in the receiver's performance. The use of the sub-harmonic sampling enables us to extract the in-phase and quadrature components. If the ratio between  $\frac{F_{\text{sampling}}}{F_{\text{IF}}}$  is set to 4 which means that the ADC samples at exactly four times the IF signal then inphase and quadrature components could easily be extracted by digital mixing. Once the inphase and quadrature components are known then the amplitude and phase of the RF signal is calculated. The absolute calibration technique to remove systematic errors within the measurement system has been presented. A one channel THA based setup was built and sequential measurement was made at the input and out of DUT. As the measurement is not simultaneous at the two ports, a time alignment method is needed to synchronize the input and output signal. The results obtained are validated with the measurement of a commercially available single channel VSA which works on the same principle of quadrature sampling.

Next a fully calibrated 4-channel time-domain test bench is built for characterization of high-power GaN amplifier in terms of power and linearity. This proposed test bench has the capability to extract the dynamic characteristics of PA under different modulation signals. This ability allows the extraction of the two-tone transfer characteristics that are highly useful in designing a digital pre-distortion linearization scheme for a static AUT. A significant improvement in the third-order inter-modulation products has been shown using the baseband pre-distortion linearization scheme. A key aspect of the four channels is that no time alignment is required to get time-aligned input and output envelope before proceeding to digital linearization scheme.

---

## BIBLIOGRAPHIE :

---

- [1] Jan H. Mikkelsen “Front-End Architectures for CMOS Radio Receivers”, *Division of Telecommunications, Aalborg University*, Internal Report; No. IR96-1003, 2006.
- [2] National instruments “What is IQ data”, *Tutorial, www.Ni.com*.
- [3] Eng. Chun Heong, “Design and development of an automated demodulator calibration station”, *Masters Dissertation –Singapore Technologies Kinetics Ltd. University of Birmingham, UK, 2000*.
- [4] Kenneth J. Hetling, “Multirate sub-harmonic sampling”, *MIT Lincoln laboratory 244 wood streets, Lexington, IEEE ICC, vol.2, pp.763-767, 2000*.
- [5] J.Verspecht, “Calibration of a measurement system for high frequency non-linear devices”, *Doctoral Dissertation - Vrije universiteit Brussel, November 1995*.
- [6] Agilent technologies“Agilent Specifying Calibration Standards for the Agilent 8510 Network Analyzer”, *Application note 8510*.
- [7] Peder Malmlof, “RF- measurement technology”, *Third edition Ericsson Radio access AB Gavle. October 2002*.
- [8] D. C. DeGroot, K. L. Reed, and J. A. Jargon, "Equivalent circuit models for coaxial OSLT standards," 54th ARFTG Conference Digest, pp. 103-115, 1999.
- [9] Tibault Reveyrand, “*Conception d’un système de mesure d’enveloppes temporelles aux accès de modules de puissance. Application à la mesure du NPR et à la modélisation comportementale d’amplificateurs.*”, doctoral dissertation, 25 April 2002, Limoges.
- [10] M. Abouchahine, “*Développement d’un Banc de Caractérisation Fonctionnelle Large Bande (Porteuses et Enveloppes) dans le Domaine Temporel de Dispositifs non linéaires microondes*”, doctoral dissertation, XLIM France, 28 Sep 2011.
- [11] M. Saad-el-Dine, “*Linéarisation des amplificateurs de puissance à haut rendement en combinant les techniques de pré-distorsion numérique et le contrôle de polarisation*””, doctoral dissertation, 18 Dec. 2009, Limoges.
- [12] J. Max and J. Lacoume, *Méthodes et techniques de traitement du signal et applications aux mesures physiques*, MASSON, Ed., 1996, vol. Tome 1.
- [13] Grégoire Nanfack Nkondem, “*Développement d’un système de caractérisation temporelle d’enveloppe d’amplificateurs de puissance. Application à la linéarisation d’amplificateurs par prédistorsion en bande de base*“, Ph.D, dissertation, Université de Limoges, 2008.
- [14] Ahmed, M. Saad-el-Dine, G. Neveux, T. Reveyrand, D. Barataud, J. Nebus, “*Time-Domain Measurement System Using Track & Hold Amplifier Applied to Pulsed RF Characterization of High Power GaN Devices*” IEEE International Microwave symposium Baltimore 2011.

- [15] Nitronex “NPTB00050 Datasheet”, NDS-007 Rev. 2, May. 2009 available at <http://www.nitronex.com>
- [16] M Saad El Dine, T. Reveyrand, G. Neveux, P. Bouysse, D.Barataud, J.-M. Nebus, W. Reberneck, “A Measurement Set-up and Methodology Combining Dynamic Biasing and Baseband Predistortion for High Efficiency and Linear Amplifier design”, International Microwave Symposium Boston USA, 2010.
- [17] Martin Weiß, “Measuring the Dynamic Characteristic of High- Frequency Amplifiers with Real Signals,” *European Wireless 2000, September 2000, Dresden.*
- [18] S. Ahmed, M. Saad-el-dine, G. Neveux, D. Barataud, J. Nebus “4-Channel, High Dynamic Range Time-Domain Measurement System Using Track & Hold Amplifier Utilized for the Characterization and Linearization of High Power GaN Amplifiers” International Journal of Microwave and Wireless Technologies, volume 4, issue 01, pp. 71-79.
- [19] M. El Yaagoubi, G. Neveux, D.Barataud, T. Reveyrand, J.-M. Nebus, Verbeyst, F.; Gizard, F.; Puech, J, “Time-Domain Calibrated Measurements of Wideband Multisines Using a Large-Signal Network Analyzer”, *IEEE Transactions on Microwave Theory and Techniques*, vol. 56, Issue 5, Part 1, pp. 1180 - 1192, May 2008.
- [20] Ilari Teikari, “Digital predistortion linearization methods for RF power Amplifiers”, *Doctoral Dissertation – Helsinki University of Technology, 26<sup>th</sup> September, 2008.*
- [21] K. A. Morris and J. P. McGeehan, “Gain and phase matching requirements of cubic pre-distortion systems,” *Electron. Letters*, vol. 36, no. 21, pp. 1822–1824, Oct. 2000.
- [22] D. Giesbers, S. Mann, K. Eccleston “Adaptive digital pre-distortion linearization for RF power amplifier”, *13<sup>th</sup> Electronics New Zealand Conference (ENZCON2006), pp. 244-248, 13-14 Nov 2006.*

## **CHAPTER IV:**

# **RF Transients Measurement**

---





## Introduction

RF measurements system as discussed earlier have a bottleneck within the system which comes from analog to digital converters (ADC) which is one of the basic part of signal processing. ADC's have a limited bandwidth and roughly the maximum sampling rate and the resolution of the ADC are inversely proportional to each other. Hence a physical bound to the digital representation of analog signals exists. Due to this constraint, an RF measurement is divided into three different steps. Primary among them is the down-conversion of the received RF signal into an IF signal, whose spectrum is contained within the bandwidth limitations of the ADC. Then the digitization of the IF signal is performed and finally the signal processing takes over.

In conventional time-domain measurement systems the down-conversion is performed either by using samplers or mixers. Both translate the RF signal into a baseband signal. The signal can then be digitized by an ADC at a high sampling rate and after it can be processed using different signal processing techniques. The final signal represented is a translated baseband signal and not an RF signal. For modulated signals this approach does not give any information regarding the envelope transients which describe the transition of a pulsed signal from one state to another. For example in case of modulated RF signals at most the pulsed envelope measurement is performed which means that evolution of the envelope of the RF signal versus time is measured. This is performed by digitizing the acquired time-domain samples and then an IQ modulator is used to generate vector demodulation and extract the I and Q signal transformation components. This is a hardware implementation from rectangular to polar coordinates. Applying trigonometric identities to the  $I(t)$  and  $Q(t)$  components allow us to extract the instantaneous amplitude,  $A(t)$ , and phase,  $\phi(t)$  of the signal.

For the characterization of high power non-linear devices which undergo different undesired phenomenon like electrical, thermal and trapping effects that ultimately affect the device performance, many different characterization techniques are available to use under modulated excitation. A pulsed characterization is commonly used and for an accurate pulsed characterization, it is very important that the bandwidth of the RF measurement system is very high so that the complete complex harmonic spectrum can be retrieved in a single take. This phenomenon is prohibitive due to huge front end bandwidth demands. One of the

methods to achieve an extremely high sampling rate is to utilize time interleaved sampling. This method is extremely used in multi-Gigahertz bandwidth oscilloscopes [1].

In this chapter a direct voltage sampling technique has been used due to the use of THA's. The advantages of this setup is that it directly feed the ADC and do not require any additional IF circuitry. Similarly the use of a common sinusoidal clock by both the THA and ADC further facilitates the application of time interleaved sampling techniques. Using this technique, an RF modulated spectrum with complete RF transients is measured and the memory effects within the device are characterized.

## I. Coherent Time-Interleaved System

### I.1. An adaption of sub-sampling principle

#### I.1.1. Real sampling frequency calculation

The goal of this work is to increase the overall direct sampling rate to measure an RF signal. The Nyquist criterion as stated in Eq.139 states that if the sampling rate is twice the highest frequency contained within the signal no aliasing is produced and accurate information is retrieved in frequency domain.

$$F_{S-RF} = n * F_{RF} \quad \text{Eq:-139}$$

Where

$$n \geq 2$$

$F_{RF}$ = fundamental RF frequency

$F_{s-RF}$ =Direct RF Sampling frequency

$n$ =Number of desirable samples contained in an RF signal period

To accurately interpret a signal in the time-domain it is necessary that the RF signal is sampled far beyond the rate specified by Nyquist which means that  $n \gg 2$ . The practical implementation of this equation is prohibitive for RF signals due to front end bandwidth limitations (ADC). Sub-sampling is one of the solutions to implement an equivalent high sampling rate for periodic signals respecting Eq.139 as followed:

$$F_{e\_RF} = n * F_{RF} \quad \text{Eq:-140}$$

Where

$F_{e-RF}$ =Equivalent RF Sampling frequency

$$n \gg 2$$

To obtain this equivalent RF sampling rate, the measurement systems use sub-sampling principle based on a real sampling frequency that is defined by the following equations

$$T_{RS} = T_{FRAME} + T_{e\_RF} \quad \text{Eq:-141}$$

$$T_{FRAME} = N_{TRF} * T_{RF} \quad \text{Eq:-142}$$

Where

$T_{RS}$ = Period of real sampling frequency (the rate at which the samples are actually taken by the instrument)

$T_{FRAME}$  = acquisition time is divided into time a time interval and for modulated signal it is equal to one modulation period minimum.

$N_{TRF}$ = an integer number that is equal to the number of fundamental RF periods falling in the frame period  $T_{FRAME}$ .

The implementation of these equations corresponds to a stroboscopic sample acquisition where the samples are sequentially acquired. The main drawback of this sequential method is that the real sampling frequency ( $F_{RS}$ ) can become very low. Consequently, the acquisition time that is required to measure the desired RF signal can become very large when the  $T_{e\_RF}$  tends to 0.

To find a trade-off between the acquisition time of a signal and the real sampling frequency, Coherent Time Interleaved Sampling (CTIS) is developed [1]. The main idea is to divide  $T_{FRAME}$  into number of (K) segments where K is also an integer (number to maintain the coherence of the sampling acquisition process).

$$T_{SEGMENT} = \frac{T_{FRAME}}{K} \quad \text{Eq:-143}$$

Hence, Eq. 141 can be re-defined by replacing  $T_{FRAME}$  to  $T_{SEGMENT}$  as follows:

$$T_{RS} = T_{SEGMENT} + T_{e\_RF} \quad \text{Eq:-144}$$

The repercussion of this change is that the acquired samples are scrambled in time and hence the measurement of the time signal requires re-ordering of the samples. The advantage of this process is that the acquisition time is reduced by a factor of K. Time interleaved samples acquisition was performed over number of frames and finally all the scrambled samples within all frames are re-ordered to represent the complete signal in one frame.

The number of samples required ( $N_{SAMPLES}$ ) to perform interleaving is equal to:

$$N_{SAMPLES} = n * N_{TRF} \tag{Eq:-145}$$

Introducing Eq. 141, 142 and 143 in Eq.144 leads to the representative equation for the coherent time interleaving process:

$$T_{RS} = T_{e\_RF} * \left[ \frac{N_{SAMPLES}}{K} + 1 \right] \tag{Eq:-146}$$

This real sampling time is used to acquire the desired number of samples of the signal under test and represent a frame period as set initially. The number of frames ( $N_{FR}$ ) falling into the acquisition interval before interleaving can be determined by the following relation Eq. 147

$$\frac{T_{RS}}{T_{FRAME}} = \frac{N_{FR}}{N_{SAMPLES}} \tag{Eq:-147}$$

The samples acquired are not in the properly ordered so re-ordering of the samples is required once the acquisition is complete as shown in Fig.IV.1.

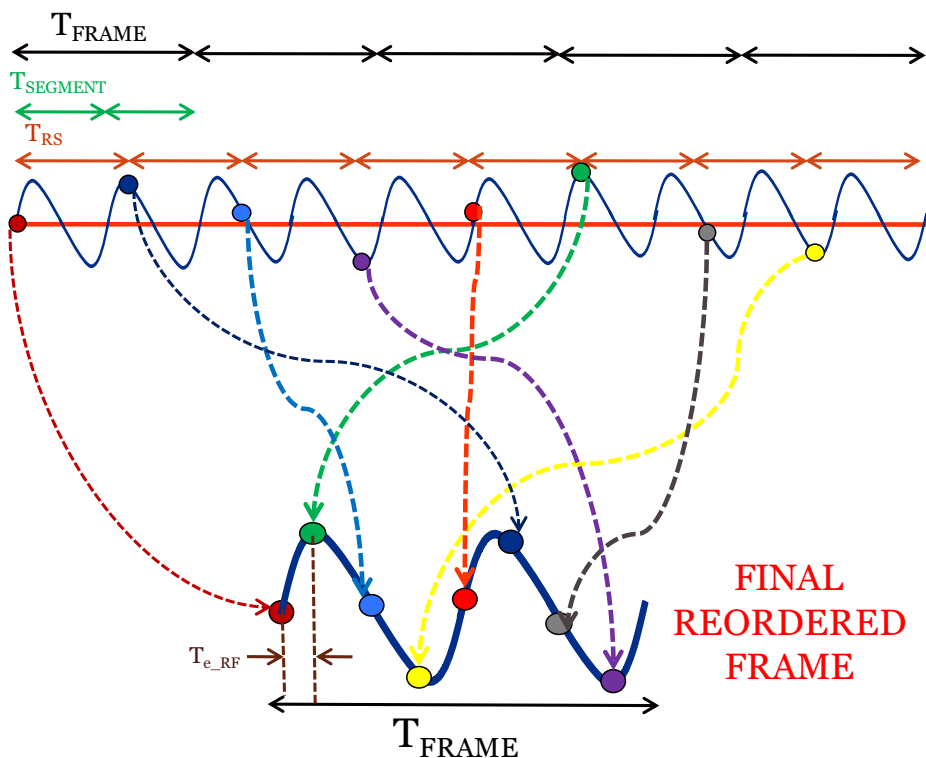


Figure IV. 1: De-scrambling phenomenon in CTIS.

### I.1.2. De-scrambling of samples

The first step that is needed to re-order samples is to determine the beginning and the end time of each frame and that to calculate the shift of the first sample (Eq. 148) corresponding to each frame starting from this beginning time instant.

$$[Shift]_{nFR} = \left[ t_{snFR} - T_{FRAME} \frac{(i_{FR} - 1)_{nFR}}{T_{e_{RF}}} \right] \quad \text{Eq:-148}$$

Where

$t_{snFR}$  = time instant of first sample corresponding to frame  $n^{\circ}n_{FR}$

$i_{FR}$  = index of frame

$n_{FR}$  varies from 1 to  $N_{FR}$

Because the non coherent sampling frequency (the sampling frequency is not an integer number) the number of samples in each frame is not constant. This can be calculated by the following Eq. 149

$$[Nbr]_{nFR} = [(i_{EFR} - i_{BFR}) + 1] \quad \text{Eq:-149}$$

Where

$Nbr$  = an array containing the number of samples present in each frame

$i_{EFR}$  = the index of the last sample in each frame

$i_{BFR}$  = the index of the first sample in each frame

The last step is to re-order (Eq.150) the sample points using the calculated scrambling information:

$$[New\_index] = [1: N_{FR} : (N_{NFR} * Nbr_{nFR})] + [Shift]_{nFR} \quad \text{Eq:-150}$$

### I.1.3. Example explaining CTIS

To explain CTIS an example is formulated that illustrates the interleaving and de-scrambling process. In this example a fundamental frequency  $F_{RF}$  of 250 MHz is chosen. This is very low but is used as an illustration that explains the CTIS phenomenon.

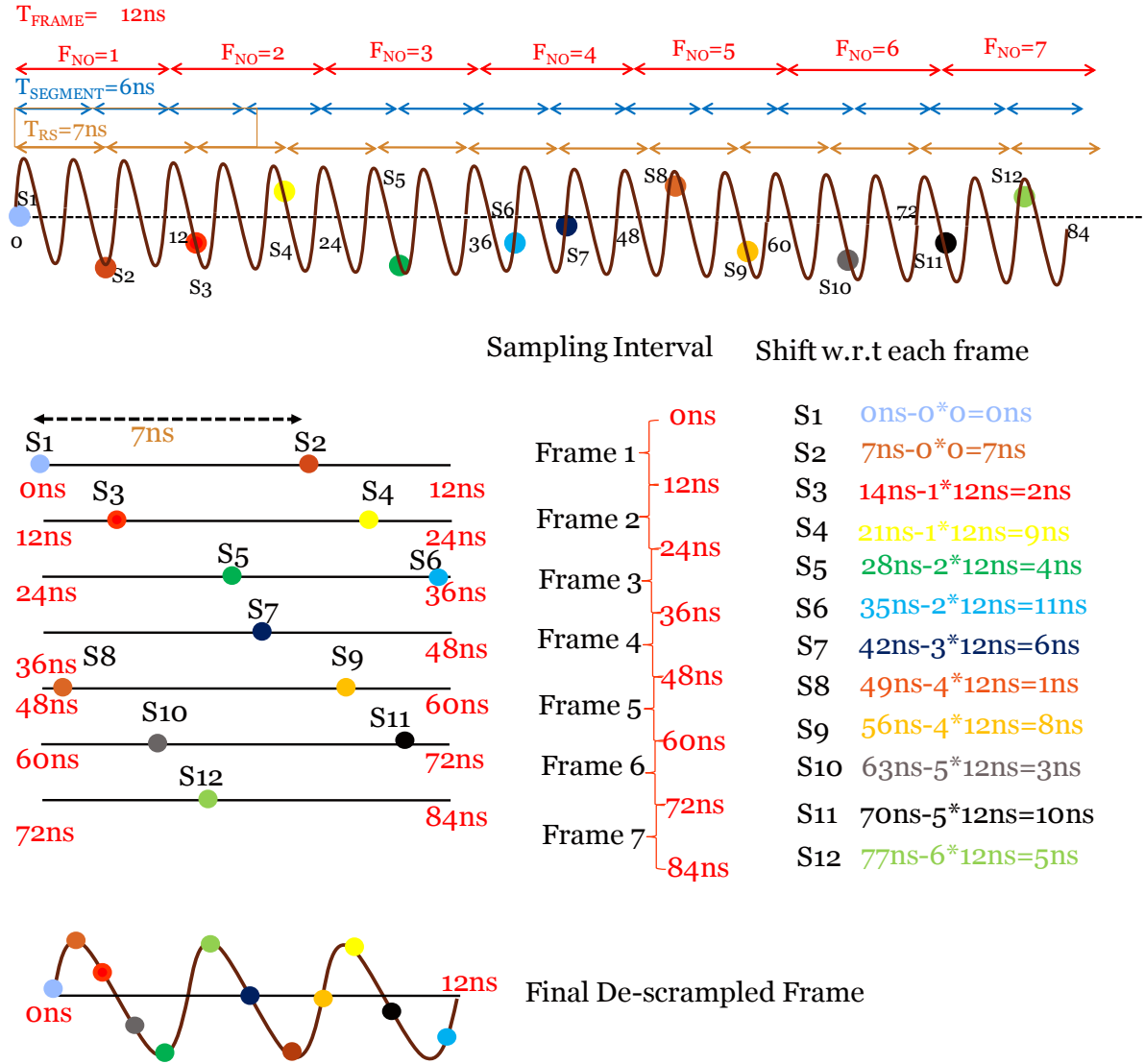


Figure IV. 2: Example explaining CTIS sampling and de-scrambling procedure.

An equivalent RF sampling frequency  $F_{e-RF}$  of  $4 * F_{RF}$  is chosen. The frame period  $T_{FRAME}$  of 12 ns is selected which ensures that 3 RF periods  $T_{RF}$  fit within the frame. This means that the final frame would contain three RF periods with 12 samples and each sample is at a time difference of 1ns as shown in Fig. IV.2. To adapt to a real sampling frequency which is less than the  $F_{RF}$  a segment time  $T_{SEGMENT}$  of 7 ns is chosen. Using Eq.142, 143 and 144 the value of K and number of samples are calculated:

$$T_{RF} = 4\text{ns}$$

$$N = 4$$

$$T_{e-RF} = 1\text{ns}$$



$$T_{\text{FRAME}} = 12\text{ns}$$

$$N_{\text{TRF}} = 3$$

$$N_{\text{SAMPLES}} = 4*3$$

$$T_{\text{SEGMENT}} = 6\text{ns}$$

$$K = 2$$

Putting these values in Eq. 146 we get the real sampling frequency  $T_{\text{RS}}$ .

$$T_{\text{RS}} = 1e^{-9} \left[ \frac{12}{2} + 1 \right] = 7e^{-9}\text{s}$$

Thus the real sampling frequency calculated is 142.8571429 MHz. A very high resolution signal generator is required to generate this non synchronous clock signals. Fig. IV.2 represents the complete sampling and descrambling process for the above example.

## II. CW Measurement System Description and Results

### II.1. CW wave measurement

#### II.1.1. CW measurement setup and calibration

The 4-channel time-domain measurement system employing the time-interleaving system is described in Fig. IV.3. A modulated signal generator unit is used to generate RF CW. The signal is linearly amplified and feeds the input of the power amplifier under test (AUT). The incident and reflected signals at the input and output of DUT are measured at the same instant by using two bi-directional couplers, and four 13 GHz bandwidth 2 GS/s THAs. The THAs are followed by differential amplifiers and a four channel 420 MS/s, high dynamic range (12 bit) ADC. A common high precision sinusoidal clock that is configured by the previously described CTIS calculation is fed into the THA and the ADC. The RF signals are then directly sampled by the THA and the ADC that are synchronized by a 10 MHz signal. The acquired data is then processed to reorder the samples.

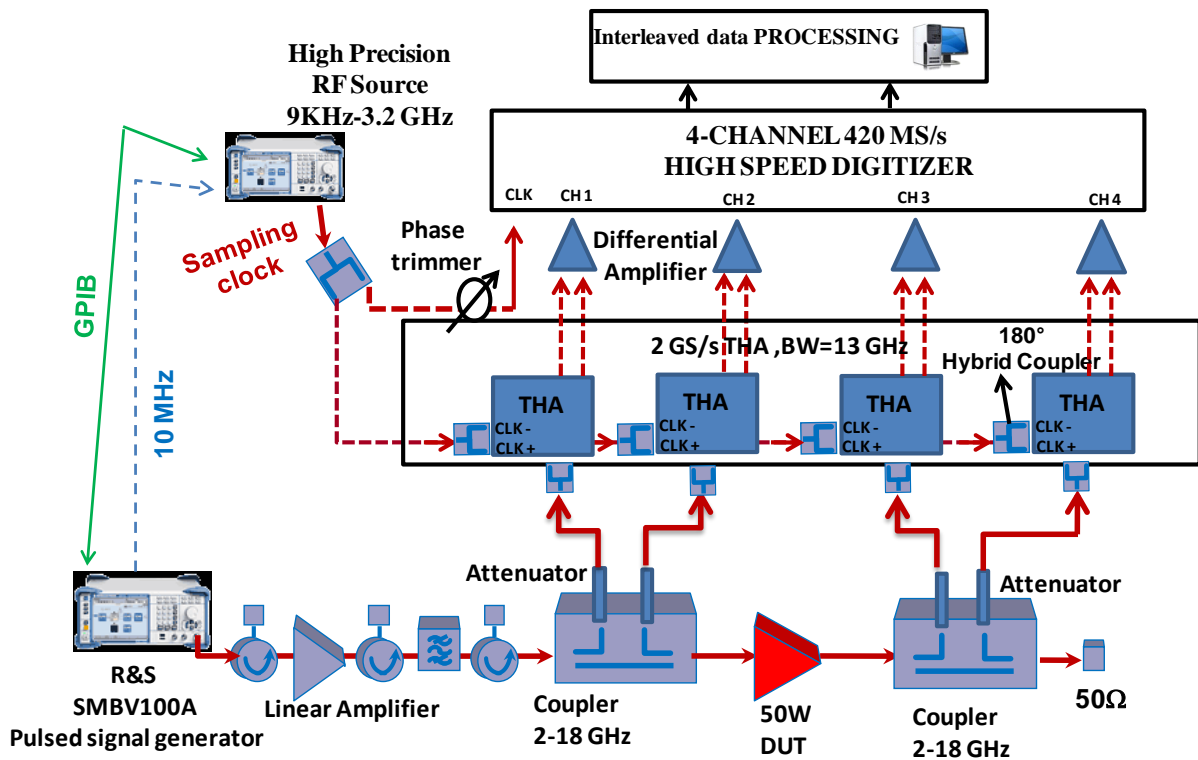


Figure IV. 3: Block diagram of measurement setup for CW measurement.

The main difference between this test bench and the test benches presented in the previous chapter is that this setup includes wide band couplers and no filters are present before the THAs. Therefore this bench characterizes the complete non-linear behaviour of the PA including the harmonics of the RF. The configuration of the clocks is different as the same non-synchronous continuous sinusoidal clock is used for THA and ADC and its frequency is set using CTIS.

An absolute SOLT system [2] calibration was performed to mathematically remove systematic errors. The goal of the calibration procedure was to determine the eight unknown complex error coefficients for each frequency (fundamental and harmonics). The first three steps are similar to the calibration procedure performed for classical vector network analyzer by connecting a priori known short, open and load standard to port 1 and port 2 respectively. Next a through connection is made between the two ports. These error coefficients are obtained from raw data provided by ADC measurement channels to the incident and scattered power waves at the input and output of device under test. The next step is to determine the coefficient  $K$  which is also a complex function of the frequency. Its amplitude is found by connecting a power meter to port one and a power measurement is taken for each frequency.

Then the signal generated by a [357-536 MHz] comb generator that is excited by a frequency of 500 MHz is fed to the measurement system and the time-domain waveform is acquired at an equivalent sampling rate of 250 Gsamples/s. The SRD is excited by a sine wave, the frequency of which is selected so that it contains all the frequencies of interest at the output of the DUT.

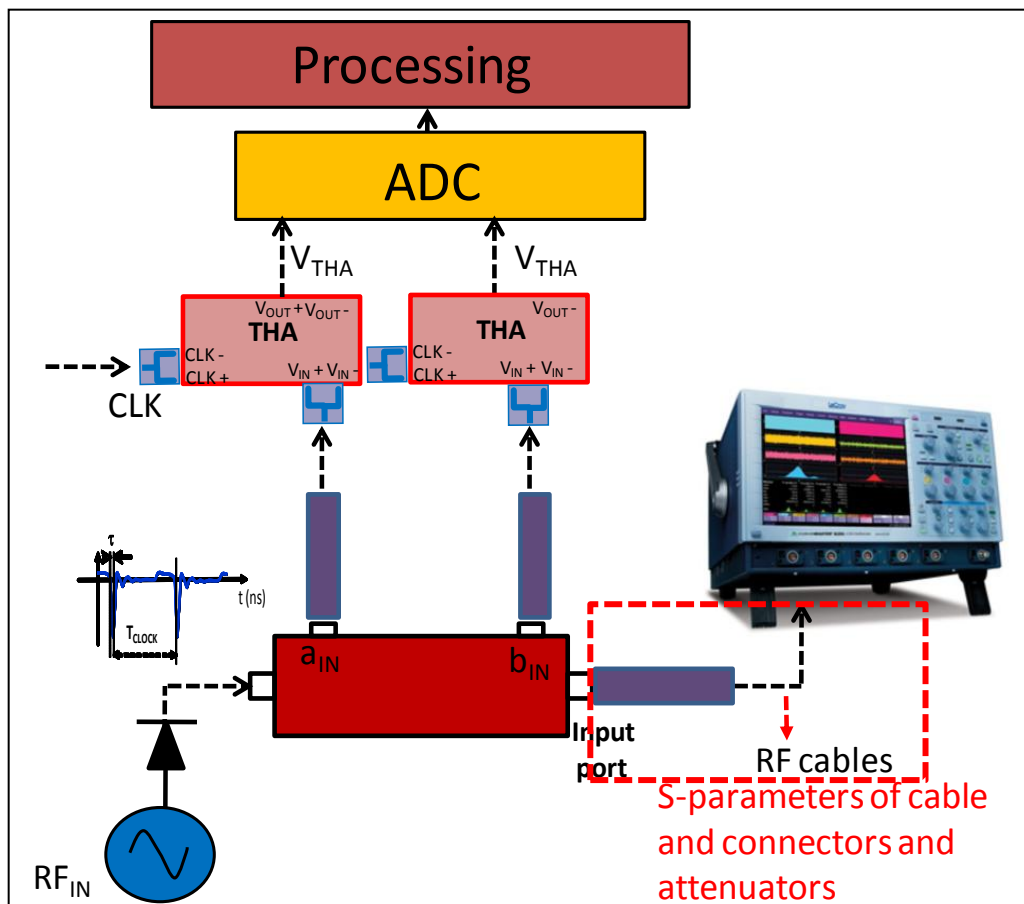


Figure IV. 4: Phase error correction using a HPR and Lecroy oscilloscope

A previously calibrated Lecroy oscilloscope is connected at the same time to port 1 as described in Fig. IV.4. The scope is used as harmonic phase reference. The Lecroy oscilloscope also works on the interleaved sampling principle. It is configured to acquire the signal at an equivalent sampling rate of 512 Gsamples/s. The acquired waveform is processed to de-embed the effect of the cable and the connectors using their respective S-parameters. Finally, a phase correction factor for the desired frequencies is calculated based on the measurement of the scope and the test bench.

### II.1.2. Automated Measurement Setup for CW signal

The complete test setup as described in Fig. IV.3 is automated using Labview and Matlab. A user friendly program is developed to calculate the calibration coefficients for multiple frequencies [1-13GHz]. The calibration coefficients are calculated automatically by the calibration program by just sequentially connecting the SOLT calibration standards to port 1 and port 2. Calibration of 4-channels was performed using the CTIS system.

The acquisition of the time-domain waveforms present at 4 channels is also automated. This means that the desired sampling rate is defined by the user, and then the algorithm is developed to which automatically calculate the time interleaving characteristics. Raw data samples are acquired using CTIS and are descrambled and error corrected in terms of amplitude and phase. A citi file is created to display the measurement results using ADS. Fig IV.5 describes the block diagram for of the software that is needed for the measurement of a CW signal.

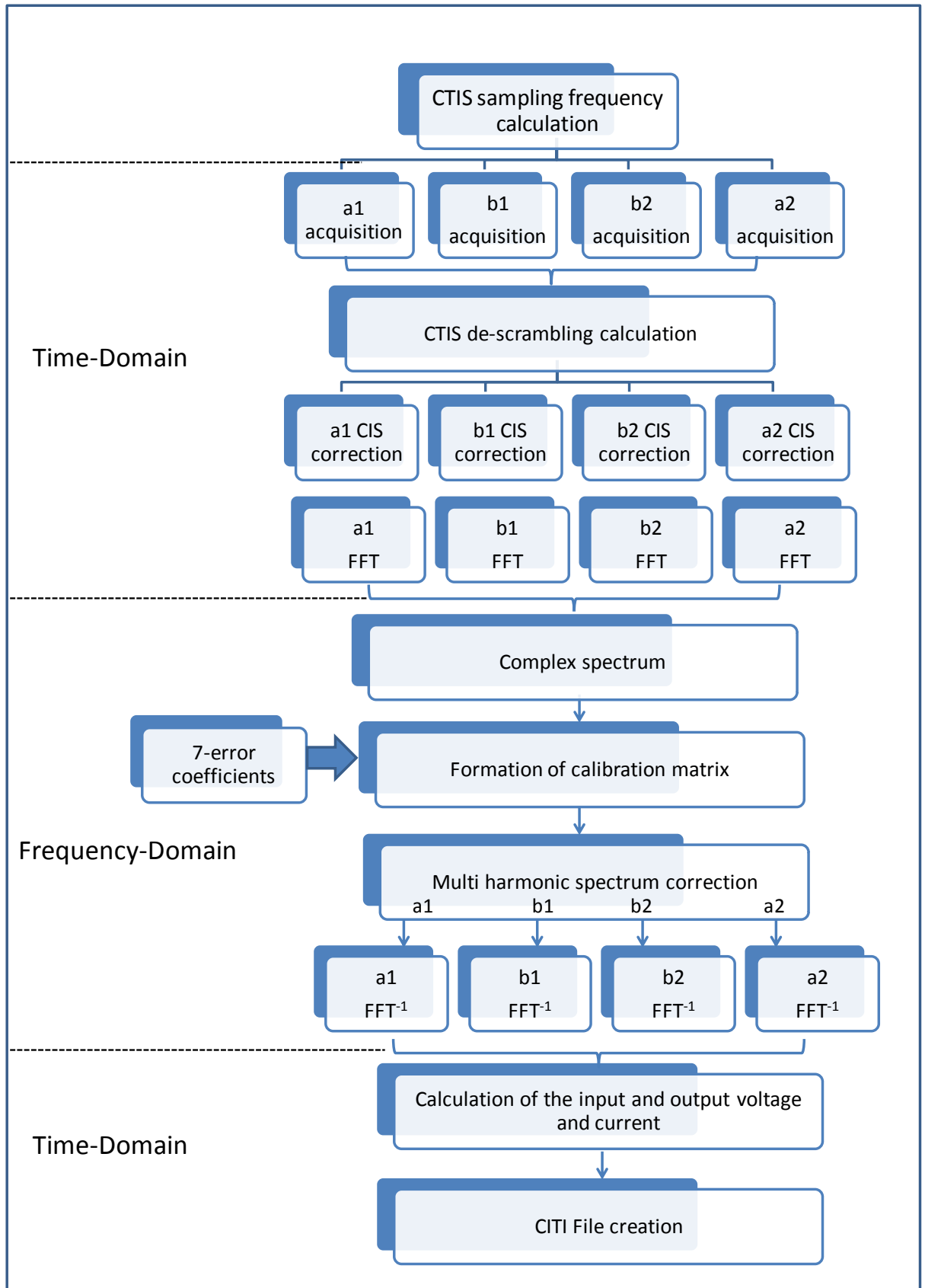


Figure IV. 5: Block diagram of measurement setup for CW measurement.

### II.1.3. CW Measurement results

The proposed CTIS based test bench has been used for the characterization of a 50 W GaN Nitronex (NPTB00050B) [3] PA. The PA is excited by a CW signal at a frequency of 2.5 GHz. A virtual sampling frequency of 250 Gsamples/s (4ps) was achieved which is 100 times the fundamental frequency. Conventional DC, RF and power characterization of the PA were performed. Fig.IV.6 presents the corrected input, output current and voltage time-domain waveforms for a power sweep at input between 5-35dBm (3 dB compression). Note that the output matching network of the PA is very well designed that no harmonics are present at the output port even at a 3 dB compression level.

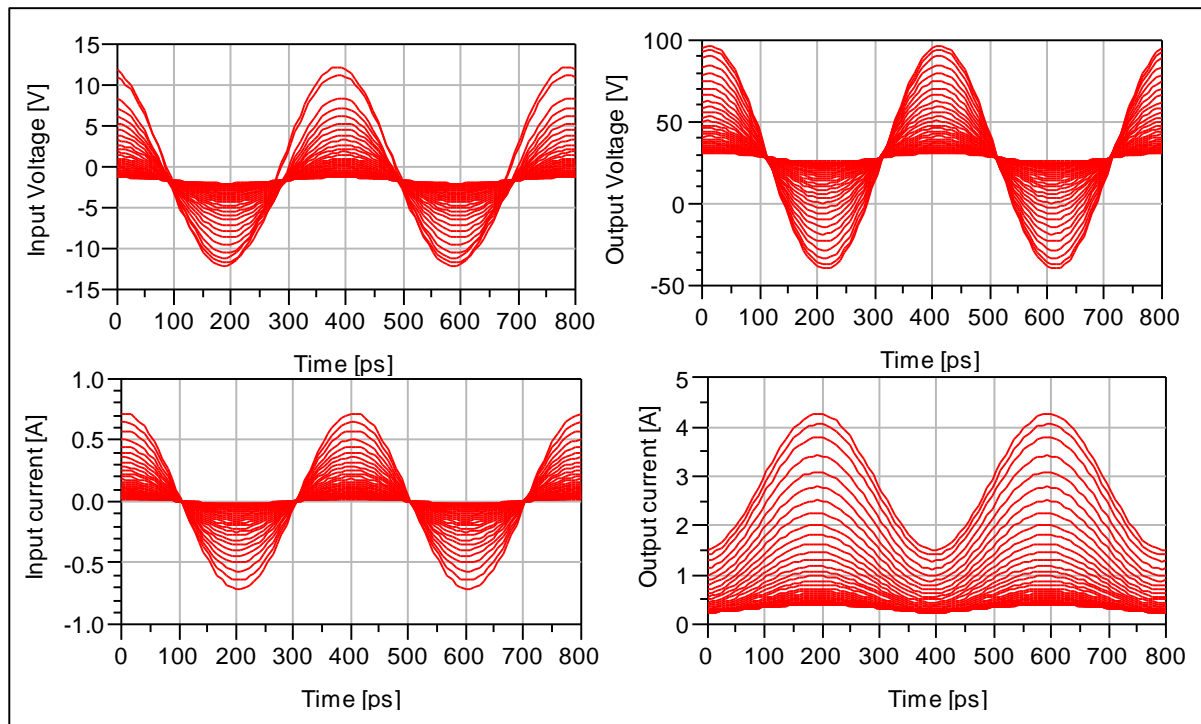


Figure IV. 6: Measured voltage and current waveforms at the input and output port

The DC characteristics are captured by the automated power supplies in this case. The gate voltage, the drain current and the drain voltage remain constant during the power sweep while the drain current varies from 300mA to 2.9A as the DC consumption increases with the input power.

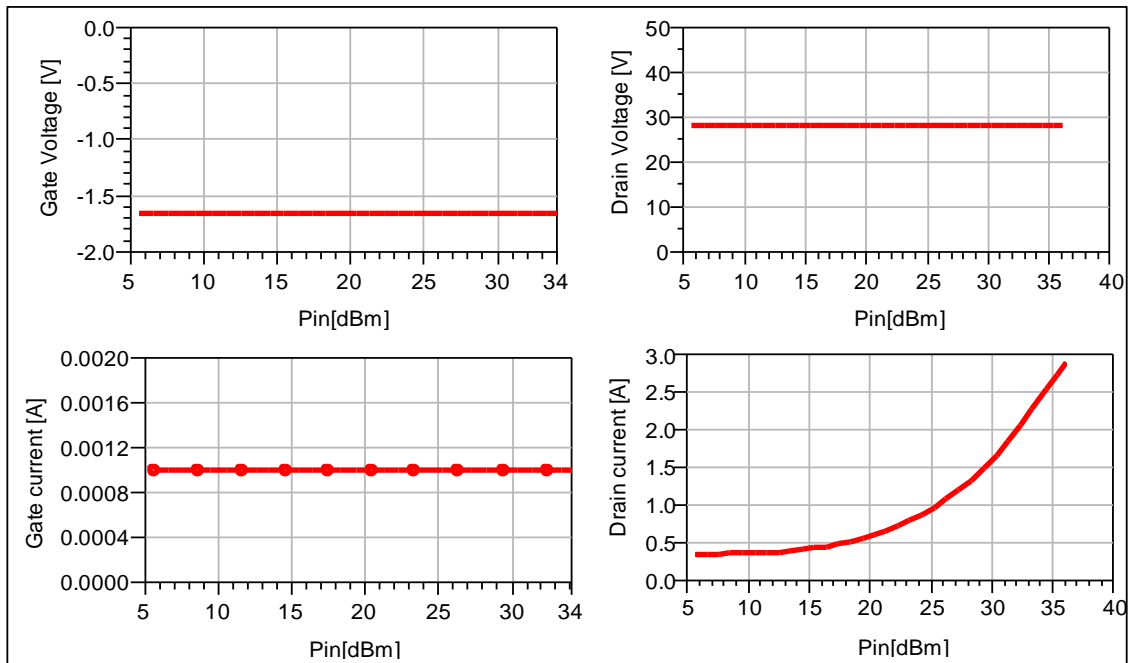


Figure IV. 7: Measured DC characteristics of the PA.

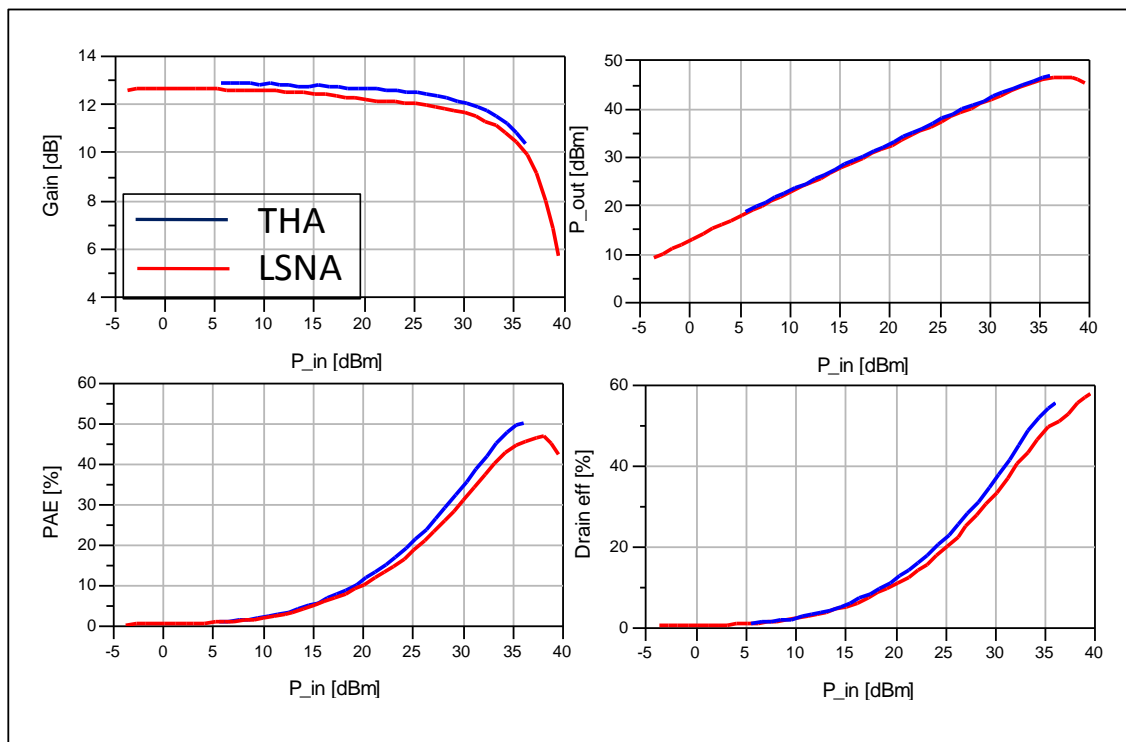
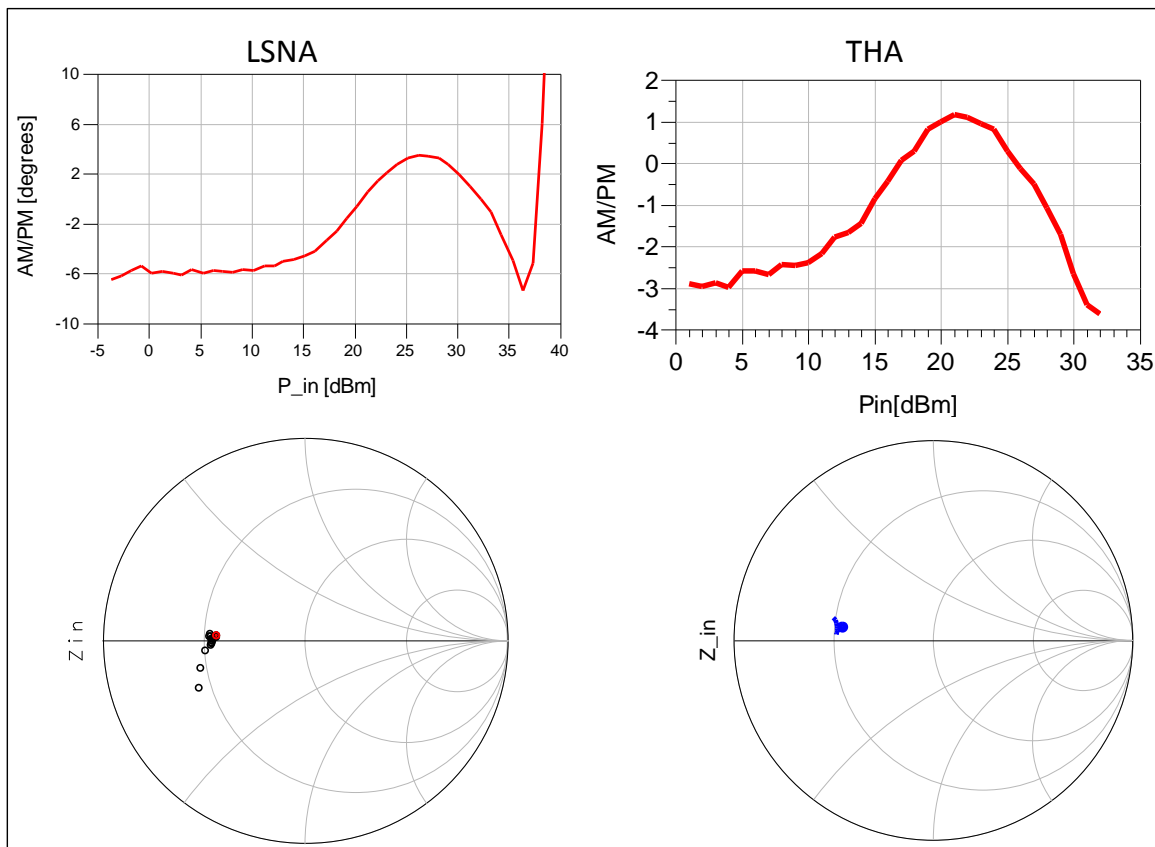


Figure IV. 8: Measured Power characteristics.

The 1 dB compression point was measured at an output power of 45.6 dBm and a power gain of almost 12 dB (Fig. IV.8) was measured. The maximal drain efficiency (Fig.IV.9) is measured to be 55 % while the PAE reaches 50 %.



**Figure IV. 9: Measured AM/PM characteristics and input impedance.**

A phase variation of 4 degrees was recorded (Fig IV.9) for the whole power sweep which ensured the linearity of the PA. The input impedance that is calculated using the captured waveforms is also displayed in Fig. IV.9. All the results are compared with the measurement results of the LSNA [4] and similar performance has been noticed in terms of power, efficiency and AM/PM.

## II.2. Measurement of a broadband amplifier

### II.2.1. CW performance

To test the capabilities of the measurement setup a broad band 1-3GHz GaN PA designed for radar applications was characterized. The test setup as explained in Fig. IV.3 is used and the PA is characterized in terms of power, linearity and efficiency. The PA is excited with a continuous sinusoidal signal and is biased at a quiescent current of 300 mA and a drain voltage of 50 Volts.



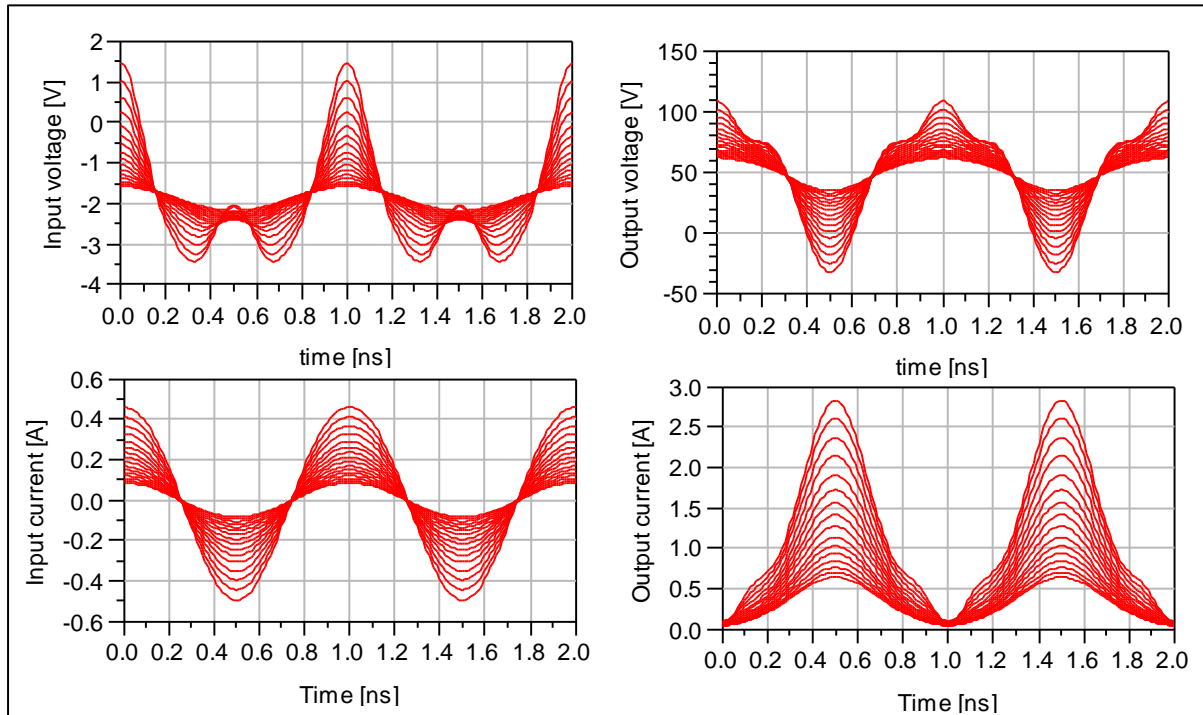


**Figure IV. 10: Corrected input, output voltage and current waveforms.**

The input, output voltage and current time-domain corrected waveforms are captured as displayed in Fig. IV.10. From the input voltage waveforms it's noticed that the input reflection coefficient is very high as we can see that the input waveform when pushed to saturation becomes highly nonlinear. Similarly, the output waveform depicts the presence of multiple harmonics.

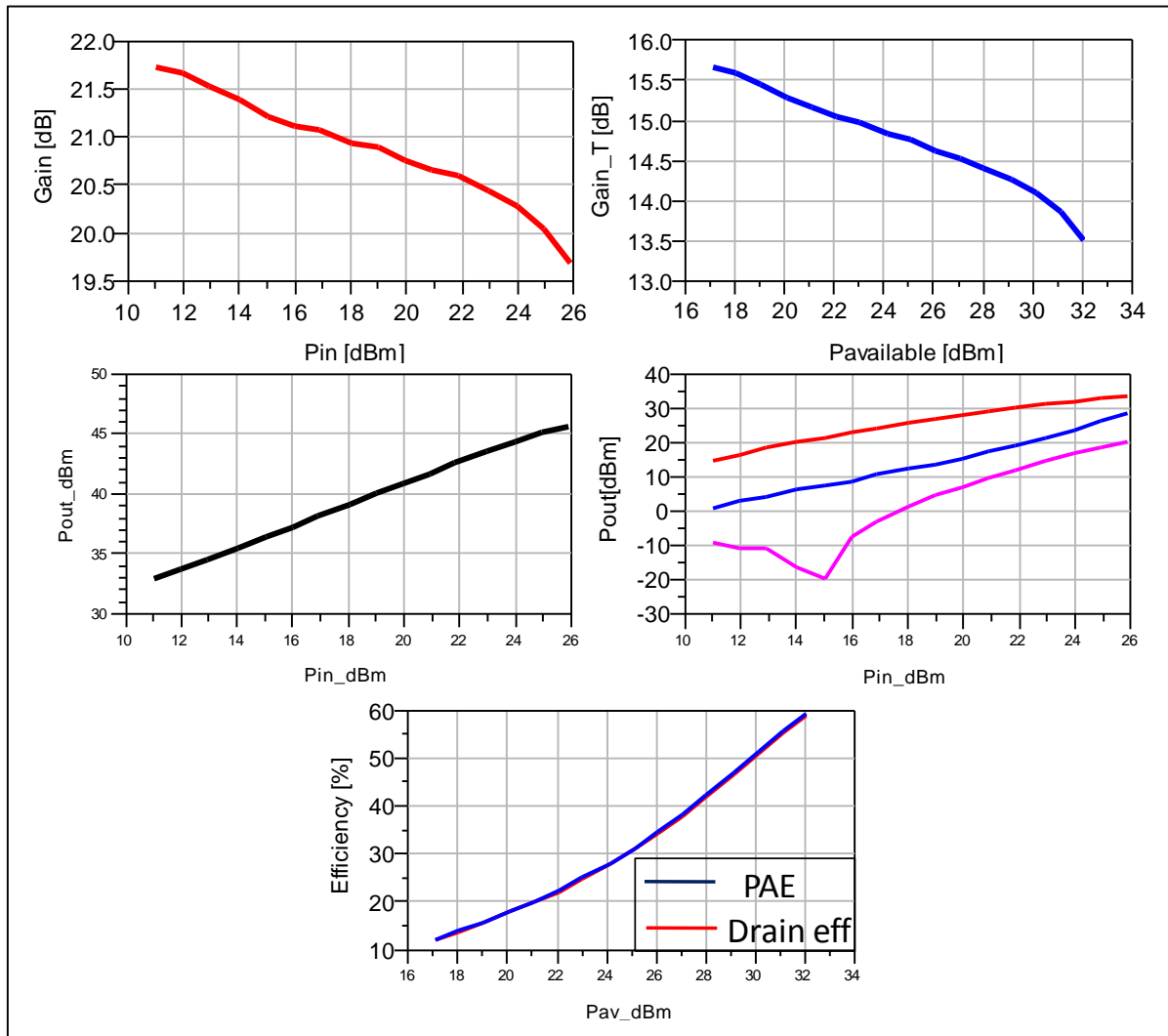


**Figure IV. 11: Measured Power characteristics for non-linear amplifier.**

Analyzing the power characteristics of the power amplifier its noticed that due to the high input reflection coefficient a difference of almost 6 dB is measured between the power and the transducer gain. The 1 dB compression output power, the output power at multiple harmonics and the efficiency of PA are displayed in Fig. IV.11. The DC measurements were made with a power supply.

### II.2.2. Quasi square signal measurement results

To verify the capability of a broadband class s PA a specific test is performed using a quasi square wave signal excitation [5]. The measurement setup as explained in Fig. IV.3 is modified and a quasi square signal (signal with odd harmonics) is generated to test the S band octave bandwidth PA behavior under multiple harmonics. The combination of the

fundamental and the third harmonic and the optimum amplitude ratio between them yields a quasi square signal. The new test setup is explained in Fig. IV.12. It can be seen that two signal generators are used to produce the fundamental ( $f_0$ ) and a third harmonic ( $3f_0$ ) component. The two signals are linearly amplified and added together using a power combiner. The phase of the third harmonics is adjusted to form a quasi square wave signal. The absolute calibration procedure described before was adopted to calibrate the fundamental and the harmonic frequencies.

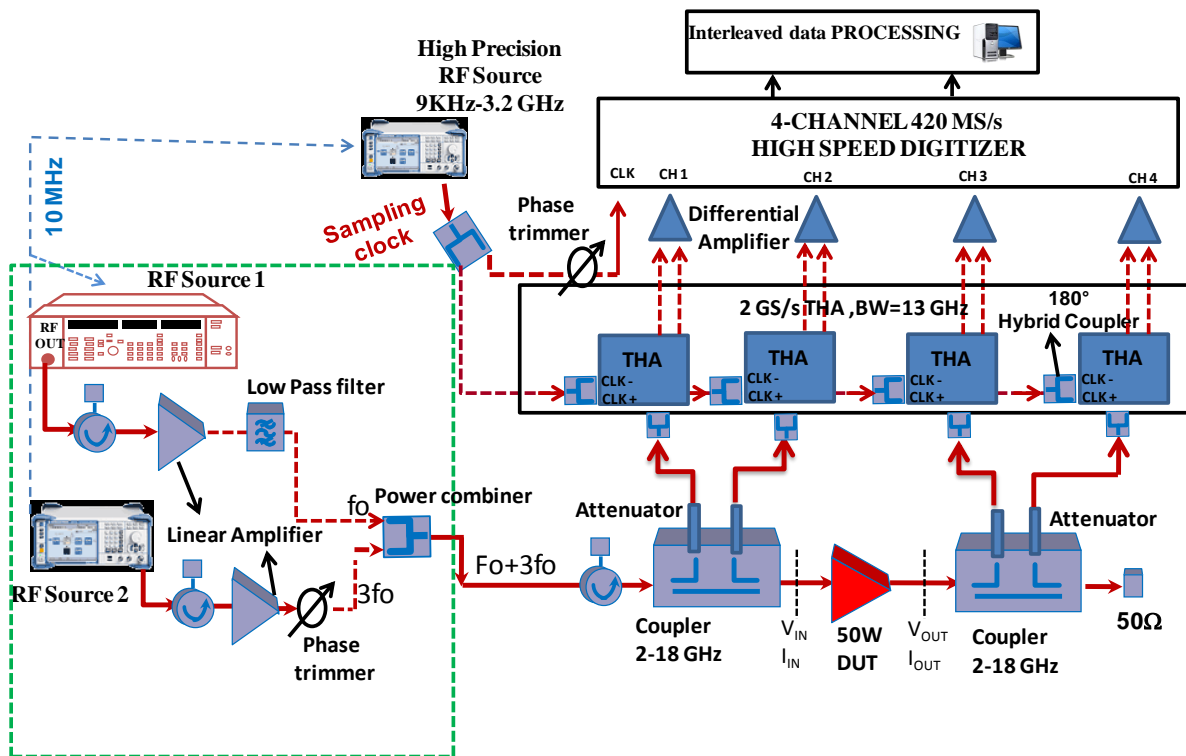


Figure IV. 12: Block diagram for time-domain test setup for quasi-square signal generation and measurement.

A quasi square signal is generated by combining the fundamental frequency of 1GHz and its third harmonic. The input time-domain waveform is measured with calibrated 4-channel proposed receiver. The waveform is then formed by controlling the magnitude of the fundamental and the third harmonic along with introducing the phase shift between the two signals which is done by using a phase trimmer. This signal then feeds the octave band PA and the input and output waveforms are simultaneously measured as displayed in Fig. IV.13. Using CTIS system the signal was sampled at a sampling interval of 10 pico-seconds (100Gsamples/s). The power spectrum at input and output of the PA along with the reflection

coefficients seen by the PA at input and output for different power levels are displayed in Fig IV.14.

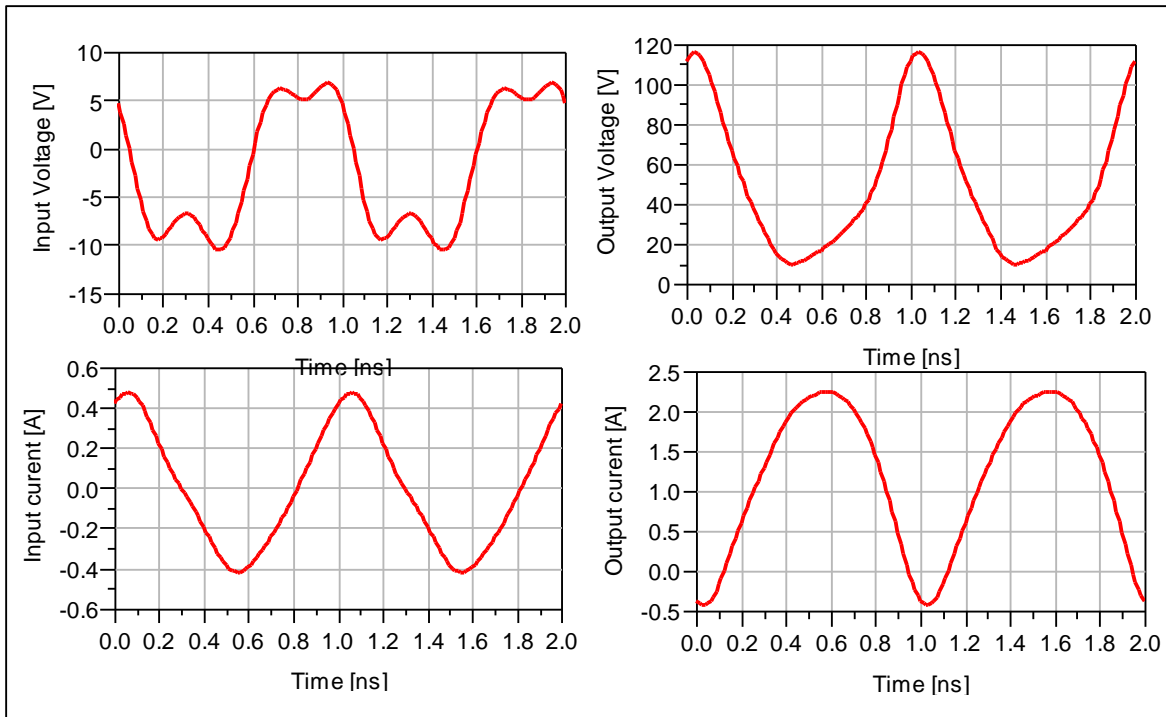


Figure IV. 13: Quasi-square input and corresponding output voltage and current waveforms.

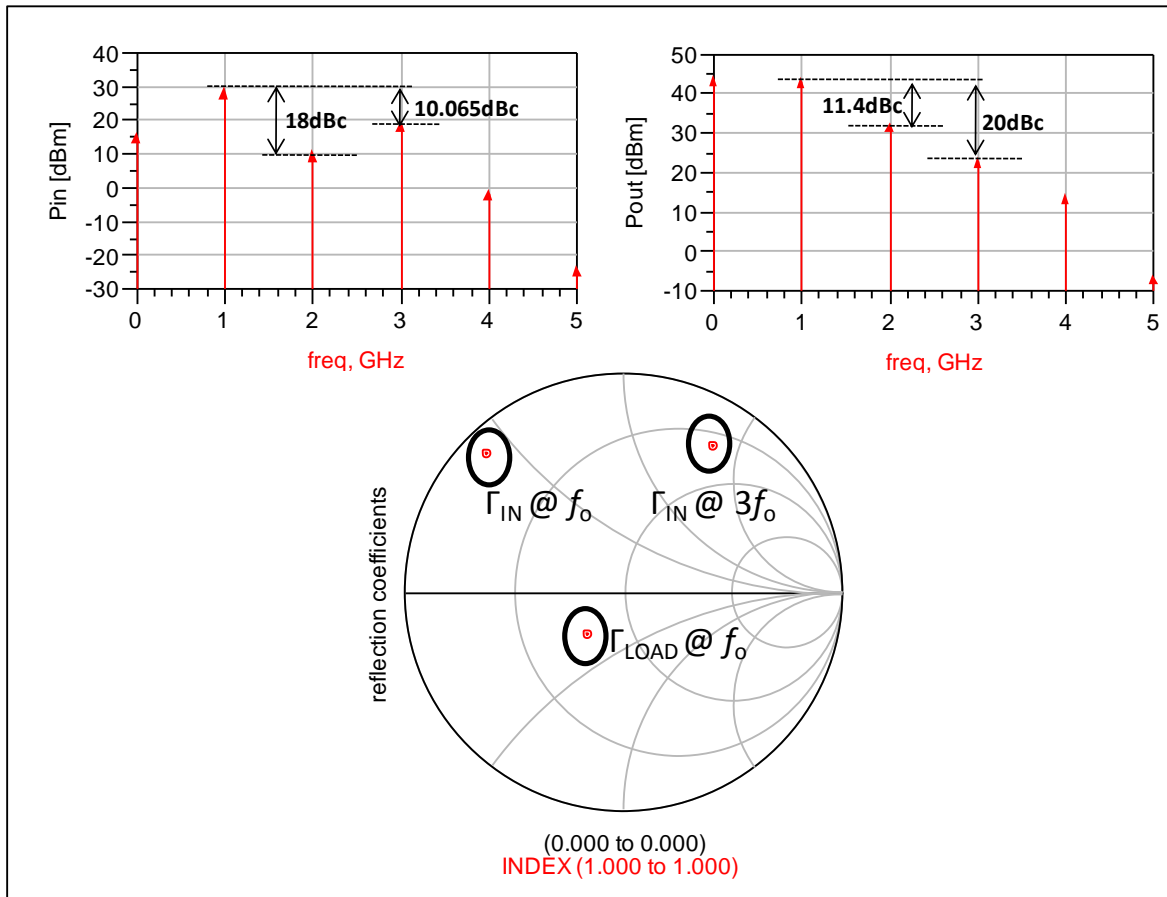
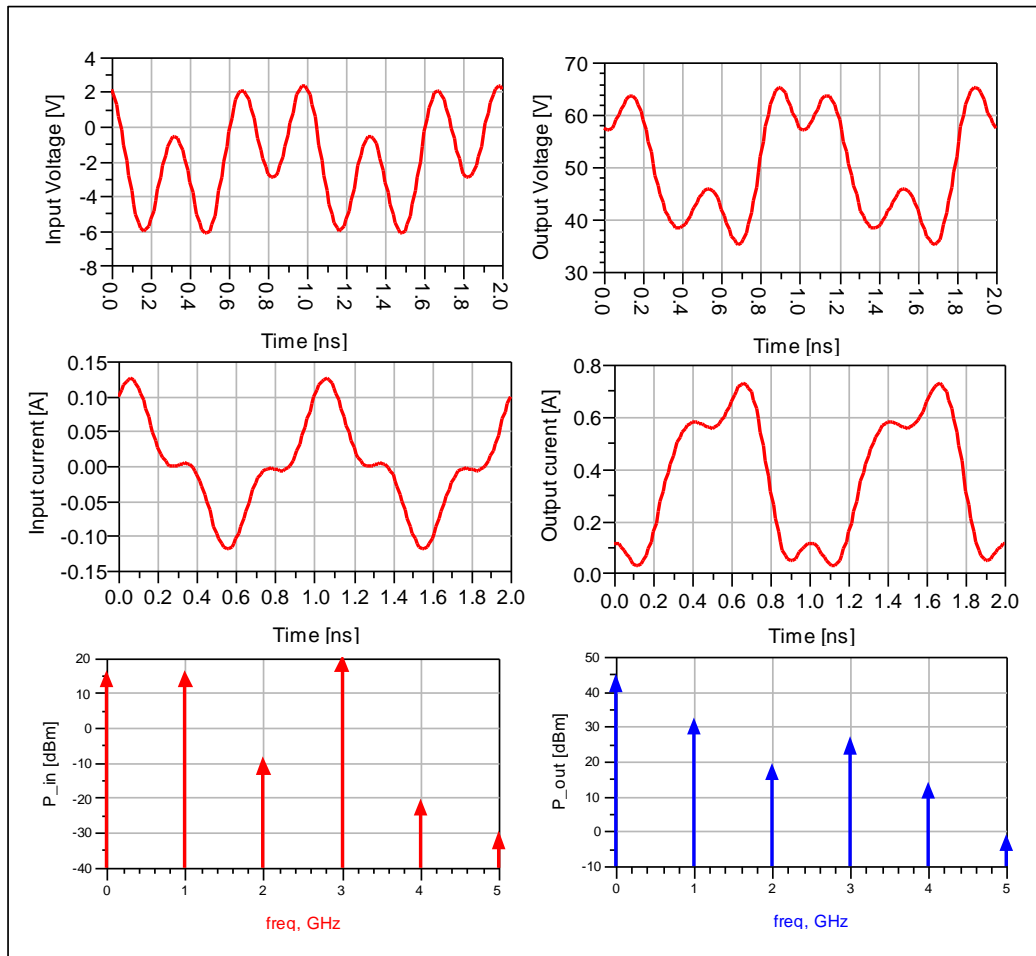


Figure IV. 14: Measured Power characteristics of quasi-square signal.

In Fig.IV.13 one can observe that even if the input voltage is forced to be a quasi square wave the output voltage wave of the amplifier is distorted with respect to the input signal because the matching circuit that are present at the input and output are not broad band and hence the third harmonic is removed.. The input and output spectrum shown in Fig.IV.14 confirms that the non-linearity of the PA contains strong second order component as the second harmonic is measured at the output while it is lower at the input. Note also that the third harmonic is curtailed. The reflection coefficients seen at input port at the fundamental frequency and its harmonics is also very high which indicates the presence of a high level of the mismatching in the input network.

In the second experiment, a similar approach was adopted and this time the phase and the amplitude ratios of the first and the third harmonics were adjusted by an active injection to obtain a quasi square voltage waveform at the output of the Power amplifier.



**Figure IV. 15: Quasi-square input, output voltage and current waveforms and the frequency spectrum at input and output**

The results of this test are shown in Fig. IV.15. Note that the level of the third harmonic at the input is much higher than at the output port. The level of third harmonic at the input is boosted to a level higher than the level of the fundamental tone. This indicates the presence of an internal attenuation of the third harmonic in the amplifier. This test setup allows verifying if the operation mode of the power amplifier is indeed class S [5]. It can also help engineers to verify their designs by using engineering waveforms [6].

### III. Pulsed Signal Measurements and Results

As discussed earlier the pulsed signal measurements offer great deal of complexities due to their infinite spectral bandwidth. For accurate characterization using pulsed signals the front end bandwidth of the receiver needs to be large. The proposed measurement test bench and the use of CTIS enable us to overcome this limitation. Following sections describe the

measurement test bench and the steps involved in pulse characterization of high power non linear devices. It also explains the RF transients occurring within the pulse.

### III.1. Pulsed signal measurement test setup

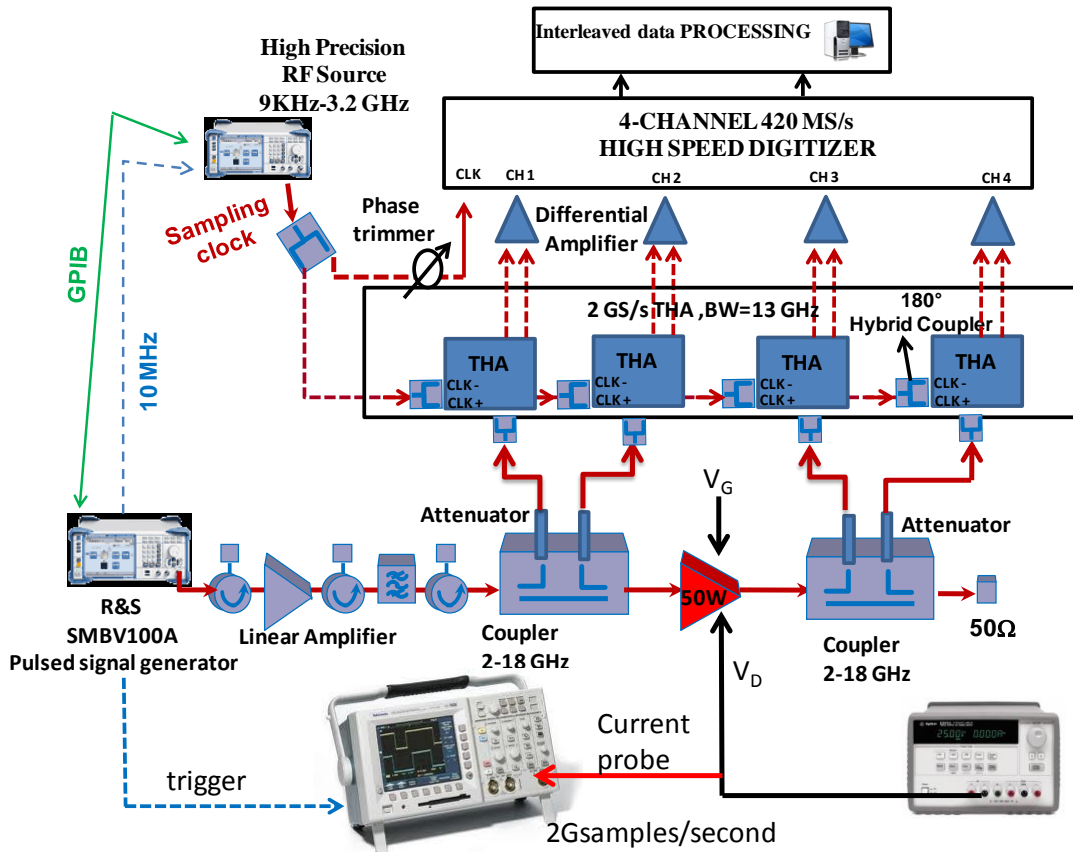


Figure IV. 16: Block diagram of the time-domain setup for pulsed signal measurement.

The 4-channel time-domain measurement system that is built for the RF pulsed characterization employs the time-interleaving sampling principle that is described in Fig. IV.16. The test setup remains the same as described in Fig.IV.3 for the CW measurement. In this setup, a signal modulation unit (SMBV100A) was used to generate a pulse modulated signal. A Focus tuner was used at the output port to test the test bench capabilities in a load pull environment. As the proposed measurement is limited to 4-channels therefore the DC current and voltage at the drain were measured by using a 2 Gsamples/s digital storage oscilloscope by Tektronix.

A similar system calibration as explained in II.1.1 was performed to mathematically remove systematic errors at the fundamental and harmonic frequencies.

## III.2. Issues related to pulsed signal excitation

### III.2.1. Effect of the bandwidth in pulsed signal

The increasing power levels that are used in wireless applications has led to many issues related to thermal and trapping effects. To counter their influence in characterization one of the methods used quite extensively is pulsed characterization of devices. This keeps the thermal issues under control but at the same time pulsed characterization is a hard task due to the multi-harmonic nature of pulsed spectrum. As discussed earlier the bandwidth of a pulsed spectrum is infinite and the frequency components contained in the spectrum depend upon the pulse repetition interval and the duty cycle of the pulsed train. As the PRI increases the resolution of spectral components within the pulse spectrum increases and due to this phenomenon an important factor involved in pulsed signal measurement is the calibration in general and phase calibration in particular. Also a large analog bandwidth of front end receiver is needed which forms a major technological challenge. Different procedures are used to calibrate the phase spectrum for the fundamental RF band and its subsequent harmonics. The Harmonic phase reference (HPR) is commonly used as a phase reference even though it has its own limitations. Other important issue related to pulsed signals is the bandwidth of the frontend due to infinite bandwidth of a sinc(x) function. This process is known as desensitization and is explained in section 2.2.1.1. A minimum front end bandwidth is required to accurately acquire the pulse spectrum and the same rule applies for correction of the amplitude and the phase during calibration meaning that the measurement system should be calibrated for a pre-specified bandwidth. This phenomenon is explained in the following paragraph.

An RF pulsed signal with a carrier at a frequency of 2.5 GHz is designed to have a pulse period of 1  $\mu$ s and duty cycle of 10 % (pulse width 100ns). It is acquired by the proposed test bench (explained in last section) and is shown in Fig. IV.17. This measurement was made in a through connection i.e. without the DUT and port 1 was directly connected to port 2. The signal was sampled at a sampling rate of 50 Gsamples/s and the corrected pulse voltage waveform measured at the input port is displayed.



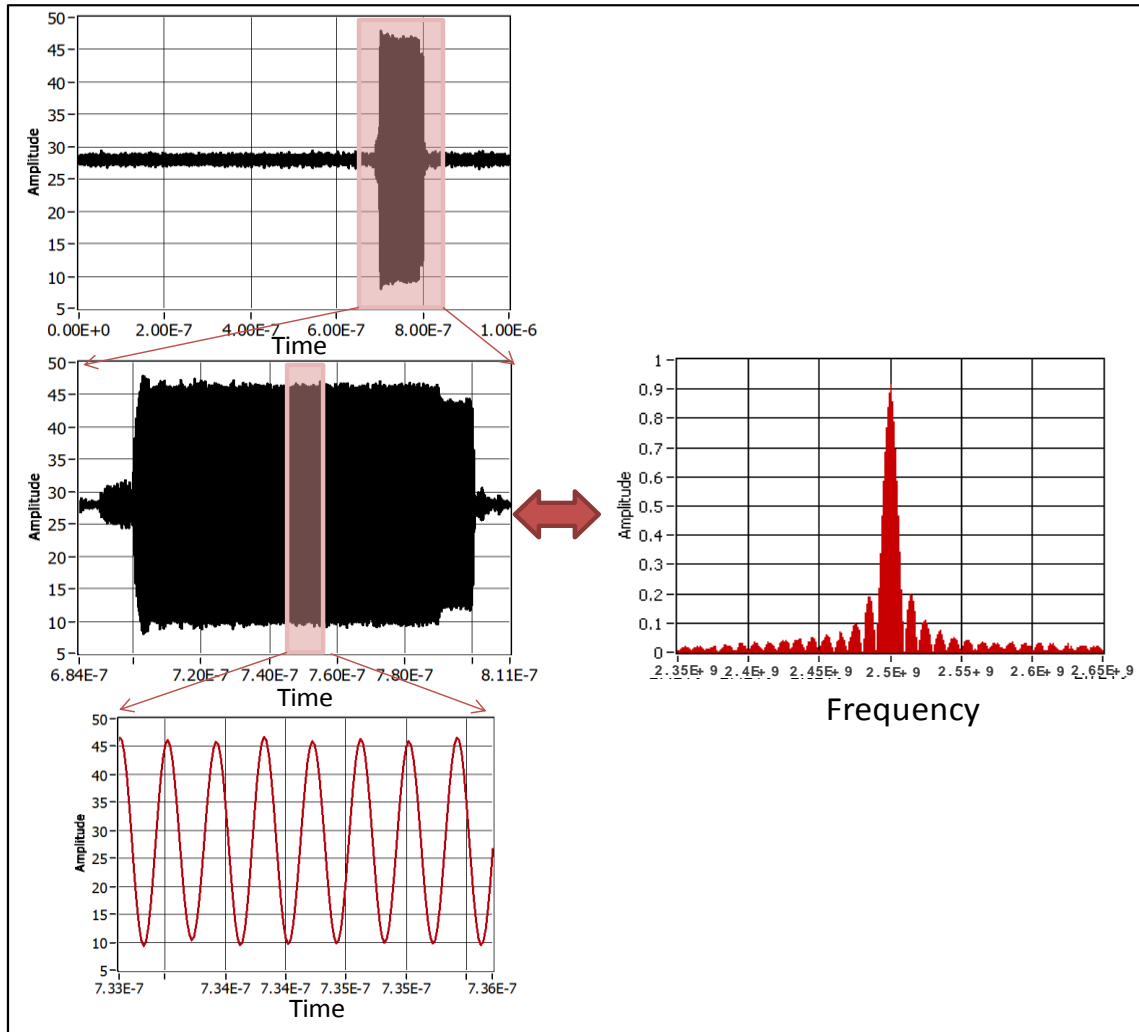


**Figure IV. 17: Acquired pulsed signal at the input port and its spectrum.**

As the proposed system does not have provisions for an IF bandwidth limitation therefore the bandwidth related phenomenon is explained by using digital filtering (ideal band-pass filtering) during the calibration process. The following flow chart explains the steps involved in this procedure:

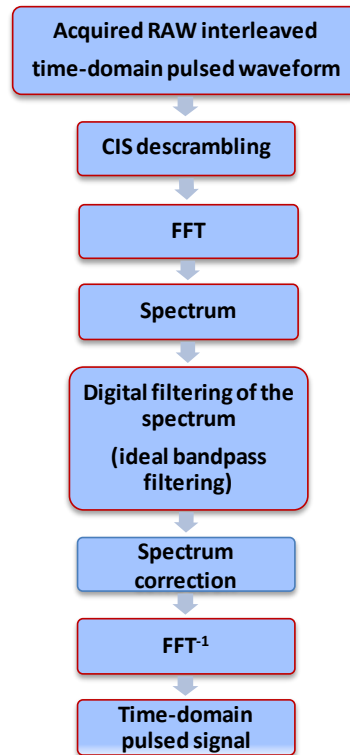


Figure IV. 18: Block diagram for calibration and digital filtering.

As the error correction is done in frequency domain therefore the acquired pulse time-domain signal is first transformed into the frequency domain using the Fourier transform. Then the pulsed spectrum is corrected for different bandwidths using an (ideal rectangular band-pass filtering) and transformed back into the time domain to see the distortion that the window imposes on the transformed pulsed signal. For this correction the complete spectrum is divided into windows of a specific (equal) bandwidth depending upon the carrier frequency, around the fundamental carrier and its subsequent harmonic frequencies as shown in Fig. IV.19.

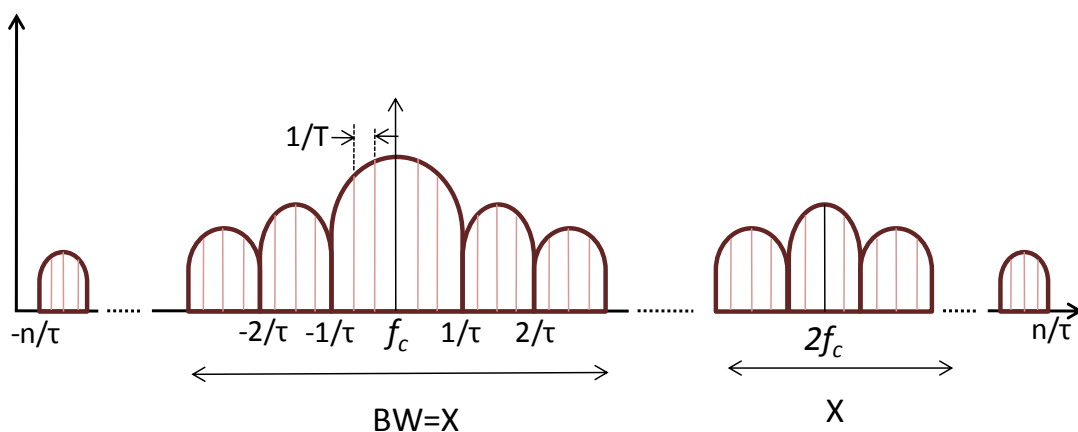


Figure IV. 19: Block diagram of measurement setup for CW measurement.

These high resolution spectral lines within the selected frequency bands are error corrected for phase and amplitude and transformed back into time-domain. To obtain an undistorted waveform, different bandwidths around fundamental and the harmonic frequencies are selected. These bandwidths are set starting from 2.5GHz to 200MHz. Note that when the calibration bandwidth was reduced during the correction process a clear distortion of the RF transients and pulse envelope appears as shown in Fig.IV.20. Finally it was observed that if the correction bandwidth equal to  $f_c$  or  $1.5 f_c$  was chosen to correct the band of spectrum around fundamental and harmonics then the transformed time-domain waveform is not significantly distorted. In this work modulation bandwidth equal to  $f_c$  was corrected so that accurate RF transient information can be retrieved. The performed analysis also gives information about the importance of the bandwidth of an analog frontend. When this bandwidth is limited it will affect the pulse modulated time-domain measurement directly.

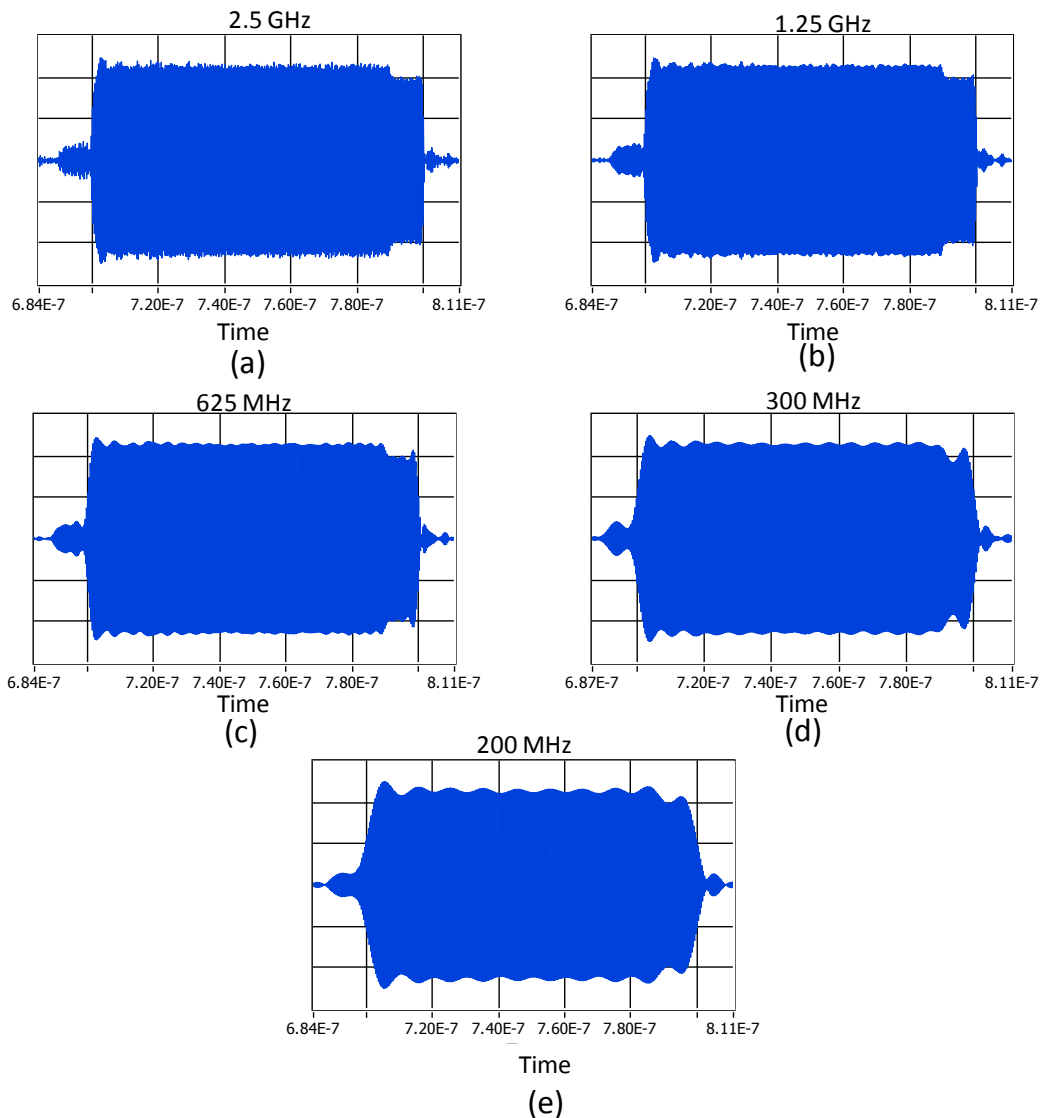


Figure IV. 20: Pulsed profile for different correction bandwidths (a-e represent bandwidth from 2.5GHz-200MHz)

### III.2.2. Spectrum correction

As discussed in the previous section that the pulsed spectrum is infinitely spread therefore a priori selected band around the fundamental and its subsequent harmonics needs to be corrected to obtain accurate measurements of pulsed signals. Within this bandwidth the frequency resolution is equal to inverse of pulse repetition interval (PRI), therefore for accurate phase calibration the calibration needs to be performed for each component of spectrum located within this band. This frequency resolution is very hard to achieve with conventional HPR as it is very difficult to generate dense harmonics, particularly for large pulse periods. Also the amplitude of HPR is limited which results in low power per spectral

component. The measurement system to be calibrated contains large attenuations in the RF path to measure high power amplifiers.

Therefore, in this work for phase corrections a constant group delay was assumed for the modulation and the absolute complex error coefficients of the fundamental and harmonic frequencies were applied to the complete band. All the spectral components in each window corresponding to fundamental and the harmonic modulation are corrected using the same complex error correction coefficient. For the power calibration, the same procedure was followed and this is not a big issue for power calibration as 90% of the power is contained in the first lobe of the modulation ( $BW=2/\tau$ ). Also for large PRI the frequency resolution is very dense and the amplitude error correction vector is assumed to remain the same.

### III.2.3. RF transients in pulsed signal

Another important issue that is related to pulsed signal measurement is the transition time which is basically the transition at the beginning and end of the pulse. This is where the state of the waveform is changed from ON to OFF and vice versa. This transition depends heavily on factors like the rise and fall time of the pulse generator used. Also these transients are affected by the dynamics of all the elements through which the pulse waveform travels on its way from being generated to being measured. All the passive and nonlinear active elements and particularly band limiting filters degrade the rise time of the pulse. Also, these transitions are intolerant to impedance changes seen by the waveform through the path. This includes the mismatches between coaxial cables, attenuators, couplers and other loads. Generally the rise time of the pulse after passing through a linear system is the square root of the sum of the squares of the rise time of all the cascaded elements.

All state of the art time-domain measurement instruments presently available measure base band RF signal which means that they down-convert the RF signal into a low frequency signal and also these instruments are limited in terms of intermediate frequency bandwidth. These factors limit the measurement of the transition effects which actually might contain several tens of RF periods during the transitions. To understand this phenomenon pulse measurements were made using the proposed THA based time-domain measurement system in a through mode which means without a non-linear DUT (Fig.IV.21) and the transition

effects were measured for different pulse periods to see the effect of the different passive and active elements included in the measurement setup.

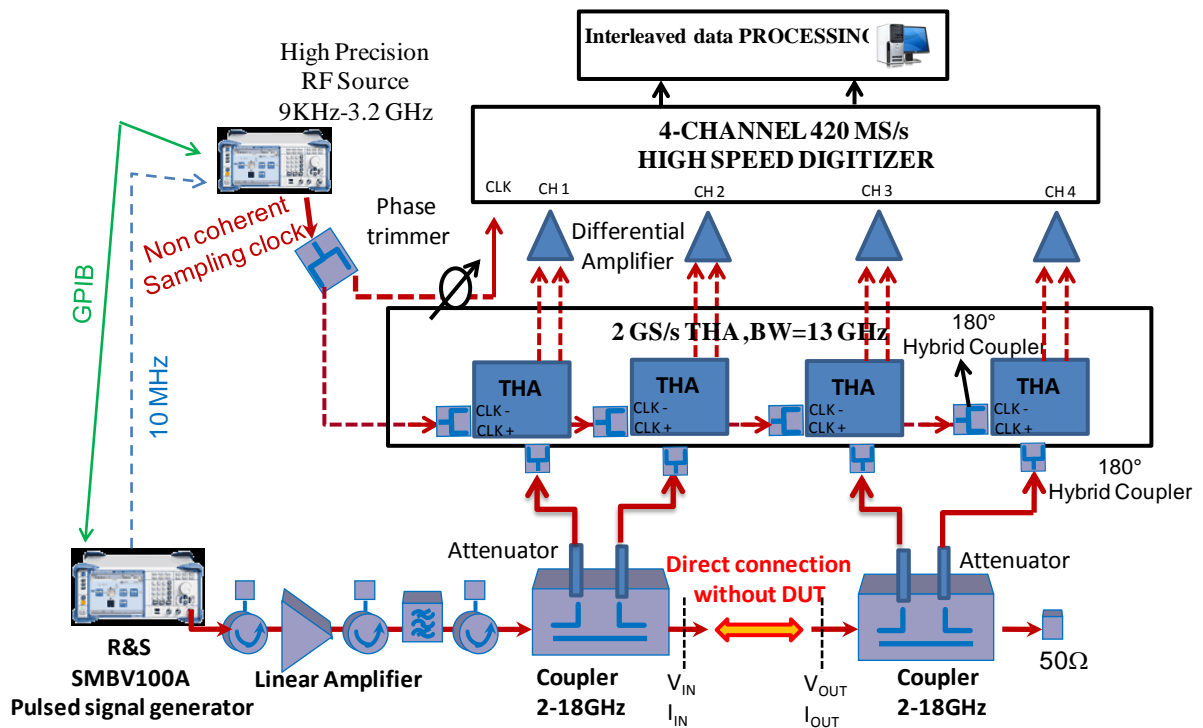


Figure IV. 21: Block diagram of the measurement system in through mode.

The time interleaving sampling was utilized which means that a sampling rate of  $10f_{RF}$  (25Gsamples/s) was obtained for an  $f_{RF}$  that is equal to 2.5 GHz. The absolute calibration procedure as described earlier was followed at a frequency of  $f_{RF}$  and  $2f_{RF}$  and corrected for the bandwidth equal to 2.5 GHz around  $f_{RF}$  and  $2f_{RF}$ . Fig.IV.22 represents the corrected input, output voltage and current waveforms for an input power of 35 dBm. It can be seen that  $V_{IN}$  is equal to  $V_{OUT}$  while  $I_{IN}$  is equal to  $I_{OUT}$ .

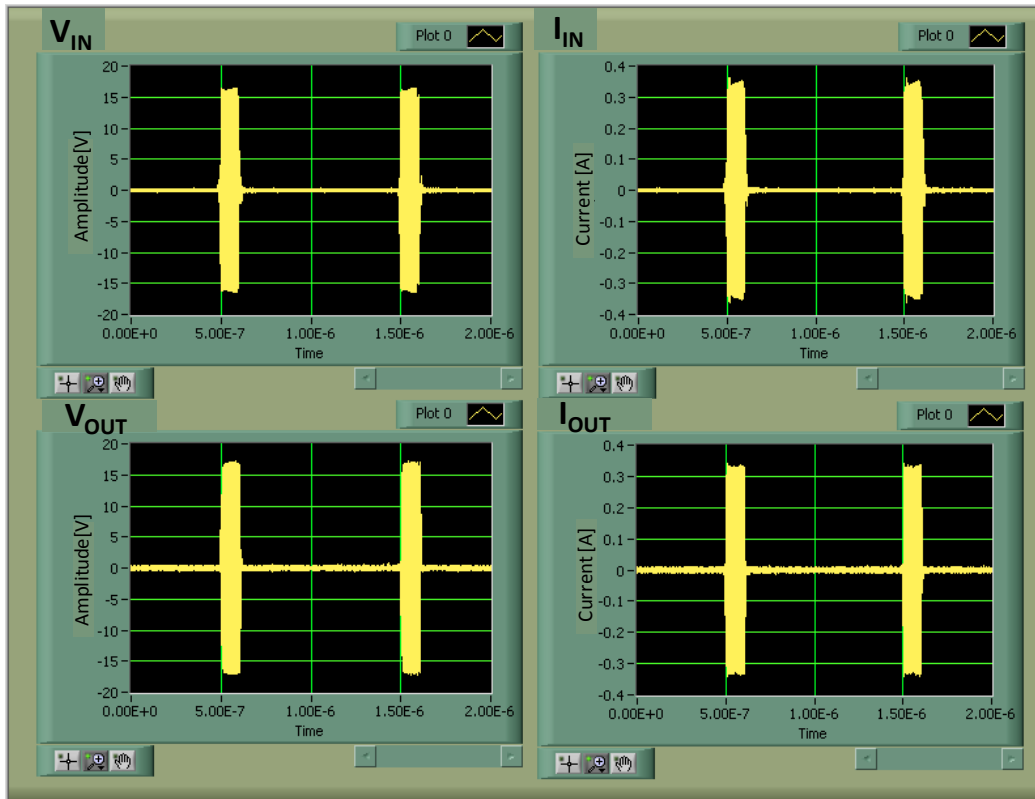


Figure IV. 22: corrected Pulse modulated RF signal with a pulse period of  $1\mu\text{s}$  and 10% duty cycle in through connection.

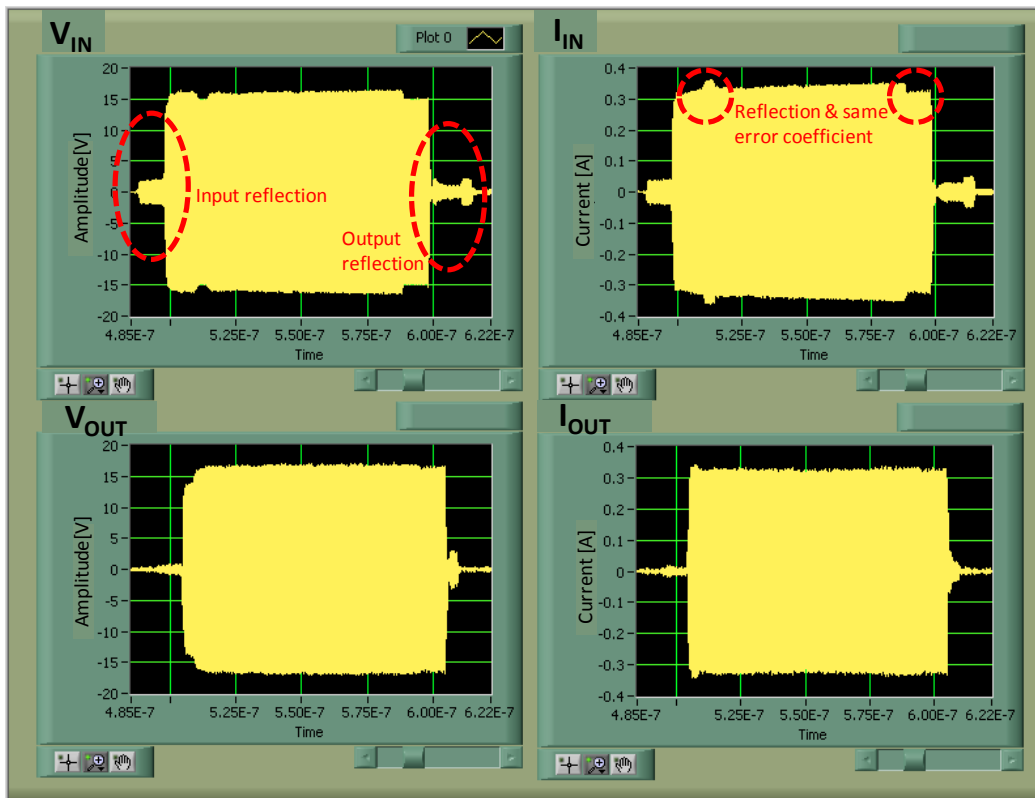


Figure IV. 23: Reflections at the beginning and end of the pulse.

Fig.IV.23 represents the pulsed width for a 1 us pulse period with a duty cycle of 10 % (100ns). Note that at the beginning and end of the pulse transition a reflection is observed while the rise and fall transition of the pulse is constant. This reflection occurs due to reflections from different impedances seen by the input and output port. Fig. IV.24 represents a pulse period of 50 us with a duty cycle of 5 % (5us) and similar reflections (Fig.IV.23) at the beginning and end of the pulses at the input, output voltage and current waveforms was noticed.

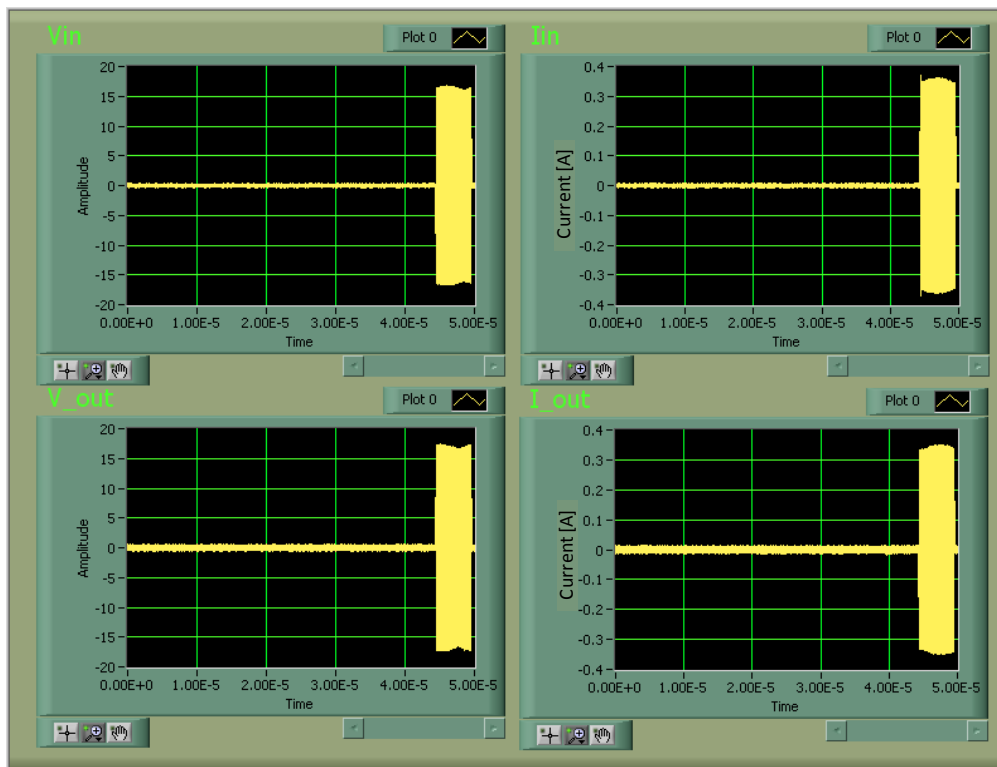


Figure IV. 24: Pulse modulated RF signal with a pulse period of 50 $\mu$ s and 5%duty cycle in through connection.

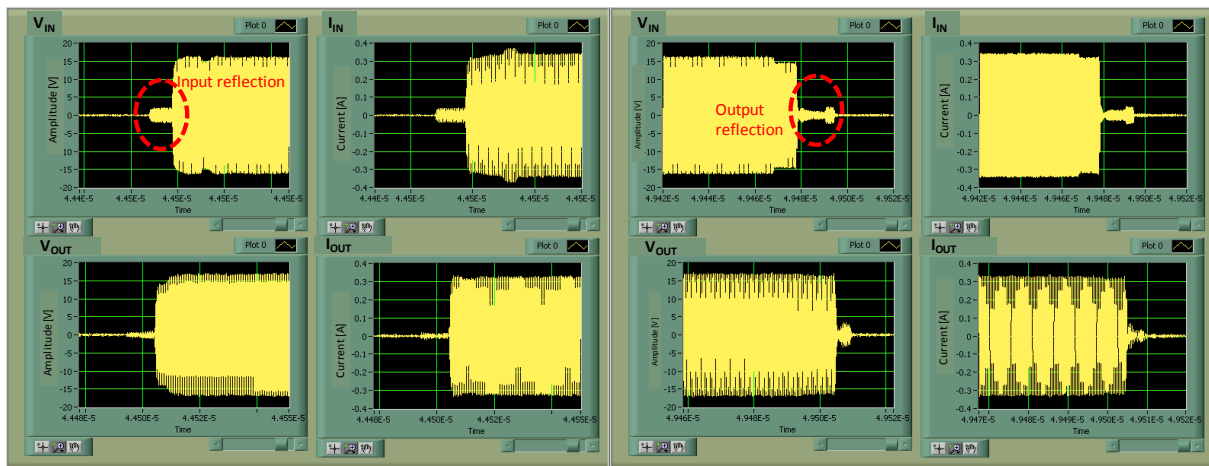


Figure IV. 25: Reflections at the beginning and end of the pulse.



A third measurement with a pulse period of 50  $\mu$ s and duty cycle of 10 % (10 $\mu$ s) was made and the current and voltage waveforms are displayed in Fig.IV.26. Similar reflections at the beginning and end of the pulse appear.

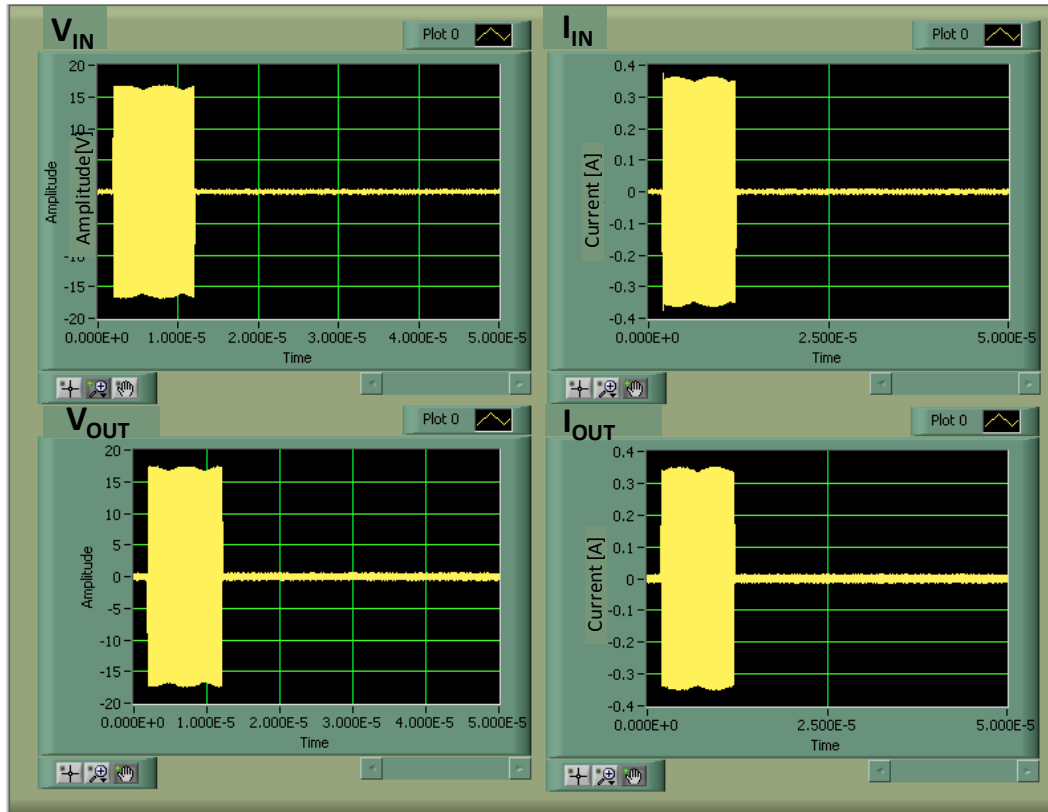


Figure IV. 26: Pulse modulated RF signal with a pulse period of 50 $\mu$ s and 10%duty cycle.

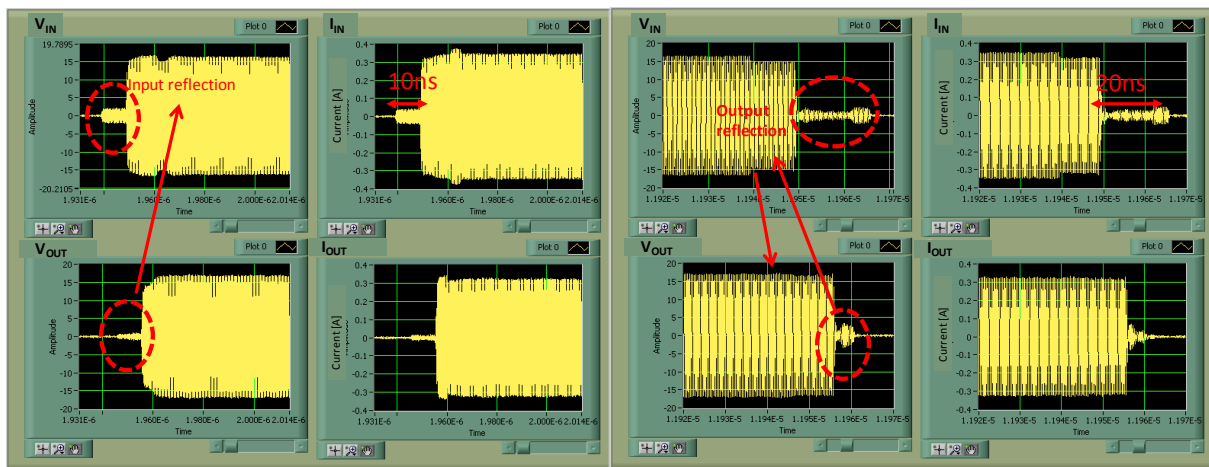


Figure IV. 27: Reflections at the beginning and end of the pulse.

All these measurements it has been noticed that that almost similar transient characteristics are obtained and the time period over which these reflections extend at the beginning and end of the pulse remains constant in all the measurements (Fig.IV.27). It means

that pulse period or the duty cycle has no effect on these reflections and they are purely due to reflections caused by different passive components cascaded in the measurement path. When characterizing a non-linear DUT all these effects should be accounted for as they are caused by the measurement system and could not be removed by calibration procedure.

### III.3. Pulsed signal automated test setup

The 4-channel time-domain measurement system for pulsed characterization employing time-interleaving sampling principle as described in Fig. IV.16 was completely automated using Labview and matlab. A program was developed to calibrate the system considering the bandwidth and taking all the assumption into account as discussed earlier in the chapter. Pulsed measurement setup also involved some additional steps, as for CTIS system since no start trigger was used; therefore the pulsed waveforms acquired at the four channels were not aligned in time when more than one measurement (power sweep) is considered. This is due to the rate of change of phase in the local oscillator of the generator. This discrepancy was removed by using a soft triggering technique. This soft triggering synchronizes all the measurements to first measurement made using the incident input of port  $a_1$ . This synchronization uses the direct linear cross correlation function. Fig IV.28 describes the block diagram for the steps involved in the complete automated test setup for measurement of pulsed signal. One drawback of using the CTIS technique for measurement of pulsed signal is that the minimum frame period that can be selected to represent the de-scrambled time interleaved data need to be equal to the modulation period. When the modulation period (e.g pulse repetition interval for pulsed signals) increases, so does the number of samples which consequently increase the acquisition time. With the test setup proposed we are limited with the memory of the ADC and therefore when long pulse repetition interval is selected then it is difficult to acquire multiple pulses. This limitation is purely a digital hardware issue and if the memory of ADC is increased then multiple pulses can easily be acquired.

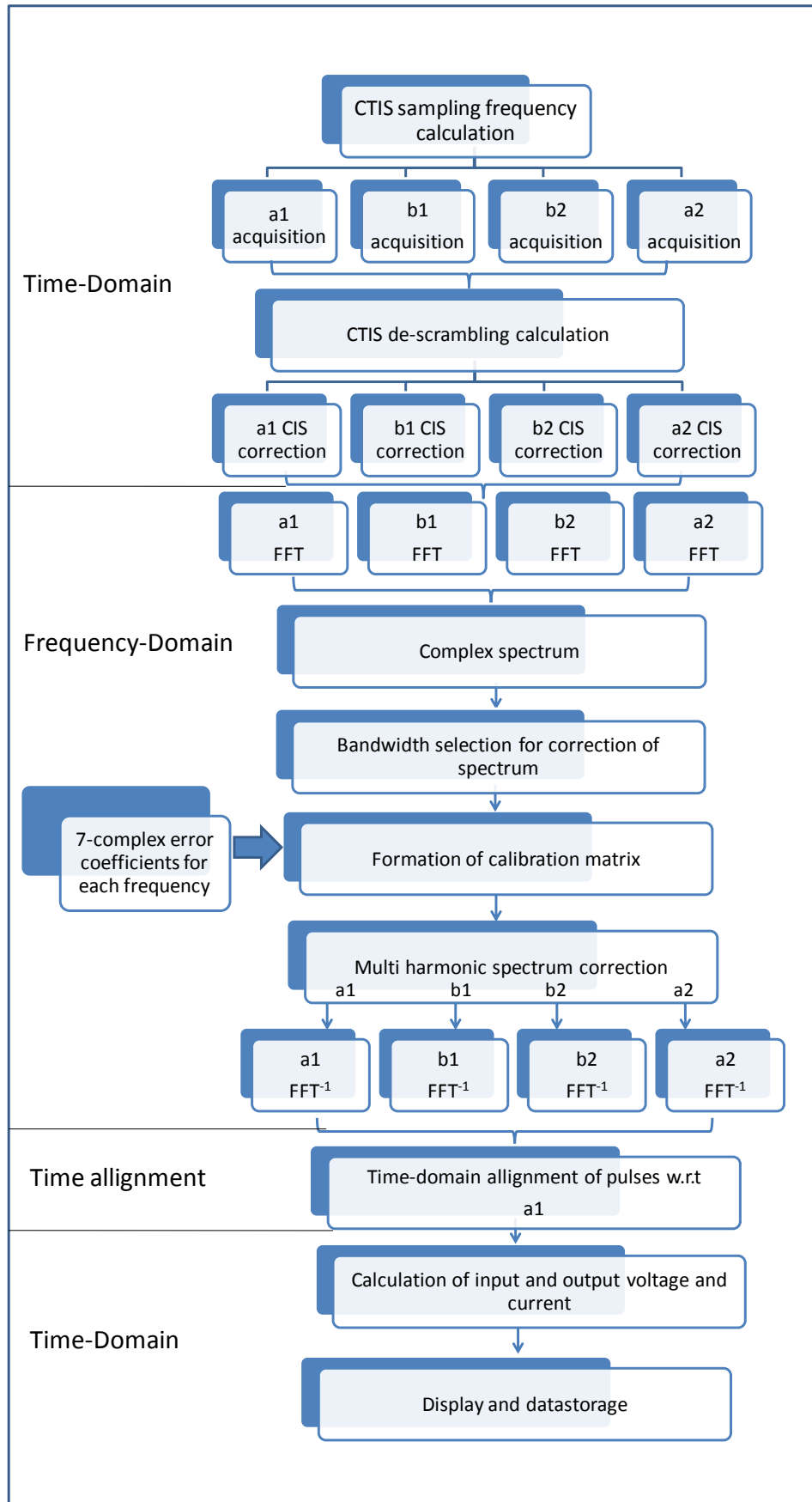


Figure IV. 28: Block diagram of the measurement setup for Pulsed signal.

### III.3.1. Results for the Pulsed signal measurement

The proposed CTIS based test bench has been used for to the characterization of an octave band 40 W GaN PA (described earlier). The RF time domain voltage and current waveforms at both ports of the AUT are measured. Pulse modulated signals with pulse repetition periods varying from 1  $\mu\text{s}$  to 50  $\mu\text{s}$  and duty cycles varying from 5 to 10 % (100ns to 10 $\mu\text{s}$ ) were applied as an excitation to the PA at a fundamental frequency of 1 GHz. The sampling rate was chosen to be 10 times the fundamental frequency (10 Gsamples/s). Frame periods ( $T_{\text{FRAME}}$ ) equivalent to the pulse repetition period were chosen which means that the number of samples acquired differ in each acquisition. For example, if a period of 50  $\mu\text{s}$  is to be measured then the minimum frame period should also be 50  $\mu\text{s}$ . It means that the no. of RF periods falling in this time frame would be 50000 and the total no of samples would be 0.5 million for each channel. These samples are taken at a high sampling frequency of 10 Gsamples/s (10 samples per RF period). Similarly, if the pulse period is increased further or multiple pulses are to be acquired that the no. of samples also increases. With our present test setup the memory of both the ADC and the operating software (labview) is limited.

#### *III.3.1.1. 1 $\mu\text{s}$ pulse repetition period*

A first measurement was made with a pulse repetition period of 1  $\mu\text{s}$  and a duty cycle of 10 % which means that pulse width ( $\tau$ ) was set to 100 ns. The measurement was made at gain compression in order to observe both the non-linearity of the AUT and the pulsed RF transients. Fig.IV.29 represents the corrected current and voltage waveform burst of two pulses at the input and output of AUT.

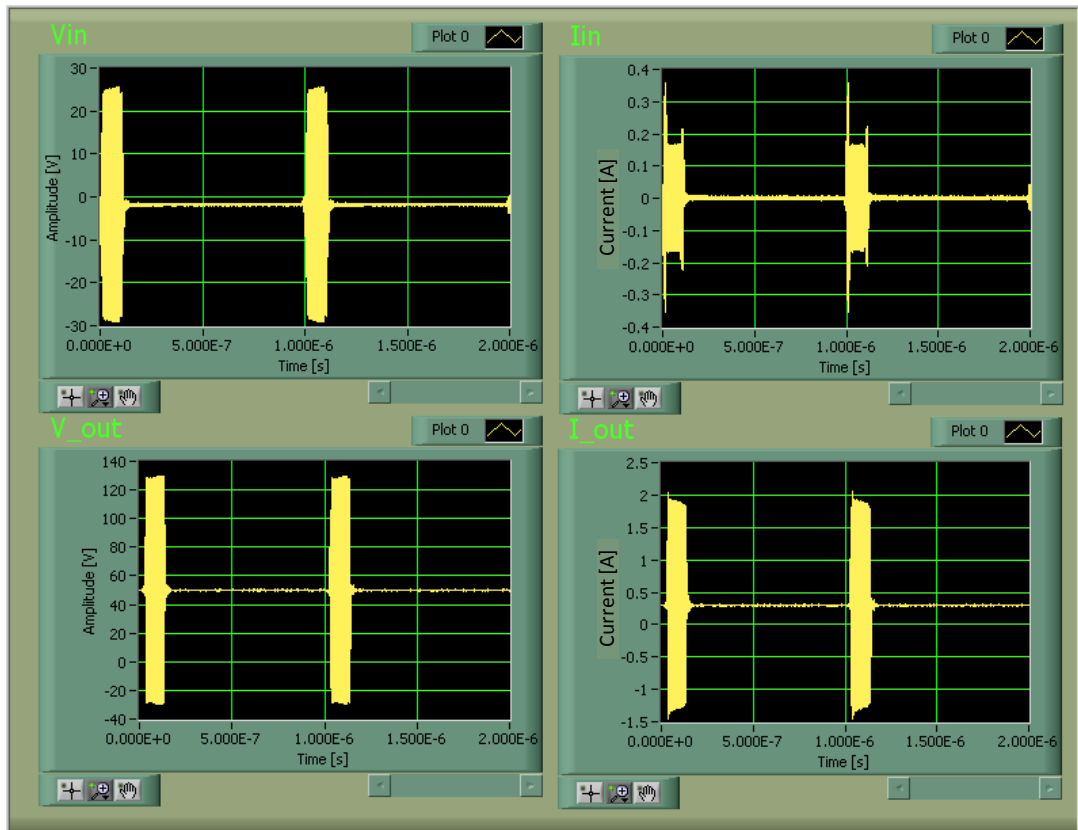


Figure IV. 29: Input and output voltage and current waveforms @ 1µs pulse period.

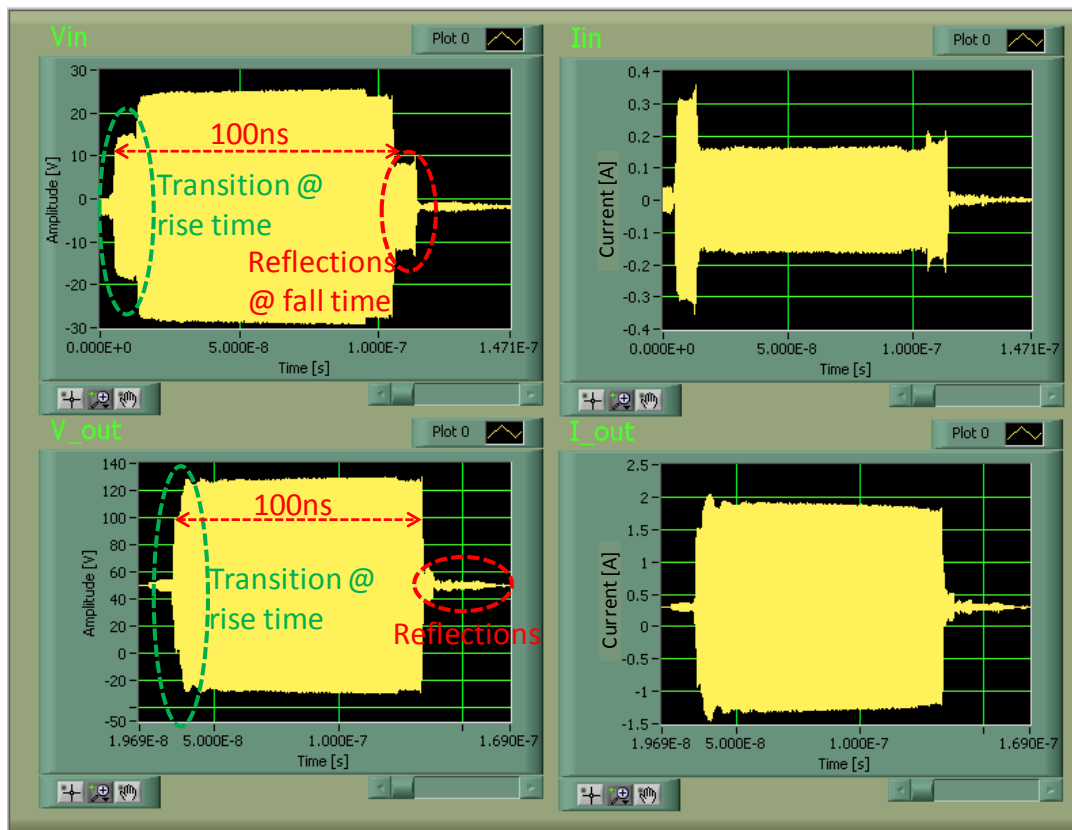


Figure IV. 30: Pulse profile @ 1µs pulse period.

Fig.IV.30 represents the pulse period for a 100 ns pulse width. Note that the transition that occurs at the rising edge of the input voltage and current waveform is not constant and this is due to high frequency dependent reflection that is present at the input. The reflection coefficient of the input matching network of the AUT is very high which means that it's poorly matched. At the beginning and the end of the pulse, a reflection that is similar to the measurements made for through connection (section III.2.3) occurs. This reflection is created by the different passive components that are cascaded in the RF measurement path. As seen in Fig.IV.30 there is a delay noticed between the input and output waveforms.

### *III.3.1.2. 50us pulse repetition period*

A measurement with a pulse period of 50 us seconds and 10 % duty cycle was made. Fig. IV.31 exhibits the voltage and current waveforms obtained at the input and output of DUT at 1dB gain compression. The DC current at the drain is captured using a digital storage oscilloscope as the proposed measurement system is limited to 4 channels. The maximum sampling rate of DSO is limited to 2Gsamples/second while the sampling rate at which the RF waveforms are captured was equivalent to 10 Gsample/s. To get around this problem the samples obtained with DSO were interpolated to have an equal number of samples for the two measurements. The rise time of the DSO and the current probe affect the acquired pulse envelope for the DC signal. An important thing to be noted is that the measurement is made on an amplifier which included a bias network with large capacitors and large inductors in the DC path. The inductance, capacitance and resistance offered by this bias network combined with the inductance, capacitance and resistance of the probe and the biasing cables creates a resonant circuit which resonates at a set of frequencies that is determined by the values of L and C. This effect is commonly known as ringing and was clearly observed during the DC measurement. To have accurate DC measurements it is necessary to measure as close as possible to the drain lead. Considering this problem of DC measurement it was not possible to add the DC current to the RF output current. Therefore the two currents are super imposed on the same graph.

Soft triggering as described before was used to align the two pulses as the DSO used an external trigger from the RF modulator while the proposed time-domain measurement system does not use a trigger signal at all. An overshoot is observed at the rising edge of the

pulse and the drain current does not settle during the pulse ON time before the pulse goes in the off state. Fig.IV.32 represents the transients at the beginning and end of the pulse.

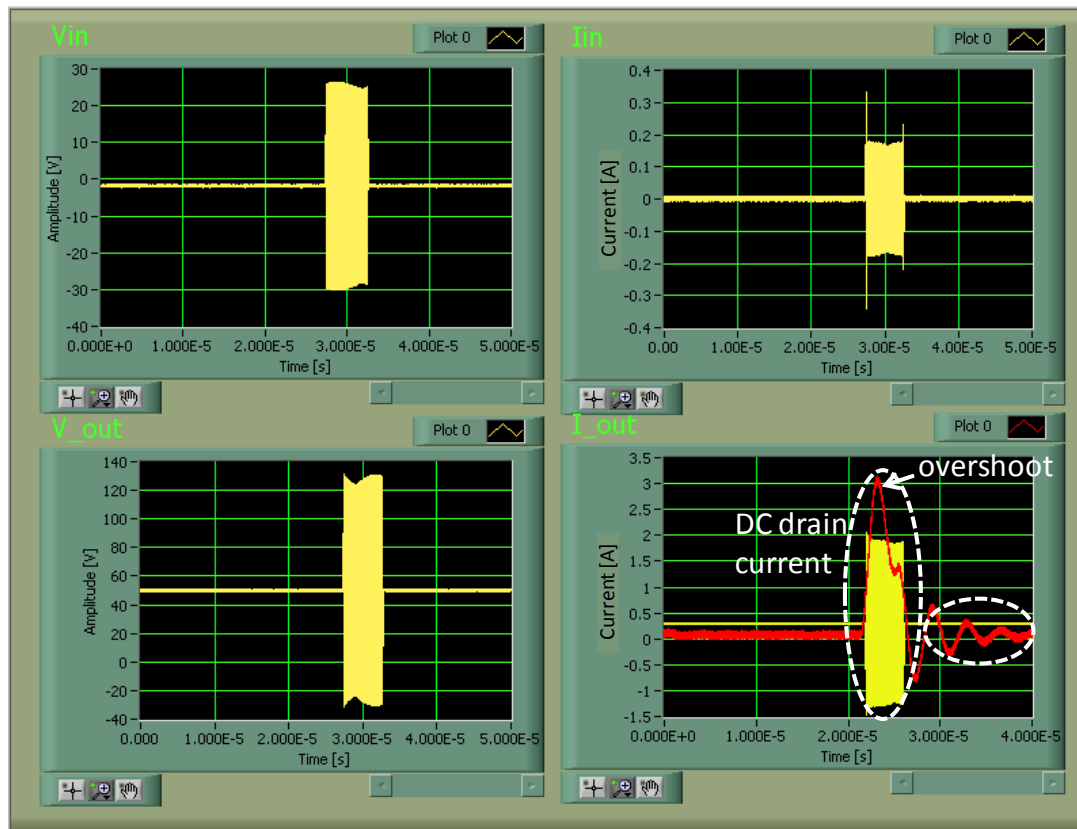


Figure IV. 31: Input and output voltage and current waveforms @ 50 μs pulse period.

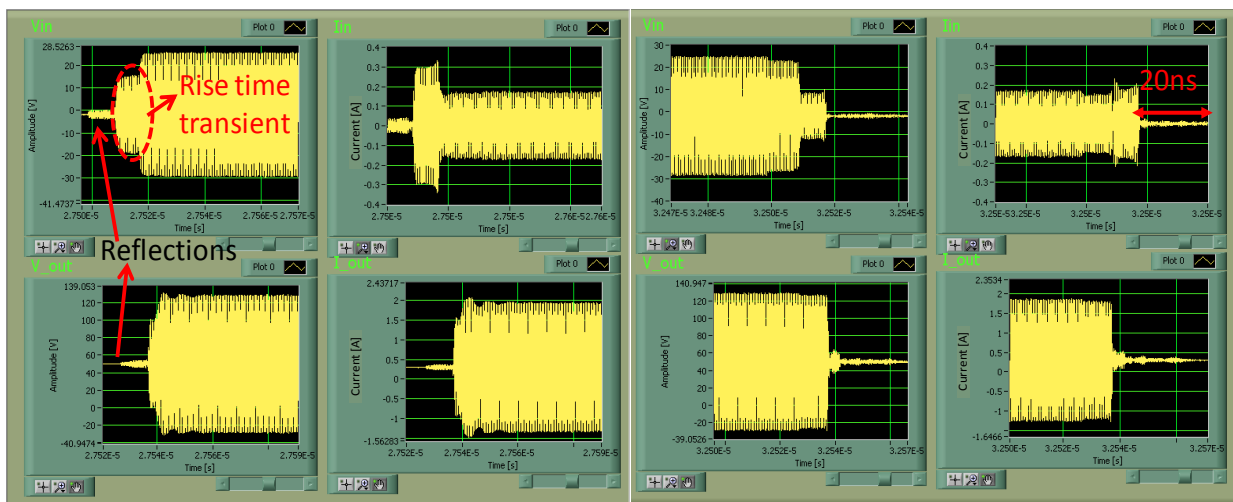


Figure IV. 32: Input and output voltage and current transients @ 5 μs pulse width.

Second measurement with a 50 us pulse width but with a 20 % duty cycle was made to analyze the effect of the duty cycle on the transients, the pulse envelope and the drain current.

Fig.IV.33 represents the acquired input, output voltage and current waveforms and the DC drain current at gain compression. Again, overshoot and ringing effects are observed in the drain current measured by the DSO.

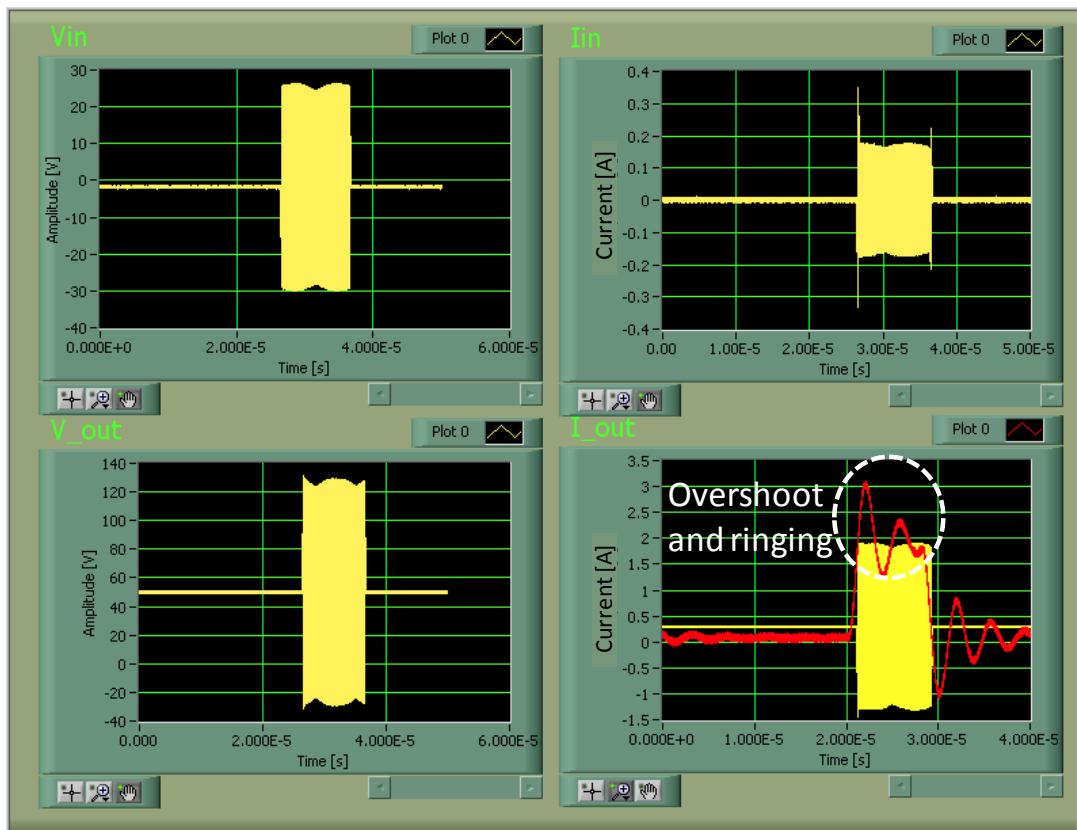


Figure IV. 33: Input and output voltage and current waveforms @ 50  $\mu$ s pulse period.

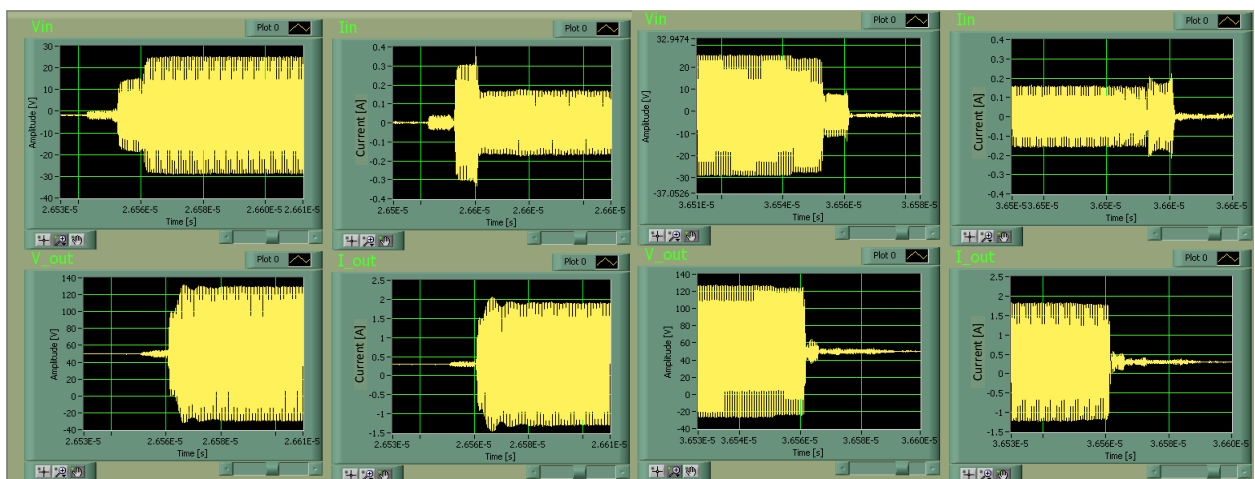


Figure IV. 34: Input and output voltage and current transients @ 10  $\mu$ s pulse width.

Fig.IV.34 represents the transient at the beginning and end of the pulse. The three measurements show that the pulse period and duty cycle has no effect on the transients and on



the reflections at the beginning and end of the pulse width. The reflection that is measured at the beginning and end of the pulse remains the same as the one obtained in through mode (that is without the non-linear DUT) while the reflections from the DUT do affect the rising edge of the pulse transient as seen in the input voltage and current waveforms for all the three cases.

### III.3.1.3. Power sweep characterization

The AUT was also characterized as a function of the input power in the pulse mode. The AUT is excited with a pulse that has a period of 10 us and a duty cycle of 10 %. An input power sweep is performed to acquire the output power and gain characteristics as displayed in Fig.IV.35. The PAE and the drain efficiency are obtained by measuring the DC power from the DC power supply. Due to the high ringing effect that is present in the DC measurement by oscilloscope it was difficult to measure the average power consumed during the on state of the pulse.

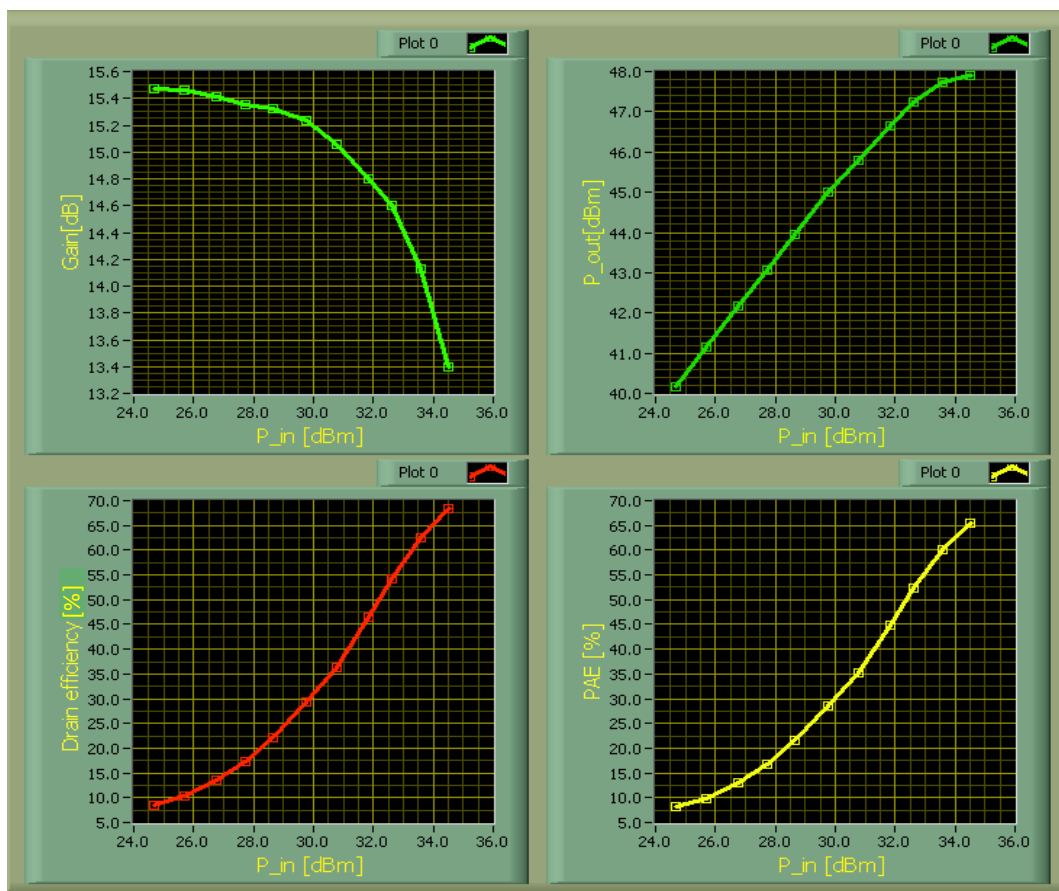


Figure IV. 35: Power characteristics in pulsed mode

The input and load impedance were also calculated (Fig. IV.36) using the measured incident and reflected signal at the input and output port of the AUT.

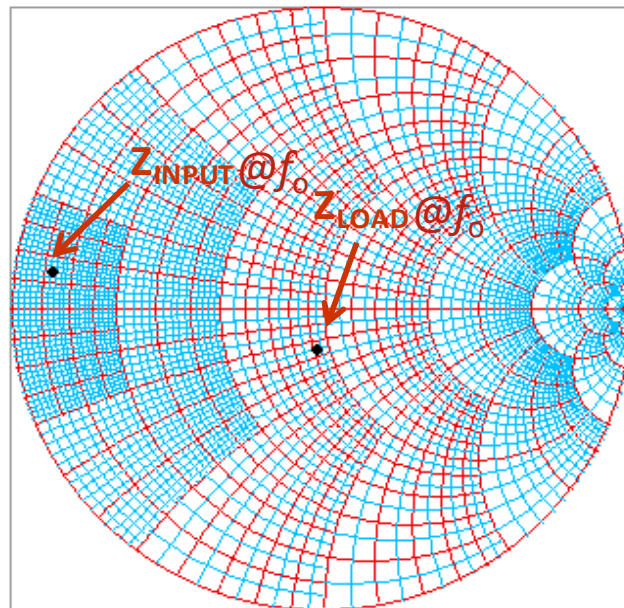


Figure IV. 36: Input and load impedance @ $f_0$

The power measurements are performed in the time-domain by measuring the average power within the pulse. Then average power within 90% of the pulse width as shown in Fig.IV.37 was calculated to remove the effect of transients at the beginning and end of the pulse.

$$P_{avg} = \frac{1}{\Delta t} \int_{t_1}^{t_2} V(t)I(t)dt \quad \text{Eq:-151}$$

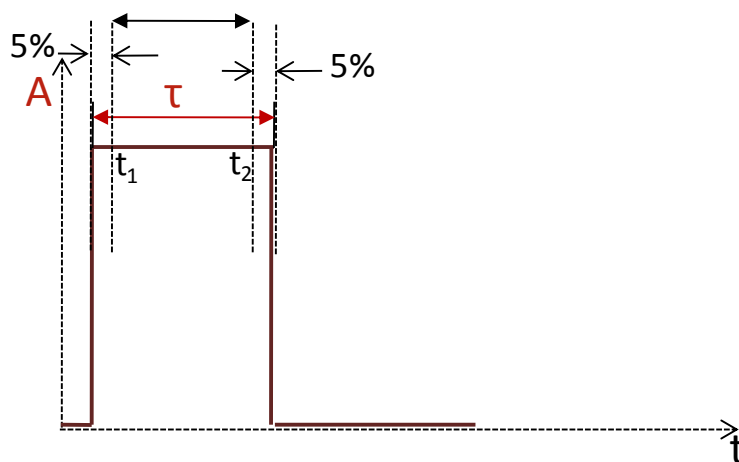


Figure IV. 37: Pulse detection to calculate average power

### III.3.2. Pulsed signal measurement under load-pull conditions

The previous section shows that neither the pulse period and nor the duty cycle has any effect on the pulse transients and the reflection at the beginning and end of the pulse. The reflections that occur are mainly due impedance mismatch. To study the effect of impedance on the pulsed transients a new measurement is made under varying load impedance using an impedance tuner connected at the output port of the AUT as described in the test setup Fig. IV.16. The AUT is excited by a pulsed signal that has a pulse repetition equal to 50  $\mu\text{s}$  and a duty cycle of 20%. The measurement is made at a relatively low power level as no attenuations were added before the tuner. The input, output voltage and current waveforms along with the DC drain current was acquired for varying impedances. Fig.IV.38 represents the measurements voltage and current waveforms at  $(25+j54)\Omega$ .

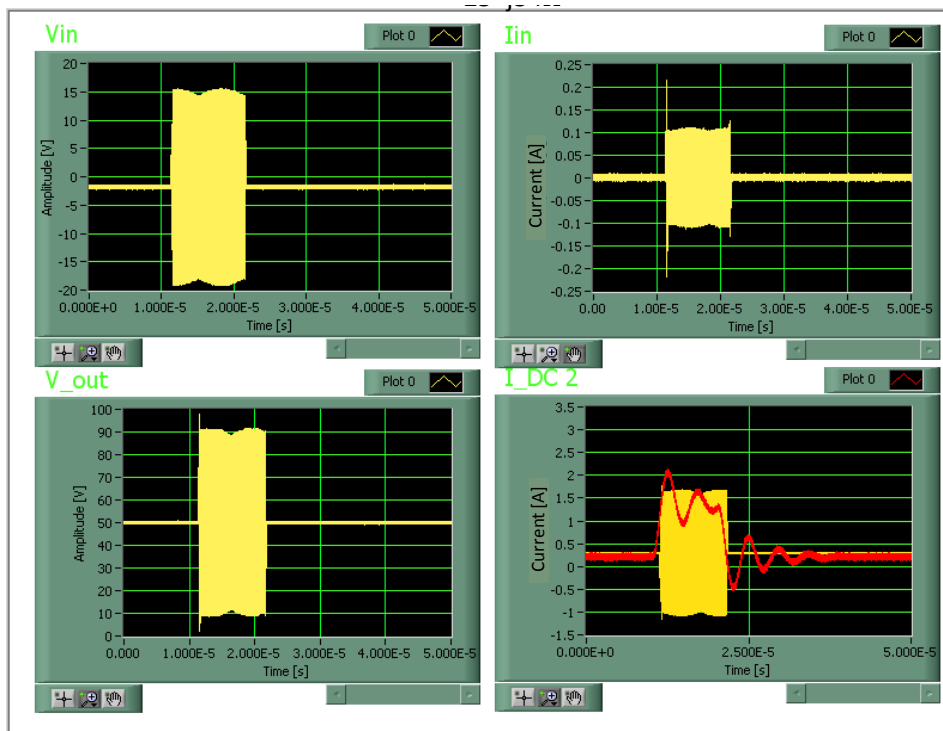


Figure IV. 38: Input and output voltage and current waveforms @ 50  $\mu\text{s}$  pulse period and  $25+j54 \Omega$  load

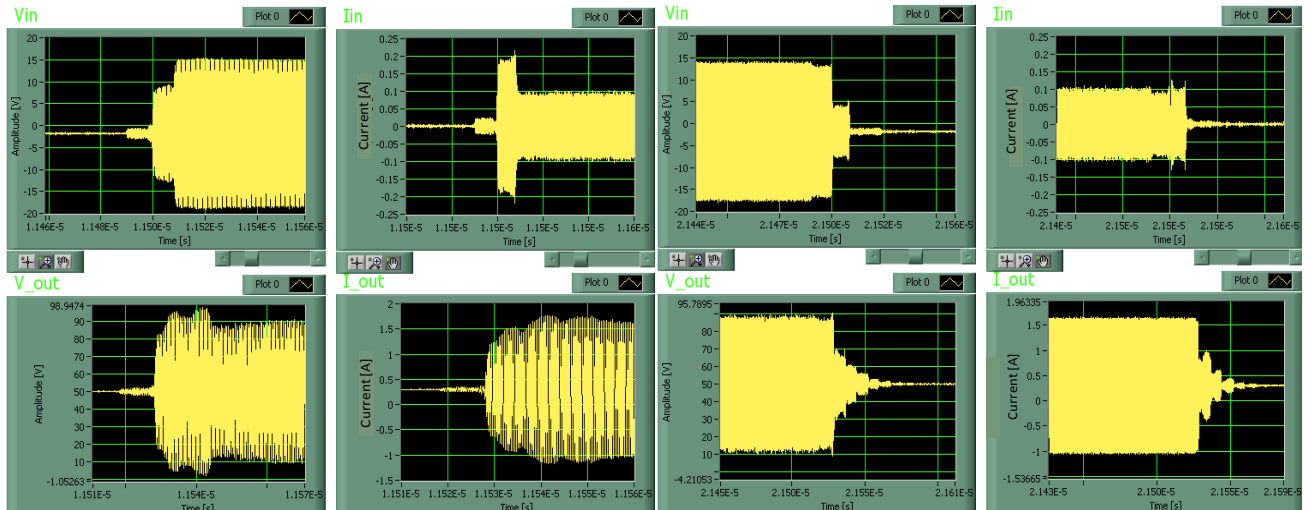


Figure IV. 39: Input and output voltage and current transients @ 10  $\mu$ s pulse width and 25+j54  $\Omega$  load

If we look into the rising and falling edge of the output pulse it's noticed that as the load impedance is changed, the voltage and current transients are highly affected. Large reflections appear at the beginning and end of the pulse as is shown in Fig.IV.39. The rising and falling edge of the input pulse remains the same as for 50 $\Omega$  pulse. The reflections seen in that case are due to the mismatch of the input matching network.

The same measurement was repeated for three different load impedances and the results are shown in the figures below.

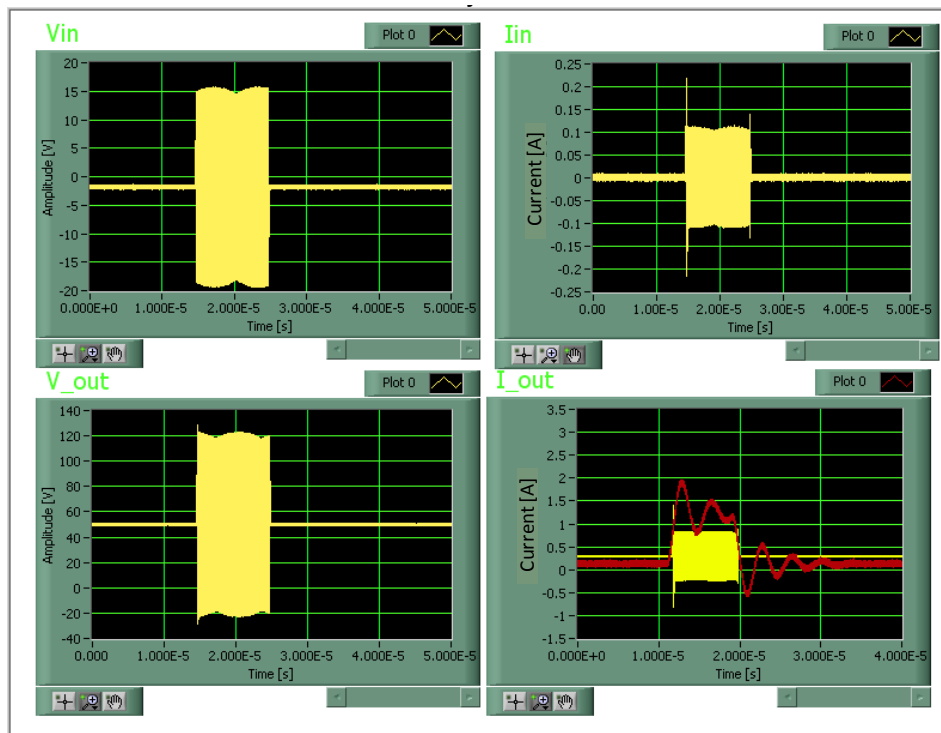


Figure IV. 40: Input and output voltage and current waveforms @ 50  $\mu$ s pulse period and 11+j4.78 $\Omega$  load

The output voltage and current transients obtained at different impedance differ from each other, while the input voltage and current transients have very little effect due to high frequency dependent reflections present due to input matching network and remain same in all the measurements.

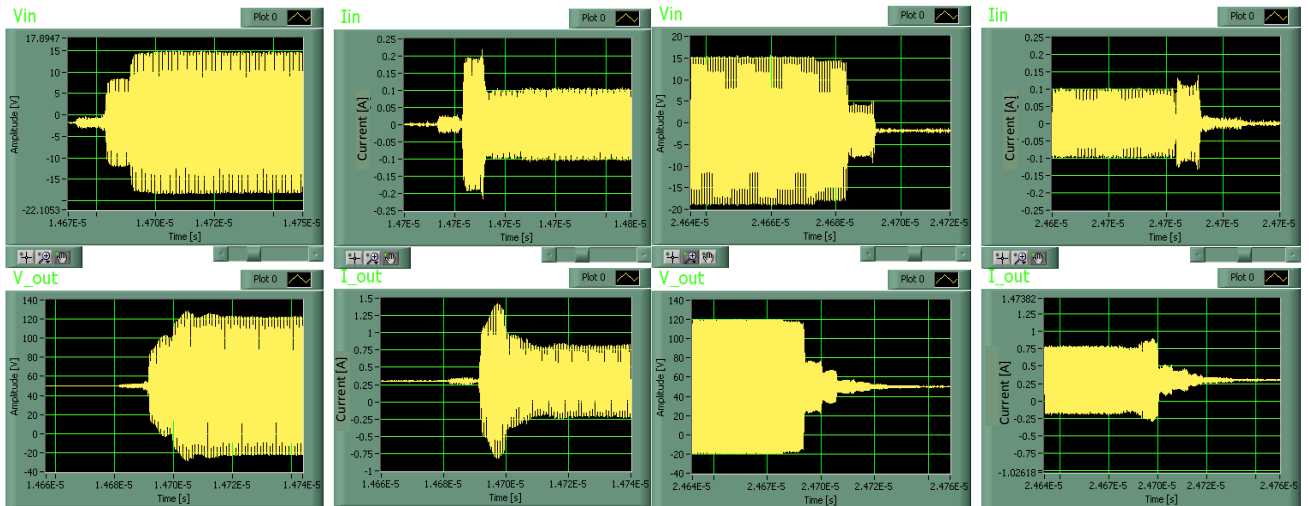


Figure IV. 41: Input and output voltage and current transients @ 10  $\mu$ s pulse width and  $11+j4.78\Omega$  load

Again if the rising and falling edge of the output pulse is analyzed the transitions are very different and also the amplitude of the RF output voltage and current differs due to impedance changes.

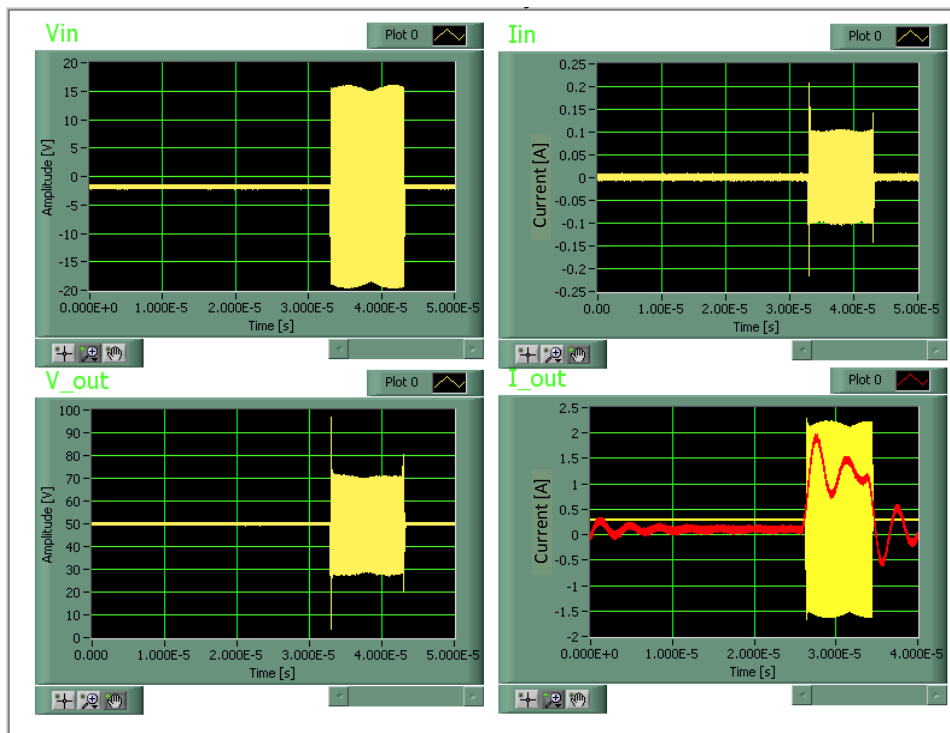
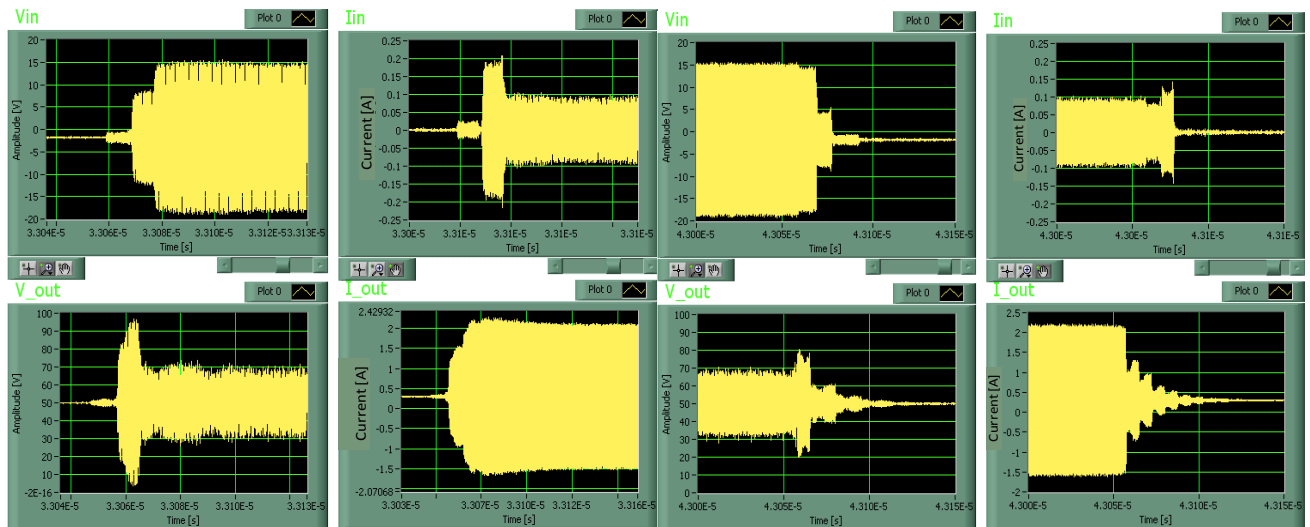


Figure IV. 42: Input and output voltage and current waveforms @ 50  $\mu$ s pulse period and  $68+j127\Omega$  load

The measurement is repeated for yet another value of impedance and similar reflections at the rising and falling edge of the output pulse transitions is noticed.



**Figure IV. 43: Input and output voltage and current transients @ 10  $\mu$ s pulse width and  $68+j127\Omega$  load.**

Due to the impedance change the current and voltage level also differed and the power characteristics for the three cases are also affected. The difference in power characteristics obtained for different measurements are displayed in table IV.1.

Load Impedance	Input Power [dBm]	Output Power [dBm]	Gain [dB]
50 $\Omega$	28.64	43.96	15.3
25+j54 $\Omega$	28.88	41.4	12.52
11+j4.78 $\Omega$	28.72	40.5	11.78
68+j127 $\Omega$	28.73	41.89	13.16

**Table IV. 1: Power characteristics for different load impedances**

All these measurements lead us to conclude that while studying the behavior of non-linear device it is very important to fully characterize the measurement system itself as the different passive components within the system offer different impedances and do affect the transients and the pulse envelope. The impedance that is presented by the load to the AUT also has huge impact. This means that memory effects occurring in a non-linear PA are very sensitive to load.

## Conclusion

In this chapter we present a method to increase the sampling frequency of a measurement system by using a time interleaved sampling process. This process allows to practically achieving sampling rate that is equivalent to 100 times the CW RF sinusoidal signal and 10 times the RF pulse modulated signal which is far beyond the physical limitations of ADC used. The repercussion of this process is that the samples obtained are scrambled in time and require reordering. Reordering is a process which is completely performed in the digital domain and a specific algorithm for this process has been developed. A fully calibrated 4-channel time-domain measurement system utilizing THA's and the CTIS has been presented. The complete characterization of a high power non-linear amplifier has been performed under CW and pulse modulated excitation. For the first time pulse RF transient measurements have been performed. The effect of the instrumentation and the bandwidth of the measurement system on the transients have been discussed. The time-domain characterization of a high power GaN amplifier under varying loads has been performed. Considerable differences are obtained in RF power characteristics, while the voltage and current transients are clearly observed.

## BIBLIOGRAPHY

---

- [1] Lecroy corp, “*Coherent Interleaving Sampling*,” patent: WO/2006/086257, August, 2006.
- [2] J.Verspecht, “Calibration of a measurement system for high frequency non-linear devices”, *Doctoral Dissertation - Vrije universiteit Brussel, November 1995*.
- [3] Nitronex “NPTB00050 Datasheet”, NDS-007 Rev. 2, May. 2009 available at <http://www.nitronex.com>.
- [4] M. El Yaagoubi, G. Neveux, D.Barataud, T. Reveyrand, J.-M. Nebus, Verbeyst, F.; Gizard, F.; Puech, J, “*Time-Domain Calibrated Measurements of Wideband Multisines Using a Large-Signal Network Analyzer*”, *IEEE Transactions on Microwave Theory and Techniques*, vol. 56, Issue 5, Part 1, pp. 1180 - 1192, May 2008.
- [5] M.P van der Heijden, M Acar, J. S. Vromans A. A. C. Cortes, “*A 19W High Efficiency Wide band CMOS Class E Chirix RF Outphasing Power Amplifier*”, *IEEE International Microwave Symposium Baltimore, June 2011*.
- [6] Paul J. Tasker, “*Practical waveform engineering*”, *IEEE Microwave Magazine* pp.65-76, December 2009.





# General Conclusion & Perspectives

---



The development of civil or military applications using GaN transistors has been on the rise since last decade. These transistors enable the realization of high power circuits design but at the same time also present some memory effects which include thermal and trapping effects. The need for an efficient time-domain instrument used to extract more information about RF transients for modulated signals is of prime importance. A lot of work has been done in this domain in the last 20 years.

The focus of this thesis is to develop a fully calibrated time-domain test bench capable of measuring the RF transient for pulse modulated signals. A detailed analysis of all the available time-domain measurements systems was carried out. For a time domain measurement setup a major step is to down-convert the RF signal into an intermediate frequency signal. This is needed due to the physical limitation imposed by the speed and the resolution of analog to digital convertor. For all the available time-domain measurement systems the principle instruments used for frequency down conversion are samplers or mixers. The RF signal is down converted into a baseband signal and then digitized by the high resolution ADC. Samplers and mixers both are three port devices that operate on a very different principle. Sampler utilizes the sub sampling principle and a pulsed clock generated by a comb generator, while mixer requires a continuous clock and produces frequencies which are the sum and difference of the RF and that of a CW clock (local oscillator). Both devices translate the fundamental RF frequency and its harmonics into intermediate frequencies (IF). Lots of undesired frequencies are also generated in the process. The conversion loss of both devices is very high, therefore an IF circuitry comprising of high gain linear amplifiers and band-pass (anti aliasing) filters is required before digitization. This IF circuitry imposes further limitations on the measurement setup in terms of bandwidth when modulated signals are used in addition to an extra complex clock requirement.

Considering all these constraints, it was considered to be necessary to apply another approach to translate the fundamental frequency spectrum into a lower frequency. In this context a commercially available 13 GHz 2 Gsamples/s track and hold amplifier (THA) was used. The first step was to understand the operating principle of THA and to assess its performance; therefore it was fully characterized in terms of power and linearity. The complete working principle of THA was analyzed and it was noticed that it follows the sub-sampling principle but does not requires a strobe signal for the clock. The output of the THA has ideal gain conversion that is equal to unity corresponding to the RF signal due to the use of Emitter Follower Amplifiers at the output of each switch. Using the sub-sampling principle

the output voltage of THA could directly be digitized by ADC without using any additional IF circuitry. The use of a differential amplifier at the output further increases the performance in terms of dynamic range. THA and ADC share the same sinusoidal clock without the IF analog circuitry thus reducing circuit complexity. A four channel 420 Msamples/s ADC with a resolution of 12 bits was utilized to directly digitize the RF voltage acquired by THAs.

After the analysis of the THA the second step was to use it as a fundamental front end in a completely automated time-domain measurement using Labview. In the beginning, a single channel time-domain measurement setup was built and for data processing a quadrature IQ modulation scheme was developed. The inphase and quadrature components were extracted from the measured data. A calibration process was developed to remove linear systematic errors and power and phase mismatch. As it was a single channel setup and sequential measurement was performed to acquire input and output waveforms, therefore it required an additional time alignment between the two measurements. The results obtained with this measurement were verified and validated by a commercially available single channel VSA (mixer based). In the next step a 4-channel test setup was built and a high power GaN amplifier was fully characterized in terms of power (sinusoidal excitation) and linearity (two-tone excitation). The performance of test bench under pulse signals was also evaluated and it was noticed that the test setup performs exceptionally well for modulated signals without the use of extra complex clock circuitries. Until this point the proposed setup was based on quadrature modulation and extracted the envelope and phase information from the measured data. This was due to the fact that the test setup was limited to a specific sampling bandwidth due to limitations imposed by the ADC.

To extract the transient information for pulsed signals it was necessary to sample the fundamental RF signal at a very high rate. The fact that ADC and THA utilize a common sinusoidal clock and the direct RF voltage sampling property of THA based systems allowed the implementation of time interleaved sampling. For this, a Coherent Time Interleaved Sampling technique was developed, the main idea of which was to sample the fundamental RF signal at a frequency that is much lower and not an integer multiple of it. A specific method was developed to calculate this sampling frequency and the drawback offered by this system is that the acquisition time became longer and the acquired samples are scrambled in time and require reordering. An algorithm was developed using DSP techniques for the descrambling of the samples.

An automated absolute calibration process for amplitude and phase calibration was developed. The system was only calibrated for the fundamental and its harmonics and a constant group delay was assumed for modulated signals. A sampling frequency of  $100f_0$  for CW signals and  $10f_0$  for pulse modulated signals was achieved. The transients for the pulsed signals were acquired for the first time and the effect of bandwidth and instrumentation on the pulse profile is presented. Pulsed time-domain characterization of high power GaN amplifier under varying loads was performed and obtained appreciable results. It also validated the test setup capabilities to work in a load pull environment.

As discussed earlier the pulse signal produces an infinite spectrum, the resolution of which is dependent upon the pulse repetition interval (PRI). As the PRI increases the resolution becomes narrower and the spectral density increases. To calibrate for such narrow resolution is very difficult as it requires a multi harmonic generator capable of producing multiple harmonics with a high resolution and with high amplitude over the entire bandwidth. For accurate pulse measurements it is very important that the test setup should be calibrated at a low resolution for a large bandwidth each for fundamental frequency and its subsequent harmonics.

An interesting perspective to this work is to build a new standard which has the capabilities of becoming a universal standard and could be valid for different modulated signals. One of the methods to achieve this feature is by using a new commercially available arbitrary waveform generator (AWG) working at very high accuracy.

Also for characterizing PA's its necessary to acquire the DC characteristics so that accurate RF output current waveform can be measured. As the measurement system is limited to 4-channels therefore a method should be developed so that the DC characteristics could be measured simultaneously with the same measurement system and no time alignment is required. One of the methods to do so is to add bias tees in the measurement path before the ADC and use DSP techniques to extract DC information from RF waveforms.

For characterizing devices and to extract models on wafer probes should be added to the test setup which would help to characterize at device level. One of the problems which could be encountered to do that would be the performance of transient simulation using the simulation tools (ADS AWR microwave office) over large modulation bandwidths.



## Publications Relative to This Thesis

---

- **Ahmed.S**, M. Saad-el-dine, G. Neveux, D. Barataud, J. Nebus “*4-Channel, High Dynamic Range Time-Domain Measurement System Using Track & Hold Amplifier Utilized for the Characterization and Linearization of High Power GaN Amplifiers*” **International Journal of Microwave and Wireless Technologies** vol.4, issue 01, pp. 71-79, 2011.
- **Ahmed.S**, M. Saad-el-dine, G. Neveux, T. Reveyrand, D. Barataud, J. Nebus “*Time-Domain Measurement System Using Track & Hold Amplifier Applied to Pulsed RF Characterization of High Power GaN Devices*” **International Microwave symposium Baltimore 2011**.
- **Ahmed.S**, M. Saad-el-dine, G. Neveux, T. Reveyrand, D. Barataud, J. Nebus “*Caractérisation temporelle RF impulsionnelle directe par des THA d’amplificateurs de très forte puissance GaN*” **17èmes Journées Nationales Microondes** 18-19-20 Mai 2011 – BREST.
- **Ahmed.S**, G. Neveux, T. Reveyrand, D. Barataud, J. Nebus “*Time-Domain Interleaved High Sampling Rate System for Characterization of Non-linear Devices*” **79<sup>th</sup> ARFTG Microwave Measurement Conference, IMS June 2012, Montreal, Quebec**.





## **4-channel Time-Domain Interleaved High Sampling Rate System based on Track & Hold Amplifiers for Pulsed Characterization of High Power Non-Linear Amplifiers.**

**Abstract:** High power communications particularly RADAR applications are based upon radio frequency pulse signal modulation. These RF pulsed signals offer high complexities when it comes to accurate measurement as it occupies infinite frequency spectrum bandwidth. Therefore to obtain instant information about amplitude and phase it's very important to measure the modulated signal with respect to change in time. Time-domain measurements have their own limitations when it comes to bandwidth and resolution. This work proposes a new measurement technique based on Track and Hold amplifiers which simplifies the analog circuitry to a great extent. A fully calibrated 4-channel time-domain measurement system has been built and was used to characterize non-linear power amplifiers under continuous sinusoidal and pulse modulated signals in terms of envelope measurement or RF transient characterization. The measurement results were analyzed and validated by existing time-domain measurement systems. Utilizing the advantages of the THA based system a coherent time interleaving sampling systems was developed and frequency sampling rate of  $100f_0$  for CW and  $10f_0$  for pulsed modulated signals was achieved. Complete RF transient response for pulse modulated signals different load conditions has been presented.

**Key words:** Radar applications, RF time-domain characterization, Power amplifier, GaN, non-Linear, pulse modulated signal, coherent time interleaving sampling, RF transients.

## **Système de mesures temporelles 4-canaux à échantillonnage entrelacé ultra haute fréquence basé sur des amplificateurs « Track & Hold » pour la caractérisation impulsionnelle d'amplificateurs de puissance non linéaires**

**Abstract :** Les communications de forte puissance, telles que celles des applications radar, sont fondées sur des modulations impulsionnelles de signaux RF. La mesure précise de ces signaux RF impulsionnels est très complexe parce que leur bande passante est infinie. Pour obtenir les informations instantanées de phase et d'amplitude, il est nécessaire de les mesurer dans le domaine temporel. Ces mesures temporelles ont aussi des limitations en termes de bande passante et de résolution. Ce travail propose une nouvelle technique de mesure temporelle fondée sur l'utilisation d'amplificateurs « Track and Hold » qui permettent de simplifier les circuits analogiques des instruments. Un système de mesure 4 canaux entièrement calibré a été créé pour caractériser des amplificateurs de puissance non linéaires excités par des signaux continus ou pulsés. L'outil de caractérisation permet l'extraction des enveloppes des signaux ainsi que la visualisation de leurs transitoires. Les résultats de mesure ont été analysés et validés par comparaison avec des instruments mesures commerciaux. Le système de mesure réalisé à base de THA est associé à une procédure de traitement temporel cohérent des données entrelacées. Des fréquences d'échantillonnage 100 fois supérieures à la fréquence porteuse pour les signaux continus et 10 fois supérieures pour les signaux impulsionnels ont été obtenus et utilisés pour extraire les variations des réponses transitoires pour différentes conditions de charges.

**Mots-clés:** Applications Radar, caractérisation RF temporelle, amplificateur de puissance, GaN, non-linéaire, signal impulsionnel, échantillonnage entrelacé cohérent, transitoire RF.